Negative Lambda Quantum Cosmology

by

Petar Simidzija

BSc, University of Waterloo, 2017
MMath, University of Waterloo, 2019

A THESIS SUBMITTED IN PARTIAL FULFILLMENT OF
THE REQUIREMENTS FOR THE DEGREE OF

DOCTOR OF PHILOSOPHY

in

The Faculty of Graduate and Postdoctoral Studies

(Physics)

THE UNIVERSITY OF BRITISH COLUMBIA

(Vancouver)

July 2024

The following individuals certify that they have read, and recommend to the Faculty of Graduate and Postdoctoral Studies for acceptance, the dissertation entitled:

Negative Lambda Quantum Cosmology

submitted by Petar Simidzija in partial fulfillment of the requirements for the degree of Doctor of Philosophy in Physics.

Examining Committee:

Mark Van Raamsdonk, Professor, Physics, University of British Columbia
Supervisor

Moshe Rozali, Professor, Physics, University of British Columbia
Supervisory committee member

Gary Hinshaw, Professor, Physics, University of British Columbia
University examiner

Jim Bryan, Professor, Mathematics, University of British Columbia
University examiner

Andreas Karch, Professor, Physics, University of Texas at Austin
External examiner

Additional Supervisory Committee Members:

Douglas Scott, Professor, Physics, University of British Columbia
Supervisory committee member

Gordon Semenoff, Professor, Physics, University of British Columbia
Supervisory committee member

Abstract

We present a model of quantum cosmology based on anti-de Sitter/conformal field theory (AdS/CFT) holography. The spacetimes in our construction are time-symmetric, big-bang/big-crunch cosmologies with a negative cosmological constant Λ. In the simplest version of our model the cosmology lives inside a spatially finite bubble within an otherwise empty AdS spacetime. By studying the thermodynamic and geometric properties of this spacetime, we provide evidence that the "bubble of cosmology" spacetime has a well-defined dual CFT description.

We also present an upgraded model in which the cosmology is spatially infinite, homogeneous, and isotropic. Although a homogeneous cosmology is not asymptotically AdS and hence cannot be described directly by AdS/CFT, the time-reflection symmetry of the spacetime allows us to perform an analytic continuation, following which the spacetime is an asymptotically AdS Euclidean wormhole. If we assume that the cosmology is spatially flat a second analytic continuation obtains a Lorentzian traversable AdS wormhole. The AdS wormhole spacetimes can be described using holography: they are dual to a pair of three-dimensional CFTs coupled via a four-dimensional theory. We explain how an anomalously large amount of negative energy can support the traversable wormhole, and we begin to populate the holographic dictionary relating observables in the wormhole/cosmology to observables in the microscopic theory. Finally we show that time-dependent scalar fields naturally enable these cosmologies to contain a period of accelerated expansion, suggesting that our $\Lambda < 0$ models could ultimately provide the framework for a fully microscopic description of our Universe.

Lay Summary

Understanding the beginning of the Universe is a worthy goal. Presently this is not possible: the very early Universe contains exceedingly energetic matter, and our standard physical model breaks down at such high energies. We propose using an upgraded, *holographic*, model to study the Universe. A key distinction with the standard model is that the energy of empty space in our holographic model is slightly negative, rather than slightly positive. This seemingly minor difference enables a *quantum* description of the Universe which is valid at all energy scales, and which we systematically investigate as we work towards an eventual understanding of the origin of everything.

Preface

This thesis is an original, unpublished work by Petar Simidzija, under the supervision of Mark Van Raamsdonk.

Chapters 1 and 2 of this work are an original synthesis of the relevant literature, providing the necessary context and technical prerequisites for later chapters.

Chapter 3 is based on the work [1] done in collaboration with Mark Van Raamsdonk. Mark came up the idea for the project and both of us contributed equally to the calculations and writing. The work greatly benefited from useful discussions with the UBC and Berkeley String Theory groups, in particular Alex May and Raphael Bousso.

Chapter 4 is based on the work [2] done in collaboration with Abhisek Sahu and Mark Van Raamsdonk. All co-authors contributed equally with ideas, calculations, and writing. Stimulating discussions with Stefano Antonini, Brian Swingle, and Chris Waddell greatly enriched this work.

Chapter 5 is based on the papers [3, 4] done in collaboration with Stefano Antonini, Brian Swingle, and Mark Van Raamsdonk. All co-authors contributed equally with ideas, calculations, and writing. This work benefitted from many useful discussions with Panos Betzios, Matt Kleban, Lampros Lamprou, Henry Maxfield, Yasunori Nomura, Liam McAllister, Douglas Scott, Eva Silverstein, Chris Waddell, David Wakeham, and Aron Wall.

Chapter 6 is based on the work [5] done in collaboration with Alex May and Mark Van Raamsdonk. All co-authors contributed equally with ideas, calculations, and writing. We are grateful to Costas Bachas, Ben Freivogel, Henry Lin, and Juan Maldacena for helpful discussions and insights.

Chapter 7 is based on the work [3] done in collaboration with Stefano Antonini, Brian Swingle, and Mark Van Raamsdonk. All co-authors contributed equally with ideas, calculations, and writing. This work benefited from insights from Rodrigo A. Silva and Wucheng Zhang.

Chapter 8 is based on the work [4] done in collaboration with Stefano Antonini, Brian Swingle, Mark Van Raamsdonk, and Chris Waddell. All co-authors contributed equally with ideas, calculations, and writing. Helpful discussions with Douglas Scott and Panos Betzios improved the quality of this work.

Table of Contents

List of Figures

Acknowledgements

I am grateful to my supervisor Mark Van Raamsdonk for his mentorship, and for giving me the freedom to work on ideas that I found interesting. I am also grateful my colleagues at UBC, many of whom are now my close friends, for making my time in Vancouver so enjoyable. Most of all I am thankful to my parents, Aleksandra and Mirko, my brother Stevan, and my wife Christine, for their love and support.

Chapter 1

Introduction

Big bang and black holes

Understanding the very early Universe and the interiors of black holes are two of the most significant outstanding challenges in physics.

Starting at the present, there is overwhelming observational evidence that the Universe is currently expanding, i.e. on large scales distances between galaxies are increasing [6, 9, 10]. This expansion is well-explained by the standard model of cosmology, which is based on the gravitational theory of general relativity (see e.g. [11]). If we imagine the expansion process in reverse we conclude that as we go further into the past the distances between galaxies decrease. This contraction can be modeled simply by reversing the direction of time in the equations of general relativity. Evolving these time-reversed equations one obtains the prediction that the distance between any two points goes to zero at a particular finite time in the past, roughly 14 billion years ago. This is the *big bang*, the time at which the Universe emerged from a state of infinite density and began its expansion and dilution. In the context of this model this represents the beginning of the Universe.

A second challenge, on par with understanding the very early Universe, is to better understand black holes. Black holes are the predicted endpoints of the gravitational collapse of an object that is too dense to prevent this collapse from occurring [12, 13]. They are black because their gravity is strong enough to prevent light from escaping past a certain surface, called the *event horizon*; inside the event horizon is the interior of the black hole, which we cannot see. Black holes are conceptually simpler to think about compared to the beginning of the Universe for two main reasons. First, while there is only one big bang, there are many black holes in the Universe. There is even one at the centre of our galaxy, which on cosmic scales is not too far away [14–16]. Moreover black holes can form at any point in time, whereas the big bang represents the beginning of time itself. It is much easier to conceptualize a black hole because there is something that came before it and that gave the initial conditions for its formation; this is not the case with the big bang in the standard model of cosmology.

Despite these differences there is an important similarity between the big bang and a black hole: our standard theory of gravity, general relativity, predicts that they are both contain a *singularity*. In general relativity singularities are limiting points in spacetime where the curvature of the geometry of spacetime becomes infinite, or equivalently points where the energy density of the contents of the spacetime becomes infinite [12, 17]. In the case of the big bang the singularity is the big bang itself, the point of zero volume from which the entire Universe supposedly emerged. In the case of a black hole the singularity is the point at which gravity compactifies the object which formed the black hole (e.g. a star) into a single point. Black hole singularities are predicted to occur behind event horizons, and thus be invisible to external observers [18]. The big bang singularity is in principle visible, but in practice the high density of the early Universe makes it difficult to see back to arbitrarily early times.

These last two points are the most important and should be emphasized: black hole and big bang singularities are predictions of a theory (general relativity) and not observed facts about the Universe. It is therefore reasonable to question whether the theory is correct in predicting these

singularities. Assuming that singularities are unphysical, it is evident that an upgrade to general relativity is necessary for a more accurate description of the very early Universe and the interiors of black holes. Two questions arise. First, when/where does general relativity break down? And second, what should we replace it with?

Quantum gravity

The lack of observational evidence of the breakdown of general relativity means that we must resort to theoretical arguments to speculate on when or where the breakdown occurs. Because singularities in general relativity are points of infinite energy density, we expect the breakdown of general relativity to be a *high energy* breakdown, i.e. the theory is invalid beyond a certain energy scale. Before giving a prediction for what this scale might be, let us consider the question of how we might upgrade general relativity so that it is valid at all energy scales.

To make progress it is instructive to compare general relativity, a theory of gravity, to the theories of the other fundamental forces (electromagnetism and the strong and weak nuclear forces). Like general relativity these are field theories, in which the dynamical degrees of freedom are functions of space and time, i.e. fields. But while the fields describing electromagnetism and the nuclear forces are quantum fields (see e.g. [19]), the gravitational field in general relativity is simply the spacetime metric, which is a classical field. Classical fields and quantum fields are mathematically very different: quantum fields are Hilbert space operators while classical fields are simply number (or tensor) valued functions of spacetime. These differences in their mathematical descriptions makes it challenging to construct a theory that incorporates both classical and quantum fields. If gravity and the other forces were completely decoupled this would not be a problem, but evidently this is not the case. Gravity in particular is a universal force, acting on particles (electrons, protons, photons, etc.), which also interact via the other forces. Thus even to completely describe the interaction between a proton and an electron, let alone the entire Universe or the interior of a black hole, we need to have a unified theory of gravity along with the other forces.

What would this unified theory look like mathematically? Making the assumption that classical and quantum theories are incompatible it appears there are three possibilities.[2] The first is to describe all the forces classically. This appears to be out of the question, since the quantum description of the non-gravitational forces agrees very well with experimental observations [27]. The second option is to promote general relativity to a quantum theory so that it is on an equal footing with the other forces. And lastly, it is possible that a unified theory of nature requires us to reformulate our description of all the forces, gravitational and non-gravitational, in some new mathematical language, which does not fit into either the classical or the quantum categorization.

It is not clear whether the second approach (quantum gravity) or the third approach (post-quantum gravity) will provide the correct unified description of physics in our Universe. Since in any case the distinction between a quantum theory and a post-quantum theory is not very clear, it is common to view these approaches as one and the same and refer to the unified theory of all forces as a theory of *quantum gravity*. With this broad definition there have been many approaches to quantum gravity. This thesis is based on two related approaches: *string theory* and *holography*. Other approaches to quantum gravity include loop quantum gravity [28], causal dynamical triangulation [29], and causal set theory [30]. Whether any of these approaches is correct is yet to be determined.

[2] There have been many arguments both for and against the statement that classical and quantum theories are incompatible, and in particular the need to quantize gravity. See [20–26] and references therein for a variety of viewpoints.

Before introducing string theory and holography, let us give an answer to our original question: At what energy density does general relativity break down and quantum gravity become necessary? We can provide an estimate using dimensional analysis. The dimensionful parameters in general relativity are Newton's constant G and the speed of light c. If quantum gravity is anything resembling quantum mechanics, then it will also depend on Planck's constant $\hbar$. These three quantities uniquely define a natural energy density scale $\rho_{\rm Pl} = c^7/\hbar G^2$, which we call the *Planck density*. In SI units this is roughly 10^{113}J/kg^3. We can similarly define a natural *Planck length* $\ell_{\rm Pl} = \sqrt{\hbar G/c^3}$, which is roughly 10^{-35}m. We expect general relativity to break down and quantum gravity to become important at densities above $\rho_{\rm Pl}$ or at distances below $\ell_{\rm Pl}$. Although these are very extreme scales, general relativity predicts an infinite density inside black holes and at the big bang. So to describe these regimes accurately it appears that quantum gravity becomes necessary. With this in mind, let us discuss how to quantize gravity.

Effective field theory

The most obvious approach to quantize gravity is to start with general relativity and quantize it. This approach follows the precedent set by electrodynamics. Originally electrodynamics was understood as a classical theory, and only after the development of quantum mechanics was it promoted to a quantum theory, with great success. For example the quantization of the energy levels of the electromagnetic field resolved the classical ultraviolet catastrophe, the prediction that the electromagnetic field in a finite temperature state should have infinite energy density [31]. Moreover, quantum electrodynamics makes very accurate predictions for the scattering of charged particles [27], so it is by all measures a highly successful quantum theory.

Since classical electromagnetism and general relativity are similar in many ways, both mathematically and physically, it might be hoped that the latter could be quantized similarly to the former. This is indeed possible and unsurprisingly the resulting quantum gravity theory exemplifies the similarities between electromagnetism and gravity [32]. For example just as the quantum particle mediating the electromagnetic force is a massless, spin-1 boson (the photon), the hypothesized quantum particle mediating gravitational interactions is a massless, spin-2 boson called the graviton. Unlike photons, gravitons have not been directly observed, but this is to be expected: the predicted coupling of gravitons to each other and to other particles is very weak, so the cross sections for scattering amplitudes involving gravitons are correspondingly small [32].

Given that this approach defines a theory of quantum gravity, is our job done? Can we use this theory to understand the big bang or the interiors of black holes? Unfortunately (or fortunately) the answer is no. To understand why, consider using this quantum gravity theory to compute the scattering cross section σ of gravitons at some energy scale E. As in quantum electrodynamics we can compute σ perturbatively in the coupling constant of the theory. In the case of quantized general relativity the coupling constant is given by the inverse Planck energy $E_{\rm Pl} \equiv \rho_{\rm Pl}\ell_{\rm Pl}^3 = \sqrt{\hbar c^5/G}$. But because this is a dimensionful scale it is not really appropriate to think of it as a perturbation parameter. What actually happens in calculations is that a positive power of the external energy scale E accompanies each negative power of $E_{\rm Pl}$, giving an effective dimensionless perturbation parameter $E/E_{\rm Pl}$. Perturbation theory works only if this quantity is much less than 1, that is if the energy scale E of the gravitons is less than the Planck scale. If E is larger than the Planck scale then this quantum theory breaks down. However this is precisely the regime in which general relativity broke down! So the quantum theory which was supposed to solve the trans-Planckian problems of general relativity has precisely these same trans-Planckian problems.

We can summarize the situation by saying that this naive quantum theory of gravity is an *effective* field theory (EFT), which we will call the *gravitational effective field theory*. Like any effective

theory [33], the gravitational EFT is only valid up to a certain energy scale, in this case the Planck scale. We will use the gravitational EFT extensively in this thesis; it is very valuable whenever we want to understand physics at scales below the Planck scale. However to fully understanding the big bang and the interiors of black holes, we must go beyond gravitational EFT. It is not enough to simply have a quantum theory of gravity. Instead we require a quantum theory of gravity which is valid at arbitrarily high energy scales. Such a theory is called *ultraviolet complete*, or *UV complete*.

String theory

To say a theory is sensible at arbitrarily high energies, i.e. that it is UV complete, is equivalent to saying that it is sensible at arbitrarily short distances. Hence gravitational EFT fails at very short distances. In fact this failure is common: many quantum field theories have divergences at short distances.[3] To understand why this is the case recall that quantum field theory is simply the result of trying to consistently describe relativistic point particles using quantum mechanics. Since point particles have zero size but carry a finite amount of energy it is perhaps not surprising that quantum field theory is generally afflicted by ultraviolet divergences.

String theory is a candidate theory of quantum gravity which is based on the idea that fundamental excitations are not zero-dimensional point particles, but one-dimensional *strings* of finite length. Just as quantum field theory is the result of quantizing relativistic point particles, string theory is the theory of quantum relativistic strings. Because the fundamental objects in string theory have a finite size, string theory avoids the short distance divergences present in quantum field theory. See [34, 35] for introductions to string theory.

String theory is not only a theory of quantum gravity, but of all interactions. It predicts that what we think of as fundamental point particles (electrons, quarks, etc.) are in fact quantum excitations of tiny strings. These strings are so small that they are effectively pointlike even at the shortest distance scales which we have been able to probe via particle colliders. We call the quantized excitations of strings the *spectrum* of string theory. Besides being UV complete, one of the most important features of string theory is that it contains a massless excitation of spin-2 in its spectrum, which we identify with the graviton. Therefore string theory is a UV complete theory of quantum gravity.

The issue with string theory is that it is far from evident that it is correct as a description of our Universe. The most obvious issue is that it is only consistent in a large number of spacetime dimensions. In the simplest version, bosonic string theory, the number of dimensions is 26, rather than the four which we observe. If fermions are included in the theory the number of spacetime dimensions drops to 10, but its not like this is any better than 26. Moreover the incorporation of fermions is achieved by requiring that the theory is *supersymmetric*, which implies that every fermionic excitation is accompanied by a partner bosonic excitation, and vice versa [36]. Unbroken supersymmetry requires that these "superpartners" have the same mass, a prediction which is in complete disagreement with particle spectra from collider experiments [27].

Despite these two seemingly egregious predictions—10 spacetime dimensions and superpartners for every particle—there may still be hope for string theory. It is possible that at the low energies of everyday experience (or even of particle colliders) these problems are not apparent. For example if six spatial dimensions are compact and very small, then it is conceivable that they are there but we just have not probed short enough distances to observe them [37]. Similarly it is possible that supersymmetry, despite being an exact symmetry of the theory, is broken at low energies, and that this is the reason superpartners have not been observed yet [38].

[3] See any textbook on quantum field theory, e.g. [19].

However, this solution comes with its own problem, which is that string theory does not just predict a single low energy solution but rather it predicts a very large (potentially infinite) number of them [39, 40]. Each of these low energy solutions, or *vacua*, of string theory come with their own values for the observable constants of nature (e.g. particle masses or coupling constants), seemingly allowing string theory to match any observation. This raises a legitimate concern that string theory is not a true scientific theory, since essentially any experiment can be matched by fine tuning to an appropriate vacuum.

Related to the notion that string theory contains a vast number of vacua is the question of whether we can find one which is consistent with observations of our Universe. Since string theory aims to be a theory of all interactions, finding such a low energy description is difficult: it must match our observations of the Universe from microscopic to cosmological scales. Thus not only must we find a vacuum with a particle spectrum matching the standard model of particle physics, but it must also match our observations of the large-scale structure of the Universe, including the observation that the Universe is presently expanding at an accelerated rate. This last requirement in particular has been a major sticking point in the quest to find a realistic string theory vacuum. The goal of this thesis is to make progress on this front.

AdS/CFT

The most popular strategy to finding a string theory vacuum which is consistent with the observed accelerated expansion of the Universe has been to look for solutions with a positive cosmological constant Λ. This is because $\Lambda > 0$ is the most straightforward way to obtain a cosmological spacetime with a period of accelerated expansion. Indeed the standard ΛCDM model of cosmology (see e.g. [19]) is based on the assumption that the Universe contains regular matter, cold dark matter (CDM), and a positive cosmological constant Λ. Unfortunately string theory vacua with $\Lambda > 0$ have been very difficult to construct, and it is presently not even agreed whether they exist [41, 42].

On the other hand string theory vacua with $\Lambda < 0$ are plentiful. The maximally symmetric spacetime with $\Lambda < 0$ and no other forms of stress-energy is called *anti-de Sitter* (AdS) spacetime, so such solutions are known as *AdS vacua* of string theory. Aside from being easier to construct, the dynamics of string theories near AdS vacua are conjectured to possess an additional remarkable property: they are thought to be dual to non-gravitational quantum field theories living on the boundary of the spacetime. The example which motivated this conjecture was found by Maldacena, who showed that the low energy effective theory describing perturbations around an AdS vacuum of type IIB superstring theory (a particular type of string theory) is dual to $\mathcal{N} = \triangle$ supersymmetric Yang-Mills (SYM) theory, where $\mathcal{N}$ quantifies the amount of supersymmetry in the theory [43]. The AdS vacuum solution in this construction is a 10-dimensional spacetime, consisting of a five-dimensional AdS spacetime multiplied by a five-dimensional sphere. Meanwhile, the $\mathcal{N} = \triangle$ SYM theory is defined on the flat, four-dimensional boundary of the five-dimensional AdS spacetime. Since this is a theory on a flat spacetime it is non-gravitational. Moreover, it happens to be a scale-invariant quantum field theory, or more precisely a *conformal field theory* (CFT) [44]. This seminal discovery by Maldacena, of a duality between a gravitational theory on an AdS spacetime and a non-gravitational CFT living on the boundary of the spacetime, was the first realization of what has come to be known as the *AdS/CFT correspondence* [43, 45, 46].

Since Maldacena's discovery many additional examples of the AdS/CFT correspondence have been found.[4] In each of these examples a gravitational theory on AdS spacetime (or more precisely a

[4] See e.g. [47, 48] for introductions to AdS/CFT.

spacetime that approaches AdS near its asymptotic boundary) is seen to be related (and conjectured to be completely dual) to a non-gravitational CFT defined on the boundary of the spacetime. The extensive study of these examples has led to the steady buildup of the *AdS/CFT dictionary*, namely the mapping which relates quantities on the AdS side of the duality to quantities on the CFT side, and vice versa.

This proliferation of examples of the AdS/CFT correspondence has led to a more modern viewpoint that AdS/CFT should be viewed not as a duality between two independently defined theories, but rather as a *definition* of a theory of quantum gravity. In this viewpoint the prescription of a CFT together with the AdS/CFT dictionary define a theory of quantum gravity on an AdS spacetime.[5] This is an attractive viewpoint because: i) CFTs can be defined relatively precisely, and ii) the fact that they are scale invariant means that they are valid at arbitrarily high energies, hence enabling the construction of UV complete theories of quantum gravity.

Holography

One of the most significant conceptual achievements of the AdS/CFT correspondence is that it provides a concrete realization of the *holographic principle* [50–52]. The motivation for this principle predates AdS/CFT and is rooted in black hole physics. In the 1970s several independent pieces of evidence were found suggesting that black holes behave like thermodynamic systems [53, 54]. In particular it was argued that the thermodynamic entropy of a black hole is proportional to its surface area [53]. But in statistical mechanics entropy is defined by the exponential of the number of microstates consistent with a given macrostate, which suggested that the total number of degrees of freedom of a black hole (the number of microstates) is proportional to its surface area. This proportionality inspired the idea that the underlying degrees of freedom of a black hole should actually be thought of as "living on" the surface of the black hole, i.e. that a UV complete theory of the black hole should be defined on its surface [55]. The extrapolation of this idea to general gravitational systems (not necessarily containing black holes) resulted in the holographic principle, the general expectation that quantum gravity inside a volume of space can be described by a theory defined on the volume's boundary [50, 51]. The AdS/CFT correspondence provided a concrete realization of this idea, at least for asymptotically AdS volumes of space.

This thesis

The goal of this thesis is to develop a model of quantum cosmology with the hope that eventually it leads to a better understanding of the very early Universe. Our model will be based on AdS/CFT holography. Following a brief Chapter 2 covering prerequisite material, the rest of the thesis is structured as follows.

In Chapter 3 we will not discuss cosmology, but instead we will investigate a basic question in holography: when can a quantum gravitational system which is holographically described by some conformal field theory CFT_1 also be described by a different conformal field theory CFT_2? We will argue that the answer is "when the two CFTs can be coupled at a boundary". In this case we will find that it is possible to construct states of CFT_2 that describe arbitrarily large bubbles of the gravitational system dual to a state of CFT_1. The main technical tools developed in this chapter—the Euclidean path integral and the Isreal junction condition formalism—will be essential in later chapters.

In Chapter 4 we begin to think about cosmology. An apparent issue with using holography to describe cosmology is that holographic spacetimes in AdS/CFT must be asymptotically empty,

[5] The conditions on a CFT to have an AdS gravity dual are discussed in [49].

whereas the cosmology we live in contains matter and radiation. Our first model of quantum cosmology resolves this issue in perhaps the most obvious way, by embedding a finite "bubble" of cosmology within an empty AdS spacetime. In this construction the cosmological region is a time-reflection symmetric, $\Lambda < 0$, big-bang / big crunch cosmology. This bubble of cosmology is homogeneous and isotropic locally, but not globally. Nevertheless we will show that the bubble can be arbitrarily large, avoiding tension with the observed large scale homogeneity and isotropy in our Universe. By studying the thermodynamic and geometric properties of these asymptotically AdS cosmologies, we will give evidence that they can indeed be described quantum mechanically via a conformal field theory.

Although this framework can accommodate arbitrarily large regions of cosmology, from a Copernican perspective it is desirable to have a quantum model in which the cosmology is globally homogeneous and isotropic. In Chapter 5 we develop such a model. The key to the construction is a simple mathematical observation: spatially flat, time-symmetric $\Lambda < 0$ homogeneous and isotropic cosmologies can be analytically continued to asymptotically AdS Euclidean and Lorentzian wormhole spacetimes. This suggests a three-way correspondence between i) time symmetric spatially flat cosmologies, ii) Euclidean AdS wormholes, and iii) Lorentzian traversable AdS wormholes. Following work in [56] we argue that the AdS wormholes are dual to a microscopic (i.e. quantum) description in which a pair of three-dimensional CFTs are coupled via a four-dimensional field theory. By analytic continuation this also provides a quantum description of the $\Lambda < 0$ cosmology. In the remainder of the chapter we explore many aspects of this cosmological model. Most of our quantitative results are at the level of the background cosmology, but we also comment on the model's implications for fluctuations about the background. An important observation which we elaborate on is that while the quantum state of the cosmology is a very complicated excited state—as it must be to describe the entire Universe—the state of the dual traversable wormhole is simply the vacuum state. Because the latter is relatively straightforward to describe using established AdS/CFT techniques, this offers a promising approach to studying quantum cosmology.

In Chapter 6 we address an important issue from the construction of the previous chapter, specifically regarding the validity of the traversable wormhole. The issue is that effective field theory straightforwardly implies that the existence of traversable wormholes requires a large amount of negative energy density. While classical matter sources always have positive energy density, there are states of quantum fields that, locally, can have a negative energy density. The most famous example of this is the Casimir effect, in which the energy density of the electromagnetic vacuum between two parallel conducting plates is negative. In this chapter we study whether this mechanism can produce enough negative energy density to support the traversable wormholes appearing in our construction. Happily we find that precisely under the conditions required for our cosmological construction to make sense, an anomalously large amount of negative energy density can exist in the traversable wormhole spacetime, thus enabling its existence and providing a non-trivial consistency check on our construction.

In Chapter 7 we continue to explore the model of homogeneous cosmologies dual to Euclidean and Lorentzian wormhole spacetimes. Specifically we begin to construct the holographic dictionary for the model, which relates observables in the gravitational theories (cosmology, Euclidean wormhole, or Lorentzian wormhole) and the non-gravitational quantum field theory defined on the boundaries of the wormhole spacetimes. Because the quantum state of the traversable Lorentzian wormhole is simply the vacuum state whereas the state of the cosmology is a complicated excited state, we primarily focus on understanding the relationship between observables in the wormhole to observables in the field theory. In particular we consider the most fundamental observable defining the wormhole spacetime, its background metric. We derive the explicit relationships between the wormhole metric and various field theory observables, such as the particle spectrum and subregion

entanglement entropies. Because the wormhole background metric is directly related, via analytic continuation, to the metric of the background cosmology, this provides a concrete and explicit mapping between observables in the quantum field theory and the cosmological scale factor.

Finally in Chapter 8 we begin to address the question of whether our model is capable of describing realistic cosmologies, i.e. ones resembling the one we live in. The most glaring apparent issue with $\Lambda < 0$ cosmologies is that by itself a negative cosmological constant cannot drive an accelerated expansion of the Universe. In fact this is not an issue in our holographic cosmological constructions, because it is generically the case in AdS/CFT that the gravitational theory contains various scalar fields dual to the many scalar operators present in the CFT. In general these scalar fields have non-trivial potentials, and in the cosmological spacetime the potential energy of the scalars can act as a time varying dark energy. This time varying dark energy can, and as we show generically does, compensate for the negative cosmological constant and results in a Universe with a period of accelerated expansion. To fully drive the point home that our negative Λ model has the capacity of describing realistic cosmologies, we show how a single scalar field with a particular potential is able to produce a cosmology with a scale factor that precisely agrees with the scale factor of standard ΛCDM cosmologies, with positive cosmological constant. This shows that at least from the perspective of the background cosmology our model has the capacity to be realistic.

Chapter 2

Prerequisites

2.1 Path integrals

Path integral techniques are central to high energy physics, and quantum gravity in particular. Here we review the basics. See [19, 57] for more details.

Path integrals in quantum mechanics

The simplest example of a path integral is in ordinary quantum mechanics. Consider the quantum mechanics of a single point particle. The states of the particle are vectors in a Hilbert space. For example we can use the eigenstates $|x\rangle$ of the position operator as a basis for the Hilbert space. The dynamics of the theory are determined once we specify the Hamiltonian operator H.

Now consider the following physical question. A particle starts out at position $|x_1\rangle$ at time $t = t_1$. What is the probability amplitude that at time $t = t_2$ the particle is at position $|x_2\rangle$? In the Schroedinger picture of time evolution, we can compute this amplitude by evolving the initial state $|x_1\rangle$ with the unitary time evolution operator

$$U(t_2, t_1) \equiv T \exp\left(-\frac{i}{\hbar}\int_{t_1}^{t_2} dt H(t)\right), \tag{2.1}$$

(where T is the time-ordering operation), and then computing the overlap with the final state. Thus the amplitude in question is $A = \langle x_2| U(t_2, t_1) |x_1\rangle$. A useful way to rewrite this amplitude is to take the time-ordered exponential, break it up into a product of a large number of small time evolutions, insert the identity $\mathbf{1} = \sum_x |x\rangle \langle x|$ in between each factor in the product, and evaluate the resulting product of matrix elements (see, e.g., [19] for details). The result is the *path integral representation* of the transition amplitude:

$$A = N \int_{x(t_1)=x_1}^{x(t_2)=x_2} [dx] e^{\frac{i}{\hbar}S[x]}, \tag{2.2}$$

where $S[x]$ is the action functional corresponding to the given Hamiltonian, and the integral is over all continuous paths/trajectories $x(t)$ which satisfy the boundary conditions $x(t_1) = x_1$ and $x(t_2) = x_2$. The normalization factor N is infinite, but it is independent of x_1 and x_2, so it can be absorbed into the measure of integration $[dx]$.

The path integral technique can be used to rewrite not only expressions for transition amplitudes but also for matrix elements of operators. Working now in the Heisenberg picture of time evolution, in which operators rather than states are time dependent, consider the matrix element of the operator $x(t)$ at time t between the eigenstates $|x_1(t_1)\rangle$ and $|x_2(t_2)\rangle$, with $t_1 < t < t_2$.[6] The path integral technique allows us to write this matrix element as

$$\langle x_2(t_2)| x(t) |x_1(t_1)\rangle = \int_{x(t_1)=x_1}^{x(t_2)=x_2} [dx] x(t) e^{\frac{i}{\hbar}S[x]}, \tag{2.3}$$

[6]The states have time labels not because they are time dependent but because they are eigenstates of an operator that is time dependent.

where we have absorbed the infinite N into the path integral measure.[7] Matrix elements of more operators would simply result in inserting the corresponding fields into the integrand of the path integral on the right hand side.

Despite the fact that it is not very well-defined mathematically (for example due to the infinite constant N), the path integral is nevertheless a useful tool in quantum mechanics because it provides a very intuitive physical picture of a transition amplitude (or a matrix element) as being the sum of amplitudes of all paths that the particle can take to go from one point to another.

Path integrals in quantum field theory

The full utility of path integrals is evident in quantum field theory (QFT), the quantum mechanics of continuous fields. The path integral expressions for transition amplitudes and matrix elements in QFT are derived in exactly the same way as the expressions above for the single quantum mechanical particle. Consider a quantum field theory of a field $\phi(x,t)$ in a flat spacetime, defined by an action functional $S[\phi]$. The matrix element of any sequence of operators between an eigenstate of ϕ at time $t=t_1$ with eigenvalue ϕ_1 and an eigenstate of ϕ at time $t=t_2$ with eigenvalue ϕ_2 is given by the following path integral:

$$\langle \phi_2(t_2)|\, \phi(t)\cdots|\phi_1(t_1)\rangle = \int_{\phi(t_1)=\phi_1}^{\phi(t_2)=\phi_2} [d\phi]\phi(t)\cdots e^{\frac{i}{\hbar}S[\phi]}. \tag{2.4}$$

These matrix elements can be directly related to scattering amplitudes of field quanta, so evaluating them is important from a practical perspective. The path integral helps in this regard. If the action $S[\phi]$ consists of a piece quadratic in the fields (the kinetic and mass terms) plus contributions that multiply small coupling constants, then the exponential in the path integral can be perturbatively expanded in these small couplings, and the resulting terms, consisting of generalized Gaussian integrals, can be computed exactly. The perturbative expansion can be represented diagrammatically, resulting in the Feynman diagram technique of computing scattering amplitudes in QFT.

Let us consider another example of a path integral in quantum field theory. This time we use a path integral to represent a state, rather than a matrix element of operators between states. Specifically, let us consider the vacuum state of the theory, $|vac\rangle$. This is a state in the abstract Hilbert space, but we can equivalently consider the wavefunction of the state with respect to some basis of the Hilbert space. Let us consider the eigenbasis of the ϕ operator, consisting of eigenvalues $|\phi\rangle$. The wavefunction of the vacuum is $\langle\phi|\, vac\rangle$, just as in quantum mechanics. This is close in form to the general path integral expression written above. The only difference is that that the state on the right is the vacuum rather than a field eigenstate. But because the vacuum is the state of lowest energy, we can write it by starting with any field eigenstate $|\phi'\rangle$ and acting on it with the *Euclidean time evolution* operator e^{-Ht} for infinite time, i.e. $|vac\rangle \propto \lim_{t\to\infty} e^{-Ht}\,|\phi'\rangle$. To understand where this expression comes from, imagine expanding out $|\phi'\rangle$ in an eigenbasis of H. Then the infinite Euclidean time evolution results in a relative exponential decay of all states with energy greater than the ground state, and the only state which remains (up to a proportionality constant N) is the vacuum state. This trick allows us to write the wavefunction of the vacuum as $\langle\phi|\, vac\rangle = N\lim_{t\to\infty}\langle\phi|\, e^{-Ht}\,|\phi\rangle'$, which we can represent using a path integral:

$$\langle\phi|\, vac\rangle = \int^{\phi} [d\tilde{\phi}]\tilde{\phi}(t)\cdots e^{-S_E[\tilde{\phi}]/\hbar}. \tag{2.5}$$

[7] The $x(t)$ on the LHS of this equation is an operator-valued function, while the $x(t)$ on the RHS is number valued. Often the former is distinguished by a hat, but we will omit hats on operators and distinguish them based on context.

There are a few things to note here. First the upper limit on the path integral is ϕ, corresponding to the $\langle\phi|$ as before. We have thus renamed the integration variable from ϕ to $\tilde{\phi}$. Moreover, we have not written the lower limit of the path integral, because it is irrelevant: the state $|\phi'\rangle$ can be taken to be *any* field eigenstate, as long as it has some overall (however small) overlap with the vacuum. What is important, however, is that the path integral is over all field configurations in the semi-infinite spacetime domain $t < 0$; the absence of an explicit lower limit in the path integral implies this domain of integration. Because this path integral represents a Euclidean time evolution, the exponential in the integrand is a damped exponential $e^{-S_E/\hbar}$ rather than an oscillatory one, and the action $S_E[\phi]$ appearing in the exponent is the *Euclidean action*, obtained from the original (Lorentzian) action by performing an analytic continuation of the time variable from real values to imaginary values. Thus this path integral should be viewed as an integral over field configurations in the *Euclidean spacetime* obtained from the initial Lorentzian spacetime via the aforementioned analytic continuation of the time coordinate. We refer to this path integral, representing the vacuum state of the field theory, as a *Euclidean path integral*. By inserting fields into the Euclidean path integral (similarly to when we computed matrix elements of a sequence of operators) we can define other (non-vacuum) states of the theory. Finally, note that the exponentially decaying rather than oscillatory weight factors in Euclidean path integrals make them somewhat better defined than Lorentzian path integrals.

Path integrals in quantum gravity

Aside from its practical utility in deriving the Feynman diagram expansion, the path integral is also very useful theoretically. One reason is that it incorporates the dynamics directly via the action functional and not the Hamiltonian, so it makes manifest the symmetries of the action. Second, the path integral is very intuitive: quantities are represented as a sum over all the different configurations of the degrees of freedom of the theory. This intuition inspires useful approximation techniques for evaluation the path integral. For example the saddle point technique is based on the idea that the dominant contributions from the path integral are those which extremize the action functional, i.e. which satisfy the classical equations of motion $\delta S[\phi]/\delta\phi = 0$. The intuition for this for Lorentzian path integrals is that extremal paths have phases $e^{iS/\hbar}$ that vary relatively little compared to other paths, and hence add up constructively rather than destructively. For Euclidean path integrals the justification is stronger, since here the non-extremal paths are individually (rather than collectively) strongly suppressed, due to the exponential decay factor $e^{-S/\hbar}$. The intuition that $\hbar \to 0$ corresponds to the classical limit also makes a lot of sense from this perspective, since in this limit only extremal paths, i.e. field configurations that satisfy the classical equations of motion, contribute to the path integral. Finally, the path integral is useful theoretically because it is very general. We have seen that completely analogous path integral expressions represent observables in ordinary quantum mechanics as well as quantum field theory. It is therefore reasonable to hope that path integrals can also be used in quantum gravity.

2.2 AdS/CFT

Here we give a brief introduction to the anti-de Sitter/conformal field theory (AdS/CFT) correspondence. See e.g. [58] or [48] for more detailed introductions.

The most concise way to state the AdS/CFT correspondence is through the language of path integrals [45, 46]. For concreteness we first state the correspondence for the most well-known example of AdS/CFT: the duality between type IIB superstring theory on $AdS_5 \times S^5$ and $\mathcal{N} = 4$ superconformal Yang-Mills (SYM) theory in a four dimensional flat spacetime, which is the boundary

of the AdS_5 sector of the gravitational theory [43]. As in any QFT a fundamental object in this CFT is the *partition function* Z_{CFT}, which is a mapping of functions $\phi_{(0)}(x)$ to numbers. To write the partition function, let us schematically denote the fields of $\mathcal{N}=4$ SYM theory as $\mathcal{O}(x)$. Then we can write Z_{CFT} as a path integral

$$Z_{\text{CFT}}[\phi_{(0)}] \equiv \int [d\mathcal{O}] \exp\left(iS_{\text{CFT}}[\mathcal{O}] + i\int d^d x \mathcal{O}(x)\phi_{(0)}(x) \right), \tag{2.6}$$

where $S_{\text{CFT}}[\mathcal{O}]$ is the action of the theory, and in this case the spacetime dimension is $d=4$. Also we have set $\hbar = 1$. In general the partition function is a useful object because it contains all the dynamical information about the theory. In particular any correlators of the operators $\mathcal{O}$ can be computed by functionally differentiating the partition function with respect to the *source* function $\phi_{(0)}(x)$.

The strongest form of the AdS/CFT correspondence is an equivalence between the CFT partition function and the partition function for the string theory, Z_{string}, namely

$$Z_{\text{CFT}}[\phi_{(0)}] = Z_{\text{string}}. \tag{2.7}$$

Unfortunately, the meaning of Z_{string} is not explicitly known, although for the equation to make any sense it must be a functional of $\phi_{(0)}$. The idea is that because the CFT is defined on the boundary of the space on which the string theory is defined, the $\phi_{(0)}$ should represent fixed boundary conditions for the fields that are presumably integrated in the definition of Z_{string}. But because the right hand side is not independently known, this equation cannot be said to be a correspondence.

On the other hand, there exists a weak form of the AdS/CFT correspondence that is much more explicit. To obtain this version of AdS/CFT we take two limits; see e.g. [48]. From the string theory perspective, we first take the limit in which the string coupling constant goes to zero, which corresponds to the limit of classical string theory. Then we take the limit in which the string length measured in units of the AdS scale also goes to zero, which corresponds to the point particle limit of string theory. In this limit the string theory is described by classical type IIB supergravity, which is an effective field theory of gravity and matter with an explicitly known action [59]. The supergravity action S_{sugra} is a functional of many fields, including the metric and various matter fields, but let us collectively denote these fields by ϕ. Then, just as we defined the partition function for $\mathcal{N}=4$ SYM, we can completely analogously define the supergravity partition function $Z_{\text{sugra}}[J]$,

$$Z_{\text{sugra}}[J] \equiv \int [d\phi] \exp\left(iS_{\text{sugra}}[\phi] + i\int d^{d+1} x \phi(x)J(x) \right). \tag{2.8}$$

Here J is a source to the various supergravity fields, just as $\phi_{(0)}$ is a source for the various CFT operators. In the weak limit that we took the string theory is described by *classical* supergravity, so we can take the classical limit of the supergravity partition function, corresponding to the saddle point approximation of the path integral, giving

$$Z_{\text{sugra}}[J] \approx \exp\left(iS_{sugra}[\phi] + i\int d^{d+1} x \phi(x)J(x) \right), \tag{2.9}$$

where the field ϕ on the right hand side satisfies the classical equations of motion. We call a field that satisfies the classical equations of motion *on-shell*. This gives the weak form of the AdS/CFT correspondence:

$$Z_{\text{CFT}}[\phi_{(0)}] \approx e^{iS_{\text{sugra}}[\phi]}|_{\phi_{(0)}}. \tag{2.10}$$

Here the source J for the supergravity fields ϕ has been set to zero, and the subscript $\phi_{(0)}$ means that ϕ is the on-shell field with boundary conditions $\phi_{(0)}$.

To make the specification of boundary conditions more precise suppose for simplicity that ϕ is a scalar field. Let us define a coordinate system for the AdS spacetime on which the supergravity theory is defined. One choice is the Poincaré AdS coordinates, in which the metric is

$$ds^2 = \frac{L_{\text{AdS}}^2}{z^2}\left(dz^2 + \eta_{\mu\nu}dx^\mu dx^\nu\right), \tag{2.11}$$

where $\eta_{\mu\nu}$ is the d dimensional Minkowski metric, L_{AdS} is the AdS length, and the boundary of the spacetime is at $z = 0$. Then the on-shell scalar field ϕ on the right hand side of Eq. (2.10) is required to have the boundary condition

$$\lim_{z\to 0}\left(\phi(z,x)z^{\Delta-d}\right) = \phi_{(0)}(x), \tag{2.12}$$

where Δ is the *scaling dimension* [44] of the CFT operator $\mathcal{O}$ dual to ϕ and is given in terms of the mass m of ϕ via

$$\Delta = \frac{1}{2}\left(d + \sqrt{d^2 + 4m^2L_{\text{AdS}}^2}\right). \tag{2.13}$$

With this specification of boundary conditions on both sides of Eq. (2.10) are independently defined, so the weak formulation of AdS/CFT is a non-trivial statement of equivalence between two very different theories.

Finally, while we defined the AdS/CFT correspondence through the most well-known example—type IIB superstring theory / supergravity on $AdS_5 \times S^5$ being dual to $\mathcal{N} = 4$ supersymmetric Yang-Mills theory—other concrete examples of the correspondence have been suggested (see [58] for a review). In all cases a gravitational theory in AdS space (perhaps times a compact manifold) is proposed to be dual to a conformal field theory on the boundary of the AdS space. Because of the plethora of examples a modern viewpoint on AdS/CFT is that a large class of CFTs are holographic, i.e. contain a dual gravitational description. The conditions for a CFT to be holographic are discussed in [49]. Moreover, because in all instances of AdS/CFT there is a one-to-one mapping of gravitational fields to CFT operators, it is often beneficial to study a truncated version of the correspondence, where we consider only a few fields/operators at a time. For example one might study the duality between a single scalar field in the gravitational theory and the corresponding dual operator in the CFT. Such a minimalist description is called the *bottom-up* approach to AdS/CFT. Of course the bottom up approach is at best an approximation, because in the explicit (i.e. *top-down*) formulations of AdS/CFT the fields on the gravity side of the duality are mutually interacting and so cannot be separated from one another, and the same goes for the CFT operators. Nevertheless the bottom-up approach retains the salient universal features of AdS/CFT holography, and thus it provides a useful framework in which to study quantum gravity. In this thesis we almost exclusively use the bottom-up approach to AdS/CFT.

Chapter 3

Bubbles of AdS

While the main theme of this thesis is the development of holographic models of cosmology, in this chapter we focus purely on holography, outside the context of cosmology. We investigate the conditions that enable a holographic conformal field theory CFT_2 to describe the gravitational physics which are dual to a state of a different holographic conformal field theory, CFT_1. We find that if the two CFTs can be non-trivially coupled at an interface then there exists a state of CFT_2 that describes an arbitrarily large bubble of the gravitational system dual to a state of CFT_1. We will mostly focus on the simplest case in which the state of CFT_1 is the vacuum state, but we also argue on general grounds that this should be true for arbitrary excited states as well. In the following chapter we will use this idea to construct holographic "bubble of cosmology" solutions.

3.1 Introduction

The focus of this chapter will be to investigate a fundamental question regarding holographic descriptions of quantum gravity. Recall that the holographic principle suggests that gravitational theories in $d+1$ spacetime dimensions can be described by non-gravitational theories living on the corresponding d-dimensional boundaries. The AdS/CFT correspondence provides an explicit realization of this idea, in which the gravitational effective theories have a negative cosmological constant, the corresponding spacetimes have asymptotically anti de Sitter (AdS) boundaries, and the dual non-gravitational theories are conformal field theories (CFTs) living on these asymptotic boundaries. Of the many features of holography that AdS/CFT brought to light, perhaps the most significant is the deep connection between the entanglement structure of quantum states of holographic systems and the geometry of the dual spacetimes they encode (see, for example [60–65], or [66] for a review). With this in mind, it is natural to ask how much information about the dual spacetime is captured by universal properties of the state such as its entanglement structure and how much relates to more detailed properties of the CFT, such as its Hamiltonian.

Here we will explore the extreme possibility that the precise microscopic degrees of freedom of the CFT are actually unimportant, and that a suitably chosen state of *any* holographic CFT (or perhaps even some arbitrary quantum field theory) can faithfully encode large regions of a spacetime dual to a completely different holographic CFT. A particular motivation for this investigation is the work [67] which argued that states of a holographic CFT can be approximated by states of a large collection of non-interacting quantum systems, each of which has almost no information about the global geometry. This suggested that the nature of these individual systems is not important, and that any quantum system with enough degrees of freedom (e.g. a simple harmonic oscillator), placed in an appropriate state, can faithfully encode the same gravitational physics. Another motivation is the work [68–70], which suggests that auxiliary radiation systems can encode the behind-the-horizon physics of late time black holes, regardless of what specific degrees of freedom the radiation system is built from.

To that end, consider a quantum state $|\Psi_1\rangle$ of some holographic conformal field theory, CFT_1, dual to a spacetime geometry M_1. When we say that the state $|\psi_1\rangle$ is dual to the spacetime M_1 what we mean more precisely is that observables of the state can be related to observables of the

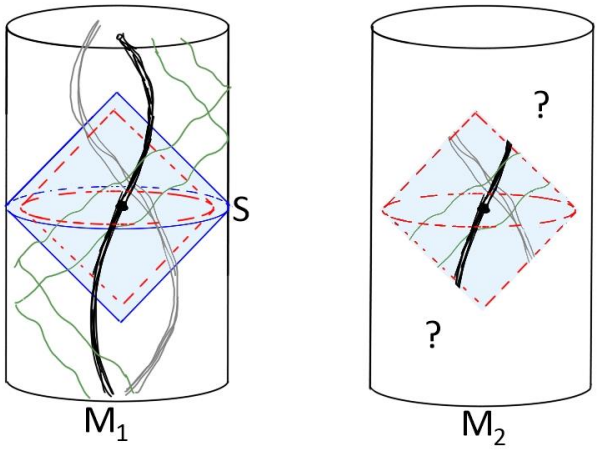

Figure 3.1: Left: The Wheeler-DeWitt patch M_1^S (shaded blue region) of spacetime M_1 dual to CFT_1 state $|\Psi_1\rangle$ defined at boundary time slice S. Physics in the Wheeler-DeWitt patch can be related to properties of the state $|\Psi_1\rangle$. Right: Geometry M_2 dual to CFT_2 state $|\Psi_2\rangle$ includes a region that approximates a large subset of M_1^S.

spacetime, and vice versa. For example, correlation functions of CFT operators in the state $|\psi_1\rangle$ can be related to correlators of quantum fields propagating in the spacetime M_1. However, in general it is not true that information about the entire spacetime M_1 can be recovered from the state $|\psi_1\rangle$. Rather, the CFT state defined on a particular boundary time slice S encodes the "Wheeler-DeWitt patch" M_1^S associated with S, defined as the union of spacelike bulk slices of M_1 ending on S, or equivalently the bulk domain of dependence of one of these slices (see Figure 3.1). Parts of the geometry outside this region would be affected by perturbations to the CFT_1 Hamiltonian that happen before or after the time defined by S. Thus, these regions of the spacetime are not strictly encoded in the state $|\Psi_1\rangle$ but require knowledge of $|\Psi_1\rangle$ and the CFT_1 Hamiltonian. We would like to argue that it is possible to find states of a different holographic conformal field theory CFT_2, whose dual geometries include regions which approximate arbitrarily large portions of M_1^S, as indicated in Figure 3.1.

An immediate objection to this idea is that in general in AdS/CFT, fields in the gravitational theory dual to a particular CFT correspond to specific operators in the CFT. For example the mass m of a scalar field in the gravitational theory is related to the scaling dimension Δ of a scalar operator in the CFT through the relation $m^2 L_{\text{AdS}}^2 = \Delta(\Delta - d)$ where L_{AdS} is the curvature lengths scale of the AdS spacetime. How then can we hope to describe the same physics using a CFT with a completely different operator spectrum? To understand this, we recall that theories of gravity with different low-energy descriptions can be related to each other non-perturbatively, so we could have an interior spacetime region described by one semiclassical gravity theory appearing as a bubble in a spacetime whose asymptotic behaviour is described by some very different semiclassical theory. In this case, the interior and exterior regions would be separated by some type of codimension-one brane.

Being able to encode CFT_1 dual geometries using CFT_2 states in this way requires that the low-energy theories of gravity which describe the asymptotic physics of these two different holographic CFTs must be part of the same non-perturbative theory of quantum gravity, which must include branes (i.e dynamical interfaces) that can connect regions with these two low-energy descriptions. Understanding which CFTs / gravitational theories are related in this way seems at first to be an impossible challenge, requiring complete knowledge of possible non-perturbative theories of quantum

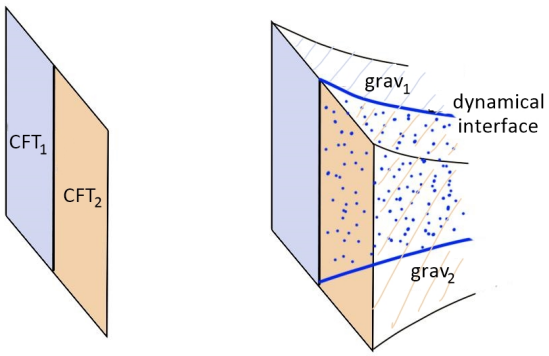

Figure 3.2: Gravity interpretation (right) of two holographic CFTs (left) coupled non-trivially at an interface.

Figure 3.3: Euclidean path integral defining a quench operator $M_{\mathcal{I},\epsilon}$ mapping states of CFT_1 to states of CFT_2. Here, I represents a non-trivial conformal interface between the CFTs.

gravity. However we will now argue for a very simple sufficient condition: theories of gravity dual to different CFTs must be part of the same theory (which includes a non-perturbative interface brane), provided that the CFTs can be coupled non-trivially at an interface, such that energy and excitations can pass from one to the other.[8]

For suppose we have holographic CFTs joined along such an interface, and that we perturb one of the CFTs so that the perturbation is later detected in the other CFT. From the gravity perspective, we have an excitation in the region of spacetime associated with our first holographic CFT, and this leads to an excitation in the region of spacetime associated with the second holographic CFT. In this gravitational description, the implication is that the two regions of spacetime are joined somehow. In a gravitational theory, we expect that any such interface must be dynamical; this would be our desired codimension one "brane" separating regions with the two different low-energy descriptions (Figure 3.2).

Given our assertion, it is very interesting to understand whether any two CFTs can be coupled non-trivially at an interface, and thus whether all low-energy gravitational theories are part of the same non-perturbative theory. The recent works [67, 72] have advocated for this picture. In this paper we will set aside such questions and instead we will simply assume that CFT_1 and CFT_2 can be coupled non-trivially as described, and focus on the question of how to construct states of CFT_2 that faithfully encode the gravitational physics of a spacetime dual to some CFT_1 state.

CFT_2 disguised as CFT_1

Consider a state $|\Psi_1\rangle$ of holographic CFT_1. Even though the CFT is holographic, it is generally not the case that the state is dual to a classical spacetime. For example, a coherent superposition of two CFT states corresponding to two very different classical spacetimes would not itself correspond, even

[8] [71] also discusses the existence of CFT interfaces as a condition for the existence of interfaces between the corresponding gravitational theories.

in an approximate sense, to a classical spacetime. Let us therefore focus attention specifically on states $|\Psi_1\rangle$ which *are* dual to classical spacetimes. We say that such states have a *good semiclassical description*, because the CFT physics of these states and their perturbations can be well-described by quantum field theory in curved spacetime in the bulk. Starting with the state $|\Psi_1\rangle$, our central idea is to define a state

$$|\Psi_2^{\mathcal{I}}(\epsilon)\rangle \equiv M_{\mathcal{I},\epsilon}|\Psi_1\rangle \tag{3.1}$$

of CFT_2 where $M_{\mathcal{I},\epsilon}$ is an operator defined by the Euclidean path-integral shown in Figure 3.3 (see next section for more details). In operator language, we have

$$M_{\mathcal{I},\epsilon} \equiv \lim_{\epsilon_1 \to 0} e^{-\epsilon H_2} \hat{Q}_{\mathcal{I}} e^{-\epsilon_1 H_1}, \tag{3.2}$$

where the operator $\hat{Q}_{\mathcal{I}}$ performs a quench, modifying the Hamiltonian from that of CFT_1 to that of CFT_2 in a specific way associated with the chosen interface $\mathcal{I}$. This is a singular operation, resulting in a state of infinite energy, since the UV structure of finite energy states for H_2 is different than the UV structure of finite energy states of H_1. The Euclidean time evolution $e^{-\epsilon H_2}$ removes the singular UV behaviour, leaving us with a state of finite energy with respect to H_2.

Since the operation $M_{\mathcal{I},\epsilon}$ corresponds to evolution for an infinitesimal Euclidean time with a local Hamiltonian, our hope is that if ϵ is sufficiently small this operator will not significantly affect the long distance properties of the states on which it acts. Therefore new state $|\Psi_2^{\mathcal{I}}(\epsilon)\rangle$ should have long-distance properties (e.g. entanglement structure) that closely resemble those of the original state $|\Psi_1\rangle$. In the gravitational description this would imply that the state $|\Psi_2^{\mathcal{I}}(\epsilon)\rangle$ faithfully encodes a large portion of the spacetime dual to $|\Psi_1\rangle$.

To check this, we would like to understand in detail the dual geometry to $|\Psi_2\rangle$. For simplicity, we assume that the state $|\Psi_1\rangle$ can also be described by a Euclidean path integral (possibly with sources). Then the Euclidean geometry dual to the CFT path integral of Figure 3.4a used to compute observables in $|\Psi_2\rangle$ will have an asymptotic region in which one strip is described by the semiclassical gravitational theory associated with CFT_2 while the remainder is described by the semiclassical theory associated to CFT_1. These two asymptotic regions must be separated by the brane associated with the chosen CFT interface.

Various topologies for the interface brane are possible, as shown in figure 3.4b,c. The key idea that motivates the investigations in this paper is that if ϵ is sufficiently small, it is plausible that solutions with the connected-brane topology of figure 3.4c will have the least action and dominate the gravitational path-integral. We see that a $\tau = 0$ slice of such a geometry (which gives the initial data for the Lorentzian geometry dual to $|\Psi_2^{\mathcal{I}}(\epsilon)\rangle$) contains a bubble of the geometry dual to CFT_1, and the size of this bubble goes to infinity as $\epsilon \to 0$. We also expect that the interior geometry of this bubble approaches the geometry dual to $|\Psi_1\rangle$. So we would have a state $|\Psi_2^{\mathcal{I}}(\epsilon)\rangle$ of CFT_2 that describes an arbitrarily large bubble of the original spacetime dual to state $|\Psi_1\rangle$ of CFT_1.

Summary of results

In the remainder of this chapter, we will check the expectations outlined in the previous paragraphs in the context of a simple model where the interface between CFT_1 and CFT_2 is associated with an interface brane with purely gravitational couplings. We show that the tension of this interface brane is directly related to the interface entropy (equation 3.20) and that a finite interval of positive tensions can describe all possible interface entropies (equation 3.21).

In the context of our model, we consider the gravitational dual of states $|\Psi_2^{\mathcal{I}}(\epsilon)\rangle$ defined above, where first we consider the state $|\Psi_1\rangle$ to be the vacuum state of CFT_1. We find the possible solutions as a function of the gravitational parameters L_1^{AdS}, L_2^{AdS}, the brane tension κ, and the

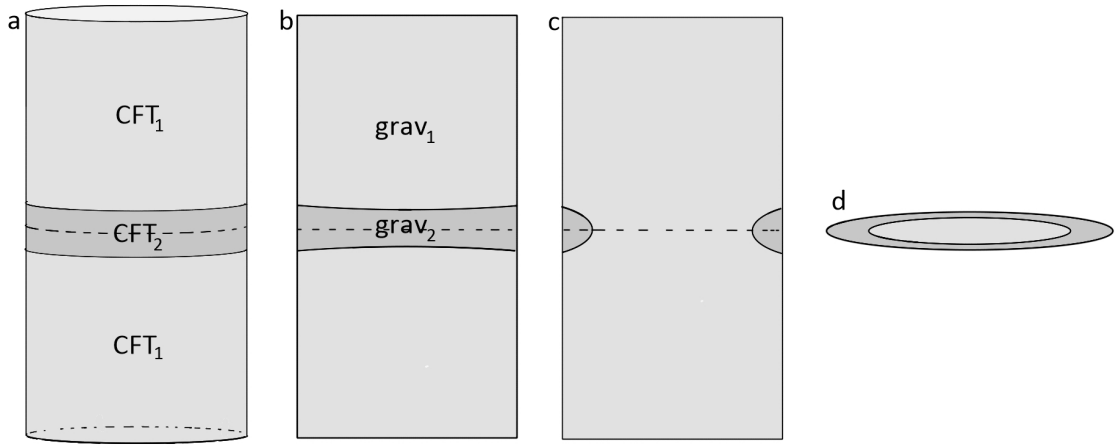

Figure 3.4: **a)** The exterior of the cylinder corresponds to the CFT path integral geometry for $\langle\Psi_2|...|\Psi_2\rangle$. Inserting CFT operators in the middle of the path integral computes the corresponding expectation value in the state $|\Psi_2\rangle$. **b),c)** Possible topologies for the interface brane in the dual Euclidean solution (showing vertical cross section). **d)** $t = 0$ slice of c), providing initial data for the time-symmetric Lorentzian geometry dual to $|\Psi_2\rangle$ in the case when solutions of the type c) have lowest action.

ratio S between the width of our strip in Euclidean time and the radius of the sphere on which the CFTs are defined. In the case of 1+1 dimensional CFTs, these gravitational parameters correspond to the CFT central charges c_1,c_2, the boundary entropy $\log g$ and the parameter ϵ appearing in (3.2), respectively.

For $c_2 > c_1$ and any boundary entropy, we find that the least action gravitational solution is always of the type **c** in figure 3.4 (connected brane topology) for sufficiently small ϵ. For larger values of brane tension / boundary entropy the bubble is behind a black hole horizon.

For $c_1/3 < c_2 < c_1$ we find that the least action solution is of type **c** for sufficiently large brane tension / interface entropy.

However, when $c_2 < c_1/3$ we find that there are no allowed solutions with topology of type **c**. This would seem to contradict our original expectation that a large part of the gravitational solution dual to a state of CFT_1 can also be described by a state of CFT_2, as long as the two CFTs can be coupled at an interface. However, we will argue that the problem is that a transition directly from CFT_1 to CFT_2 with a much smaller central charge is too severe to preserve the desired properties of the original state. We proceed to consider more general interfaces that involve one or more intermediate CFTs and show that in this more general setup, it is always possible to choose a state of CFT_2 such that the dual geometry contains an arbitrarily large causal patch of pure AdS geometry dual to the vacuum state of CFT_1, in accord with our expectations.

In summary, within the context of our model, any CFT has states that can approximate arbitrarily large regions of the geometry dual to the vacuum state of any other CFT.

In the Lorentzian geometries dual to our CFT_2 states, the picture from the interior of the interface brane is that we have a bubble of pure AdS spacetime that eventually collapses. The exterior picture meanwhile consists of an asymptotically Schwarzschild-AdS spacetime with a spherically symmetric bubble wall that may initially be inside or outside the horizon but eventually falls in, collapsing to zero size at the singularity. This is shown in Figure 3.11.

In Section 3.5, we argue that exactly the same construction used to approximate the vacuum state of CFT_1 also works to approximate geometries dual to excited states of CFT_1. Here we consider

both states perturbatively close to the vacuum and high-energy states dual to black hole geometries. In Section 3.6, we discuss some properties of the CFT_2 states that encode CFT_1 geometries, for example how much energy is needed to encode the physics of a bubble of size r_0 as a function of the central charges c_1 and c_2. We end with a discussion in Section 3.7, mentioning some directions for future work and offering a few more comments on the general picture.

3.2 Interface CFTs

Given two different CFTs, we can define a single theory on some spacetime where the local degrees of freedom on half of the space are those of CFT_1 and the local degrees of freedom of the other half of the space are those of CFT_2. At the interface, we can have some coupling between the CFTs on each side, possibly with some extra degrees of freedom living on the interface.[9]

For our application, it will be important that the coupling between the CFTs is such that excitations/energy in one CFT can pass to the other CFT. We will say that two CFTs are *compatible* if is possible to couple these CFTs to each other along an interface in a non-trivial way so that excitations/energy in one CFT can pass to the other CFT. More generally, we say CFT_a and CFT_b are in the same *compatibility class* if there is a sequence $(CFT_a, CFT_1, \ldots, CFT_n, CFT_b)$ such that neighbouring CFTs in the sequence are compatible.

It seems plausible that most CFTs are compatible. Generally speaking, when we have two ordinary physical systems, it is possible to couple them together in such a way that energy can be transferred from one to the other. It is also plausible that any two CFTs in the same compatibility class are compatible, since we could define an interface between them consisting of a set of layers involving $\{\text{CFT}_i\}$, and then consider the IR limit of this theory.

A useful way to think about an interface between two different CFTs is as a boundary condition for the CFT which is the tensor product between CFT_1 and CFT_2.[10] Here, we are using the so-called "folding trick" [73], where the half-space on which CFT_1 is defined is identified with the half-space on which CFT_2 is defined. From this perspective, we can say that CFT_1 and CFT_2 are compatible if there is a boundary condition for the product theory that couples the two bulk theories non-trivially. Note that some boundary conditions for the tensor product theory correspond to choosing separate boundary conditions for CFT_1 and CFT_2 and taking the tensor product theory $\text{BCFT}_1 \otimes \text{BCFT}_2$. These boundary conditions, or more general boundary conditions corresponding to linear combinations of these (i.e. linear combinations of the path integral amplitudes for various trivial choices), give rise to interfaces that we would describe as trivial, where excitations on one side of the interface simply reflect off the interface and are not transmitted to the other CFT.

The allowed boundary conditions for the $CFT_1 \otimes CFT_2$ tensor product CFT are constrained by crossing symmetry and unitarity, and thus might in principle be classified by a bootstrap approach (see e.g. [74]).

[9] There are various ways we can imagine coupling two CFTs. If it is possible to understand the CFTs as arising from the IR limit of some UV lattice theories, we could consider the half-space version of each of these lattice theories (possible including additional degrees of freedom at the boundary) and then couple the two theories at the boundary in some way. The resulting theory should flow to a conformal theory in the IR with the local physics on either side of the interface described by CFT_1 and CFT_2. Similarly, if we can define the CFTs as the IR limits of UV theories with a field theory Lagrangian description, we can consider each of these UV theories on a half space and couple the fields in the two theories at the boundary. Again, the resulting theory should flow in the IR to a conformal theory with the local physics on either side of the interface described by CFT_1 and CFT_2.

[10] More precisely, we should take the mirror image of CFT_2 if this is different that CFT_2.

3.2.1 Interface entropy

For interface CFTs (where the interface theory is scale invariant) or for the UV or IR limits of interface renormalization group (RG) flows, we can define an interface entropy to be the boundary entropy [75] of the associated boundary conformal field theory (see e.g. [76]). For 1+1 dimensional BCFTs, this boundary entropy is denoted $\log g$ and may be defined as the difference between the vacuum entanglement entropy S for an interval of length l that includes the boundary, and the vacuum entanglement entropy of an interval of the same length which does not include the boundary. The latter quantity is universally known to equal $(c/6)\log(2l/\epsilon)$ where c is the central charge of the CFT and ϵ is a regulator. Therefore, since the bulk central charge in the tensor product theory is the sum of central charges for CFT_1 and CFT_2, we define the boundary entropy as

$$\log g = S - \frac{c_1 + c_2}{6} \log\left(\frac{2l}{\epsilon}\right). \tag{3.3}$$

In higher dimensions, the boundary entropy can be defined via the vacuum entanglement entropy of a hemisphere centered on the boundary (see e.g. [77]).

3.2.2 Approximating CFT states

The central idea of this paper is to approximate a state of some holographic CFT_1 by a state of another CFT_2, preserving the entanglement structure and other "universal" properties of the state as much as possible at least above some UV length scale ϵ.

If CFT_1 and CFT_2 were ordinary quantum systems with the same degrees of freedom (e.g. finite collections of qudits or harmonic oscillators), then they could be described using the same Hilbert space, and we could simply take $|\Psi_2\rangle = |\Psi_1\rangle$. However, for conformal field theories, it is not generally possible to identify the Hilbert spaces of the two systems, so we require a mapping from the states of one theory into the states of the other.

We can define such a mapping by making use of a Euclidean interface CFT, where the Euclidean versions of CFT_1 and CFT_2 are joined along an interface. Let S_{12} denote the Euclidean action of the interface CFT. Then we can define a map $M_{\mathcal{I},\epsilon}$ via its matrix elements:

$$\langle\tilde{\phi}_2|M_{\mathcal{I},\epsilon}|\tilde{\phi}_1\rangle = \lim_{\epsilon_1\to 0}\int_{\phi_1(-\epsilon_1)=\tilde{\phi}_1}^{\phi_2(\epsilon)=\tilde{\phi}_2}\int[d\phi_i]e^{-S_{12}}\,. \tag{3.4}$$

Using the techniques discussed in Chapter 2, we can write this in operator language as

$$M_{\mathcal{I},\epsilon} = \lim_{\epsilon_1\to 0} e^{-\epsilon H_2}\hat{Q}_{\mathcal{I}}e^{-\epsilon_1 H_1}, \tag{3.5}$$

where the operator $\hat{Q}_{\mathcal{I}}$ corresponds to the terms in the action which describe the interface interaction between the CFTs. We can think of this as a *quench operator*, i.e. an operator which modifies the Hamiltonian from that of CFT_1 to that of CFT_2. Using the operator $M_{\mathcal{I},\epsilon}$ we define the state of CFT_2 corresponding to the original state of CFT_1 as

$$|\Psi_2^{\mathcal{I}}(\epsilon)\rangle = M_{\mathcal{I},\epsilon}|\Psi_1\rangle\,. \tag{3.6}$$

As we discussed in the introduction to this chapter, following the quench the state of CFT_2 has infinite energy since the UV structure of finite energy states for H_2 is different than the UV structure of finite energy states of H_1. However the subsequent Euclidean time evolution $e^{-\epsilon H_2}$ regulates the bad UV behaviour, leaving us with a finite energy state of H_2. If ϵ is small, we expect that $e^{-\epsilon H_2}$ does

not significantly change the entanglement structure, so the new state provides an approximation to the original state as far as the IR entanglement structure is concerned. The parameter ϵ_1 which we have introduced to make the path integral expression well-defined, can safely be taken to zero.

Our goal will be to investigate the gravitational dual of the approximated state $|\Psi_2\rangle$ and compare this with the gravitational dual of the original state $|\Psi_1\rangle$. We take $|\Psi_1\rangle$ to be a state constructed using a Euclidean path integral, possibly with sources for various operators. In this case, it will be possible to directly understand the gravitational duals of both $|\Psi_1\rangle$ and $|\Psi_2\rangle$ provided that we understand the gravitational physics associated with the CFT interface.

We emphasize that with our construction, we only expect the states $|\Psi_1\rangle$ and $|\Psi_2\rangle$ to be similar at the time when they are constructed. Since they evolve with different Hamiltonians, the state of CFT_2 at some later time may bear little resemblance to the state of CFT_1. However, it is expected that the CFT states encode the physics of a bulk region consisting of all bulk spatial slices anchored on the boundary slice at $t = 0$ (or the domain of dependence region of one of these slices), as shown in Figure 3.1. Thus, it is reasonable to hope that $|\Psi_2(t = 0)\rangle$ faithfully encodes the physics of a large portion of the interior of this spacetime region in the geometry dual to $|\Psi_1\rangle$.

3.3 Holographic interface CFTs

We now consider the dual gravitational physics of the situation where we have two holographic CFTs coupled at a non-trivial interface.

We have argued in Section 3.1 that a physical system constructed from compatible CFTs joined by a non-trivial interface is dual to single gravitational theory with a *dynamical interface* separating two asymptotically AdS regions with different semiclassical descriptions. We can think of the interface as a codimension one "brane" across which the low-energy description of the gravitational physics (cosmological constant, light fields, etc...) changes from that corresponding to the first CFT to that corresponding to the second CFT. Such a brane could involve microscopic branes of the gravitational theory, or correspond to a region of spacetime in which the internal space makes a transition from one geometry to another. In some special cases, the brane can be described within the context of a single low-energy effective theory, for example where we have a scalar field making a transition between two possible extrema of its potential. This could correspond to an interface between CFTs for which CFT_2 is the IR limit of an RG flow obtained by perturbing CFT_1 with a relevant operator $\mathcal{O}$. In this case, the interface CFT can be understood as CFT_1 with a spatially dependent coupling for $\mathcal{O}$ that transitions from zero on one side of the interface to infinity on the other side of the interface.

In this section, we introduce a simple holographic model where the gravitational dual includes different low-energy gravitational theories corresponding to the two CFTs and an interface brane that can connect regions described by these two low-energy theories.

3.3.1 Bottom up model for holographic interface CFTs

Gravity duals for interface CFTs have been considered various times in the literature. Precise gravitational solutions dual to the vacuum state of various supersymmetric interface CFTs have been worked out in [78–83] for example. In these 10-dimensional microscopic solutions, there is often no sharp interface brane, but rather a smooth ten-dimensional geometry with a region where the internal space makes a transition from one configuration to another. In a lower-dimensional description, the interface brane represents this transition region.

In this paper, we will employ a bottom-up approach, modelling the dual geometry for a $(D-1)$-dimensional interface CFT as a D dimensional spacetime with two regions connected by an $(D-1)$-

dimensional interface brane. This is similar to the bottom-up dual for BCFTs studied in [84–86] or the models in [76, 87] used in the case of identical CFTs coupled at a defect. We take the gravitational action to be the Einstein action with a cosmological constant in each region related to the central charge of the corresponding CFT. In general, we can also have a bulk matter action in each region. At the interface, we have a Gibbons-Hawking-York boundary term associated with each side of the interface, plus an action for matter localized to the brane. This interface matter action can include couplings between fields on the interface and bulk fields. For our investigation, we will consider the simplest case where the interface brane is a constant-tension brane that couples only gravitationally to the bulk. The solutions we consider will then be purely gravitational and we can ignore the bulk matter actions. In summary, the relevant terms in the action in the Euclidean case are

$$\mathcal{I} = -\frac{1}{16\pi G_D}\Bigg[\int_{\mathcal{M}_1} d^D x\sqrt{g_1}\,(R_1 - 2\Lambda_1) + \int_{\mathcal{M}_2} d^D x\sqrt{g_2}\,(R_2 - 2\Lambda_2) + 2\int_{\mathcal{S}} d^{D-1}y\sqrt{h}(K_1 - K_2) - 2(D-2)\int_{\mathcal{S}} d^{D-1}y\sqrt{h}\kappa\Bigg], \tag{3.7}$$

where G_D is the D dimensional Newton constant, we have defined a tension parameter $\kappa \equiv 8\pi G_D T/(D-2)$ in terms of the brane tension T, and the cosmological constants Λ_i are negative and related to the AdS lengths L_i as $\Lambda_i = -(D-1)(D-2)/(2L_i^2)$. The equations of motion arising from varying this action are the Einstein equations with cosmological constant on each side of the interface, together with the second Israel junction condition [88],

$$K_{1ab} - K_{2ab} = \kappa h_{ab}, \tag{3.8}$$

where K_{1ab} and K_{2ab} represent the extrinsic curvatures for the interface, computed with the bulk metrics on either side, with the normal vector pointing from region 1 to region 2 in each case. Note that we are also assuming the first junction condition, that the induced metric on the brane when viewed from side 1 is the same as the induced metric viewed from side 2, i.e.

$$h_{1ij} - h_{2ij} = 0\,. \tag{3.9}$$

The first junction condition can be viewed as a condition for the full geometry to be continuous, while the second junction condition ensures that the geometry satisfies Einstein's equations across the junction.

In the next sections, following similar work in [85] for boundary CFTs and [76] for defect CFTs, we establish a connection between the interface tension parameter κ and the interface entropy for the corresponding interface CFT, by comparing the general result (3.3) for interface entropy with a holographic calculation using the Ryu-Takayanagi formula [61].

3.3.2 Planar interface solution

We first derive the gravitational solution dual to the vacuum state of the interface CFT with a planar interface.

We consider two asymptotically AdS$_3$ spacetimes $(\mathcal{M}_1, g_1)$ and $(\mathcal{M}_2, g_2)$ with AdS lengths L_1 and L_2, separated by a domain wall of constant tension $T = \kappa/(8\pi G)$. Near the AdS boundary, the metrics g_1 and g_2 can be written as

$$ds_i^2 = d\rho_i^2 + \frac{L_i^2}{y_i^2}\cosh^2\left(\frac{\rho_i}{L_i}\right)\left(-dt_i^2 + dy_i^2\right), \tag{3.10}$$

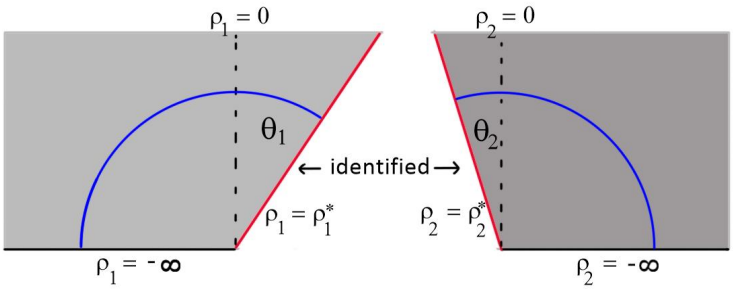

Figure 3.5: Gravity dual of an interface CFT in bottom up model with a constant tension-brane. The brane is shown in red and the boundary of AdS corresponds to $\rho_1 = -\infty$ and $\rho_2 = -\infty$. The angles θ_1 and θ_2 in Poincare coordinates are determined by the AdS lengths L_1, L_2 and the brane tension κ. These are related to the CFT parameters c_1, c_2 and $\log g$. The RT surface for a spatial subsystem including points in each CFT within distance l from the interface is shown in blue.

where $i \in \{1, 2\}$, such that the AdS boundary occurs at $y_i = 0$. A coordinate change $z_i = y_i/\cosh(\rho_i/L_i)$, $x_i = y_i \tanh(\rho_i/L_i)$ relates these coordinates to the usual Poincaré coordinates

$$ds_i^2 = \frac{L_i^2}{z_i^2}(dz_i^2 - dt_i^2 + dx_i^2). \tag{3.11}$$

The location of the domain wall that separates these two regions can be determined by requiring that the junction conditions are satisfied. We make the ansatz that in the (t_i, ρ_i, y_i) coordinates the domain wall is given by the embedding $\rho_i = \rho_i^*$, where we keep the part of spacetime $\mathcal{M}_i$ with $-\infty < \rho_i < \rho_i^*$, as shown in Figure 3.5. Then the induced metric h_{ab} on the domain wall $\mathcal{S}$, viewed as a surface in region $\mathcal{M}_i$, is

$$ds_{\mathcal{S},i}^2 = \frac{L_i^2}{y_i^2}\cosh^2\left(\frac{\rho_i^*}{L_i}\right)\left(-dt_i^2 + dy_i^2\right). \tag{3.12}$$

We see that the induced metric is independent of which embedding we use — i.e. the first junction condition Eq. (3.9) is satisfied — if we make the following identifications at the interface:

$$y_1 = y_2 \qquad t_1 = t_2 \qquad L_1 \cosh\left(\frac{\rho_1^*}{L_1}\right) = L_2 \cosh\left(\frac{\rho_2^*}{L_2}\right). \tag{3.13}$$

Next let us impose the second junction condition, Eq. (3.8). It is straightforward to show that the extrinsic curvatures K_{1ab} and K_{2ab} of the domain wall embedded in regions $\mathcal{M}_1$ and $\mathcal{M}_2$ are given by

$$K_{1ab} = \frac{1}{L_1}\tanh\left(\frac{\rho_1^*}{L_1}\right)h_{ab} \qquad K_{2ab} = -\frac{1}{L_2}\tanh\left(\frac{\rho_2^*}{L_2}\right)h_{ab}, \tag{3.14}$$

Then the second junction condition gives

$$\frac{1}{L_1}\tanh\left(\frac{\rho_1^*}{L_1}\right) + \frac{1}{L_2}\tanh\left(\frac{\rho_2^*}{L_2}\right) = \kappa, \tag{3.15}$$

Equations (3.13) and (3.15) have the unique solution

$$\tanh\frac{\rho_1^*}{L_1} = \frac{1}{2}\left(\kappa L_1 + \frac{1}{\kappa L_1} - \frac{L_1}{\kappa L_2^2}\right), \tag{3.16}$$

$$\tanh\frac{\rho_2^*}{L_2} = \frac{1}{2}\left(\kappa L_2 + \frac{1}{\kappa L_2} - \frac{L_2}{\kappa L_1^2}\right). \tag{3.17}$$

Note that $\tanh \frac{\rho_i^*}{L_i} = \sin(\theta_i)$, where θ_i is the angle by which the domain wall deviates from the normal to the AdS boundary in Poincaré coordinates.

Brane tension vs interface entropy

Using our gravity solution, we can use the Ryu-Takayanagi (RT) formula [61] to compute the interface entropy in terms of the bulk parameters and then compare the result with the CFT expression (3.3) to come up with a relation between the brane tension and the interface entropy.

Starting from (3.3), we note that the interface entropy can be expressed as

$$\log g = S^{\mathcal{I}}_{[-l,l]} - \frac{1}{2} S^1_{[-l,l]} - \frac{1}{2} S^2_{[-l,l]} \tag{3.18}$$

, where $S^{\mathcal{I}}$ is the vacuum entanglement entropy for the interval $[-l, l]$ in the interface CFT with interface at $x = 0$, while S^1 and S^2 are the vacuum entanglement entropies for the same interval when CFT_1 and CFT_2 are defined on the whole real line.

The RT surface associated with the entropy of the interval $[-l, l]$ is built from extremal surfaces in the two regions which meet at the interface. The extremal surfaces are described in Poincaré coordinates as semicircular geodesic curves which intersect the AdS boundary orthogonally. In order that the two parts of the surface meet at the interface without a kink (which we require for an extremal area surface), it is also necessary that the curves meet the interface orthogonally on each side.[11] Thus, the RT surface is simply the curve $t_i = 0, y_i = l$ (or $z^2 + x^2 = l^2$ in Poincaré coordinates), as shown in Figure 3.5.

According to the RT formula, the entropy difference on the right side of (3.18) is equal to $1/4G$ times the area of this $y_i = l$ surface (which covers $\rho_i = [-\infty, \rho_i^*]$) minus the area of the same surface $y_i = l$ for $\rho_i = [-\infty, 0]$ in the pure AdS spacetimes corresponding to each side. From the metric (3.10), we see that the area of a segment of the RT surface is just the coordinate length in the ρ direction. Thus, we have simply

$$\log g = \frac{1}{4G}(\rho_1^* + \rho_2^*) \tag{3.19}$$

where ρ_1^* and ρ_2^* are given in (3.16). Using (3.16) and (3.17) we can rewrite the result as

$$\log g = \frac{L_1 + L_2}{4G} \operatorname{arctanh}\left(\frac{\kappa}{\frac{1}{L_1} + \frac{1}{L_2}}\right) + \frac{L_1 - L_2}{4G} \operatorname{arctanh}\left(\frac{\frac{1}{L_1} - \frac{1}{L_2}}{\kappa}\right). \tag{3.20}$$

In the case $L_1 = L_2$, our result agrees with the earlier result [76] for the entropy in defect CFTs.

It is straightforward to check that for any positive L_1, L_2, we have a monotonic relation between $\log g$ and κ in the interval

$$I = (\kappa_-, \kappa_+) \equiv \left(\left|\frac{1}{L_1} - \frac{1}{L_2}\right|, \frac{1}{L_1} + \frac{1}{L_2}\right). \tag{3.21}$$

that takes (κ_-, κ_+) to $(-\infty, \infty)$. Thus, we have a bijection between CFT parameters $\{c_1 > 0,$ $c_2 > 0, \log g \in \mathbb{R}\}$ and gravitational parameters $\{L_1 > 0,\ L_2 > 0,\ \kappa \in I\}$.

It may be useful to note that the interface brane tension in holographic models has also been related [89] to the *transmission coefficient* [90, 91], a quantitative measure of the extent to which excitations can pass from one CFT to another across a particular interface.

[11] To see this, we note that the Poincaré coordinate distance from the $x = 0, z = 0$ to the point where the geodesic intersects the interface is larger/smaller than l if the intersection angle is larger/smaller than $\pi/2$. The intersection angles on the two sides sum to π if there is no kink, so the only way for the distance along the interface to be the same on the two sides is to have both intersections be orthogonal.

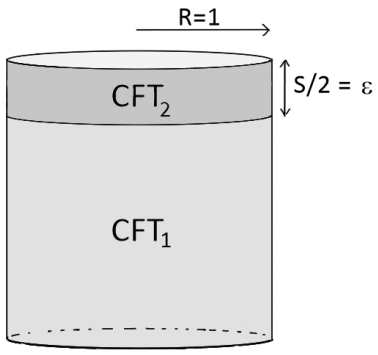

Figure 3.6: Euclidean path integral defining state $|\Psi_2(I,\epsilon)\rangle$ of CFT_2 approximating the vacuum state of CFT_1.

3.4 Gravity duals for approximated states

In this section, we make use of the holographic model for interface CFTs outlined in the previous section to investigate the geometries dual to the states (3.6), where a state of holographic CFT_1 is approximated by a state of holographic CFT_2 by a Euclidean quench. In this section, we will focus on the case where the state $|\Psi_1\rangle$ is the vacuum state of CFT_1. This can be constructed via the path integral on a semi-infinite cylinder, so the state $|\Psi_2\rangle$ arises from the Euclidean interface CFT path integral of figure 3.6. We follow the standard AdS/CFT recipe to understand the dual geometry to this state; the same type of geometries were considered recently in [92]; some of our technical results overlap with results in that paper, but we present the solutions for completeness. First we consider the Euclidean geometry dual to the doubled path integral of figure 3.4a. This will be a Euclidean time-reversal symmetric geometry whose $t = 0$ slice provides the initial data for the Lorentzian geometry dual to state $|\Psi_2\rangle$.

The boundary theory for the path integral in figure 3.4a is a Euclidean CFT with two interfaces separated by some distance S (which we will later take to be a small parameter 2ϵ). These partition the Euclidean cylinder $\mathbb{R} \times S^{D-2}$ into three sections. Since the theories we are dealing with are scale-invariant, we can set the radius of the S^{D-2} to be $R = 1$ without loss of generality. The top and bottom sections are semi-infinite cylinders with a CFT of central charge c_1, while the middle section is a finite cylinder of height S and contains a CFT of central charge c_2. We assume that both interfaces are the same, with defect entropy, $\log g \in \mathbb{R}$. We would like to find the possible bulk geometries corresponding to this setup.

As we have discussed, the dual geometries will have a dynamical interface brane separating regions in which the physics is described by the semiclassical gravitational theories dual to CFT_1 and CFT_2. In general, we expect two different possible topologies for this interface brane, as shown in Fig. 3.4b,c. The first type of geometry has two domain walls, with each wall ending on a single defect. The second type of geometry has a single domain wall running from one defect, into the bulk, and then ending on the other defect in a time symmetric manner. In some cases, solutions with each topology are possible for the same set of boundary data, and we will need to choose the one with least action.

We will assume that the bulk geometries preserve the $SO(D-1)$ symmetry of the CFT setup. Then, assuming that the bulk solution is purely gravitational, the local geometry in each region

must be Schwarzchild-AdS, which we describe with the usual metric

$$ds_i^2 = f_i(r)dt^2 + \frac{dr^2}{f_i(r)} + r^2 d\Omega_{D-2}^2 \, . \tag{3.22}$$

Here, $i \in \{1, 2\}$ denotes whether the asymptotic region of the geometry corresponds to CFT_1 or CFT_2, and $f_i(r)$ is defined as

$$f_i(r) = 1 + \lambda_i r^2 - \frac{\mu_i}{r^{D-3}} \, . \tag{3.23}$$

The parameter μ_i is proportional to the mass of the corresponding Lorentzian black hole. The dual for the CFT_1 vacuum state $|\Psi_1\rangle$ corresponds to the full Euclidean AdS geometry, with $\lambda_1 = 1/L_1^2$ and $\mu_1 = 0$. For non-zero S, the Euclidean geometry at large $|t|$ should approach this pure AdS geometry, so we must have $\mu_1 = 0$. On the other hand, we can have μ_2 either zero or non-zero, and we will find that these two possibilities correspond to the two cases in Fig. 3.4b,c. For this reason we refer to the geometry in Fig. 3.4b as the *pure AdS phase*, and the geometry in Fig. 3.4c as the *black hole phase*. The Lorentzian geometries corresponding to the black hole phase will involve a black hole at late times, while the Lorentzian geometries in the AdS phase will be pure AdS at the classical level.

3.4.1 Interface trajectories

All geometries that we describe are symmetric under time-reversal and can be constructed by gluing together patches of AdS / Schwarzschild AdS with boundaries described by interface trajectories which we describe either by $t_i(r)$ or by $(t_i(s), r(s))$ where s corresponds to the proper distance along the interface in the $r-t$ directions. Since the coordinate r corresponds to the physical radius of the S^{D-2}, the first junction condition implies that the r coordinate of a point on the interface must be the same in the coordinates on each side. There is no such relation between the t coordinates, so we need to provide $t_1(r)$ and $t_2(r)$ separately.

For AdS geometries, the upper half is a patch $\{r \in [0, \infty), t_1 \in [t_1(r), \infty)\}$ of pure AdS with $\lambda_1 = 1/L_1^2$ joined to a patch $\{r \in [0, \infty), t_2 \in [0, t_2(r)]\}$ of pure AdS with $\lambda_2 = 1/L_2^2$. For black hole geometries, we have a patch $\{r \in [0, r_{\min}], t_1 \in [0, \infty)\} \cup \{r \in [r_{\min}, \infty), t_1 \in [t_1(r), \infty)\}$ of pure AdS joined to a patch $\{r \in [r_{\min}, \infty), t_2 \in [0, t_2(r)]\}$ of AdS Schwarzschild geometry with $\lambda_2 = 1/L_2^2$ and some nonzero $\mu_2 = \mu$. We will see that μ can be related to the CFT parameter S.

In either case, the range of the t coordinate in the large r asymptotic region of the middle section of the geometry is $\sqrt{\lambda_2} t_2 \in [-S/2, S/2]$, since this gives the appropriate ratio between the height and the radius of the central portion of the cylinder in the asymptotic region.

The precise form of the trajectories may be determined by solving the junction conditions. As we explain in appendix A, the second junction condition

$$K_{1ab} - K_{2ab} = \kappa h_{ab}. \tag{3.24}$$

leads to the relation

$$f_1 \frac{dt_1}{ds} + f_2 \frac{dt_2}{ds} = \kappa r \tag{3.25}$$

while the definition of the proper length parameter s (and the first junction condition that induced geometries on either side of the interface match) gives

$$f_i \left(\frac{dt_i}{ds}\right)^2 + \frac{1}{f_i}\left(\frac{dr}{ds}\right)^2 = 1 \, . \tag{3.26}$$

Using (3.25) and (3.26) we find

$$\left(\frac{dr}{ds}\right)^2 - V_{\text{eff}}(r) = 0 \qquad V_{\text{eff}}(r) \equiv f_1 - \left(\frac{f_2 - f_1 - \kappa^2 r^2}{2\kappa r}\right)^2 , \tag{3.27}$$

and

$$\begin{aligned} \frac{dt_1}{dr} &= \frac{1}{f_1\sqrt{V_{\text{eff}}}}\left(\frac{1}{2\kappa r}(f_1 - f_2) + \frac{1}{2}\kappa r\right) \\ \frac{dt_2}{dr} &= -\frac{1}{f_2\sqrt{V_{\text{eff}}}}\left(\frac{1}{2\kappa r}(f_2 - f_1) + \frac{1}{2}\kappa r\right) . \end{aligned} \tag{3.28}$$

The first equation tells us that $r(s)$ will be the trajectory of a particle with zero energy in a potential $-V_{\text{eff}}(r)$.[12]

3.4.2 AdS solutions

We first describe the pure AdS phase solutions. The results of this section are valid in any dimension.

From equation (3.27), we find that for $\mu_1 = \mu_2 = 0$, $V_{\text{eff}} = 1 + Ar^2$, where

$$A = \frac{1}{4\kappa^2}(\sqrt{\lambda_1} + \sqrt{\lambda_2} + \kappa)(\sqrt{\lambda_1} + \sqrt{\lambda_2} - \kappa)(\sqrt{\lambda_1} - \sqrt{\lambda_2} + \kappa)(\sqrt{\lambda_2} - \sqrt{\lambda_1} + \kappa) . \tag{3.29}$$

From (3.21), the range of allowed values of κ is $\kappa \in (|\sqrt{\lambda_1} - \sqrt{\lambda_2}|, \sqrt{\lambda_1} + \sqrt{\lambda_2})$, we see that A is always positive,[13] so dr/ds cannot change sign and the solution to equation (3.27) will be a monotonic function from $[s_0, \infty)$ to $[0, \infty)$. Choosing $s_0 = 0$, we have

$$r(s) = \frac{1}{\sqrt{A}} \sinh\left(\sqrt{A}s\right) . \tag{3.30}$$

From (3.28), we find that $t_1(r)$ and $t_2(r)$ are monotonic, with the following signs:

$$\begin{array}{lll} \lambda_2 < \lambda_1 : & \sqrt{\lambda_1} - \sqrt{\lambda_2} < \kappa < \sqrt{\lambda_1 - \lambda_2} & \dot{t}_1 > 0, \dot{t}_2 > 0 \\ & \sqrt{\lambda_1 - \lambda_2} < \kappa < \sqrt{\lambda_1} + \sqrt{\lambda_2} & \dot{t}_1 > 0, \dot{t}_2 < 0 \\ \lambda_2 > \lambda_1 : & \sqrt{\lambda_2} - \sqrt{\lambda_1} < \kappa < \sqrt{\lambda_2 - \lambda_1} & \dot{t}_1 < 0, \dot{t}_2 < 0 \\ & \sqrt{\lambda_2 - \lambda_1} < \kappa < \sqrt{\lambda_1} + \sqrt{\lambda_2} & \dot{t}_1 > 0, \dot{t}_2 < 0 . \end{array} \tag{3.31}$$

The trajectories $t_1(r)$ and $t_2(r)$ can be determined analytically by integrating (3.28). Taking $t_2 = 0$ to be the time-symmetric point in the geometry, we must have $t_2(r = \infty) = S/(2\sqrt{\lambda_2})$. We can choose $t_1(r = \infty) = 0$. The result is

$$\begin{aligned} t_1(r) &= \frac{1}{\sqrt{\lambda_1}} \operatorname{arctanh}\left(\frac{\kappa^2 - \lambda_2 + \lambda_1}{2\kappa\sqrt{\lambda_1(1 + Ar^2)}}\right) \\ t_2(r) &= \frac{S}{2\sqrt{\lambda_2}} + \frac{1}{\sqrt{\lambda_2}} \operatorname{arctanh}\left(\frac{\lambda_1 - \lambda_2 - \kappa^2}{2\kappa\sqrt{\lambda_2(1 + Ar^2)}}\right) \end{aligned} \tag{3.32}$$

Below, it will be useful to have expressions for $\Delta t_i = t_i(\infty) - t_i(0)$, which we can write as

$$\Delta t_1 = \frac{1}{\sqrt{\lambda_1}} \operatorname{arctanh}\left(\frac{\kappa^2 - \lambda_2 + \lambda_1}{2\kappa\sqrt{\lambda_1}}\right) \qquad \Delta t_2 = \frac{1}{\sqrt{\lambda_2}} \operatorname{arctanh}\left(\frac{\lambda_1 - \lambda_2 - \kappa^2}{2\kappa\sqrt{\lambda_2}}\right) \tag{3.33}$$

[12] In the corresponding Lorentzian geometries, the trajectories will be governed by the potential $V_{\text{eff}}(r)$.

[13] More precisely, we have $0 < A \leq \min(\lambda_1, \lambda_2)$.

In order that the two domain walls asymptoting to $t_2 = \pm S/2$ do not intersect in the interior of the geometry, we have a constraint that $\Delta t_2 < S/2$. This is relevant only to the case $\lambda_2 < \lambda_1, \sqrt{\lambda_1} - \sqrt{\lambda_2} < \kappa < \sqrt{\lambda_1 - \lambda_2}$. Explicitly, we require

$$S > \frac{2}{\sqrt{\lambda_2}} \operatorname{arctanh}\left(\frac{\lambda_1 - \lambda_2 - \kappa^2}{2\kappa\sqrt{\lambda_2}}\right) \tag{3.34}$$

For smaller values of S, no AdS solution exists.

3.4.3 Black hole solutions

Let us now consider the solutions with $\mu_2 = \mu > 0$. In this case

$$V_{\text{eff}}(r) = Ar^2 + 1 + \frac{B}{r^{D-3}} - \frac{C}{r^{2D-4}}, \tag{3.35}$$

where $A > 0$ is defined in (3.29) and B, C are defined as

$$B = -\mu\left(\frac{\lambda_1 - \lambda_2 + \kappa^2}{2\kappa^2}\right) \qquad C = \frac{\mu^2}{4\kappa^2}\ . \tag{3.36}$$

Since A and C are positive, the potential V_{eff} is positive for large r and negative for small r so must have a root for positive r. For $D \geq 3$ it can be shown [92] that the root is unique, and we call this r_0. Domain wall trajectories that reach the asymptotic boundary of AdS reach a minimum radius at r_0 before returning to $r = \infty$. Thus, solutions for $\mu > 0$ are "black hole" solutions of the type shown in figure 3.4c. For $D = 3$, we have explicitly that

$$r_0 = \frac{\mu}{\sqrt{2\sqrt{\mu^2\kappa^2\lambda_1 + \mu\kappa^2(\lambda_2 - \lambda_1 - \kappa^2) + \kappa^4} + \mu(\lambda_2 - \lambda_1 - \kappa^2) + 2\kappa^2}} \qquad D = 3 \tag{3.37}$$

Euclidean AdS-Schwarzschild geometry

Before proceeding, we recall a few useful facts about the Euclidean AdS/Schwazschild geometry in (3.22). We have that $f_2(r) = 0$ at $r = r_H$, where r_H is the horizon radius, determined by

$$1 + \lambda_2 r_H^2 - \frac{\mu}{r_H^{D-3}} = 0\ . \tag{3.38}$$

For $D = 3$, we have[14]

$$r_H = \sqrt{\frac{\mu - 1}{\lambda_2}} \qquad D = 3\ . \tag{3.39}$$

The geometry is smooth at $r = r_H$, provided that t is taken to be periodic with period

$$\beta = \frac{4\pi}{f_2'(r_H)} \tag{3.40}$$

which reduces in $D = 3$ to

$$\beta = \frac{2\pi}{\sqrt{\lambda_2(\mu - 1)}} \qquad D = 3\ . \tag{3.41}$$

For our solutions, the black hole region includes only a finite interval $t \in [-S/2, S/2]$ in the asymptotic region $r \to \infty$.

[14] For $0 < \mu < 1$, we have a conical singularity at $r = 0$.

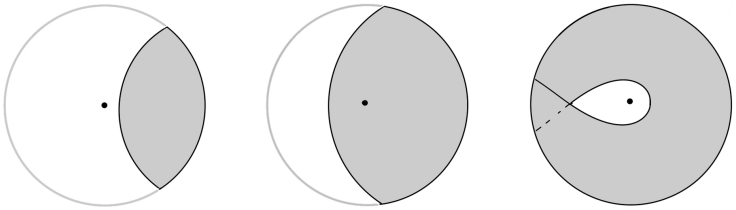

Figure 3.7: Possibilities for the geometries exterior to the interface brane in the Euclidean picture. The shaded region corresponds to the portion of the space which is kept, while the unshaded region is discarded. Left: part of Euclidean AdS-Schwarzschild without a horizon. Centre: part of Euclidean AdS-Schwarzschild including the horizon (centre point). Right: solution without a horizon with $\Delta t_2 > \beta/2$.

We have two types of black hole solutions, characterized by whether or not the horizon is included in the spacetime region between the domain wall and the asymptotic AdS boundary (see left/centre panels in figure 3.7). For the no-horizon solutions, $\dot{t}_2$ is positive near $r = r_0$, while for solutions with a horizon, $\dot{t}_2$ is negative for $r = r_0$. From (3.28), we find that the solution will include the Euclidean horizon[15] if

$$f_2(r_0) - f_1(r_0) + \kappa^2 r_0^2 > 0 \ . \tag{3.42}$$

For $D = 3$, together with (3.37), this gives

$$\kappa > \sqrt{\lambda_1} \qquad \mu > 1 + \frac{\lambda_2}{\kappa^2 - \lambda_1} \qquad D = 3 \ . \tag{3.43}$$

We note that when the horizon is not included, our geometry can be a portion of a multiple cover of the Euclidean Schwarzschild solution, as shown in the right panel in figure 3.7.

Interface trajectories

The interface trajectories are again determined by integrating 3.28. As for the AdS solutions, it will be useful to have expressions for Δt_1 and Δt_2. In this case, we have

$$\begin{aligned} \Delta t_1 &= \int_{r_0}^{\infty} \frac{dr}{f_1 \sqrt{V_{\text{eff}}}} \left(\frac{1}{2\kappa r}(f_1 - f_2) + \frac{1}{2}\kappa r \right) \\ \Delta t_2 &= -\int_{r_0}^{\infty} \frac{dr}{f_2 \sqrt{V_{\text{eff}}}} \left(\frac{1}{2\kappa r}(f_2 - f_1) + \frac{1}{2}\kappa r \right) \ . \end{aligned} \tag{3.44}$$

For $D = 3$, we can give an explicit result in terms the of elliptic integral functions Π and K defined as

$$\Pi(\nu, z) = \int_0^1 \frac{dt}{(1 - \nu t^2)\sqrt{(1 - t^2)(1 - z^2 t^2)}} \qquad K(z) = \Pi(0, z) \tag{3.45}$$

We have that

$$\Delta t_1 = z r_0 (K(z) + C_1 \Pi(\nu_1, z)) \qquad \Delta t_2 = \frac{z r_0}{1 - \mu}(K(z) + C_2 \Pi(\nu_2, z)) \qquad D = 3 \tag{3.46}$$

[15] In the Lorentzian picture, this translates to the property that the domain wall is behind a black hole horizon at $t = 0$. For the Euclidean solutions without a horizon, the domain wall is initially not behind a horizon but collapses to form a black hole at later times.

where

$$\begin{aligned} z &= \frac{\mu}{\sqrt{\mu^2 + 4r_0^4\kappa^2 A}} \qquad \nu_1 = \frac{1}{1+\lambda_1 r_0^2} \qquad \nu_2 = \frac{1-\mu}{1-\mu+\lambda_2 r_0^2} \\ C_1 &= \frac{r_0^2\nu_1}{\mu}(\kappa^2 - \lambda_2 - \lambda_1(\mu-1)) \qquad C_2 = \frac{r_0^2\nu_2}{\mu}(-\kappa^2 + \lambda_1 + \frac{\lambda_2}{\mu-1}) \end{aligned} \tag{3.47}$$

For the black hole solutions without a horizon (figure 3.7 left and right), t_2 is 0 at the time-symmetric point and $S/(2\sqrt{\lambda_2})$ at the boundary, so

$$S/2 = \sqrt{\lambda_2}\Delta t_2 \ . \tag{3.48}$$

For the black hole solutions with a horizon (figure 3.7 centre), t_2 decreases from $\beta/2$ at the time-symmetric point to $S/(2\sqrt{\lambda_2})$ at the boundary, so

$$S/2 = \sqrt{\lambda_2}(\Delta t_2 + \frac{\beta}{2}) \ , \tag{3.49}$$

where β is given in (3.40). In either case, we have a constraint that

$$S \geq 0 \tag{3.50}$$

in order that the brane does not intersect itself.

Existence of solutions

The gravitational solutions depend on dimensionless parameters $\sqrt{\lambda_2/\lambda_1}$, $\kappa/\sqrt{\lambda_1}$, and μ. The dimensionless quantity S is a function of these parameters. The plots in figure 3.8 indicates the region of μ-κ parameter space for which black hole solutions of each type exist (for various values of $\sqrt{\lambda_2/\lambda_1}$) and also shows contour plots for the value of S. We find that black hole solutions satisfying the constraint $S > 0$ exist only for $\sqrt{\lambda_2/\lambda_1} < 3$. For $\sqrt{\lambda_2/\lambda_1}$ in this range, we typically have solutions with horizons for larger values of κ and solutions without horizons for smaller κ.

For fixed $\sqrt{\lambda_2/\lambda_1}$ and $\kappa/\sqrt{\lambda_1}$, we see that there can be two different values of μ that give rise to the same S. In our application, we are fixing the CFT parameter S, so we need to consider both solutions, along with the AdS solution with the same value of S to determine which has least action.

3.4.4 Comparing actions

In cases where more than one gravity solution exists for the same CFT parameters c_1, c_2, $\log g$, S, the one that dominates the path integral and correctly computes CFT observables will be the one with least action. In Appendix C, we derive expressions for the action starting from the general expression (3.7). For $D = 3$, the results are particularly simple. After removing a divergent term that is the same for each type of solution, we find that for the AdS geometries, the regulated action is

$$4G_3\mathcal{I}^{reg}_{\text{AdS}} = \Delta t_2 - \Delta t_1 \tag{3.51}$$

where Δt_1 and Δt_2 are given in (3.33) while for black hole geometries, the regulated action is

$$4G_3\mathcal{I}^{reg}_{BH} = (1-\mu)\frac{S}{2\sqrt{\lambda_2}} - \Delta t_1 \ , \tag{3.52}$$

where Δt_1 is given in (3.46).

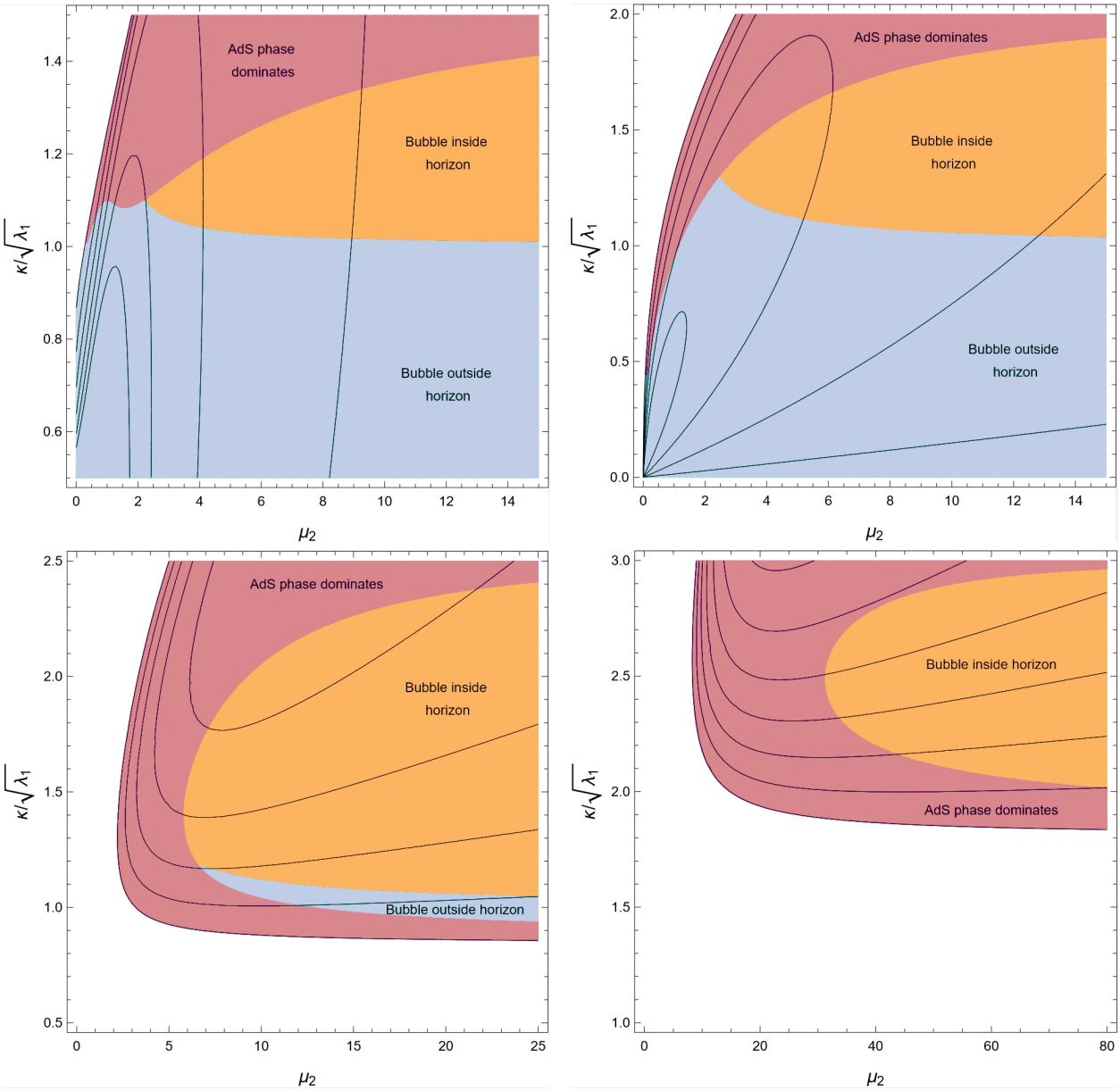

Figure 3.8: Possible bulk solutions with S contours shown (see Figure 3.6 for definition of S). $\sqrt{\lambda_2/\lambda_1} = 1/2, 1, 3/2, 2$ from top left to bottom right. The unshaded regions, corresponding to $S < 0$, admit no black hole solutions.

Phase diagrams for $D = 3$

Making use of the results in the previous section, we can compute the actions for the various solutions that are possible for fixed parameters $\lambda_1, \lambda_2, \kappa, S$. The diagrams in Figure 3.8 indicate which of the allowed black hole solutions have the least action compared with other black hole solutions or AdS solutions with the same parameter values.

With this information, we can assemble phase diagrams showing the preferred solution as a function of S and κ for fixed $\sqrt{\lambda_2/\lambda_1}$. These are shown in figure 3.9.

3.4.5 Small S

For our application, we are mainly interested in the limit $S = \epsilon \to 0$, so that the Euclidean evolution with H_2 in (3.2) does not significantly alter the long-distance properties of the CFT state. From the results in the previous section, we find that the least action solution is always a black hole solution with large μ when such a solution exists, or an AdS solution otherwise.

As we show in Appendix B.1, in this large μ limit, we can write the relation between S and μ explicitly as

$$S = \frac{1}{\sqrt{\mu}} \left(2\pi\Theta(\hat{\kappa} - 1) - \sqrt{\frac{\hat{\lambda}_2}{\hat{\kappa}}} K(z_\infty) - \sqrt{\frac{\hat{\lambda}_2}{\hat{\kappa}}} \frac{\hat{\kappa} + 1}{\hat{\kappa} - 1} \Pi \left(1 - \frac{\hat{\lambda}_2}{(\hat{\kappa} - 1)^2}, z_\infty \right) \right), \tag{3.53}$$

where

$$z_\infty = \sqrt{\frac{\hat{\lambda}_2 - (\hat{\kappa} - 1)^2}{4\hat{\kappa}}} \qquad \hat{\lambda}_2 = \frac{\lambda_2}{\lambda_1} \qquad \hat{\kappa} = \frac{\kappa}{\sqrt{\lambda_1}} , \tag{3.54}$$

so we see that $\mu \sim 1/S^2$ for small S. Legitimate black hole solutions exist provided that $S > 0$. From (3.43) these include the Euclidean horizon if and only if $\kappa > \sqrt{\lambda}_1$.

Examining the expressions (3.51) and (3.52) for the regulated actions, we see that the leading contribution at large μ to the action difference between a black hole solution and an AdS solution is

$$S^{BH} - S^{\text{AdS}} = -\frac{\mu S}{2\sqrt{\lambda_2}} + \mathcal{O}(\mu^{-\frac{1}{2}}) \tag{3.55}$$

since the regulated action for the pure AdS solutions does not depend on μ and Δt_1 goes as $1/\sqrt{\mu}$ according to (B.9). Thus, provided that a black hole solution exists (i.e. $S > 0$), it will have lower action.

Combining these results, we obtain the small S phase diagram showing the least action solution as a function of $\sqrt{\lambda_2/\lambda_1}$ and $\kappa/\sqrt{\lambda_1}$ in Figure 3.10.

At large μ, the expression (3.37) becomes

$$r_0 = \frac{\sqrt{\mu}}{\sqrt{\lambda_2 - (\sqrt{\lambda_1} - \kappa)^2}} \tag{3.56}$$

so we see that provided the black hole solution exists, the bubble of AdS vacuum can be made arbitrarily large by taking the limit of large μ, or equivalently, small $\epsilon = S/2$.

3.4.6 Summary of the results for small S

We find that for $\lambda_2 < \lambda_1$ (i.e. if CFT_2 has a larger central charge), the small S solutions for any κ are black hole solutions with a large bubble of the vacuum AdS geometry dual to CFT_1. For

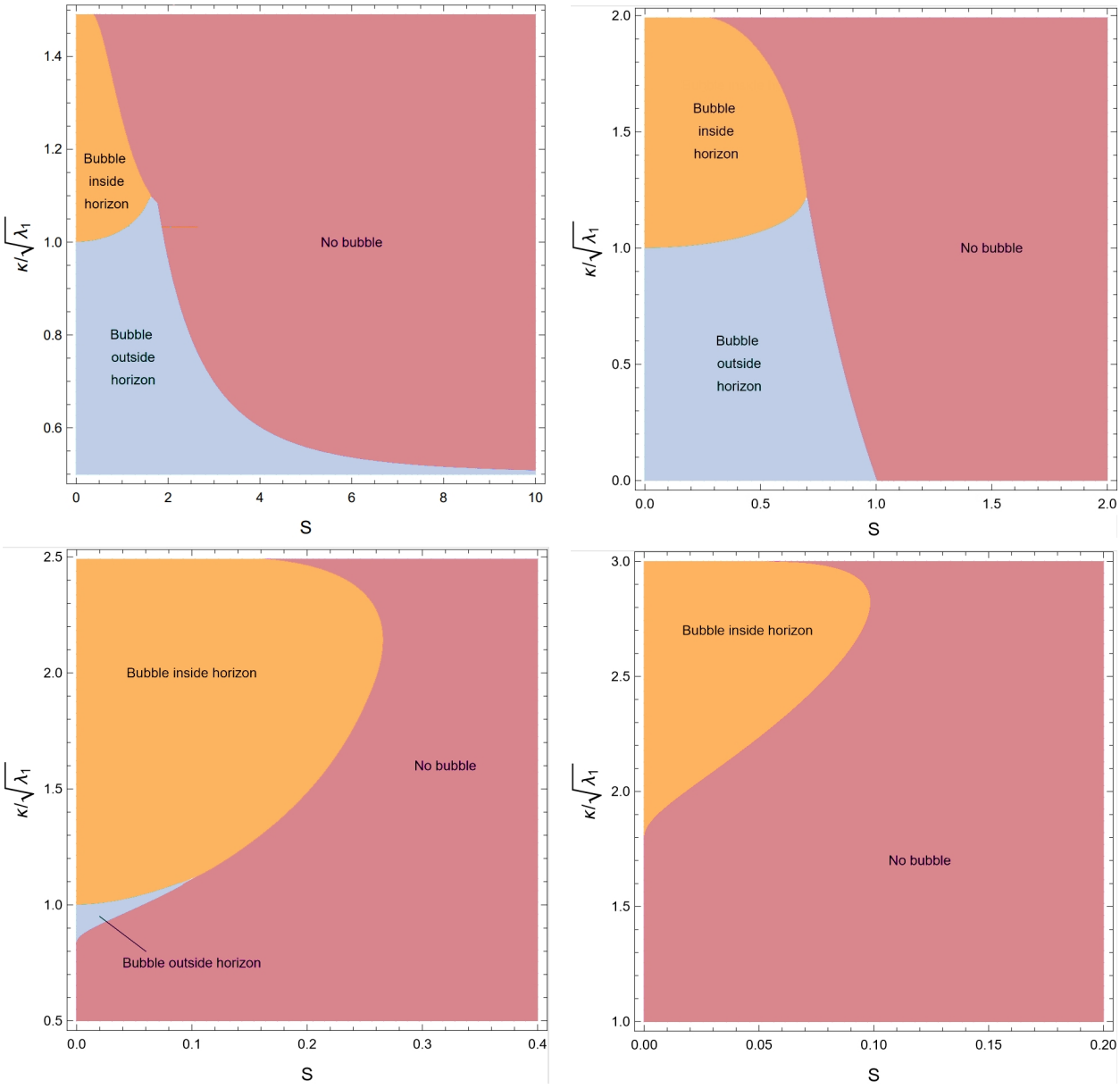

Figure 3.9: Phase plots showing least action gravity solution with $\sqrt{\lambda_2/\lambda_1} = 1/2, 1, 3/2, 2$ from top left to bottom right. For $\sqrt{\lambda_2/\lambda_1} > 3$, only AdS solutions exist.

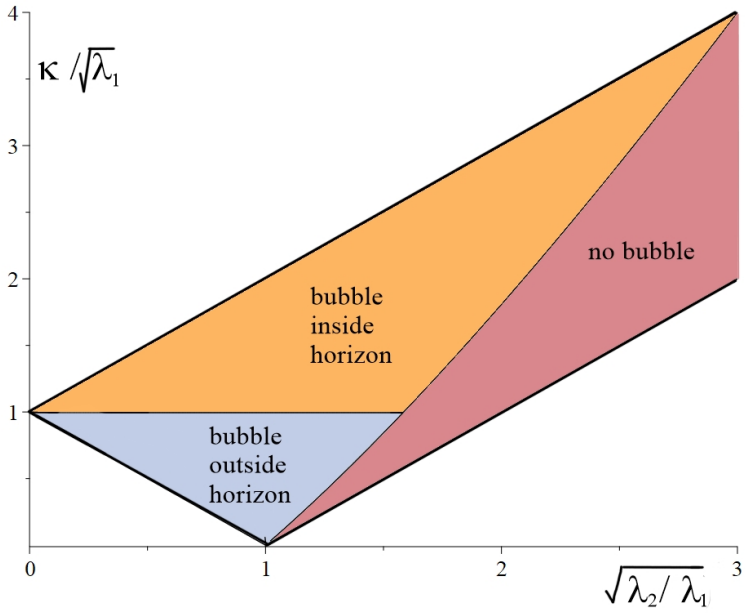

Figure 3.10: Phase diagram of least action bulk solutions in the limit of small S.

$\kappa < \sqrt{\lambda_1 - \lambda_2}$, the solution does not include a Euclidean horizon. We will see below that the domain wall in the corresponding Lorentzian solutions is not initially behind a black hole horizon, but later collapses to form a black hole. For $\kappa > \sqrt{\lambda_1 - \lambda_2}$, the solution includes a Euclidean horizon and the domain wall in the Lorentzian solution is behind the black hole horizon at all times.

For $\lambda_2 > \lambda_1$ (i.e. when CFT_2 has a smaller central charge), we have black hole solutions for some choice of κ only when $\lambda_2 < 9\lambda_1$ (or $c_2 > c_1/3$). For larger λ_2, all solutions are of AdS type, so apparently no CFT_2 states of the form (3.6) encode the gravitational physics of the geometry dual to the CFT_1 vacuum. On the other hand, we will see in Section 3.4.8 that this goal can be achieved by considering CFT_2 states using a path-integral with multiple interfaces.

3.4.7 Lorentzian Solutions

To find the Lorentzian geometries associated with our states, we use the $t = 0$ slice of the Euclidean geometry as initial data for Lorentzian evolution. The resulting geometry is a portion of the maximally extended black hole geometry, truncated at some time-dependent radial location by the interface brane, with a portion of Lorentzian AdS glued on to the interior. Similar Lorentzian geometries have been discussed previously in [93–95].

The Lorentzian interface brane trajectory is described by analytically continued versions of the Euclidean equations (3.27) and (3.28). The brane radius as a function of the proper time satisfies

$$\left(\frac{dr}{ds}\right)^2 + V_{\text{eff}}(r) = 0 \qquad V_{\text{eff}}(r) \equiv f_1 - \left(\frac{f_2 - f_1 - \kappa^2 r^2}{2\kappa r}\right)^2 . \tag{3.57}$$

Here, the sign of the potential is switched relative to the Euclidean case, so now the brane radius starts at $r = 0$, expands to $r = r_0$ and then contracts again. From the interior point of view, this means that the size of our AdS bubble shrinks with time after $t = 0$. From the exterior point of view, the interpretation is that the bubble emerges from the past singularity, grows, and then collapses to $r = 0$ at the future singularity, as shown in Firgure 3.11. For solutions that include the Euclidean

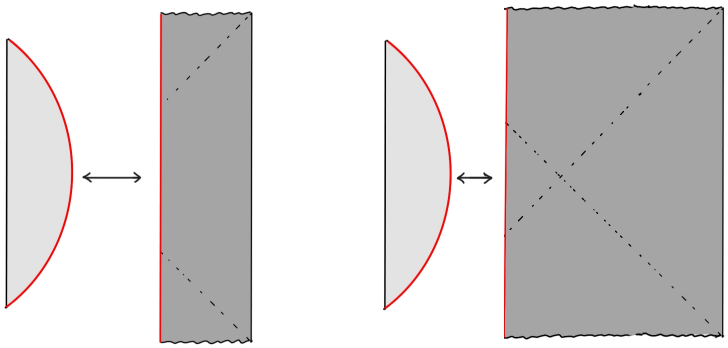

Figure 3.11: Schematic causal diagrams for Lorentzian solutions corresponding to Euclidean black hole phase solutions without (left) and with (right) a Euclidean horizon. In either case we have a collapsing bubble of pure AdS.

horizon, the bubble is behind the Lorentzian horizon at all times. For solutions without a Euclidean horizon, the bubble begins at the past singularity, emerges from the past horizon, falls back into the horizon, and then hits the future singularity. This description makes use of the worldvolume time on the brane. In terms of the exterior Schwarzchild time, the brane emerges from the horizon at $t = -\infty$ and falls back at $t = \infty$.

3.4.8 Multi-interface solutions

In the previous section, we have found that when the central charge of CFT_2 is too small, $c_2 < c_1/3$, we have only AdS solutions, suggesting that states $|\Psi_2\rangle = e^{-\epsilon H_2}\hat{Q}_{\mathcal{I}}|\Psi_1\rangle$ cannot provide an approximation to the CFT_1 vacuum state that faithfully encodes the gravitational physics of a large region of the original pure AdS spacetime. On the other hand, we have found that states of a CFT_2 with smaller central charge *can* faithfully encode large regions of the AdS spacetime dual to the CFT_2 vacuum provided that c_2/c_1 is not too small. Below, we will argue that the construction (3.6) also works for excited states. This suggests the following procedure to construct a state of CFT_n with central charge smaller than $c_1/3$ that can properly encode the physics dual to the CFT_1 vacuum:

1. start with the vacuum state of CFT_1;
2. consider a sequence CFT_2, CFT_3, $\ldots$ CFT_n of CFTs with c_{i+1}/c_i in the range $(1/3, 1)$;
3. construct a state $|\Psi_{i+1}\rangle$ of CFT_{i+1} from state $|\Psi_i\rangle$ of CFT_i by the map (3.6).

All together, we have a state of CFT_n defined from the CFT_1 vacuum by a series of Euclidean quenches involving a series of intermediate CFTs (see left panel in Figure 3.12):[16]

$$|\Psi_n\rangle = e^{-\epsilon_n H_n}\hat{Q}_{\mathcal{I}_{n\,(n-1)}} e^{-\epsilon H_{n-1}} \cdots e^{-\epsilon_2 H_2}\hat{Q}_{\mathcal{I}_{21}}|\Psi_1\rangle \ . \tag{3.58}$$

One motivation for considering these states is that the quench operator $\hat{Q}_{\mathcal{I}}$ may necessarily result in too severe a modification to the original state when passing to a new CFT with much smaller central charge than the original CFT. By including more steps, we can try to make the transition more gradual, so that the final state can faithfully encode the original geometry.

[16] A similar construction was considered in [92] when constructing "bag-of-gold spacetimes".

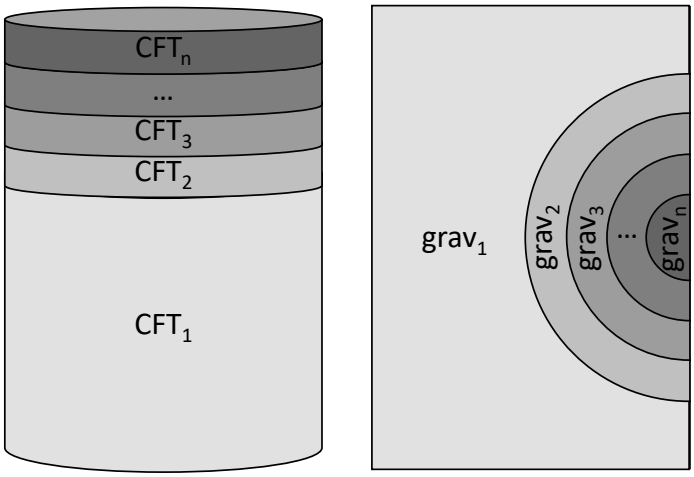

Figure 3.12: Left: construction of the state $|\Psi_n\rangle$ of CFT_n from the state $|\Psi_1\rangle$ of CFT_1. Right: dominant gravitational dual in the case of large μ_i, with $i \geq 2$.

We will consider a sequence of CFTs such that the ratio of central charges c_{i+1}/c_i for neighbouring CFTs is only slightly less than one, and the tension associated with the interface brane between these two CFTs is small. We take the width in Euclidean time of the strip with CFT_i to be $S_i/2$. On the gravity side, we have parameters $\lambda_i = 1/L_i^2$, μ_i $(i = 1, \ldots, n)$, and κ_i $(i = 1, \ldots, n-1)$, where $\mu_1 = 0$.

For the interface between the ith and $(i+1)$st region, the trajectory is determined by

$$\left(\frac{dr}{ds}\right)^2 = V_{\text{eff}} \tag{3.59}$$

with

$$V_{\text{eff}} = 1 + \lambda_i r^2 - \mu_i - \left[\frac{(\lambda_{i+1} - \lambda_i - \kappa_i^2)}{2\kappa} r - \frac{\mu_{i+1} - \mu_i}{2\kappa r}\right]^2 . \tag{3.60}$$

The ith region is bounded by the $(i-1)$st and ith domain walls, whose trajectories are described by $t_i^+(r)$, $t_i^-(r)$, satisfying

$$\begin{aligned} \frac{dt_i^-}{dr} &= \frac{1}{f_i\sqrt{V_{\text{eff}}}}\left(\frac{1}{2\kappa_i r}(f_i - f_{i+1}) + \frac{1}{2}\kappa_i r\right) \\ \frac{dt_i^+}{dr} &= -\frac{1}{f_i\sqrt{V_{\text{eff}}}}\left(\frac{1}{2\kappa_{i-1} r}(f_i - f_{i-1}) + \frac{1}{2}\kappa_{i-1} r\right) . \end{aligned} \tag{3.61}$$

For a valid solution where the domain walls do not intersect, we require that $\Delta t_i^+ > \Delta t_i^-$, and $t_i^+(r) > t_i^-(r)$ for $r \geq (r_0)_{i+1}$.[17]

We would like to show that there is a valid solution with λ_n/λ_1 arbitrarily large (c_n/c_1 arbitrarily small). To see this, we consider the series of parameters

$$\lambda_{i+1}/\lambda_i = (1+\epsilon) \qquad \kappa_i/\sqrt{\lambda_i} = \delta \ . \tag{3.62}$$

[17]Here, we will always be choosing $\kappa_i < \sqrt{\lambda_{i+1} - \lambda_i}$, so all $\dot{t}$s are positive.

We define $\mu_1 = 0$ and take μ_2 to be some large value (this will ensure that the values S_i are small). We now try to find μ_{i+1} for $i > 1$ so that

$$\Delta t_i^- = p \Delta t_i^+ \tag{3.63}$$

for some fraction $p \in (0, 1)$. For the specific example $\epsilon = \delta = 0.01$ we find numerically that the necessary μ_i values exist and form an increasing sequence for which μ_i/μ_{i-1} converges quickly (e.g. to $\mu_i/\mu_{i-1} = 4.23$ for $p = 1/2$ or $\mu_i/\mu_{i-1} = 1.067$ for $p = 0.99$). The solutions corresponding to these parameters appear to satisfy our desired properties for arbitrarily large n, though we have not proven this analytically. Since $\lambda_n = 1.01^{n-1}\lambda_1$, we see that λ_n/λ_1 can be made arbitrarily large, so based on the numerical evidence we have solutions corresponding to states of CFT_n with arbitrarily small central charge that include a bubble of the spacetime dual to CFT_1.

For these solutions, the regulated action is

$$\mathcal{I}_{reg} = -\Delta t_1^- + \sum_{i=2}^{n-1} (1 - \mu_i)(\Delta t_i^+ - \Delta t_i^-) + (1 - \mu_n)\Delta t_n^+ \ . \tag{3.64}$$

Defining $S_i/2$ to be the width of the ith CFT strip in units where the sphere radius is 1, we have

$$\Delta t_i^+ - \Delta t_i^- = \frac{S_i}{2\sqrt{\lambda_i}} \ , \tag{3.65}$$

so we can rewrite the action as

$$\mathcal{I}_{reg} = -\Delta t_1^- + \sum_{i=2}^{n} (1 - \mu_i) \frac{S_i}{2\sqrt{\lambda_i}} \tag{3.66}$$

We should compare this to the action for the other possible solutions where $\mu_1 = \cdots \mu_k = 0$ so that the first $k - 1$ domain walls extend to $r = 0$. For those solutions, the expression (3.64) for the action still applies, though the parameters $\mu_{i>k}$ must be chosen to obtain the same S_i values as those arising from (3.62).

For the examples described above, we have checked numerically that for the other possible solutions, the μ value in each region for our original solution with only one AdS region will always be larger than the μ value in the same region for any of the other solutions.[18] In the case where all the μ values are large, it then follows from the form of the action (3.66) that the action for the solution with only one AdS region is always smallest (see right panel in Figure 3.12).

3.5 Approximating non-vacuum states

So far, we have focused on defining CFT_2 states that encode a large region of the pure AdS spacetime dual to the CFT_1 vacuum. However, given some other CFT_1 state dual to a non-vacuum geometry, we can consider exactly the same mapping (3.6) to define a CFT_2 state that approximates this. Very general perturbations to the AdS vacuum geometry can be included by adding sources for various operators to the Euclidean path integral defining the vacuum state (see, for example, [96–98]).[19]

[18] To find the other solutions, we note that given μ_{k+1}, the remaining μ_i for $i = k + 2, \ldots, n$ are fixed via the procedure above by demanding that S_i matches with the previous solution for $i = k + 1, \ldots, n - 1$. The value of S_n for the new solution will be some function of μ_{k+1}, and we must choose μ_{k+1} so that this matches with S_n in the original solution.

[19] Alternatively, we can consider the insertion of a discrete set of operators.

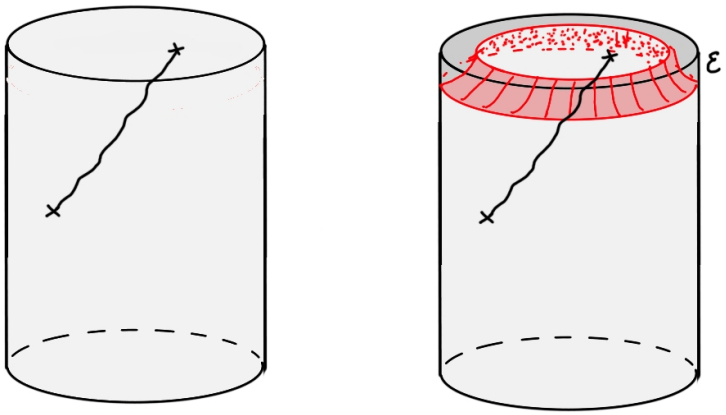

Figure 3.13: Approximating excited states. In the limit $\epsilon \to 0$, we expect that the boundary-to-bulk propagators on the right approach those on the left, so the interior geometry of the CFT_2 state on the right should provide a good approximation to the interior geometry of the CFT state on the left. The red surface is the interface separating the regions of the bulk corresponding to the different CFTs.

These sources modify the boundary conditions for the corresponding bulk fields, leading to changes in the initial data. Perturbatively, these changes are governed by some Euclidean boundary-to-bulk propagator, as depicted in Figure 3.13. We expect that the boundary-to-bulk propagator in the background geometry dual to the approximated vacuum state (right side of figure 3.13) should approach the original boundary-to-bulk propagator in the limit $\epsilon \to 0$, so the interior geometry of an approximated state with sources should approach the original perturbed interior geometry in this limit.[20] Assuming that our parameter choices are such that the approximated vacuum geometry with a bubble has least action, the same will be true when we add sources provided that these sources are not too large.

It would be interesting to investigate in more detail how accurately a set of bulk perturbations are reproduced in the interior of a bubble when ϵ is some small finite value.

3.5.1 Approximating black hole geometries

We can also consider the case of highly-excited CFT states, where the bulk geometry is far from pure AdS. In the generic situation, we expect that the bulk geometry should be well-approximated by an AdS/Schwarzschild black hole, so we will consider the case where CFT_1 is in a thermal state, purified as the thermofield double state of two copies of CFT_1. In this case, we can approximate the state as an entangled state of CFT_1 and CFT_2, defined by[21]

$$\begin{aligned} |\Psi\rangle &= \mathbb{1} \otimes M_{\mathcal{I},\epsilon} |\Psi_{TFD}\rangle_{LR} \\ &= \frac{1}{Z^{\frac{1}{2}}} \sum_i e^{-\frac{\beta}{2} E_i} |E_i\rangle_L \otimes M_{\mathcal{I},\epsilon} |E_i\rangle_R. \end{aligned}$$

The state arises from the Euclidean path integral shown at the left in Figure 3.14.

[20] It is apparent from the figure that for sources $\lambda_\alpha(x,\tau)$ in the original state, the best approximation to the original state at small finite ϵ may be obtained by taking sources $\lambda_\alpha(x,\tau+\sqrt{\lambda_1}\Delta t_1)$ in the approximated case so that the bulk $\tau = 0$ slice is at the same location relative to the sources in both pictures.

[21] Alternatively, we could have considered replacing both sides with CFT_2.

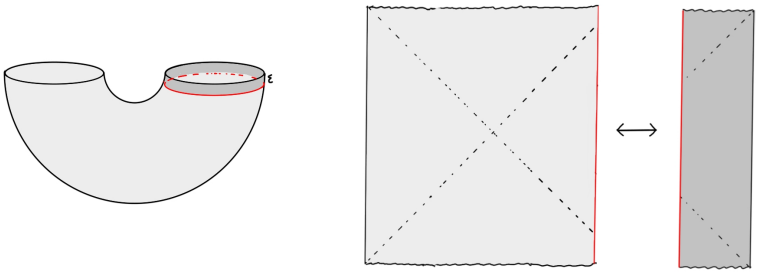

Figure 3.14: Approximating black hole geometries. A thermofield double state of two copies of CFT_1 is replaced by an entangled state of CFT_1 and CFT_2. The dual geometry is a Lorentzian wormhole connecting regions described asymptotically by the low-energy gravitational theories dual to CFT_1 and CFT_2, with an interface brane between them.

In this case, the dual geometry (either in the Euclidean or in the Lorentzian picture) will be one where both parts are portions of Schwarzschild-AdS geometries with different values of μ. One possibility for the Lorentzian geometry is shown at the right in Figure 3.14, though we can also have the situation that the domain wall is inside the horizon on the right. Similar geometries have been discussed in [99].

For these black hole geometries the interface trajectories are determined in the same way as before. The explicit results for Δt_1 and Δt_2 in this general case with nonzero μ_1 and μ_2 are given in appendix B.

Phases

A basic way to characterize the solutions corresponding to entangled states of CFT_1 and CFT_2 is to understand whether the interface brane lies behind the horizon on the CFT_1 side, the CFT_2 side, or both sides. Since the two CFTs have no interaction, the interface must be behind the horizon on at least one side, otherwise we could send a signal from one asymptotic region to the other.

The interface brane will be behind the horizon on the CFT_1 side (as in Figure 3.14) if and only if $\dot{t}_1(r_0) > 0$, while the interface brane will be behind the horizon on the CFT_2 side if and only if $\dot{t}_2(r_0) < 0$. From equation (3.61), these give:

$$\begin{aligned} &(\lambda_1 - \lambda_2 + \kappa^2) r_0^2 + (\mu_2 - \mu_1) > 0, && \text{interface behind } \mathrm{CFT}_1 \text{ horizon;} \\ &(\lambda_1 - \lambda_2 - \kappa^2) r_0^2 + (\mu_2 - \mu_1) < 0, && \text{interface behind } \mathrm{CFT}_2 \text{ horizon,} \end{aligned} \tag{3.67}$$

The phase boundaries lie at $\dot{t}_1(r_0) = 0$ and $\dot{t}_2(r_0) = 0$; when these are satisfied, we also have $r_0 = r_H^1$ and $r_0 = r_H^2$ respectively, since the phase boundary is the boundary in parameter space where the interface crosses the Euclidean horizon. Using (3.39) in (3.67), the phase boundaries simplify to:

$$\begin{aligned} &\lambda_1(\mu_2 - 1) > (\lambda_2 - \kappa^2)(\mu_1 - 1), && \text{interface behind } \mathrm{CFT}_1 \text{ horizon;} \\ &\lambda_2(\mu_1 - 1) > (\lambda_1 - \kappa^2)(\mu_2 - 1), && \text{interface behind } \mathrm{CFT}_2 \text{ horizon.} \end{aligned} \tag{3.68}$$

Figure 3.15 shows the types of black hole geometries that are possible and for which parameter values each phase is realized. The slopes of the various lines can be read off from (3.68).

Generally, we find that configurations similar to that shown in Figure 3.14 with CFT_2 occupying a small fraction of the thermal circle corresponds to parameter values $\mu_2 \gg \mu_1$.

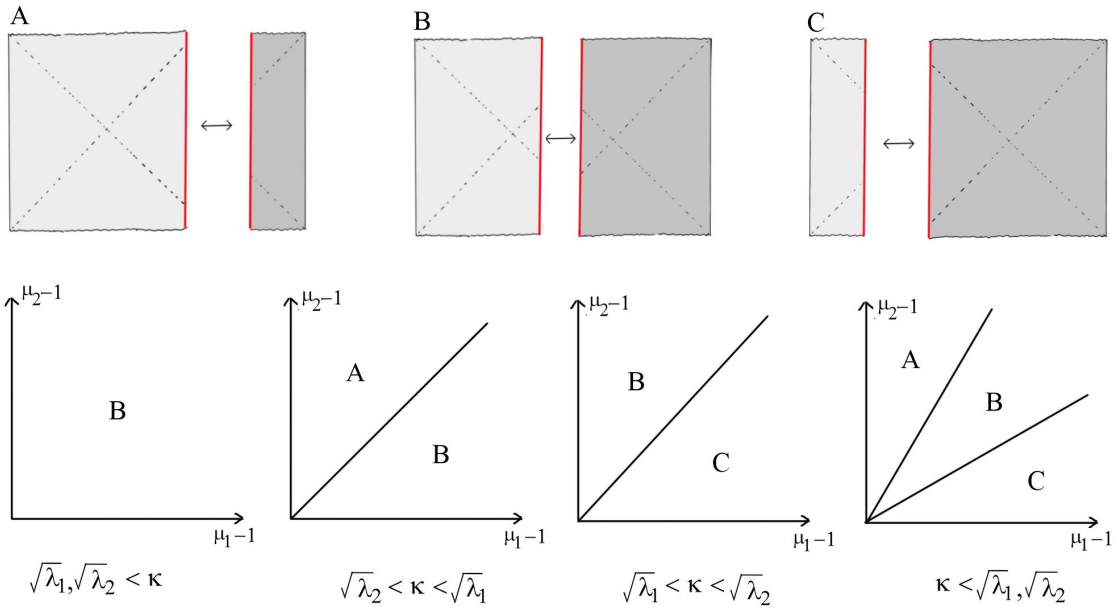

Figure 3.15: Top row: possible black hole geometries corresponding to approximations of a thermal state of one CFT_1 by a state of CFT_2. Bottom row: Phase diagram showing the solution consistent with given parameter values.

3.6 Properties of the CFT state

It is interesting to consider the properties of the CFT states which are able to encode a bubble of pure AdS spacetime with size r_0. In particular, we can ask what is the minimum amount of energy needed in CFT_2 to describe a state that includes a bubble of size r_0 for the AdS spacetime dual to CFT_1.

For $D = 3$, the energy and (coarse-grained) entropy of the CFT_2 state can be related to the parameter μ as[22]

$$\begin{aligned} E_{\mathrm{CFT}} &= \frac{c_2}{12}\mu \\ S_{\mathrm{CFT}} &= \frac{c_2}{3}\pi\sqrt{\mu - 1} \end{aligned} \tag{3.69}$$

where we have that

$$\begin{aligned} \mu &= 2\kappa r_0(1+\lambda_1 r_0^2)^{\frac{1}{2}} + r_0^2(\lambda_2 - \lambda_1 - \kappa^2) \\ &= r_0^2[\lambda_2 - (\sqrt{\lambda_1} - \kappa)^2] + \frac{\kappa}{\sqrt{\lambda_1}} + \mathcal{O}(r_0^{-2}) \,. \end{aligned} \tag{3.70}$$

For a given large value of r_0, μ is minimized for $\kappa \to \sqrt{\lambda_1} + \sqrt{\lambda_2}$ (corresponding to $\log g \to \infty$) when $\lambda_2 > \lambda_1$ and for $\kappa \to \sqrt{\lambda_1} - \sqrt{\lambda_2}$ (corresponding to $\log g \to -\infty$) when $\lambda_2 < \lambda_1$. Thus, the least energy will be achieved by choosing the interface with the largest value of $\log g$ when $c_2 > c_1$ and the smallest value of $\log g$ when $c_2 < c_1$.

In terms of CFT parameters, we have that the energy of a CFT_2 state required to describe a bubble of size $r_0 = nL_1$ of the AdS spacetime dual to the CFT_1 vacuum (i.e. for a bubble whose

[22]Here, the entropy can be derived using the Bekenstein-Hawking formula $S = A_H/(4G)$ while the energy can be obtained using $dE = TdS$, taking $E = 0$ for $\mu = 0$ so E_{CFT} is the energy relative to the vacuum. The temperature is the inverse periodicity of the CFT time, $T^{-1} = \beta_{\mathrm{CFT}} = \sqrt{\lambda}\beta_{\mathrm{grav}}$, where β_{grav} is given in (3.40).

radius is n AdS lengths) satisfies

$$E > \begin{cases} \frac{1}{12}(c_2+c_1)(1-\frac{1}{4n^2}+\mathcal{O}(n^{-4})) & c_2 < c_1 \\ \frac{1}{12}(c_2-c_1)(1-\frac{1}{4n^2}+\mathcal{O}(n^{-4})) & c_2 > c_1 \end{cases} \tag{3.71}$$

We recall that $c_2/12$ is the energy of the CFT state associated with the lightest BTZ black hole. Thus, when approximating the CFT_1 vacuum with a CFT with less degrees of freedom the state necessarily has energy in the black hole range, while for a CFT_2 with more degrees of freedom, a lighter state is possible. While these infimum values for the energies (which require taking $\log g \to \pm\infty$) have a finite limit for $r_0 \to \infty$, we see that for a fixed choice of CFT parameters, the energy of a CFT_2 state approximating an AdS bubble of radius r_0 always scales as r_0^2 for large r_0.

Energy of approximated black hole states

When approximating a bubble of radius r_0 of a black hole geometry with mass parameter μ_1, we find that the equation (3.70) for the parameter μ that determines the energy and entropy of the CFT_2 state via (3.69) generalizes to

$$\begin{aligned} \mu_2 &= \mu_1 + 2\kappa r_0(1+\lambda_1 r_0^2 - \mu_1)^{\frac{1}{2}} + r_0^2(\lambda_2 - \lambda_1 - \kappa^2) \\ &= r_0^2[\lambda_2 - (\sqrt{\lambda_1}-\kappa)^2] + \frac{\kappa}{\sqrt{\lambda_1}} + \mu_1\left(1 - \frac{\kappa}{\sqrt{\lambda_1}}\right) + \mathcal{O}(r_0^{-2})\,. \end{aligned}$$

where we are assuming that $\dot{t}_1(r_0) > 0$ so that bubble at $t = 0$ contains the black hole as in Figure 3.15A,B. An interesting feature is that for $\kappa > \sqrt{\lambda_1}$ the CFT_2 state energy actually decreases as the black hole mass parameter μ_1 increases, though this dependence is only in the subleading $\mathcal{O}(r_0^0)$ behaviour. So, for fixed r_0, it does not necessarily require more energy in CFT_2 to approximate an excited state of CFT_1.

3.7 Discussion

In the context of a simple holographic model that captures the central charges of CFTs and the interface entropy of possible interfaces between them, we have found that it is always possible to find states of CFT_2 whose dual geometries include arbitrarily large causal patches of the geometry dual to the vacuum state of CFT_1, or a very general class of excited states. Our result should hold generally provided that there is always some choice of interface (or series of interfaces) and some sufficiently small S for which the topology of the interface brane takes the form shown in Figure 3.4c rather than the form shown in Figure 3.4b. It would be interesting to see whether this is true in more general models, for example, in models with more general bottom-up actions or microscopic models arising from string theory.

In our simple model, the interface brane is assumed to couple only gravitationally. Combined with the assumed spherical symmetry this implies that the interior geometry of our bubbles is precisely pure AdS with AdS length L_1, i.e. the geometry of the bubble interior for the approximated state is precisely the same as the geometry that we started with. In more general cases, the interface brane can couple to other fields in the geometry, so it is interesting to ask whether the bubble interior would still be approximately pure AdS in these cases. The following argument suggests that this should be the case.

Suppose that the interior geometry at $t = 0$ contained some massive particle. In the Euclidean geometry, this particle will lie on a time-symmetric geodesic. If this geodesic is not too close to the bubble wall, it will intersect the asymptotically AdS boundary at points in the past and the future

in the asymptotic region associated with CFT_1. But such an intersection would imply the insertion of a heavy operator in the CFT, and we have assumed that there are not any such insertions. Similarly, we expect that extra light matter in the bubble interior would imply a modification of the asymptotic behaviour of fields in the CFT_1 region of the asymptotic geometry, corresponding to sources for various light operators in the CFT. Assuming that these sources are not present, we expect that the bubble interior away from the bubble wall should be very close to vacuum AdS. It would be interesting to investigate this further, for example in a model where the interface brane action includes a source for a scalar field.

Probing the bubble interior with CFT_2

In cases where the dual geometry to our CFT_2 state includes a bubble of the AdS spacetime dual to the CFT_1 vacuum or to perturbative excitations around this geometry, it is interesting to ask which CFT_2 observables can be used to probe the physics inside the bubble. In simple cases, where the bubble wall is not always behind a black hole horizon, we expect that an HKLL-type construction [100, 101] should work to express interior bulk operators in terms of boundary operators. Here, we need a propagator from the interior of the bubble to the asymptotically AdS region outside the bubble; this will generally involve different fields on either side of the bubble, and will require detailed knowledge of the physics of the interface brane to understand how excitations on one side will be transmitted to the other side.

Calculations of entanglement entropy for various spatial regions of CFT_2 should also probe the bubble interior in some cases, even when the bubble lies behind the black hole horizon. Calculations similar to those in [102] could be used to investigate which portion of the interior region is reached by RT surfaces (for various values of the parameters) and in which cases some or all of this region lies in the "entanglement shadow". When we consider bubbles of cosmology in the next chapter we will see examples of such RT surface calculations.

In general, we expect that the local description of physics inside the bubble should be quite complicated from the CFT_2 perspective when the bubble lies behind the black hole horizon. Even without an interface, understanding the description of local physics behind a black hole horizon is a significant open question.

General picture

To conclude this chapter, we summarize the speculative picture that has motivated our study and that we have found evidence for using our simple holographic model. First, we have suggested the following conjecture:

- Theories of gravity dual to CFTs that can be non-trivially coupled at an interface are part of the same non-perturbative theory. This includes dynamical interface branes that can connect regions of spacetime described by the low-energy gravitational theories associated with the individual CFTs.

According to this, distinct non-perturbative theories of quantum gravity would correspond to different equivalence classes of CFTs, where two CFTs are in the same equivalence class if they can be coupled non-trivially at an interface. An interesting possibility is that there is only one equivalence class (or at least, only one containing holographic theories), in which case all low-energy gravitational theories (with asymptotically AdS vacua) would be part of a single non-perturbative theory of gravity, as advocated recently in [67, 72].

The idea that many apparently different gravitational theories may all be related is familiar from string theory,[23] and is central to the multiverse picture of cosmology (see e.g. [104]), in which bubbles with physics described by one low-energy effective theory may form and expand in an ambient spacetime described by another low-energy effective theory. However, suppose there were some other theory of quantum gravity, apparently unrelated to string theory, describing physics in an asymptotically AdS spacetime. According to the general principles of AdS/CFT, the asymptotic observables of this theory should define a dual CFT (see e.g. [105]). Provided that this CFT can be nontrivially coupled at an interface to some CFT dual to a gravitational theory arising from string theory, then the gravitational physics of the interface theory should involve both low-energy gravitational theories in different regions separated by a dynamical interface, and thus be part of a single non-perturbative theory.

Our main focus has been to provide evidence for the following idea:

- Given $|\Psi\rangle_{\mathrm{CFT}_1}$ dual to an asymptotically AdS spacetime, and given CFT_2 that can be nontrivially coupled to CFT_1 at an interface, we can find a state $|\Psi\rangle_{\mathrm{CFT}_2}$ whose dual geometry includes an arbitrarily large portion of the Wheeler-DeWitt patch associated with $|\Psi\rangle_{\mathrm{CFT}_1}$

We have given an explicit construction of the states $|\Psi\rangle_{\mathrm{CFT}_2}$ in terms of a quench operator defined using a Euclidean path integral for the interface CFT.

We emphasize that the interior regions of the bubbles described by these states of CFT_2 include all the usual low-energy fields of the gravitational theory associated with CFT_1, even if CFT_2 and CFT_1 have very different operator spectra.

According to this general picture, different holographic CFTs correspond to different possible asymptotically AdS behaviours for quantum gravity, while the gravitational physics of finite patches of spacetime is something that can be encoded in any CFT in the same equivalence class as the original one. That this same physics can be described by many different holographic theories suggests that the gravitational physics of such finite-volume patches of spacetime may be dual to some more universal physics that is present in the IR physics of any holographic CFT (such as the evolution of entanglement structure or complexity [106] of the states). In fact, our CFT construction of states applies just as well for non-holographic CFTs (i.e. where the "gravity" description would not be in terms of a conventional low-energy effective theory of gravity), so an interesting possibility is that the precise physics of quantum gravity could in principle be simulated through the IR quantum dynamics of an ordinary material, though setting up an appropriate state and understanding the proper observables to measure in order to extract interesting physics is clearly a significant challenge.

[23] That all consistent gravitational theories should come from string theory and be related to each other has been advocated recently in [103].

Chapter 4

Bubbles of cosmology

The goal of this thesis is to develop a quantum model of cosmology using AdS/CFT holography. A simple observation is that $\Lambda < 0$ gravitational effective theories, which are associated with holographic CFTs, have cosmological solutions, which are typically big-bang/big-crunch cosmologies. But because these solutions are themselves not asymptotically AdS they cannot be dual to any finite-energy state of the CFT, and hence cannot be directly described using standard AdS/CFT techniques.

In the last chapter we showed how a large part of the spacetime dual to a state of some holographic CFT_1 can equivalently be described using the state of a completely different holographic CFT_2, as long as the two CFTs can be coupled at an interface. The full gravitational solution in this case consisted of a finite volume bubble of the original spacetime embedded in an asymptotically AdS spacetime dual to CFT_2. This suggests that to obtain a description of cosmology using AdS/CFT we should consider a finite *bubble of cosmology* within an otherwise empty asymptotically AdS spacetime. In this chapter we explore such solutions and their possible CFT dual descriptions.

Starting with a cosmological solution with $\Lambda < 0$ plus arbitrary matter density, radiation density, and spatial curvature, we show that a comoving bubble of arbitrary size can be embedded in a geometry with AdS-Schwarzschild exterior across a thin-shell domain wall comprised of pressureless matter. We show that in most cases (in particular, for arbitrarily large bubbles with an arbitrarily small negative spatial curvature) the entropy of the black hole exceeds the radiation entropy in the cosmological bubble, suggesting that a faithful CFT description is possible. We show that unlike the case of a de Sitter bubble [92], the Euclidean continuation of these cosmological solutions is sensible and suggests a specific construction of CFT states dual to the cosmological solutions via a Euclidean path integral.

4.1 Introduction

The holographic approach to quantum gravity provides a fully microscopic definition for certain quantum gravitational theories in terms of dual non-gravitational quantum systems. The best understood examples describe gravitational physics in spacetimes that are asymptotically empty and negatively curved. On the other hand, observations suggest that our own Universe is qualitatively different, an approximately homogeneous and isotropic expanding spacetime filled with matter and radiation. It is a challenge to understand whether the holographic approach can be extended to describe such cosmological spacetimes. Various approaches have been considered in the past; see [107–116] for examples.

In this Chapter, we will consider $\Lambda < 0$ cosmological spacetimes that are most similar to spacetimes that we can already describe holographically. Pure AdS itself is an example of a spacetime that can be written in Friedmann-Robertson-Walker (FRW) form (with negative spatial slices) as

$$ds^2 = -dt^2 + L^2 \cos^2(t/L) dH_{n-1}^2 \tag{4.1}$$

where L is the AdS radius and dH_{n-1}^2 is the unit hyperbolic metric. This FRW metric covers only a patch of the full global AdS spacetime (see figure 4.1), equivalent to the domain of dependence

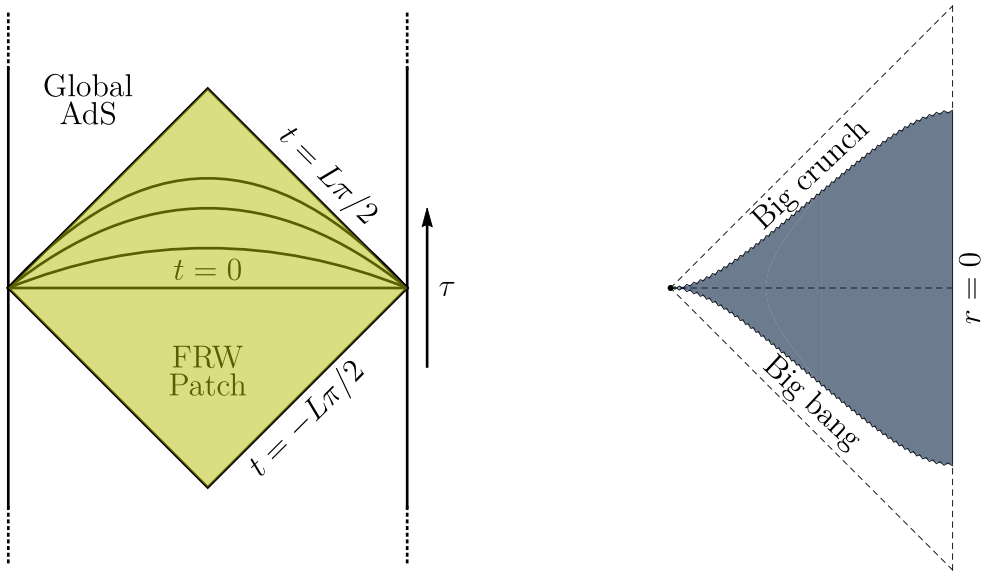

Figure 4.1: Left: FRW patch of Global AdS spacetime showing constant FRW time Cauchy slices. The surfaces $t = \pm L\pi/2$ represent coordinate singularities. Right: Adding an arbitrarily small matter or and/or radiation density gives a $\Lambda < 0$ big-bang big crunch cosmology with Penrose diagram shown here. The spacetime is no longer asymptotically AdS.

of a constant global-time slice of global AdS. The dual CFT vacuum state provides a holographic description of this trivial cosmology. The "big bang" and "big crunch" at $t = \mp L\pi/2$ are only coordinate singularities in this case. However, by adding an arbitrarily small homogeneous and isotropic density of matter and/or radiation to the $t = 0$ slice, we obtain a big bang/big crunch cosmology with genuine curvature singularities. The spacetime diagram for the resulting cosmology is shown in Figure 4.1. This spacetime is no longer asymptotically AdS, so the new spacetime does not correspond to a state in the dual CFT. This is understandable: while the energy *density* that we are adding to the $t = 0$ slice can be arbitrarily small, the total energy on the infinite volume slice is infinite, so would correspond to a state of infinite energy from the CFT perspective.

In order to make progress, we could attempt to define the cosmology from the CFT by taking a limit. Instead of including a uniform density of matter and/or radiation everywhere on the $t = 0$ slice, we could have a finite-sized ball filled with a uniform density of matter and/or radiation, with empty negatively curved spacetime outside. The full spacetime obtained by taking this slice as initial data will contain an interior region that is a patch of the FRW cosmology and an exterior region that is a part of a Schwarzschild AdS of some mass (Figure 4.2). We will call the interior region a *bubble of cosmology*. In between the bubble and the external region will be some transition region that interpolates between the two spacetimes. As in the last Chapter, for simplicity we will model this transition region using a dynamical codimension-1 domain wall. If the bubble is large enough, the interior cosmological region will include the the full causal patch associated to a complete geodesic from the big bang to the big crunch, so one might argue that a holographic description of such a spacetime would be entirely satisfactory for describing the physics accessible to any single observer in the cosmology.

Since these bubble of cosmology spacetimes are again asymptotically AdS, it is plausible that they correspond to valid finite-energy states of the dual CFT. These states can be understood as special microstates of the bulk black hole geometry where the black hole interior includes a patch

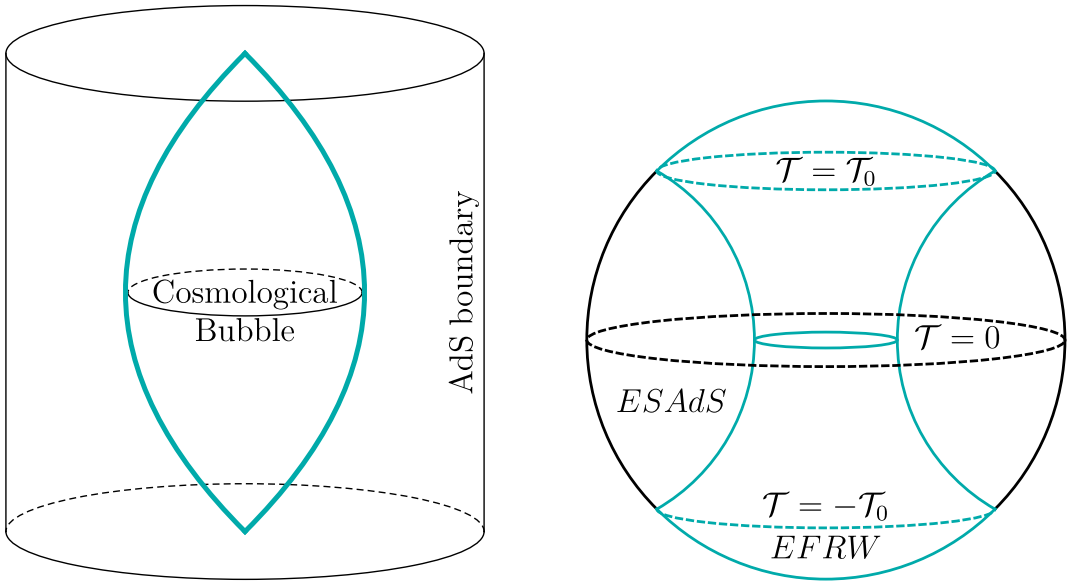

Figure 4.2: Left: schematic representation of the Lorentzian spacetime where the interior geometry is a portion of FRW and the exterior geometry is a portion of an AdS black hole spacetime. The blue surface is an interface brane separating the interior from the exterior. Note that the portion of the black hole spacetime which we keep may or may not contain the black hole horizon. Right: Euclidean continuation where the interior region is part of an AdS Euclidean wormhole.

of cosmological spacetime.

The goal of this Chapter is to construct such solutions for various types of cosmologies, to investigate whether these solutions can arise from legitimate dual CFT states, and to ask in this case how the cosmological physics is encoded in the dual CFT. Related earlier work along these lines is described below.

It is natural to ask what advantage such a construction would have over a typical semiclassical description of cosmological physics. First, as we motivated in Chapter 1, we expect that certain questions in cosmology, for example the nature of the big bang and/or the initial conditions for the cosmological evolution, will require a microscopic description to answer satisfactorily. Next, in at least some cases, CFT states encoding the cosmological physics can arise from a Euclidean path integral construction. In this case, the precise state of the cosmology is determined by the construction, and cosmological correlators could be related directly to correlators in an underlying CFT. This could provide new insights into their structure and help explain some of their unusual features e.g. the horizon problem. More generally, it might be that various semiclassical solutions are actually inconsistent, i.e. they have no microscopic construction. Showing that a certain semiclassical cosmology can arise from a holographic or other microscopic construction provides a check that the cosmology of interest does not have any subtle inconsistencies (i.e. is not in the "swampland"). We will explore these ideas in more detail in future chapters.

We now present a brief outline and summary of the results of this Chapter.

Constructing solutions

In Section 4.2, we construct a family of cosmological bubble solutions. By construction we will take the interior geometry to be a comoving bubble (i.e. with fixed coordinate radius in FRW coordinates)

of a cosmological solution with arbitrary spatial curvature, matter density, and radiation density. The exterior geometry is a part of the maximally extended AdS-Schwarzschild solution. We find that (in four dimensions) these two regions can always be joined across a domain wall that is a thin shell of dust whose density depends only on the radiation density in the interior.

Depending on the parameters, the cosmological bubble may lie completely behind the horizon of the black hole, or may start outside the horizon and fall through the horizon at some later time.

Potential entropy puzzle

For sufficiently small bubbles, it seems clear that there should be a CFT description - the spacetimes just correspond to a small amount of matter and/or radiation localized in some region of an otherwise empty AdS. However, for larger bubbles, there is a potential puzzle. Since the exterior spacetime is Schwarzschild-AdS, it has a naturally associated Bekenstein-Hawking entropy given by $1/(4G)$ times the area of the horizon. We can also associate an entropy to the interior of the bubble. For example, in a Universe with radiation, this interior entropy should be bounded below by the entropy of the radiation. As we increase the size of the bubble, the interior entropy might eventually exceed the black hole entropy (plausible since the interior entropy scales as a volume but the exterior entropy scales like an area). In this case, the CFT Hilbert space (restricted to the relevant energy band) would not be large enough to accommodate all the interior radiation microstates as independent states. Then either the bulk geometries do not correspond to valid CFT states, or the black hole interiors must be encoded non-isometrically (as in [117]).

We investigate these entropies in section 4.3. We find that with arbitrarily small negative spatial curvature, the black hole entropy always exceeds the radiation entropy in the cosmology. This is natural since for negative curvature, volume and area are proportional. For flat cosmologies, the radiation entropy eventually exceeds the black hole entropy, but only for bubbles that are parametrically larger than the cosmological scale (by a factor that is a positive power of $\ell_{\rm AdS}/\ell_{\rm Planck}$). There is never an issue with describing the region accessible to a single observer.

Euclidean construction

Another hint about the existence or not of a dual CFT state for a cosmological bubble geometry comes by looking at whether the solution has an analytic continuation to a well-behaved Euclidean geometry. If it is well-behaved, the corresponding Euclidean solution might represent the saddle point of a gravitational path integral whose dual CFT description constructs the CFT state. For de Sitter bubbles embedded in AdS (considered originally in [112]), the analytic continuations are not sensible since they have self-intersecting domain walls [118]. In our case, we find in Section 4.4 that the domain wall trajectories are sensible in the Euclidean picture for all cases with $K \leq 0$ and for any bubble smaller than half of the full spatial sphere in the $K > 0$ case.

When the Euclidean solution is sensible, the boundary has the topology of a sphere S^3, and the Euclidean domain wall has the topology of a cylinder ($S^2 \times I$) that intersects the sphere on a pair of S^2s, as shown in Figure 4.2. As we discuss in Section 4.5, this suggests that the Euclidean geometry arises holographically from a Euclidean CFT on S^3 with insertions of sources and/or operators restricted to a pair of polar regions. As a simple example, we can consider the case with pure matter, where the matter is a collection of heavy particles sitting at fixed coordinate locations in the FRW description. In this case, the CFT description involves the insertion of heavy CFT operators as specific locations on the sphere corresponding to the endpoints of the geodesics in the Euclidean picture, similar to the construction of shells of matter in [119, 120]. In order that the desired Euclidean solution provides the dominant saddle of the CFT path integral with such

insertions, it may be necessary to consider an ensemble of such insertions with a certain degree of correlation between the insertions on the two sides of the sphere. We discuss this in more detail in Section 4.5.

RT surface probes

If a bubble geometry does have a valid CFT state, it is interesting to ask how we can probe the cosmological region inside the bubble using CFT quantities. We study this question in Section 4.6. The spherical boundary at a given time is contractible in the bulk geometry, so the entanglement wedge of the boundary is the entire spacetime. This suggests that reconstruction is possible in principle. However, in the cases where the cosmology is entirely behind the black hole horizon, the horizon provides a non-minimal extremal surface for the full boundary. In this case, the cosmology is in a "Python's lunch," and the general arguments of [121] suggest that accessing the cosmology from the CFT state will be exponentially complex. We give a precise condition for when this occurs (equation (4.20)). We also investigate the behavior of RT surfaces for ball-shaped regions in the CFT to gain insight into how much of the cosmological region is encoded in proper subsystems of the boundary.

Even if the cosmology is fully behind the horizon in a Python's lunch, if there is a Euclidean construction of the state as described above, we should be able to use this Euclidean picture in order to calculate cosmological observables in a straightforward way. Thus, extracting the physics from the underlying CFT physics can be simple even if the extraction from the Lorentzian CFT state is complex.

Relation to earlier work

Describing cosmology as a bubble in AdS was considered previously in [112], where the authors described solutions with a bubble of de Sitter spacetime embedded in AdS with thin constant tension bubble wall. Though there is no problem in constructing the solutions, it is unclear whether these geometries are dual to legitimate CFT states. In particular, [118] found evidence that these solutions cannot arise from a Euclidean path integral construction of states since the domain walls appearing in the Lorentzian geometries are badly-behaved in the Euclidean continuation.

In [1, 118], the authors considered bubbles of vacuum AdS in exterior asymptotically AdS spacetimes with a different cosmological constant. In this case, the solutions often do have sensible Euclidean continuations, suggesting a Euclidean path integral construction of the states that involves an interface between CFTs. These can be viewed as constructions of bubbles of a trivial cosmology.

4.2 Spherical Bubbles of Cosmology

In this section, we construct a family of solutions with an interior region that is a bubble of FRW cosmology separated by a thin domain wall from an exterior region that is a portion of an AdS-Schwarzschild black hole spacetime. The cosmology will containing a negative cosmological constant $\Lambda < 0$, radiation, and matter. We will assume that the cosmological constant is the same throughout the spacetime, taking $\Lambda = -3/\ell_{\text{AdS}}^2$, and working in units where $\ell_{\text{AdS}} = 1$. The negative cosmological constant ensures that the bubble is a big-bang / big-crunch cosmology. We will also assume that the domain wall is comoving when viewed from the cosmology. This will require the domain wall to contain dust / non-relativistic matter.

Inside the bubble, we have an FRW metric

$$ds^2 = -dt^2 + a^2(t)\left(dr^2 + R_K(r)^2(d\theta^2 + \sin^2\theta d\phi^2)\right) \quad R_K(r) = \begin{cases} \sin(\sqrt{K}r)/\sqrt{K} & K > 0 \\ r & K = 0 \\ \sinh(\sqrt{|K|}r)/\sqrt{|K|} & K < 0 \end{cases} \tag{4.2}$$

where the scale factor $a(t)$ is taken to be dimensionless and K is the Gaussian curvature of the spatial slices. The scale factor satisfies the Friedmann equation

$$\left(\frac{\dot{a}}{a}\right)^2 = \frac{\rho_M}{a^3} + \frac{\rho_R}{a^4} - \frac{K}{a^2} - 1 \,, \tag{4.3}$$

where a dot denotes a t derivative. As the Universe expands, the matter and radiation dilute so eventually there is a time where $\dot{a} = 0$, after which the Universe contracts to a big crunch. The full solutions are time-reversal symmetric about this recollapse point. Without loss of generality, we will define this time to be $t = 0$ and choose $a(0) = 1$. In this case, ρ_R and ρ_M represent the radiation and matter densities at $t = 0$ as a fraction/multiple of the "critical" energy density $3/(8\pi G\ell_{\text{AdS}}^2)$ for a flat cosmology. The Friedmann equation at $t = 0$ gives

$$K = \rho_M + \rho_R - 1 \tag{4.4}$$

so the spatial curvature at the time-symmetric slice is fixed in terms of the matter and radiation densities. For empty AdS, we get $K = -1$ as expected.

We assume that the space outside of the ball is empty and spherically symmetric, so by Birkhoff's theorem, the domain of dependence of the exterior of the ball must be a part of the maximally extended Schwarzschild-AdS geometry. We can use Schwarzchild coordinates

$$dS^2 = -F(R)dT^2 + \frac{dR^2}{F(R)} + R^2(d\theta^2 + \sin^2\theta d\phi^2) \,, \tag{4.5}$$

to describe the various patches of that geometry, where

$$F(R) = R^2 + 1 - \frac{\mu}{R} \,. \tag{4.6}$$

Here, μ is related to the mass of the black hole by $\mu = 2MG_N$. Defining the horizon radius by $F(R_H) = 0$, we have that the past and future wedges are described using coordinates in the range $R \in (0, R_H), T \in (-\infty, \infty)$ (where $R = 0$ represents the past/future singularity), while the left and right wedges are described using coordinates in the range $R \in (R_H, \infty), T \in (-\infty, \infty)$ (Figure 4.3).

In our ansatz, the surface of the bubble is assumed to be comoving with respect to the FRW interior, so it has fixed coordinate radius $r(t) = r_0$. It is natural to use the FRW coordinates (t, θ, ϕ) to parameterize the bubble surface in the FRW spacetime. The intrinsic metric on the bubble is then

$$ds^2 = -dt^2 + a^2(t)R_K(r_0)^2 d\Omega_2^2 \,. \tag{4.7}$$

We will consider a shell of dust / non-relativistic matter living on the bubble. This can be described via the stress-energy tensor

$$8\pi G_N S^t{}_t = -\frac{\rho_s}{a(t)^2} \,.$$

Note that the energy density dilutes as $1/a^2$ since the bubble is 2+1 dimensional.

We require that the Israel junction conditions (3.8) and (3.9) be satisfied for the bubble. As we discussed in the last Chapter, the first junction condition requires that the induced metric from

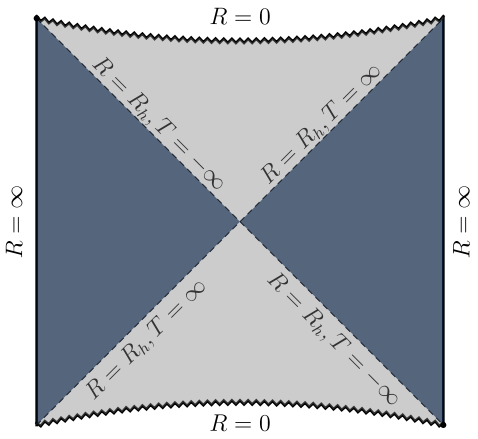

Figure 4.3: Penrose diagram of a maximally extended AdS Schwarzschild black hole.

the exterior spacetime agrees with the induced metric (4.7) from the interior spacetime. Thus, the trajectory of the bubble in the exterior spacetime can be described as $(R(t), T(t))$ where we require that

$$R(t) = a(t)R_K(r_0) \qquad\qquad F(R(t))\dot{T}^2 - \frac{\dot{R}^2}{F(R(t))} = 1 \tag{4.8}$$

The second junction condition requires that the difference of extrinsic curvatures between the interior and exterior spacetimes is determined by the surface stress-energy tensor as

$$K^{\text{in}}_{ab} - K^{\text{out}}_{ab} = 8\pi G_N(S_{ab} - \frac{1}{2}h_{ab}S) \tag{4.9}$$

where $K_{ab} = \nabla_\mu n_\nu e^\mu_a e^\nu_b$, and n is a unit normal vector to the surface in the relevant spacetime, chosen to point outward (away from the FRW interior) in both cases. In the FRW geometry, we can describe an outward pointing unit normal vector to the surface as

$$n_\mu = (0, a(t), 0, 0) \ .$$

From this, we find that the extrinsic curvature has non-zero components

$$K^\theta{}_\theta = -h^{\theta\theta}\Gamma^r_{\theta\theta}n_r = \frac{1}{2}g^{rr}\partial_r g_{\theta\theta}n_r = \frac{R'_K(r_0)}{R_K(r)a(t)} \tag{4.10}$$

$$K^\phi{}_\phi = -h^{\phi\phi}\Gamma^r_{\phi\phi}n_r = \frac{1}{2}g^{rr}\partial_r g_{\phi\phi}n_r = \frac{R'_K(r_0)}{R_K(r)a(t)} \tag{4.11}$$

$$\tag{4.12}$$

In the Schwarzschild geometry near the $t = 0$ slice, the outward pointing unit normal vector to the surface is

$$n_\mu = \epsilon(-\dot{R}, \dot{T}, 0, 0) \ .$$

where $\epsilon = 1$ if the n is outside the Schwarzschild horizon pointing towards the asymptotic region, and $\epsilon = -1$ if n is inside the Schwarzschild horizon pointing outward (i.e. if the bubble is completely inside the horizon). In this case, we can write the non-zero components of the extrinsic curvature as

$$K^\theta{}_\theta = K^\phi{}_\phi = \frac{\beta}{R_K(r_0)a(t)} \qquad K^t{}_t = \frac{\dot{\beta}}{R_K(r_0)\dot{a}(t)} \qquad \beta \equiv \epsilon\sqrt{F[a(t)R_K(r_0)] + R_K(r_0)^2\dot{a}^2(t)} \ . \tag{4.13}$$

We are now ready to write the second junction condition. The ${}^{\phi}{}_{\phi}$ and ${}^{\theta}{}_{\theta}$ components of (4.9) give

$$\frac{R'_K(r_0)}{R_K(r_0)a(t)} - \frac{\beta}{R_K(r_0)a(t)} = \frac{1}{2}\frac{\rho_S}{a^2(t)}. \tag{4.14}$$

The ${}^{t}{}_{t}$ component gives

$$-\frac{\dot{\beta}}{R_K(r_0)\dot{a}(t)} = -\frac{1}{2}\frac{\rho_S}{a^2(t)}.$$

We can check that this is satisfied provided that (4.14) is satisfied by solving for β and differentiating. Thus, we will have a solution provided that

$$\epsilon\sqrt{F[a(t)R_K(r_0)] + R_K^2(r_0)\dot{a}^2} = R'_K(r_0) - \frac{1}{2}\frac{\rho_S R_K(r_0)}{a(t)}\ . \tag{4.15}$$

Squaring this, and substituting the explicit expression for F from (4.6) and the result for $\dot{a}^2$ from the Friedmann equation (4.3), we find the equation holds only if

$$\begin{aligned} \rho_S &= 2\sqrt{\rho_R} \\ \mu &= R_K^3(r_0)\rho_M + 2\sqrt{\rho_R}R_K^2(r_0)R'_K(r_0) \end{aligned} \tag{4.16}$$

where we recall that r_0 is the proper distance from the middle of the bubble to the bubble wall at $t = 0$ and $R_0 \equiv R_K(r_0)$ is the proper bubble wall (areal) radius at $t = 0$. The first equation shows that there is a particular density ρ_S of dust on the shell that is required to "contain" the cosmology. If there is no radiation, this density goes to zero; the resulting solution (described earlier in [122]) is an AdS version of the Oppenheimer-Snyder solution for the collapse of a uniform ball of dust in Minkowski space.

Mass and horizon radius of the black hole

The second equation above gives the mass parameter of the black hole in terms of the ball radius and the matter and radiation densities inside.[24] We can also relate the black hole horizon radius to these parameters using the relation

$$\mu = R_H(R_H^2 + 1)\ . \tag{4.17}$$

We can express the result for the mass completely in terms of ρ_M, ρ_R, and R_0 using

$$R'_K(r_0) = \pm\sqrt{1 - KR_0^2} = \pm\sqrt{1 - R_0^2(\rho_M + \rho_R - 1)} \tag{4.18}$$

where the minus sign corresponds to the case where the curvature is positive ($K = \rho_R + \rho_M - 1 > 0$) and the bubble includes more than half of the full sphere, $r_0\sqrt{K} > \pi/2$. Thus

$$\mu = R_H(R_H^2 + 1) = R_0^3\rho_M \pm 2\sqrt{\rho_R}R_0^2\sqrt{1 - R_0^2(\rho_M + \rho_R - 1)}\ . \tag{4.19}$$

In the positive curvature case where we have more than half of the sphere, there is a restriction $R_0 > 2\sqrt{\rho_R}/\sqrt{(\rho_M + 2\rho_R)^2 - 4\rho_R}$ in order that the black hole has positive mass.[25] We can check that $R_0 > R_H$ in all cases, which is required since R_H is the smallest sphere radius on the $T = 0$ slice of the Schwarzchild geometry. To see this it is sufficient to check the sign of $F(R_0)$. Using the black hole mass from Eq. (4.16), we see $F(R_0) = (\sqrt{\rho_R}R_0 + R'_K(r_0))^2$ which is positive, implying $R_0 > R_H$.

[24] Using $\mu = 2MG$ and the relationship between ρ_M and ρ_S to the physical energy densities, we see that when $K = 0$ this equation says that the black hole mass is precisely equal to the energy of the dust inside the bubble plus the energy of the dust on the bubble. Since dust energy does not redshift, this is true at any time slice.

[25] It is interesting that as this critical value of of R_0 is approached from above, the solution degenerates into two disconnected parts, the exterior spacetime becoming pure AdS and the interior spacetime becoming a closed Universe with a bubble of FRW spacetime glued together with a bubble of pure AdS spacetime.

Condition for bubbles behind the horizon

The bubble cosmology will be completely behind the black hole horizon if and only if $\epsilon < 0$. Considering Equation (4.15) at $t = 0$, we see that this is equivalent to

$$\frac{R'_K(r_0)}{R_K(r_0)} < \sqrt{\rho_R}\,. \tag{4.20}$$

This will be true if and only if

$$\rho_M + 2\rho_R > 1 \qquad \text{and} \qquad r_0 > r_c$$

where r_c is the smallest value of r_0 such that

$$R_K(r_0) = 1/\sqrt{2\rho_R + \rho_M - 1}\,.$$

Condition for a complete causal patch

If we want the cosmology to contain the entire causal patch of a comoving observer, we require that $r_0 > r_{\text{obs}}$, where r_{obs} is the proper radius at $t = 0$ of the forward light cone of a point on the big bang singularity. This light cone is described by a trajectory with $dt = a(t)dr$. Expressing dt in terms of da using the Friedmann equation, we have

$$r_{\text{obs}} = \int_0^1 \frac{da}{\sqrt{\rho_M a + \rho_R - a^4 - (\rho_M + \rho_R - 1)a^2}}\,. \tag{4.21}$$

Full Lorentzian solutions

Since the bubble wall follows a comoving trajectory (by construction) in the FRW region, the bubble geometry exists for finite proper time, starting from zero size at the big bang singularity in the past and ending at zero size at the big crunch singularity. In the Schwarzchild geometry, the bubble wall trajectory must also be timelike, with finite proper time, and from this perspective the interpretation is that the bubble starts at the past singularity of the black hole and ends at the future singularity of the black hole. If the bubble starts outside the horizon, it must cross the horizon at some finite proper time. If the bubble starts inside the horizon, it remains inside the black hole at all times. The causal structures of the full Lorentzian solutions are depicted in Figure (4.4).

4.2.1 Examples

It will be useful to have some explicit examples.

Pure radiation

For pure radiation, we can solve the Friedmann equation explicitly to find

$$a(t) = \sqrt{(1 + \rho_R)\cos^2(t) - \rho_R} \qquad \text{pure radiation.} \tag{4.22}$$

The spatial curvature is $K = \rho_R - 1$, so $\rho_R = 1$ gives the special case of flat cosmology, where $a(t) = \sqrt{\cos(2t)}$.

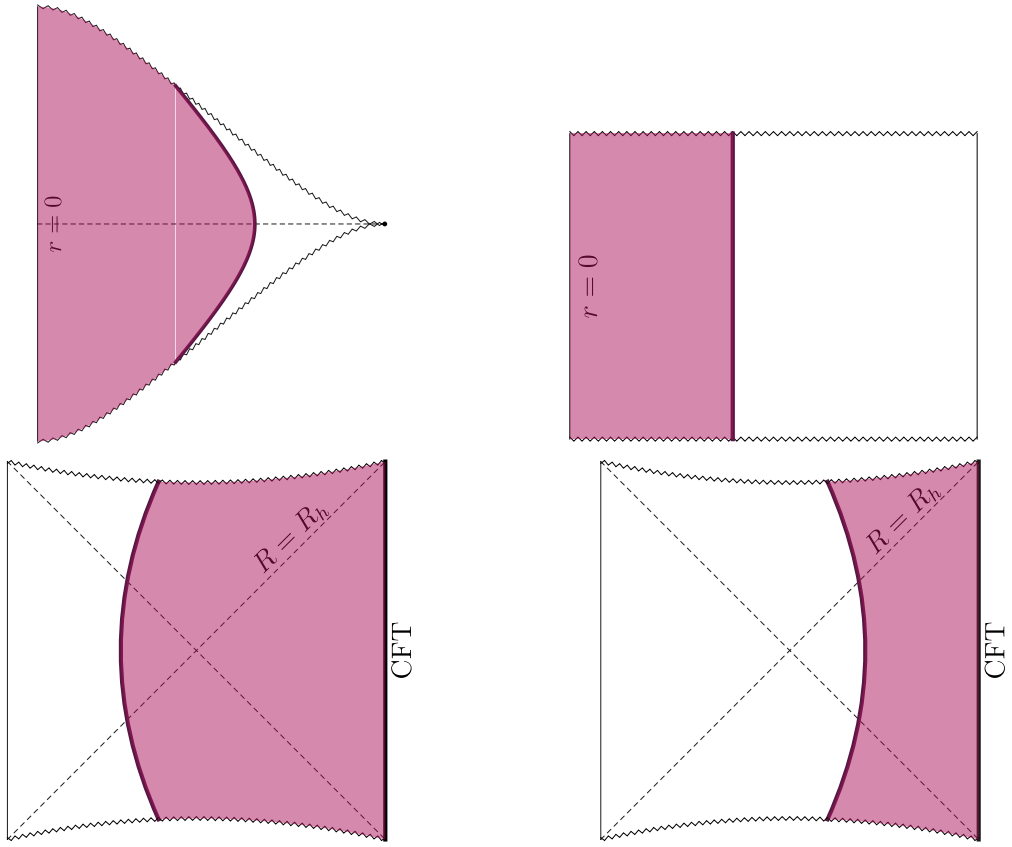

Figure 4.4: Lorentzian spacetime diagrams for solutions with an FRW bubble inside a Schwarzschild geometry. Top: shaded regions indicate spherical bubble of flat/open (left) and closed (right) $\Lambda < 0$ FRW cosmology, bounded by a comoving domain wall. The jagged lines represent big-bang / big-crunch singularities. Bottom: these bubbles are patched on part of an AdS-Schwarzschild spacetime indicated by the shaded region. The bubble may be completely inside the horizon (left) or begin outside the horizon (right). The jagged lines correspond to black hole singularities.

From (4.21), we find that the size of a bubble corresponding to the causal diamond of a single observer is[26]

$$r_{\rm obs} = \frac{1}{\sqrt{\rho_R+1}} K\left(\frac{1}{\sqrt{\rho_R+1}}\right) \qquad \text{pure radiation.} \tag{4.23}$$

In the flat case $\rho_R = 1$, we have

$$r_{\rm obs} = \sqrt{\pi}\Gamma(5/4)/\Gamma(1/4) \approx 1.311 \qquad \text{flat, pure radiation .}$$

Pure matter

For bubbles of pure matter cosmology, the black hole mass parameter μ is simply

$$\mu = R_0^3 \rho_M. \tag{4.24}$$

In the flat case, this equal to the total mass of matter inside the bubble.

For a flat cosmology with pure matter, we have $\rho_M = 1$ and the Friedmann equation can be solved explicitly to give

$$a(t) = \cos^{\frac{2}{3}}\left(\frac{3}{2}t\right) \qquad \text{flat, pure matter.} \tag{4.25}$$

Here, the proper radius of the causal patch accessible to a single observer is

$$r_{\rm obs} = 2\sqrt{\pi}\Gamma(7/6)/\Gamma(2/3) \approx 2.43 \qquad \text{flat, pure matter .}$$

4.3 Thermodynamics

We have seen that it is possible to construct a solution for which a bubble of $\Lambda < 0$ cosmology with arbitrary matter and radiation densities and arbitrary size is embedded in an asymptotically AdS Schwarzchild geometry. We would like to understand whether such solutions can correspond to legitimate states of a CFT.

An initial worry is a sharp version of the well-known bag-of-gold puzzle. For cosmologies with radiation, we can calculate the entropy of this radiation and compare it with the Bekenstein-Hawking entropy of the black hole that contains the cosmological bubble. If the black hole entropy is smaller, then the putative dual CFT cannot accommodate all of the states of the radiation as independent states. It's still possible that these bulk states are encoded non-isometrically; this would imply that certain cosmological bubble states can be expressed as linear combinations of other such states.

The Bekenstein-Hawking entropy of the black hole is

$$S_{BH} = \frac{A_H}{4G_N} = \frac{\pi R_H^2}{G_N} \ . \tag{4.26}$$

Below, it will also be useful to have the black hole temperature and energy

$$T = \frac{1+3R_H^2}{4\pi R_H} \qquad E = \frac{1}{2G_N}(R_H + R_H^3) \ . \tag{4.27}$$

The volume of the bubble of cosmology can be calculated as

$$V_K(r_0) = \int_0^{r_0} 4\pi R_K^2(r) dr = \begin{cases} \pi K^{-\frac{3}{2}}\left(2r_0\sqrt{K} - \sin(2r_0\sqrt{K})\right), & K > 0; \\ \frac{4}{3}\pi r_0^3, & K = 0; \\ \pi|K|^{-\frac{3}{2}}\left(\sinh(2r_0\sqrt{|K|}) - 2r_0\sqrt{|K|}\right), & K < 0. \end{cases} \tag{4.28}$$

[26]Here $K(x)$ is the elliptic integral that approaches $\pi/2$ for small x and $\ln(8/(1-x))/2$ as $x \to 1$.

Assuming an order one number of light fields in the cosmology and ignoring factors of order one, the entropy density s of radiation is related to the energy density u by $s \sim u^{3/4}$. We defined ρ_R as $8\pi G_N/3$ times the energy density, so the entropy of radiation is

$$S_{\rm rad} \sim V \left(\frac{\rho_R}{G_N}\right)^{\frac{3}{4}} .$$

If r_0, ρ_M, and ρ_R are all of the scale set by the cosmological constant, the black hole entropy will be much larger, $S_{\rm BH}/S_{\rm rad} \sim \sqrt{\ell_{\rm AdS}/\ell_P} \gg 1$. In particular, this will hold for bubbles containing the full region accessible to a single observer, but also much larger bubbles that are not parametrically larger.[27]

If we consider bubbles much larger than the cosmological scale (for the $K \leq 0$ cases), we have for $K < 0$ that

$$R_H \approx R_0 \left(\rho_M + 2\sqrt{\rho_R(1-\rho_M-\rho_R)}\right)^{\frac{1}{3}} .$$

In this negatively curved case, the volume behaves for large R_0 like $R_0^2/\sqrt{|K|}$, so the black hole entropy and the radiation entropy both scale as R_0^2 for large R_0. In this case, the black hole entropy remains larger than the radiation entropy by a factor of $\sqrt{\ell_{\rm AdS}/\ell_P}$ for bubbles of all size.

In the flat case, we can have sufficiently large bubbles such that an entropy puzzle arises. Here, for large R_0, we have $V \sim R_0^3$. If there is matter, we find for large R_0 that

$$R_H \approx R_0 \rho_M^{\frac{1}{3}}$$

and the entropy of the radiation becomes larger than the black hole entropy when

$$\frac{R_0}{\ell_{\rm AdS}} \gtrsim \frac{\rho_M^{\frac{2}{3}}}{\rho_R^{\frac{3}{4}}} \sqrt{\frac{\ell_{\rm AdS}}{\ell_P}} .$$

For a flat Universe with radiation only, we have for large R_0 that

$$R_H \approx R_0^{\frac{2}{3}} \rho_R^{\frac{1}{6}}$$

In this case the entropy of the radiation will exceed the black hole entropy when

$$\frac{R_0}{\ell_{\rm AdS}} \gtrsim \left(\frac{\ell_{\rm AdS}}{\ell_P}\right)^{\frac{3}{10}} . \tag{4.29}$$

Both of these critical bubble sizes would become infinite in the usual large N limit of the CFT where $\ell_{\rm AdS}/\ell_P \to \infty$.

In both of these cases, the geometries would correspond to extremely large CFT energies. In units of the CFT sphere radius, the energies are $E \gtrsim \rho_M^3/\rho_R^{9/4}(\ell_{\rm AdS}/\ell_P)^{7/2}$ in the case with matter and radiation and $E \gtrsim (\ell_{\rm AdS}/\ell_P)^{13/5}$ in the pure radiation case.

In general, we should also expect some interior entropy associated with the matter, but the details of this will depend on the construction. In situations where a significant fraction of the energy density is in radiation, we would expect the matter entropy to be smaller. For pure matter cases, it could be interesting to perform an analysis similar to that of [120], replacing the shells of matter with the approximately uniform ball of matter that we are considering here.

[27] We do have a special case for $K > 0$ when considering bubbles containing more than half of the sphere. Here, the black hole mass and entropy decrease as r_0 increases and go to zero at $R_0 = 2\sqrt{\rho_R}/\sqrt{(\rho_M+2\rho_R)^2-4\rho_R}$. At this point, the spacetime pinches off into pure AdS outside and a disconnected closed Universe with a cosmological bubble joined to a bubble of pure AdS. Here, the cosmology is clearly not described by a dual CFT state.

4.4 Euclidean continuations

We have constructed asymptotically AdS geometries containing a bubble of $\Lambda < 0$ cosmology with arbitrary initial matter densities ρ_M and ρ_R and arbitrary radius r_0 (subject to the constraint of footnote 27 in the positive curvature case). In order to understand better whether these can correspond to some legitimate states of a dual CFT, we will consider in this section the possibility of constructing such states directly via a Euclidean path integral construction. In the previous Chapter we described bubbles of pure AdS (which can be viewed as a trivial FRW cosmology) inside asymptotically AdS spacetimes with a different cosmological constant. On the other hand, [118] found that geometries with a bubble of de Sitter cosmology inside AdS appear not to have a path-integral construction.

Pure global AdS spacetime corresponds to the CFT vacuum state, which can be constructed via the Euclidean path integral on an infinite cylinder $S^2 \times \mathbb{R}$ where the $\mathbb{R}$ direction represents Euclidean time. This CFT path integral corresponds to a gravity path integral whose saddle-point geometry is pure global AdS. By inserting operators or sources into this CFT path integral, we can construct other states. To produce time-reversal invariant Lorentzian geometries, we can choose sources in the Euclidean picture to be symmetric under Euclidean time reversal. The Lorentzian geometry can be obtained by determining the dual Euclidean geometry via the rules of AdS/CFT (where the sources and operator insertions determine the boundary conditions for the Euclidean spacetime) and then performing an analytic continuation $\tau \to it$ of the Euclidean time coordinate, where $t = \tau = 0$ represents the time-reversal / reflection invariant slice.

Since we are starting from a set of Lorentzian geometries, we will try to apply this procedure in reverse, first performing an analytic continuation to Euclidean geometries and then (if these are sensible) looking at the asymptotic behaviour to understand what types of insertions/sources are required in the dual CFT path integral.

FRW part

The FRW part of the spacetime continues to a geometry

$$ds^2 = d\tau^2 + a_E^2(\tau)(dr^2 + R_K(r)d\Omega^2) \tag{4.30}$$

with boundary $r(\tau) = r_0$. Here, the Euclidean scale factor is defined via $a_E(\tau) = a(i\tau)$ and satisfies the analytically continued Friedmann equation

$$\left(\frac{a'}{a}\right)^2 = -\frac{\rho_M}{a^3} - \frac{\rho_R}{a^4} + \frac{K}{a^2} + 1 \equiv H(a)^2 \, . \tag{4.31}$$

In the Euclidean picture, the scale factor grows away from $\tau = 0$ so that the cosmological constant term comes to dominate and we have $a_E(\tau) \sim e^{\pm\tau}$ for $\tau \to \pm\infty$. We thus have asymptotically AdS regions for Euclidean times $\tau \to \pm\infty$; for this reason, this solution is sometimes described as an asymptotically AdS Euclidean wormhole.

Schwarzschild exterior

The exterior region forms a part of the Euclidean AdS-Schwarzschild geometry. This can be described as

$$ds^2 = \frac{dR^2}{F(R)} + F(R)d\mathcal{T}^2 + R^2 d\Omega^2 \qquad F(R) = R^2 + 1 - \frac{\mu}{R} \, , \tag{4.32}$$

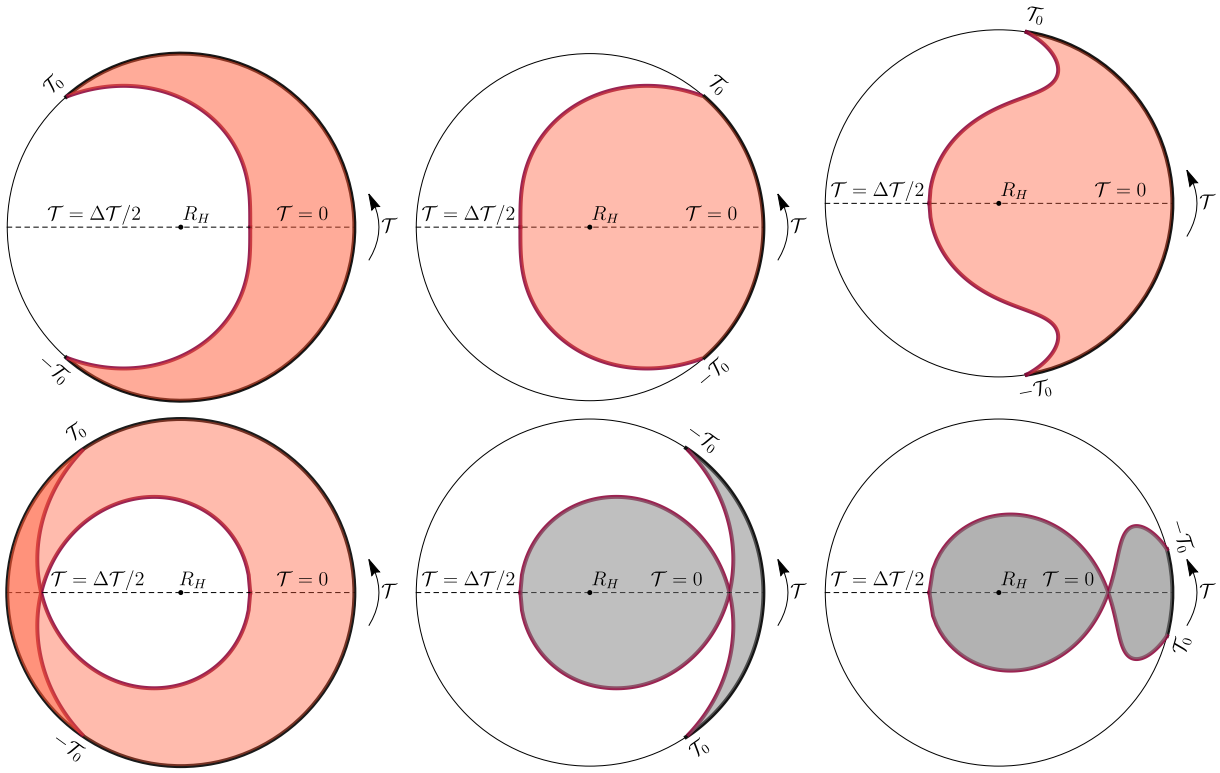

Figure 4.5: Possible domain wall trajectories (thick maroon lines) in the Euclidean Schwarzschild spacetime with the shaded region corresponding to the part that is glued to the Euclidean FRW bubble. The first column corresponds to spacetimes where the domain wall is initially outside the horizon in the Lorentzian solution. In the bottom row, the bubble wall self-intersects (shaded in gray) in the second and third examples and the spacetime is not sensible. The first example on the bottom is sensible as it corresponds to a part of the covering space with $\mathcal{T} \in (-\infty, \infty)$.

with $F(R)$ as before. We have $F(R) = 0$ at $R = R_H$. If this point is part of our solution (required when the bubble is fully inside the black hole), it is necessary that $\mathcal{T}$ is taken to be periodic with period

$$\Delta\mathcal{T} = \frac{4\pi R_H}{1 + 3R_H^2} \tag{4.33}$$

to avoid a conical singularity. Matching the induced metric from the the FRW region with the induced metric from the Schwarzchild region, the bubble trajectory in this Euclidean spacetime must satisfy

$$R(\tau) = a_E(\tau)R_0 \equiv a_E(\tau)R_K(r_0) \qquad \frac{R'(\tau)^2}{F(R(\tau))} + F(R(\tau))(\mathcal{T}'(\tau))^2 = 1 \ , \tag{4.34}$$

the analytically continued version of (4.8). It is convenient to parametrize the trajectories in terms of a_E (which we will write as a going forward). In this case, we have

$$R(a) = R_0 a \qquad \frac{d\mathcal{T}}{da} = \pm\frac{1}{F(R_0 a)aH(a)}\sqrt{F(R_0 a) - R_0^2 a^2 H^2(a)} \tag{4.35}$$

The square root here is precisely the one appearing in the analytically continued version of (4.15), so we can rewrite the $\mathcal{T}$ equation as

$$\frac{d\mathcal{T}}{da} = \frac{1}{F(R_0 a)aH(a)}\left(R_1 - \sqrt{\rho_R}\frac{R_0}{a}\right) \tag{4.36}$$

where $R_1 \equiv R'_K(r_0)$. The expression in brackets is exactly the quantity that is positive if bubble is initially outside the horizon and negative otherwise.

Bubble initially outside horizon

If the bubble is initially outside the black hole horizon, the expression (4.36) is initially positive (when $a = 1$) and therefore positive on the entire trajectory, since $a \geq 1$ in the Euclidean solution. We can take the region $\{\mathcal{T} = 0, R > R_0\}$ of the Schwarzschild geometry as the initial slice for the part of the solution we are keeping (leftmost figures in 4.5). The boundary of the region we keep is determined by solving (4.36).

The $\mathcal{T}$ coordinate increases from 0 to some maximum value $\mathcal{T}_0$ with

$$\mathcal{T}_0 = \int_1^\infty \frac{da}{F(R_0 a)aH(a)}\left(R_1 - \sqrt{\rho_R}\frac{R_0}{a}\right) \tag{4.37}$$

Since the solution in this case does not include the Euclidean horizon (the point $R = R_H$), there is no restriction on how large the range can be (i.e. we do not require $2\mathcal{T}_0 \leq \Delta\mathcal{T}$).

Bubble initially inside horizon

When the cosmological bubble is fully inside the horizon, we can take the region $\{\mathcal{T} = 0\} \cup \{\mathcal{T} = \Delta\mathcal{T}/2, R < R_0\}$ of the Schwarzschild geometry as the initial slice for the part of the solution we are keeping (four figures on the right in 4.5).

In this case, the $\mathcal{T}$ coordinate initially decreases. If $R_1 < 0$ (positive curvature with more than half of the sphere), $\mathcal{T}'$ remains negative for all time. If $R_1 > 0$, $\mathcal{T}'$ will initially be negative, but drops to zero when $a = a_0 \equiv \sqrt{\rho_R}R_0/R_1$ and switches sign afterwards.

In either case, the range of $\mathcal{T}$ on the Euclidean boundary corresponding to the part of the geometry we are keeping is $[-\mathcal{T}_0, \mathcal{T}_0]$

$$\mathcal{T}_0 = \frac{\Delta\mathcal{T}}{2} + \int_1^\infty \frac{da}{F(R_0 a) a H(a)} \left(R_1 - \sqrt{\rho_R} \frac{R_0}{a} \right) . \tag{4.38}$$

For the geometry to make sense, we require that the domain wall is not self-intersecting. In the $R_1 < 0$ case, this requires that $\mathcal{T}_0 > 0$. In the other case when $\mathcal{T}'$ switches sign at $a = a_0$, we require that

$$\frac{\Delta\mathcal{T}}{2} + \int_1^{a_0} \frac{da}{F(R_0 a) a H(a)} \left(R_1 - \sqrt{\rho_R} \frac{R_0}{a} \right) > 0 . \tag{4.39}$$

The region of parameter space for which the geometries with the bubble initially inside the horizon have good Euclidean asymptotics (i.e. the domain wall does not self intersect) are shown in Figure 4.6

Exploring these conditions numerically, we find that for $K \leq 0$ where the spatial geometry is infinite, the solutions make sense for arbitrarily large bubbles. For cases with $K > 0$ (positively curved spatial geometry), we find that there is generally some $r_{\rm int}$ above which the boundary self-intersects in the Euclidean solution. As far as we can tell, this is always larger than half the sphere diameter $r_{\rm max} = \pi/\sqrt{K}$ but smaller than the value $r_{\rm pinch}$ at which the exterior black hole mass goes to zero.

For the $K > 0$ case with fixed ρ and $f_R = \rho_R/\rho$ we generally have $0 \leq r_{\rm out} \leq r_{\rm int} \leq r_{\rm pos} \leq r_{\rm max}$, where the cosmological bubble is outside the horizon for $r_0 < r_{\rm out}$, the Euclidean continuation of the solution makes sense (the domain wall does not self-intersect) for $r_0 < r_{\rm int}$, the Lorentzian solution has positive mass if $r_0 < r_{\rm pos}$, and $r_{\rm max} = \pi/\sqrt{K}$ is the maximum value of r corresponding to the sphere diameter. In Figure 4.7, we show the behaviour of $r_{\rm out}/r_{\rm max}$, $r_{\rm int}/r_{\rm max}$, and $r_{\rm pos}/r_{\rm max}$ as a function of ρ for a few different fixed ratios $f_R = \rho_R/\rho$. We note that in all cases, both Euclidean and Lorentzian solutions are sensible if the cosmological bubble includes less that half of the spatial sphere (i.e. $r_0 < \pi/(2\sqrt{K})$.

Arbitrarily large bubbles with $K = 0$

It is possible to show analytically that flat cosmology bubbles always have sensible Euclidean asymptotics, i.e. for any values of r_0, ρ_R, ρ_M satisfying $K = 0$.

As we explained above, if the bubble is initially outside the horizon, the Euclidean solution does not include the point $R = R_H$ and so it is always a sensible geometry.

On the other hand, if the bubble is initially inside the horizon, the solution has good Euclidean asymptotics only if condition (4.39) is satisfied. For $K = 0$ this condition is equivalent to the requirement $f_1(r_0, \rho_R) - f_2(r_0, \rho_R) > 0$, where we define

$$f_1(r_0, \rho_R) \equiv \frac{2\pi R_H}{1 + 3R_H^2} \tag{4.40}$$

$$f_2(r_0, \rho_R) \equiv \int_1^{\sqrt{\rho_R} r_0} da\; g(a, r_0, \rho_R) \tag{4.41}$$

$$g(a, r_0, \rho_R) \equiv -\frac{a\left(a - \sqrt{\rho_R} r_0\right)}{\sqrt{(a-1)\left(a^3 + a^2 + a + \rho_R\right)} \left[a^3 r_0^2 + a + r_0\left((\rho_R - 1) r_0 - 2\sqrt{\rho_R}\right)\right]}. \tag{4.42}$$

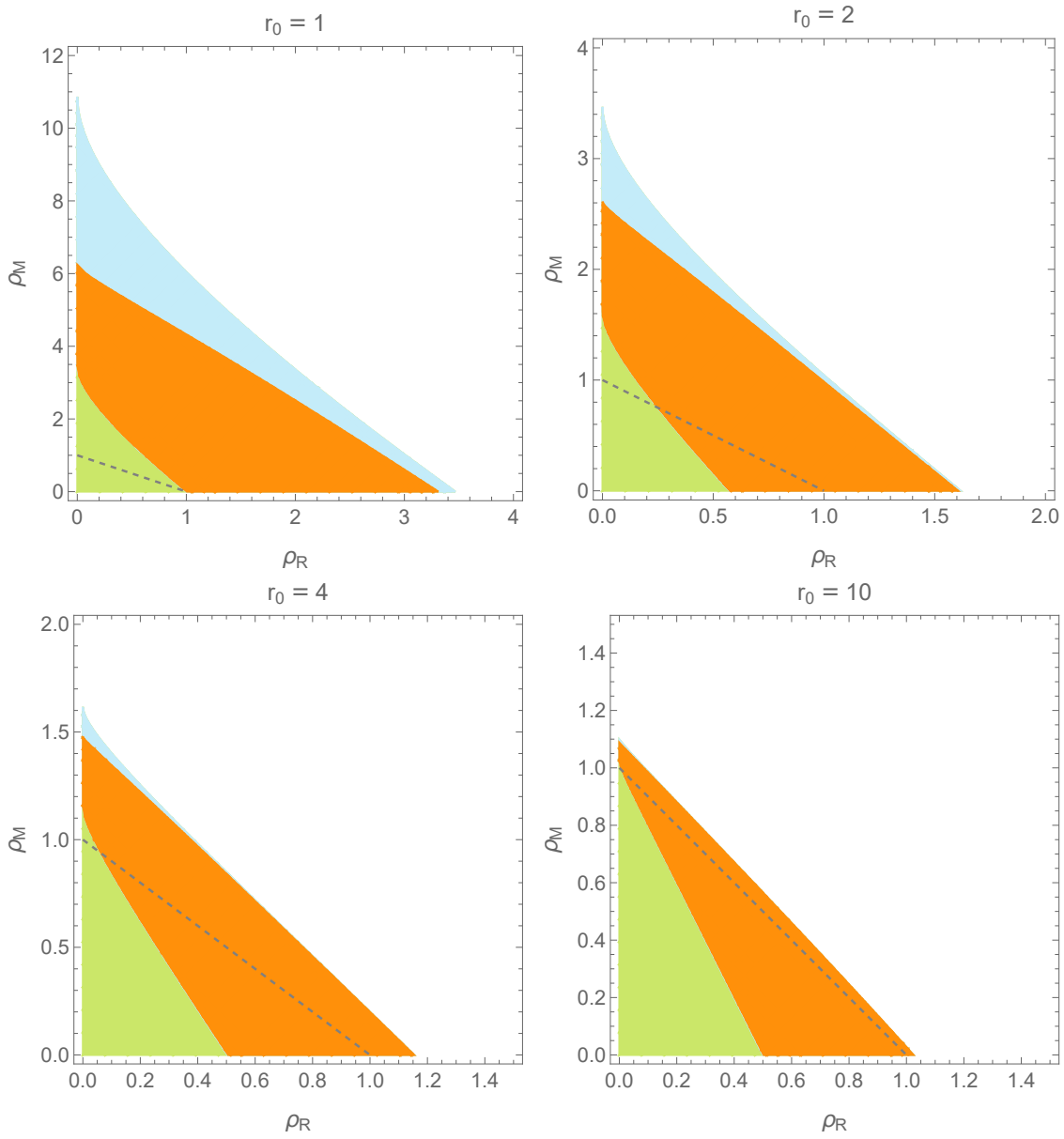

Figure 4.6: Possible bulk solutions as a function of the radiation and matter densities, ρ_{R} and ρ_{M}. The shaded regions are parameter values for which the Lorentzian solution has a positive mass black hole. The orange and green regions correspond to Euclidean solutions in which the domain wall does not self-intersect, while the blue region corresponds to solutions with a self-intersecting domain wall. The cosmological bubble is initially outside the horizon in the green region. The dashed line corresponds to $K = 0$; below it $K < 0$ and above it $K > 0$.

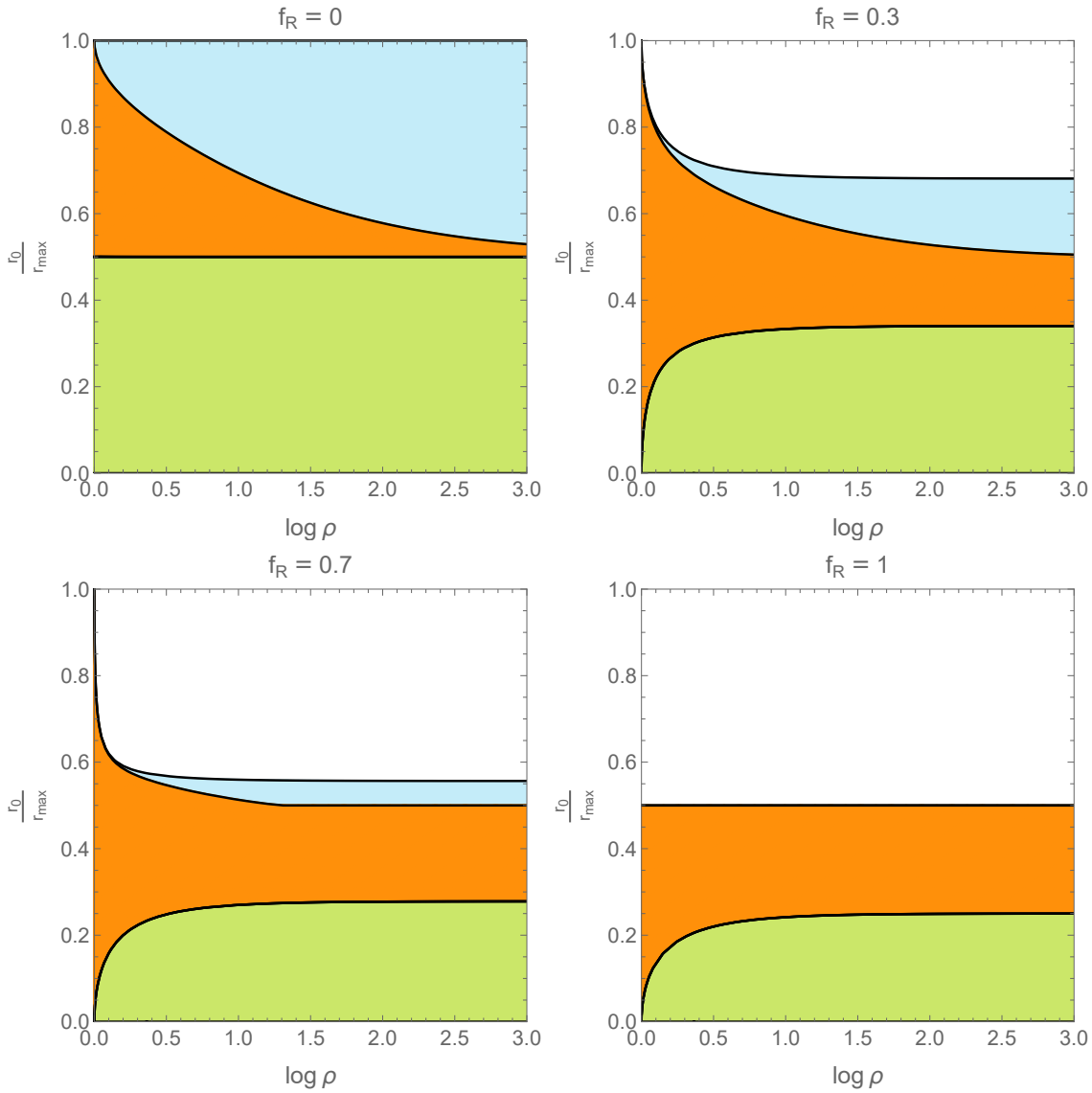

Figure 4.7: Behaviour of $r_{\rm out}/r_{\rm max}$ (green-orange boundary), $r_{\rm int}/r_{\rm max}$ (orange-blue boundary), and $r_{\rm pos}/r_{\rm max}$ (blue-white boundary) with varying $\log\rho$ for fixed $f_R = \rho_R/\rho$ in the $K > 0$ case, where $r_{\rm max} = \pi/\sqrt{K}$ is the sphere diameter. In the shaded regions, the Lorentzian solution has a positive mass black hole. The orange and green regions correspond to Euclidean solutions in which the domain wall does not self-intersect, while the blue region corresponds to solutions with a self-intersecting domain wall. The cosmological bubble is initially outside the horizon in the green region.

We can obtain an analytic upper bound $f_2^{\rm ub}$ of f_2 as follows

$$f_2 \leq f_2^{\rm ub} \equiv -\int_1^{\sqrt{\rho_R} r_0} da\, \frac{a\left(a-\sqrt{\rho_R} r_0\right)}{\sqrt{(a-1)a^3}\left((a-1)\left(3r_0^2+1\right)+\left(\sqrt{\rho_R} r_0-1\right)^2\right)} \tag{4.43}$$

$$= \frac{2}{y}\left(\frac{(x+y-1)\tan^{-1}\left(\sqrt{\frac{y-(x-1)^2}{(x-1)x}}\right)}{\sqrt{y-(x-1)^2}} - \sinh^{-1}\left(\sqrt{x-1}\right)\right), \tag{4.44}$$

where $x \equiv r_0\sqrt{\rho_R}$ and $y \equiv 1+3r_0^2$. Comparing this to the analytic expression for f_1 it is straightforward to check that $f_1(r_0,\rho_R) - f_2(r_0,\rho_R) \geq f_1(r_0,\rho_R) - f_2^{\rm ub}(r_0,\rho_R) > 0$ for all values of r_0 and ρ_R. In particular, for large bubbles, we have

$$\lim_{r_0\to\infty} \frac{f_1}{f_2^{\rm ub}} = \frac{\pi\sqrt{3-\rho_R}}{3(1-\rho_R)^{1/3}\sin^{-1}\left(\frac{\sqrt{3-\rho_R}}{\sqrt{3}}\right)}, \tag{4.45}$$

which is greater than 1 for all values of ρ_R. This shows that geometries containing arbitrarily large bubbles of flat cosmology (with arbitrary matter to radiation density) have sensible Euclidean analytic continuations. It is interesting that we apparently have a Euclidean construction even for the extremely large flat bubbles where an entropy puzzle arises; in this case it would appear that any possible encoding of the possible states of the cosmological spacetime into the CFT would have to be non-isometric.

4.5 CFT construction

In cases where we have a sensible Euclidean construction, we can look at the asymptotics of this solution to understand the properties of a potential CFT dual construction.

For the Schwarzschild part of the geometry, the asymptotic solution behaves as

$$ds^2 = \frac{1}{Z^2}\left(dZ^2 + d\mathcal{T}^2 + d\Omega^2\right), \tag{4.46}$$

where we have defined $Z = 1/R$. From this metric in Fefferman-Graham form, we can see that the boundary metric is conformal to part of a cylinder

$$ds^2 = d\mathcal{T}^2 + d\Omega^2 \qquad\qquad \mathcal{T} \in [-\mathcal{T}_0, \mathcal{T}_0]\,. \tag{4.47}$$

The part of the Euclidean solution corresponding to the FRW regions has two asymptotic regions. We can represent the geometry of each of these in Fefferman-Graham form as

$$ds^2 = \frac{1}{z^2}\left(dz^2 + z_0^2(dr^2 + R_K^2(r)d\Omega^2)\right) \tag{4.48}$$

where we have taken $|\tau| = \ln(z_0/z)$ for $\tau \to \pm\infty$. The boundary geometry is then conformal to

$$ds^2 = z_0^2(dr^2 + R_K^2(r)d\Omega^2) \tag{4.49}$$

which has the topology of a ball. Choosing $z_0 = 1/R_K(r_0)$ makes the S^2 at the boundary of this ball of unit radius so that the two balls corresponding to the two asymptotic regions of the Euclidean FRW geometry can be glued in to the two boundaries of the cylinder (4.47). Thus, the full boundary geometry has the topology of a sphere. By a conformal transformation, this can be mapped to an infinite cylinder.

Constructing matter cosmologies by operator insertion

As a simple case, we can consider the situation where there is no radiation and the matter is made up of heavy particles travelling along geodesics specified by fixed (r, θ, ϕ) in the FRW spacetime. In the Euclidean picture, these geodesics continue to spatial geodesics, also at fixed (r, θ, ϕ) extending between the two asymptotic regions. These particles can be obtained via the insertion of heavy operators in the CFT, similar to the construction of shells of matter in [119, 120].

If we consider particles of mass $m \gg 1/\ell_{\text{AdS}}$ in the bulk, the total number of these particles is

$$n = \frac{3}{8\pi G \ell_{\text{AdS}}^2} \frac{\rho_M V_K(r_0)}{m} \tag{4.50}$$

where $V_K(r_0)$ is the proper volume of the FRW bubble given in (4.28). For the CFT construction, we thus insert n scalar operators with dimension

$$\Delta \approx m\ell_{\text{AdS}} \tag{4.51}$$

uniformly on the boundary geometries (4.49) associated with two asymptotic regions of the Euclidean FRW spacetime. Of course, we need to pick specific locations for these operators, but we can also imagine some ensemble of such insertion locations, so that the resulting state would be a mixed state corresponding to an ensemble of cosmologies with the matter particles in some ensemble of locations. In order to achieve an approximately uniform matter distribution, we can take the number of operators to be large while still requiring the corresponding operators to be heavy. This gives:

$$1 \ll m\ell_{\text{AdS}} \ll \left(\frac{\ell_{\text{AdS}}}{\ell_P}\right)^2 , \tag{4.52}$$

assuming that r_0 is of order ℓ_{AdS}.

When considering a CFT path integral with operator insertions suggested by a certain Euclidean solution, it is important to understand whether the Euclidean solution of interest is actually the dominant saddle corresponding to that path integral. Otherwise, leading order calculations based on the CFT path integral might correspond to some other geometry that dominates the gravitational path integral. For the construction with the insertion of heavy operators, we are interested in a dual solution with Euclidean particle trajectories connecting the two ends of the wormhole. For these to be favoured over other solutions (e.g. where the geodesics connect operator insertions on the same side of the wormhole), it may be necessary to assume a correlated insertion of operators on the two sides (e.g. to consider a sum $\sum_i p_i \mathcal{O}_i(x_+)\mathcal{O}_i(x_-)$) where x_+ and x_- correspond to the two ends of a geodesic, rather than just a single insertion $\mathcal{O}(x_+)\mathcal{O}_i(x_-)$ (see Figure 4.8 for a schematic picture). We plan to discuss this in more detail in a forthcoming publication.

4.6 Probing the cosmology from CFT physics

Given a CFT state describing a bubble of cosmology spacetime, it is interesting to ask how the spacetime can be reconstructed, e.g. to extract cosmological observables.

A first observation is that in all of our spacetimes, the full spatial boundary is homologous to a point, so the entanglement wedge of the boundary is the full spacetime geometry. This suggests that the cosmological physics should be reconstructible in principle from the CFT [123, 124].

On the other hand, reconstruction of black hole interiors in AdS/CFT is famously challenging, and in many cases, most or all of the cosmological region lies behind the black hole horizon. When the states we describe have a Euclidean CFT construction, this should not be a problem.

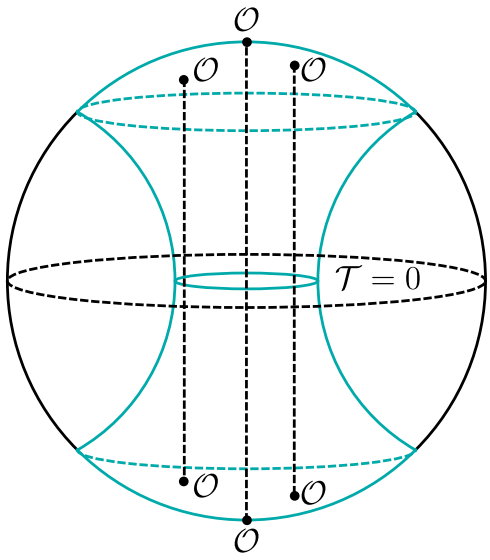

Figure 4.8: Schematic diagram illustrating the preparation of the CFT state using correlated operator insertions in the Euclidean path integral, and the corresponding bulk solution. Operators are inserted in polar regions. Vertical dashed lines correspond to bulk geodesics on which the matter particles live. To achieve the desired connected bulk geometry we may require an ensemble of such insertions.

Working in the Euclidean picture, it should be possible to use standard bulk reconstruction techniques (e.g. HKLL [125, 126]) to calculate observables in the Euclidean geometry. The Lorentzian observables are related to these by analytic continuation.

Now suppose that we don't have a Euclidean construction or we wish to probe the cosmological physics directly from the Lorentzian state. Here, the recently proposed "Python's Lunch" criterion gives a precise suggestion for when the reconstruction will be difficult. According to the conjecture in [121] and [127], the reconstruction of local bulk physics from the Lorentzian CFT state is highly complex when the region of interest lies in a Python's Lunch, that is, behind a non-minimal extremal surface. Our geometries have such a surface precisely when the bubble of cosmology lies completely behind the black hole horizon. In this case, the horizon at the $t = 0$ slice is the non-minimal extremal surface. Spatially, this is a place where the S^2 areas begin to increase in size again as we move inward from the boundary. From our analysis above, the geometry will contain a python's lunch if and only if

$$\rho_M + 2\rho_R > 1 \qquad \text{and} \qquad r_0 > r_c$$

where r_c is the smallest value of r_0 such that

$$R_K(r_0) = 1/\sqrt{2\rho_R + \rho_M - 1}\,.$$

In other cases, reconstruction of the entire spacetime should be simple; according to [127] it can be accomplished by a combination of HKLL, the application of various Lorentzian sources and forward and backward evolution with the CFT Hamiltonian.

Probing with Ryu-Takayanagi surfaces

In order to understand further how the cosmological spacetime is encoded in the boundary CFT state, it is useful to understand the Ryu-Takayanagi surfaces corresponding to various spatial sub-

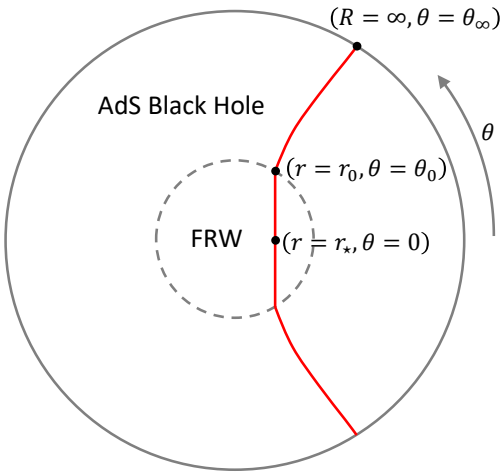

Figure 4.9: Schematic plot of an extremal surface (red) at the time symmetric slice which probes the FRW region of the spacetime.

systems of the boundary. These surfaces can indicate the extent of the entanglement wedge of a boundary spatial region of the CFT. The entanglement entropies of the boundary regions (suitably regularized e.g. by vacuum subtraction) also provide direct geometrical information about the interior via the usual Ryu-Takayanagi formula.

We will focus on ball-shaped sub-regions B of the $T = 0$ spatial slice of the boundary spacetime. We can choose angular coordinates so that $\theta = 0$ is the centre of the ball and the boundary of B is $\theta = \theta_\infty$; see Figure 4.9. By the time-reversal and spherical symmetries of the bulk spacetime, the Ryu-Takayanagi surface is expected to lie on the time-symmetric slice in the bulk and preserve the rotational symmetry that leaves B invariant. We can describe the RT surface trajectory as $R(\theta)$ in the Schwarzschild region and $r(\theta)$ in the cosmological region (if the surface extends into the bubble). In cases where the cosmology is completely inside the horizon, we need to consider separate Schwarzchild coordinate patches corresponding to the exterior region and the region past the horizon but outside the bubble.

The RT surface is the surface homologous to B that minimizes the area functional. The area functional may have multiple extremal surfaces homologous to B, in which case we need to compare the areas. It is convenient to parametrize the extremal surfaces by the location of their deepest point in the bulk (e.g. the distance r_* from the centre of the bubble), where $dr/d\theta = 0$ or $dR/d\theta = 0$. There will be a unique extremal surface for each such point, and we can integrate the extremal surface equations (below) to find the asymptotic behavior of this extremal surface. This gives some function $\theta_\infty(r_*)$, as schematically shown in Figure 4.9.

When the surface lies entirely in the Schwarzschild exterior region, the area functional is

$$\Sigma(B) = 2\pi \int_{R_*}^{\infty} R \sin\theta \sqrt{R^2 d\theta^2 + \frac{dR^2}{F(R)}} \,,$$

where we can take $\theta(R)$ or $R(\theta)$. When r_* corresponds to a point in the FRW region, we have

(assuming that the bubble is initially outside the horizon)

$$\begin{aligned}\Sigma(B) =&2\pi\int_{r_*}^{r_0} dr R_K(r)\sin\theta_-(r)\sqrt{R_K^2(r)(\theta'_-(r))^2+1}\\ &+2\pi\int_{R_K(r_0)}^{\infty} dR R\sin\theta_+(R)\sqrt{R^2(\theta'_+(R))^2+\frac{1}{F(R)}}\,.\end{aligned}$$

where $\theta_-(r)$ and $\theta_+(R)$ parameterize the surface in the FRW and Schwarzschild regions respectively. Taking a variation $\theta\to\theta+\delta\theta$ of this functional with fixed $\theta_+(R=\infty)=\theta_\infty$ and $\theta_-(r_*)=0$, we get

$$\begin{aligned}\delta\Sigma &= 2\pi\int_{r_*}^{r_0}\mathrm{d}r\Big(R_K(r)\cos\theta_-\sqrt{L_-}-\frac{\mathrm{d}}{\mathrm{d}r}\frac{R_K^3(r)\sin\theta_-\theta'_-}{\sqrt{L_-}}\Big)\delta\theta\\ &\quad+2\pi\int_{r_0}^{\infty}\mathrm{d}R\Big(R\cos\theta_+\sqrt{L_+}-\frac{\mathrm{d}}{\mathrm{d}R}\frac{R^3\sin\theta_+\theta'_+}{\sqrt{L_+}}\Big)\delta\theta_+\\ &\quad+\Big[\frac{R_K^3(r)\sin\theta\theta'_-\delta\theta_-}{\sqrt{L_-}}\Big]_{r_0}-\Big[\frac{R^3\sin\theta_+\theta'_+\delta\theta_+}{\sqrt{L_+}}\Big]_{R_K(r_0)}\end{aligned}\tag{4.53}$$

where

$$L_-=R_K(r)^2\theta'_-(r)^2+1,\qquad L_+=R^2\theta'_+(R)^2+\frac{1}{F(R)}\,.\tag{4.54}$$

For the variation to vanish in general, the two integrands must vanish, giving differential equations for $\theta(r)$ and $\theta(R)$ in the FRW and Schwarzchild regions. Furthermore, the variations in the last line must also cancel, giving

$$\frac{\theta'_-(r_0)}{\sqrt{R_0^2(\theta'_-(r_0))^2+1}}=\frac{\theta'_+(R_0)}{\sqrt{R_0^2(\theta'_+(R_0))^2+1/F(R_0)}}\,,\tag{4.55}$$

where we have defined $R_0=R_K(r_0)$. This condition can be simplified to

$$\theta'_-(r_0)=\theta'_+(R_0)\sqrt{F(R_0)}.\tag{4.56}$$

In the FRW region, we have a symmetric space, so it is straightforward to derive an analytic expression for the extremal surfaces. For the surface with closest approach $r=r_*$ to $r=0$ at $\theta=0$, we find[28]

$$\cos(\theta)=\begin{cases}\frac{\tan(r_*\sqrt{K})}{\tan(r\sqrt{K})} & K>0\\ \frac{r_*}{r} & K=0\\ \frac{\tanh(r_*\sqrt{|K|})}{\tanh(r\sqrt{|K|})} & K<0\end{cases}\tag{4.57}$$

To investigate the extremal surfaces starting at some radius r_* in the FRW region, we can use the expressions (4.57) to calculate $\theta_0=\theta_-(r_0)$. The exterior portion of the RT surface can be determined by solving the differential equation for that region with $\theta_+(R_0)=\theta_0$ and $\theta'_+(R_0)$ obtained using (4.55). In cases where two different values of r_* give the same θ_*, we need to compare the areas of the surfaces and choose the one with smaller area.

[28]For positive curvature, we can describe the sphere as $\sum x_i^2=1/K$ in Euclidean space. An extremal surface with closest distance r_* to $(1/\sqrt{K},\vec{0})$ is the plane $\vec{x}\cdot(-\sin(r_*\sqrt{K}),\cos(r_*\sqrt{K}),\vec{0})=0$. The change of variables $x_1=\cos(r\sqrt{K})/\sqrt{K}, x_2=\sin(r\sqrt{K})/\sqrt{K}\cos(\theta)$ maps back to our coordinates, giving the result. The flat and negatively curved results can be obtained by taking K to be zero or negative, respectively.

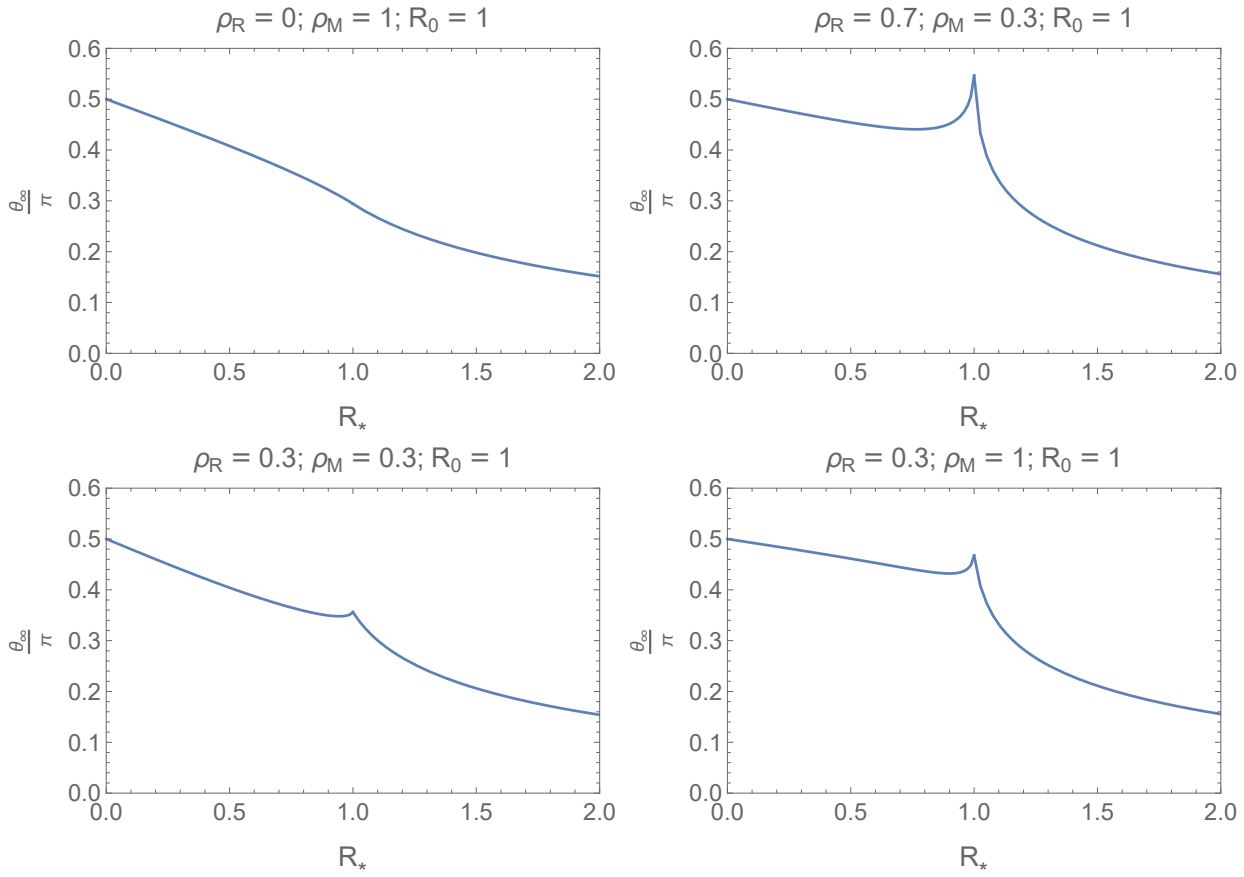

Figure 4.10: Angular size θ_∞ of spherical caps in the CFT, versus the smallest areal radius R_* probed by corresponding extremal surfaces. We see that in some cases a given CFT region (defined by a particular value of θ_∞) corresponds to multiple extremal surfaces. In this case the RT surface is the extremal surface with minimal area.

We show plots of θ_∞ as a function of R_* in Figure 4.10, where we define R_* to be the areal radius corresponding to the deepest point of the extremal surface. In these plots we fix the areal radius of the bubble separating the FRW region from the Schwarzschild region to be $R_0 = 1$. As a result $\theta_\infty(R_*)$ has a discontinuous first derivative at $R_* = 1$. Also notice that in all cases $R_* = 0$ implies $\theta_\infty = \pi/2$, i.e. the extremal surface passing through the centre of the FRW region corresponds to the hemispherical cap of the boundary CFT.

Notice that for some parameter values (e.g. a flat bubble of dust; top left in the figure), θ_∞ is a monotonically decreasing function of R_*. In such cases the function $\theta_\infty(R_*)$ is invertible to $R_*(\theta_\infty)$, and thus there is a unique extremal surface homologous to a CFT cap of a given angular size. By the usual RT prescription this extremal surface must be the RT surface corresponding to the spherical cap. Furthermore, $R_*(\theta_\infty)$ ranges from ∞ to 0 as θ_∞ ranges from 0 to π, and hence the RT surfaces probe all parts of the spacetime, including all parts of the cosmological bubble.

More generically however (remaining plots in Figure 4.10), $\theta_\infty(R_*)$ fails to be monotonic for values of R_* close to R_0. This can occur for spatially flat FRW bubbles (top right), spatially hyperbolic bubbles (bottom left), and spatially spherical bubbles (bottom right). When there are multiple values of R_* which give the same θ_∞, the areas of the surfaces must be compared and the RT surface would correspond to the minimum area extremal surface.

There are two possible manifestations of this non-monotonicity. In the first case when $\theta_\infty(R_0) < \pi/2$ there is some range $\theta_\infty \in (\theta_1, \theta_2)$, with $\theta_1, \theta_2 < \pi/2$ where there are multiple candidate RT surfaces for the same θ_∞. However, for large enough CFT balls, i.e $\theta_2 < \theta_\infty < \pi/2$, there is a unique extremal surface (and hence RT surface) passing through the cosmological region. This is illustrated in the bottom two figures of Figure 4.10.

In the second case the non-monotonicity is more severe, and $\theta_\infty(R_*)$ for $R_* > R_0$ covers the entire range $(0, \pi/2)$. An example of such a case is illustrated in the top right plot in Figure 4.10. In this case surface areas of extremal surfaces would have to be compared in order to check whether any RT surfaces probe the cosmological bubble.

4.7 Discussion

In this Chapter, we have analyzed a family of exact solutions of $\Lambda < 0$ gravitational effective field theories where a comoving bubble of an FRW spacetime is embedded in an exterior spacetime that is Schwarzschild-AdS. We found that for arbitrary matter and radiation densities and an arbitrary bubble size, the two parts of the spacetime can be patched across a thin shell of pressureless matter with density proportional to the square root of the interior radiation density. Physically, we can think of this as some perfectly reflecting dust. This construction appears to be special to 3+1 dimensions; in other dimensions, with both matter and radiation the required domain wall requires more complicated physics. Our choice to consider a domain wall with pressureless dust was purely for convenience; this allowed explicit analytic solutions that we could analyze. Of course, we could have more general solutions where the domain wall is not a thin shell. For example, there should exist a solution with only radiation, where the radiation is initially localized inside a ball-shaped region; while the radiation will spread out, the domain of dependence of the initial ball will still be FRW. In [128], the authors provide numerical evidence for formation of de-Sitter bubbles dynamically by collapse of massless scalar matter in asymptotically AdS spacetime; in many cases with several reflections of the shell of matter off the AdS boundary.

We found some promising signs that these cosmological bubble solutions, in some cases with arbitrarily large radius, can be dual to legitimate CFT states. The entropy of the exterior black hole is larger than the entropy associated with the cosmology except in the flat case for bubbles

parametrically larger than the cosmological scale. The Euclidean continuations of the solutions appear to make sense for almost all cases and suggest a Euclidean CFT construction where operators and/or sources are inserted in ball shaped regions centered at opposite poles of an S^3 on which the CFT lives. We plan to investigate and discuss the Euclidean construction in more detail in a future work.

We note that for a given cosmology, the physics accessible to a single observer can likely be encoded holographically via dual CFT physics in many different ways, with various choices for the physics of the bubble wall and of the exterior spacetime. As we saw in Chapter 3, bubbles of pure AdS spacetime (the trivial $\Lambda < 0$ cosmology) can be described via many different possible dual CFTs by considering specific states of those theories defined by performing a Euclidean quench operation starting from the vacuum state of the CFT dual to the full AdS spacetime. Via a similar quench [67, 129, 130], we can also encode the physics in the state of a collection of many non-interacting quantum systems. Similar constructions should exist for the more general cosmological spacetimes considered here. Thus, there may be many possible ways to holographically encode the physics accessible to a single observer in a cosmological spacetime. It would be interesting to understand if there is some more minimal description that avoids the excess baggage of an asymptotically AdS exterior spacetime.

Finally, let us mention two limitations of the model of quantum cosmology developed in this chapter. First, although the cosmology in our construction is locally homogeneous and isotropic, the presence of the bubble wall means that this is not globally true. Since we can generally make the bubble as large as we like this is not necessarily a problem, but from a Copernican perspective it is nevertheless desirable to have a construction in which the cosmology is fully homogeneous and isotropic. And second, the cosmologies we considered here are not realistic in that they have constant negative vacuum energy and never accelerate. The goal of the following chapters will be to solve these problems.

Chapter 5

Homogeneous cosmology

In the previous chapter we studied a model of quantum cosmology based on AdS/CFT holography. AdS/CFT is only able to provide a direct quantum gravitational description of asymptotically AdS spacetimes, which, aside from a negative cosmological constant, are empty near the asymptotic boundary. To deal with this limitation we were forced to embed a spatially finite bubble of cosmology containing matter and radiation in an otherwise empty spacetime. In the present chapter we will improve upon this construction by using an indirect approach to AdS/CFT to describe homogeneous and isotropic cosmologies with flat spatial slices of infinite extent. Let us summarize how this will work.

Our construction is based on a simple fact which we already observed in the previous chapter, namely that FRW cosmologies with a negative cosmological constant are time-reversal symmetric big-bang/big-crunch cosmologies. This $\mathbb{Z}_2$ time-reversal symmetry ensures that if we analytically continue the time coordinate from real to imaginary values we obtain a Euclidean spacetime with a sensible (real valued) metric. Because of the negative vacuum energy this spacetime turns out to be a two boundary asymptotically AdS Euclidean wormhole. Following a second analytic continuation (this time of a spatial variable) we obtain a traversable Lorentzian AdS wormhole spacetime. Therefore, unlike the original cosmological spacetime, the Lorentzian and Euclidean wormholes both contain asymptotically AdS regions and can thus be described microscopically/quantum mechanically using the standard tools of AdS/CFT holography. Then, by performing a reverse analytic continuation, we can obtain a quantum mechanical description of the spatially infinite cosmological spacetime.

5.1 Introduction

Holographic models from string theory [43, 45–47] have been extremely successful in describing a great variety of quantum gravitational phenomena, including the physics of high-energy scattering processes where gravitational effects are important, the formation, dynamics, and evaporation of black holes, and even the emergence of spacetime and gravitation from intrinsically quantum mechanical phenomena. However, it remains a significant open challenge to find a quantum gravitational description of the physics in cosmological spacetimes like our own Universe.

Cosmology with $\Lambda < 0$

A possible misconception is that the obstruction to describing realistic cosmological physics using holography is that holographic models naturally describe spacetimes with a negative cosmological constant while our own Universe appears to have a positive cosmological constant. However, the observational evidence [131, 132] tells us not that there is a positive cosmological constant, but that the expansion of the Universe is currently accelerating, i.e. that $\ddot{a} > 0$ where a is the scale factor. Einstein's equations then imply that $3p + \rho < 0$ where p and ρ are the pressure and energy density. This could be explained *either* by a positive cosmological constant, *or* by the potential energy associated with time-dependent scalar fields that are currently at a positive value of their

potential [133–135]. While the ΛCDM model with $\Lambda > 0$ provides a good fit to cosmological data, the possibility of $\Lambda < 0$ with time-dependent scalars is not ruled out (see [136–138] for recent discussions). Time-dependent scalars are also natural to consider from an effective field theory point of view since they preserve the same symmetries as an FRW spacetime. In this case, there is no particular reason why the scalars can't be evolving towards a minimum or extremum of the potential with a value (which we can define to be the fundamental cosmological constant in the effective theory) that is zero or negative.

In the absence of current observations that can tell us more definitively whether the fundamental cosmological constant is positive, negative, or zero, we might ask which possibility is most natural from a theoretical perspective. The current situation in string theory is that we have (via holography) a wealth of deeply understood models that describe quantum gravitational physics with a negative cosmological constant and no fully microscopic models of four-dimensional quantum gravity with zero or positive cosmological constant.[29] Even at the level of effective field theory, it is still controversial whether metastable string compactifications with $\Lambda > 0$ exist (see e.g. [41, 42] for recent discussions). So at present, the possibility that seems most likely to admit a fully non-perturbative theoretical description based on our current understanding is $\Lambda < 0$.

Given that we already have a good theoretical understanding of other types of spacetimes with $\Lambda < 0$ through holography, a natural next step toward understanding cosmology from a quantum gravity point of view is to try to understand $\Lambda < 0$ cosmologies microscopically, especially since it seems possible that our Universe could have $\Lambda < 0$.[30]

Why it is hard to describe $\Lambda < 0$ cosmological models holographically?

Even if we presume $\Lambda < 0$, there is still a significant obstacle in using holography to describe models of cosmology: cosmological models assume a homogeneous and isotropic Universe filled with matter and radiation, while usual holographic models describe spacetimes that are *asymptotically empty*. While holography has no trouble describing spacetimes with black holes, gravitational waves, radiation, etc... these interesting features are always in the interior of a spacetime that asymptotically looks just like pure AdS. This rigid asymptotic behaviour is related to the fact that any finite energy state of the dual field theory has the same UV physics (e.g. short distance correlators).

A complementary way to view the difficulty is that cosmological spacetimes with $\Lambda < 0$ are typically big-bang / big-crunch geometries with no asymptotically AdS regions that could be associated with a dual field theory.

Asymptotically AdS regions in complex time

A hint for how to make progress is that these $\Lambda < 0$ cosmological spacetimes often do have asymptotically AdS regions if we consider complexifying the coordinates. In an expanding Universe with $\Lambda < 0$, the negative cosmological constant eventually comes to dominate the evolution, and this causes the scale factor to decelerate and eventually turn around. In cases where any scalar fields also have zero time derivative at this point, the full solution for the background geometry is time-reversal symmetric about this turn-around point. In such time-symmetric geometries, we can analytically

[29] See [95, 107–111, 113–115] for various approaches to describing $\Lambda > 0$ cosmology.

[30] This was also emphasized recently in [137]. It is certainly still interesting to understand whether string theory can produce $\Lambda > 0$ models and whether these can be given a non-perturbative description, but it seems to us that comparatively little effort has been expended exploring what may be a simpler possibility.

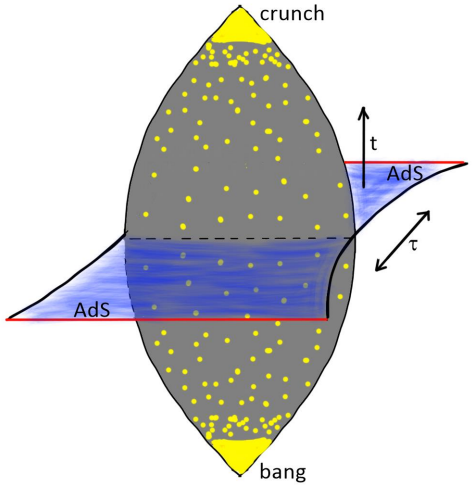

Figure 5.1: Schematic of a time symmetric $\Lambda < 0$ Lorentzian big-bang / big-crunch cosmology and the corresponding Euclidean Asymptotically AdS wormhole spacetime obtained by analytic continuation of the time coordinate. The asymptotically AdS Euclidean gravity theory can be given a microscopic holographic description, and this can be used to define a special state for the cosmology.

continue the time direction to obtain a real Euclidean geometry.[31] This analytically continued geometry has a pair of asymptotically AdS regions at Euclidean time $\tau = \pm\infty$ (see Figure 5.1) provided that the scalar fields asymptote to some value with a negative potential. In the special case of a flat cosmology (that we will focus on), we can perform a further analytic continuation of one of the spatial directions to obtain a *static* Lorentzian geometry with a pair of asymptotically AdS regions.

So far, this is a mathematical curiosity: starting from a time-reversal symmetric $\Lambda < 0$ flat cosmological spacetime, we can associate via analytic continuation a Euclidean geometry and a static horizon-free Lorentzian geometry each with a pair of asymptotically AdS regions.

However, the observation suggests a path forward to find a microscopic description of the $\Lambda < 0$ cosmology:

1. Find a microscopic description for the physics of the associated spacetimes with asymptotically AdS regions using holography.

2. Use this microscopic description of the Euclidean theory to define a special state for the Lorentzian cosmology and to give a holographic description of the physics of this state.

Before turning to the holographic descriptions, let us further motivate the second point here.

A special state for cosmology

In quantum field theory, if we have a time-reversal symmetric background Lorentzian spacetime related by analytic continuation to a reflection-symmetric Euclidean spacetime, the quantum field

[31] The scale factor is typically analytic around the time-reversal symmetric point since it is a solution of the Friedmann equation, and the analytically continued Friedmann equation is sensible for typical equations of state.

theory on this Euclidean spacetime[32] defines a special state of the Lorentzian theory, obtained by slicing the path integral defining the Euclidean theory. Observables for this state in the Lorentzian theory are related by analytic continuation to observables in the Euclidean theory. For example, as we discussed in Section 2.1, for a field theory in Minkowski space the state defined by the associated Euclidean field theory is the vacuum state.

In our case, the spacetimes are dynamical, but we will argue that the Euclidean version of the gravitational theory describing the Lorentzian cosmology can still be used to define a preferred quantum state for the cosmology. This is similar to the idea of Hartle and Hawking [139], who argued that a natural state for cosmology is provided by a Euclidean gravitational path integral with no boundary in the Euclidean past.

In our case, the Euclidean spacetimes we consider do have a boundary in the Euclidean past, namely an asymptotically AdS boundary. This is important for us as it will permit us to define the gravitational path integral non-perturbatively using holography.

Holographic description of spacetimes with two asymptotically AdS regions

We now return to the question of how to holographically describe the physics of these spacetimes. For our discussion, we focus on the most phenomenologically relevant case of four-dimensional flat cosmology; we comment on the generalization to other cases in the discussion.

We have argued that for a large class of $\Lambda < 0$ flat cosmological spacetimes, analytic continuation gives a Euclidean geometry of the form

$$ds^2 = d\tau^2 + a^2(\tau)\delta_{ij}dx^i dx^j, \tag{5.1}$$

(sum over i implicit) with asymptotically AdS regions for $\tau \to \pm\infty$. A further analytic continuation gives a Lorentzian static spacetime

$$ds^2 = d\tau^2 + a^2(\tau)\eta_{\mu\nu}dx^\mu dx^\nu \ , \tag{5.2}$$

Such geometries are sometimes described as asymptotically AdS planar *wormholes*, since they have two asymptotically AdS regions connected by a "throat" with a planar cross section. The two asymptotically AdS regions here suggest a dual holographic description that involves a pair of three-dimensional CFTs, where the coordinates labeled by x correspond to the directions on which the field theory lives, and the τ direction is the emergent radial direction.[33]

For the Lorentzian wormhole, since it is possible to go (causally) from one asymptotically AdS region to the other through the geometry, the two CFTs in the holographic description must be interacting somehow.[34] The physical separation between the boundaries in the wormhole geometry

[32] The Euclidean field theory may require additional boundary conditions for fields to complete its definition, e.g. if the analytically continued spacetime has asymptotically AdS regions. In this case, we have a family of states, each associated with a choice of boundary conditions.

[33] The AdS/CFT description of Euclidean wormholes was first discussed in [140], where the possible connection to cosmological physics via analytic continuation was also pointed out. More recent discussions of the holographic description of the types of wormholes we are discussing here appears in [141, 142].

[34] For Euclidean wormhole solutions in general, it has been suggested that the dual description may be in terms of some type of ensemble of CFTs, since the connected geometry suggests correlations between the two sides, but such correlations will be absent for a single pair of non-interacting CFTs [140, 143–147]. In the special case where the wormhole cross-section has a translation-invariant direction so that we can analytically continue to a static Lorentzian wormhole, we can make the stronger statement that the CFTs must be interacting [3, 148]. As discussed in [148], when this interaction is mediated via auxiliary degrees of freedom, integrating these degrees of freedom out in the Euclidean picture does give rise to something like an ensemble of CFTs, where the ensemble is over possible sources for local operators.

Figure 5.2: Left: two non-interacting 3D CFTs are dual to a pair of disconnected AdS spacetimes. Right: two 3D CFTs interacting via a non-holographic 4D CFT, proposed to be dual (in some cases) to a Lorentzian wormhole with two asymptotically AdS boundaries.

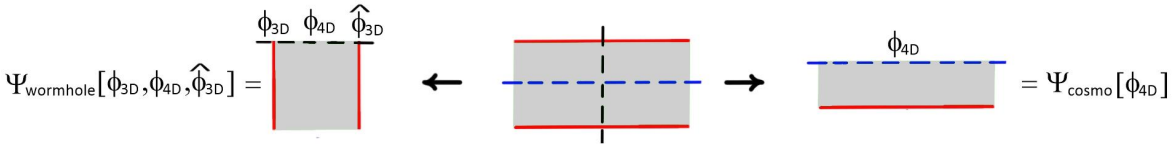

Figure 5.3: Two different slicings of the same microscopic Euclidean path integral give states dual to the Lorentzian wormhole and the cosmology. The pictures on the left and right indicated a Euclidean path integral over field configurations with the specified boundary conditions at the top surface. See also Figure 5.6 for the gravity interpretation of these states.

indicates that the interactions between the two CFTs are not instantaneous and do not induce arbitrarily strong correlations [142, 148]. These features suggest that the interaction is not a local field theory interaction; in [148], it was argued that the interaction likely involves some auxiliary degrees of freedom and that a natural possibility is for these extra degrees of freedom to take the form of a four-dimensional quantum field theory on $\mathbb{R}^3$ times an interval, to which the two CFTs are coupled at the edges of the interval (see Figure 5.2). The proposed dual for the asymptotically AdS wormhole geometry is the vacuum state of this 3D-4D-3D theory.

To preserve the four-dimensional character of the dual gravitational theory, the four-dimensional field theory should have many fewer local degrees of freedom than the 3D CFTs so that it represents a small perturbation to the physics in the UV. Nevertheless, via a long RG flow, this perturbation leads to a large amount of entanglement between the 3D CFTs in the IR, giving rise to the connected dual geometry [148]. We review some additional motivations and evidence for this construction in Section 5.2.

Holographic description of the cosmological physics

Assuming this dual description of the Lorentzian wormhole spacetime, we can now try to understand the dual of the cosmological physics.

The proposed dual for the Euclidean wormhole is the Euclidean version of the same field theory: a pair of Euclidean 3D CFTs on $\mathbb{R}^3$ coupled via a Euclidean 4D CFT on $\mathbb{R}^3$ times an interval.[35] This Euclidean theory can be used to construct the Lorentzian vacuum state dual to the Lorentzian wormhole by slicing the path integral perpendicular to the direction that is to be analytically continued (one of the $\mathbb{R}^3$ directions), as shown in Figure 5.3.

[35] More precisely, the wormhole is the dominant saddle point geometry in a gravitational path integral dual to this field theory path integral.

To define a state associated with the cosmological spacetime, we slice the same path integral in a different way, perpendicular to the direction between the two 3D CFTs, along the surface fixed by the reflection symmetry that exchanges the two 3D CFTs. We can understand this via the right-hand figure of Figure 5.2: the sliced CFT path integral corresponds to the sliced gravitational path integral that constructs a state for the cosmology at the time-symmetric point.

This second slicing defines a state of the 4D CFT on spatial $\mathbb{R}^3$. The 3D CFT appears only in the Euclidean path integral used to construct the state, not in the physical degrees of freedom. Even though the 4D CFT is not conventionally holographic, the presence of the holographic 3D CFT in the Euclidean past of the path integral produces a state that is sufficiently complex to encode the semiclassical physics of the cosmological spacetime.

The physics here is similar to how, as we saw in Chapter 4, bubbles of spacetime associated with a holographic CFT can be encoded in the state of a different CFT, or how black hole interiors can be encoded in auxiliary radiation systems [65, 149–151].

Extracting cosmological observables

The 4D CFT state that encodes the cosmological spacetime is a high-energy state that will look almost completely thermal. Thus, extracting the cosmological observables from this state would appear to be extremely difficult, similar to extracting local behind-the-horizon physics from a CFT state describing a single-sided black hole. Indeed, in the special case where the 4D CFT is holographic, the cosmological physics can be understood as living on an end-of-the-world (ETW) brane behind a black hole horizon.[36]

However, because we are considering a special state that arises from a Euclidean path integral, observables in the Lorentzian cosmology can be extracted in a simple way from this Euclidean theory, or alternatively from the vacuum physics of the Lorentzian wormhole. Since both the cosmology and the Lorentzian wormhole arise from the same Euclidean path integral through different slicings, there is a precise relationship between observables in the cosmology picture and observables in the wormhole picture. We have already seen that the scale factors in these two pictures are related by analytic continuation. But the correlation functions of local operators in the cosmology (which include all standard cosmological observables) will also be related by analytic continuation to the correlation functions in the wormhole picture. The wormhole geometry is static and horizon-free, so local observables in this picture are related in a much simpler way (e.g. by an HKLL procedure [100]) to the dual quantum field theory, which is in its vacuum state. Thus, we can understand cosmological observables by calculating the *vacuum* observables in the wormhole picture (via effective field theory or using the vacuum observables of the dual QFT), and then analytically continuing these to the cosmology picture. As a special case, correlation functions in the cosmology at $t = 0$ (the turn-around point) in which all operators live in a single 2D plane are simply equal to some corresponding vacuum correlation functions at the midpoint of the wormhole, as shown in Figure 5.4.

In the wormhole picture, there is no big bang or big crunch, and the spacetime is weakly curved everywhere. Thus, an effective field theory description should be valid everywhere. This should permit a computation of cosmological observables without having to explicitly understand physics in the vicinity of the Big Bang, and without having to use the underlying microscopic description.

[36] This was the case in the first examples of models of this type [102, 152], where the approach was dubbed "black hole microstate cosmology".

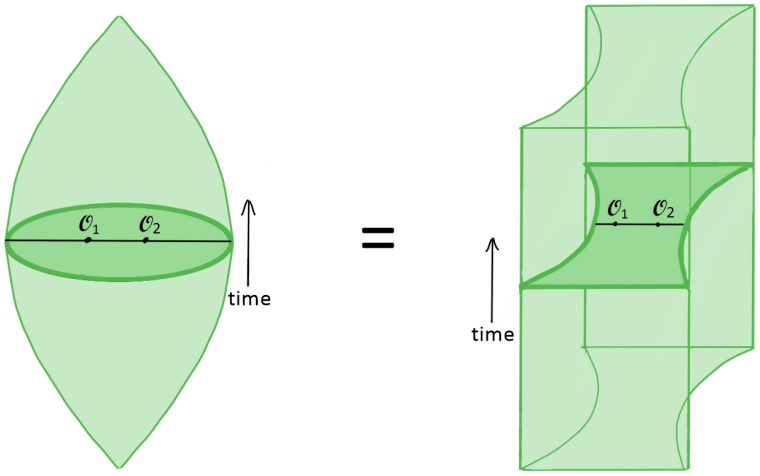

Figure 5.4: Observables $\mathcal{O}_i$ restricted to an $\mathbb{R}^2$ at the time-reflection symmetric surface in the cosmology (black line in the left spacetime) are equal to corresponding observables on the $\mathbb{R}^2$ in the middle of the Lorentzian wormhole (black line in the right spacetime). More general observables are related by double analytic continuation.

Naturalness problems in cosmology

If this framework can support realistic models of cosmology it may help resolve various naturalness problems. Extrapolating our present observations of the Universe back to early times we find that the Universe at early times must have been extremely flat and extremely homogeneous, and must have contained correlations between regions that were apparently never in causal contact since the big bang. Thus, the required initial state would appear to be finely tuned and/or unnatural in various ways. Inflation seeks to explain how such an initial state could have arisen naturally by postulating an earlier period of exponential expansion with many e-foldings.

In our framework, the Euclidean theory constructs a state at the time-symmetric point, and the initial state close to the big bang is most naturally understood as the result of quantum evolution backwards to the big bang. Thus, features of the state in the early Universe are natural provided that they arise from the backward evolution of a state at the time-symmetric point that is produced by the Euclidean path integral.

The construction of the state via a Euclidean theory with $\mathbb{R}^3$ symmetry naturally produces a Universe that is flat and very homogeneous. Also, since correlations in the cosmology picture at the time-symmetric slice are equal to vacuum correlators in the wormhole picture, we *naturally have correlations in the cosmology picture between regions of the Universe that were never in causal contact*, since all points in the static wormhole picture have intersecting past light cones.

While the model appears to alleviate many of the problems that inflation was introduced to explain, it remains to be seen whether it can reproduce the detailed quantitative results for the cosmological perturbations that arise from inflationary models and that agree with observations. An interesting point is that inflationary physics may still be present in our framework and may provide a dual explanation for the origin of perturbations/correlations, but since we can also compute these via the wormhole picture, *no explicit knowledge of the inflationary potential or any other early Universe physics is required to compute the perturbations.*

Generic cosmological predictions

In this chapter we focus on the generic predictions of this class of models. In all cases, the underlying $\mathbb{R}^3$ symmetry gives rise to a cosmology that is flat, homogeneous, and isotropic. The background is always time-symmetric so that the Universe will eventually recollapse. For models based on 3D CFTs with relevant operators, we generically have time-dependent scalar fields whose potential energy decreases from a positive value to a negative value before rising to a larger negative value at the time-symmetric point (so we have time dependent dark energy). In some cases, the positive potential *leads to a phase of accelerated expansion before the collapse*. The models could have inflation in the early Universe, but it is not clear whether this is generic. However, as we emphasized above, direct knowledge of the physics of the early Universe is not needed to extract the physics of cosmological perturbations from the model, and these perturbations naturally contain correlations at all scales. Further, the standard flatness and horizon problems (explaining why the Universe is so flat and why the temperature is nearly the same in all directions) are explained by the symmetries of the model and the fact that the state of the cosmological spacetime is naturally defined at the time-symmetric point rather than at the big bang. Thus the setup may solve the standard problems that inflation addresses without the need for inflation. However, it remains to be seen whether the possibilities for the scale factor evolution and the details of the cosmological perturbations are realistic.

The specific predictions of the model will depend on the 4D effective field theory, which is in turn determined by our choice of 3D and 4D QFTs in the microscopic setup. This choice is the only input for the physics of the model. The curvature scale in the Universe is related to the number of degrees of freedom in the 3D holographic CFT, and the gauge group in the 4D effective theory is related to the global symmetry group of the 3D CFT. Some of this gauge symmetry (and supersymmetry) may be broken by the time-dependent scalars, whose values would set the scale of the symmetry breaking.

Outline

In the remained of this chapter, we flesh out these basic observations and explore their consequences. In Section 5.2, we review the basic setup and motivations for this class of models and explain how the cosmological observables are related to vacuum observables in the dual wormhole picture. In Section 5.3, we explore the general properties and predictions for the background cosmology, making explicit the relation between cosmological observables and vacuum physics of the wormhole. We show that the simplest toy model gives rise to a standard $\Lambda < 0$ plus radiation cosmology with a big bang and a big crunch, but that more generic models will include time-dependent scalar fields that can naturally yield a phase of accelerated expansion before the collapse. In Section 5.4, we discuss fluctuations about the background geometry and how cosmological perturbations (including physics of the CMB) are related to vacuum correlators in the wormhole. We conclude in Section 5.5 with a discussion, including the steps necessary to verify that fully microscopic models of this scenario can work. Even if the models we consider turn out not to be viable to describe realistic cosmology, they have a number of interesting general features that might be employed in future microscopic models of cosmology based on string theory and/or holography.

Relation to earlier work

This chapter represents the present stage of evolution of a class of cosmological models originally proposed in [102], and further developed in [56, 148, 152, 153] (see also [154, 155]). In the original models, the 4D CFT was assumed to be holographic, and the cosmological physics was on an ETW

brane behind the horizon of a black hole. These models built on the AdS/BCFT proposal, see [156–160]. The present manifestation of the models with specific suggestions for microscopic realizations appeared in [56, 148]. The work here is the first to explicitly consider in detail the phenomenological consequences and point out that examples making use of 3D CFTs with relevant operators can lead to accelerated expansion.

Related models of cosmology for low dimensions were discussed in [161–163]. The "holographic cosmology" of [113] has similarities to our model in that they propose to relate cosmological physics to geometry associated with a 3D RG flow. However in that case, the transformation relating the geometries involves an analytic continuations of parameters as well as coordinates, and it is not clear whether the cosmology picture can be directly associated with an underlying physical theory. The paper [164] discussed a different approach to relating accelerated expansion to $\Lambda < 0$ physics. The recent model of [165] also assumes a time-symmetric Universe with an associated special state, but in that case, the point of time-reflection symmetry is the big bang, and $\Lambda > 0$ is considered.

5.2 Basic setup

In this section, we explain our basic holographic construction, focusing on the physically relevant case of flat $\Lambda < 0$ four-dimensional cosmology.

Our starting point is a three-dimensional holographic superconformal field theory on $\mathbb{R}^{2,1}$ dual to gravity on an asymptotically AdS_4 spacetime. For a realistic cosmology, we want to choose an example with many degrees of freedom so that the curvature scale is very small relative to the Planck scale, i.e. $L^2_{AdS}/G \ll 1$. We would also like the size of the extra dimensions to be small.[37] We can choose the global symmetry group $\mathcal{G}$ of the SCFT to correspond to some desired gauge group for the matter in the four-dimensional gravitational theory. As we discuss below, this gauge symmetry may be further broken by time-dependent scalar field expectation values in the cosmology.

The Lorentzian wormhole and its dual

The next step promotes the asymptotically AdS_4 geometry to a Lorentzian traversable wormhole with two asymptotically AdS_4 regions. To do this, we consider a second copy of the 3D SCFT, but with reversed orientation, so that the new copy preserves a complementary set of supersymmetries [56]. This is dual to gravity on a second asymptotically AdS_4 spacetime. To connect these two asymptotically AdS spacetimes, we couple the two three-dimensional theories weakly, via an intermediate four-dimensional CFT with relatively few degrees of freedom [148], as in Figure 5.2. The coupling introduces a scale (the distance between the 3D CFTs), and in the examples we require, the theory confines at lengths much larger than this scale. The vacuum state has a large amount of entanglement between the two 3D CFTs, and this leads to the connected wormhole geometry in the gravity dual.[38] Models with the correct vacuum structure will exhibit a symmetry breaking $\mathcal{G} \times \mathcal{G} \to \mathcal{G}$ corresponding to the fact that the bulk gauge field in one asymptotically AdS region is the same as the one in the other asymptotically AdS region [169]. The IR field theory will have massless Goldstone bosons associated with this symmetry breaking.

The main evidence that this 3D-4D-3D field theory construction can give a holographic description of the Lorentzian wormhole is [3, 56, 148]:

[37] The recent papers [166, 167] provide an explicit construction of supersymmetric AdS string vacua with negative cosmological constant whose magnitude is less than 10^{-123} in Planck units and whose extra dimensions are very small. These 3D SCFTs dual to these solutions may be an appropriate starting point for our construction.

[38] See [3, 56, 148] for a detailed discussion of this claim, and [168] for more recent discussion of the idea.

1. In examples where the 4D theory is also holographic, the dual geometry has the interpretation of a geometrical brane and its corresponding anti-brane separated at the asymptotic boundary of a 5D spacetime. Parallel brane-antibrane systems are typically unstable, and the natural endpoint of the instability in this case is for the branes to connect up, forming the wormhole. We expect that the basic field theory physics responsible for this effect continues to apply even when the four-dimensional CFT is not holographic.

2. By coupling the two 3D CFTs with a 4D CFT, we break conformal invariance and supersymmetry. The resulting theory will have an RG flow, and it is natural that the degrees of freedom in the two 3D CFTs will become more and more entangled as we go to the IR. It is also generic that the IR theory should be confining rather than having a non-trivial IR fixed point. The wormhole dual is consistent both with the large amount of entanglement between the two 3D theories and with the confinement (since the middle of the wormhole gives an IR end to the spacetime at a finite proper distance from any point in the geometry).

3. As we review below, the effective field theory description of the wormhole requires an unusual quantum field theory phenomenon (anomalously large negative Casimir energies) that had not previously been understood. As we discuss in the next chapter, this phenomenon was searched for and found to exist in a holographic quantum field theory setup [5, 56].

4. The basic mechanism of coupling two holographic CFTs to generate a traversable wormhole is similar to that used in [170, 171], though our mechanism crucially involves auxiliary degrees of freedom to achieve the coupling.

Going forward, we will assume that this holographic description is correct; in the discussion we comment on ways that this could be verified explicitly in microscopic examples.

The Euclidean wormhole and its dual

So far, we have the vacuum state of a 3D-4D-3D QFT dual to a geometry with a four-dimensional planar Lorentzian wormhole. The wormhole geometry can be described using a metric

$$ds^2 = d\tau^2 + A^2(\tau)(-d\zeta^2 + \delta_{ij}dx^i dx^j) \,. \tag{5.3}$$

Here, $A(\tau)$ is symmetric under reversal of τ and grows exponentially for $\tau \to \pm\infty$ corresponding to the two asymptotically AdS boundaries. The ζ and x^i $(i = 1, 2)$ are the coordinates of the original 3D CFT.

The vacuum state of our Lorentzian field theory is naturally associated with a Euclidean version of this theory, where the 3D CFTs are on $\mathbb{R}^3$ and the 4D theory is on $\mathbb{R}^3$ times an interval I. Specifically, the vacuum wavefunctional is obtained by slicing the path integral defining the Euclidean theory perpendicular to one of the $\mathbb{R}^3$ directions, as reviewed in Chapter 2.

The Euclidean theory is dual to the analytically continued ($\zeta = iw$) wormhole geometry, with metric:

$$ds^2 = d\tau^2 + A^2(\tau)(dw^2 + \delta_{ij}dx^i dx^j) \,. \tag{5.4}$$

More precisely, this is the saddle point geometry for the gravitational path integral of the dual theory.

The cosmology and its dual

The cosmological spacetime that we desire is obtained from this Euclidean wormhole spacetime by analytic continuation $\tau = it$, which gives the planar FRW geometry

$$ds^2 = -dt^2 + a^2(t)(dw^2 + \delta_{ij}dx^i dx^j) \ . \tag{5.5}$$

In this case, the function $a(t) \equiv A(it)$ is time-symmetric and will generally correspond to a big-bang / big-crunch cosmology, though other time-symmetric scale factors might be possible.[39]

The holographic construction gives rise to a special state describing the quantum physics of this cosmology. This is obtained by slicing the path integral for the Euclidean theory in a different way, at the midpoint of the interval I, as shown in Figure 5.3. This new slicing does not intersect the 3D CFTs at all, so the interpretation is that we have an excited state of the 4D CFT on $\mathbb{R}^3$ produced by a path integral that has the "insertion" of a 3D holographic CFT in the Euclidean past.

Unlike usual examples of holography, the underlying degrees of freedom are not associated with any boundary of the cosmological spacetime. We will understand this better presently.

5.2.1 Higher dimensional description with a 4D holographic CFT

To develop intuition for this class of models, it is useful to understand a special case, where the 4D auxiliary theory is also holographic. This was the case considered in [102, 152] where such models were originally proposed.

Here, each geometry described above is now the geometry of an end-of-the-world (ETW) brane that lives at the boundary of a five-dimensional spacetime (bottom row of Figure 5.6).

For the Lorentzian and Euclidean wormhole geometries, the five-dimensional geometry is asymptotically AdS with boundary geometry $\mathbb{R}^{2,1} \times I$ or $\mathbb{R}^3 \times I$, and the ETW brane reaches the asymptotically AdS region at the boundaries of I. In the cosmology picture, the higher-dimensional geometry is asymptotically AdS with boundary geometry $\mathbb{R}^{3,1}$, and the ETW brane does not intersect the boundary. The dual state is a high-energy excited state of the 4D CFT, so the geometry can be interpreted as a particular planar black hole microstate. The ETW brane housing the FRW geometry lives behind the horizon of this black hole. The cosmological singularities of the FRW spacetime are part of the past and future singularities of the black hole.

This last picture provides intuition for how the 4D cosmological spacetime can be described by some state of the 4D CFT which is not associated with any boundary in the cosmology. From the 5D point of view, the cosmology and the asymptotically AdS boundary are separated in the 5D radial direction. In examples where the 4D theory is not holographic, there is no 5D geometrical space, so the cosmology is like an island (using the terminology of [65, 149–151]). Other examples where a holographic theory in the Euclidean past is used to encode a geometrical spacetime in a quantum theory that is not necessarily holographic were discussed recently in [1] (see Chapter 3) and [172]. This is also similar to the way that black hole interiors can be encoded in auxiliary radiation systems [65, 149–151].

5.2.2 Auxiliary systems in the effective field theory description

We now return to the generic case to better understand the effective field theory description in the cosmology, wormhole, and Euclidean pictures. We will see that the 4D CFT plays an important role as a non-gravitational auxiliary system in the effective descriptions.

[39] See [152] for a possible construction of bouncing cosmology.

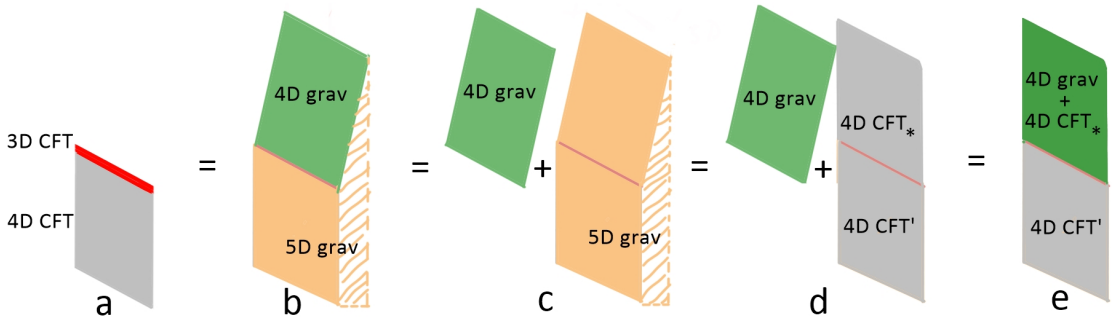

Figure 5.5: Effective field theory description of holographic 3D-4D coupled theories with $c_{3D} \gg c_{4D}$. **a)** Microscopic picture. **b)** Higher-dimensional gravity picture: 4D gravitational physics of the 3D theory appears as the physics of an ETW brane near the AdS boundary. **c)** Isolating the 5D bulk gravitational physics. **d)** 5D gravitational physics is equivalent to physics of the dual 4D CFT with a cutoff (indicated by *) on half the space. **e)** Final effective description: a 4D CFT coupled to a 4D gravity theory + cutoff CFT. The state of the lower 4D CFT in the final picture is different than the state in the micoscopic picture.

Single 3D theory:

The 3D holographic CFT that we start with is dual to some gravitational theory whose 4D effective description has gravity with a negative cosmological constant and matter with gauge symmetry given by the global symmetry group of the 3D CFT.

Single 3D theory + 4D theory:

Next, we would like to understand the effect of coupling a single copy of the 3D CFT to a 4D CFT on a half-space.

This can be understood most easily by thinking about the case where the 4D CFT is holographic (see Figure 5.5). Here, we have a higher-dimensional dual description where the 4D gravity theory dual to the 3D CFT now gives the effective description of physics on an ETW brane in a 5D asymptotically AdS spacetime whose boundary geometry is a half space.[40] In the limit of interest where the 3D theory has many more local degrees of freedom than the 4D CFT, the ETW brane makes an angle close to $\pi/2$ with the bulk radial direction and lies on a surface that cuts off the would-be second half of the asymptotic region.

From the higher-dimensional perspective, the extra physics that we have added via the 4D CFT is a gravitational theory on asymptotically AdS spacetime with a cutoff surface that removes one half of the asymptotic region. In field theory language, this should correspond to the 4D CFT on Minkowski space with a UV cutoff on half of the spacetime. In this half of the spacetime the cutoff 4D CFT is coupled locally to the 4D gravitational theory dual to the 3D CFT (Figure 5.5e).[41] While we have motivated this final picture by higher-dimensional holography, we expect it to hold also when the 4D CFT is not holographic.

[40] Such models were considered originally in [84, 156, 173]. Microscopic examples starting with $\mathcal{N} = 4$ SYM theory were discussed in [174], and explicit gravity dual solutions were found in [80–83], based on the general $OSp(2,2|4)$-symmetric solutions of type IIB supergravity found in [80, 81]. The limit of $c_{3D} \gg c_{4D}$ was considered in [175–177].

[41] According to [178], this coupling can also be understood as a modification to the gravitational effective action, in which the graviton develops a small mass, related to the ratio c_{4D}/c_{3D} of degrees of freedom, and certain higher curvature terms are induced.

Two 3D theories + 4D theory:

In the full construction for the Lorentzian wormhole, we have two boundary 3D CFTs that are coupled together by a 4D CFT. In this case, we have two copies of the four-dimensional gravitational theory just described, each with an asymptotically AdS region, but these join up in the IR to give the wormhole geometry. The fields at the two asymptotically AdS boundaries are coupled via the auxiliary non-gravitational 4D CFT on an interval. This is depicted in the middle-left picture of Figure 5.6.

This auxiliary 4D theory coupling the two asymptotically AdS boundaries is an essential part of the construction. Without it, the vacuum state of the quantum fields on the wormhole would be significantly different and would not exhibit the type of vacuum energy to support the wormhole in the first place. We will discuss this further in the following section, and also in the next chapter.

Euclidean picture:

The effective field theory description of the Euclidean picture is essentially the same as that in the Lorentzian wormhole picture, but with the translation-invariant time direction replaced by a spatial direction (Figure 5.6, middle).

Cosmology picture:

The Euclidean effective field theory (Figure 5.6, middle) has a reflection symmetry in the direction between the two asymptotically AdS boundaries of the wormhole. The surface fixed by this reflection (labeled B in the centre picture of Figure 5.6) has two disconnected parts, one in the gravitational theory at the midpoint of the wormhole, and one in the 4D CFT. This surface corresponds to the $t = 0$ surface in the cosmology picture, so that picture also includes a gravitational theory (housing the cosmology) and an auxiliary 4D CFT. These do not interact with each other directly, but are entangled. The connection between these two parts in the lower half of the Euclidean picture leads to entanglement between the two parts in the cosmology picture, similar to how a thermofield double path integral connects two quantum systems in the Euclidean past.

When we have a 5D gravity description, we can think of the state of the 4D CFT as describing the physics outside the black hole horizon and the 4D gravitational theory as describing the physics inside the black hole including the physics of the ETW brane.

The role of the 4D CFT in the effective description (Figure 5.6, middle-right) is different from its role in the microscopic description (Figure 5.6, top-right). In the micsrocopic picture of the cosmology, we only have a complicated pure state of the 4D CFT. The physics of the ETW brane is encoded in the IR physics of this state. In the effective field theory picture, we have a simpler mixed state of the 4D CFT that encodes the physics outside the horizon, and this is purified by the state of the 4D gravitational theory that describes the cosmological physics. As we describe in the discussion, this implies the presence of "islands" and explains the appearance of cosmological islands in the work of [179].

As summarized in Figure 5.6, the different analytic continuations, together with the holographic duality and the possibility of a higher-dimensional holographic description give up to nine different pictures of the physics.

5.2.3 Cosmology from vacuum physics

In our setup, we have two Lorentzian spacetimes, the cosmology and the Lorentzian wormhole, whose holographic descriptions arise from slicing the same Euclidean path integral in two different ways.

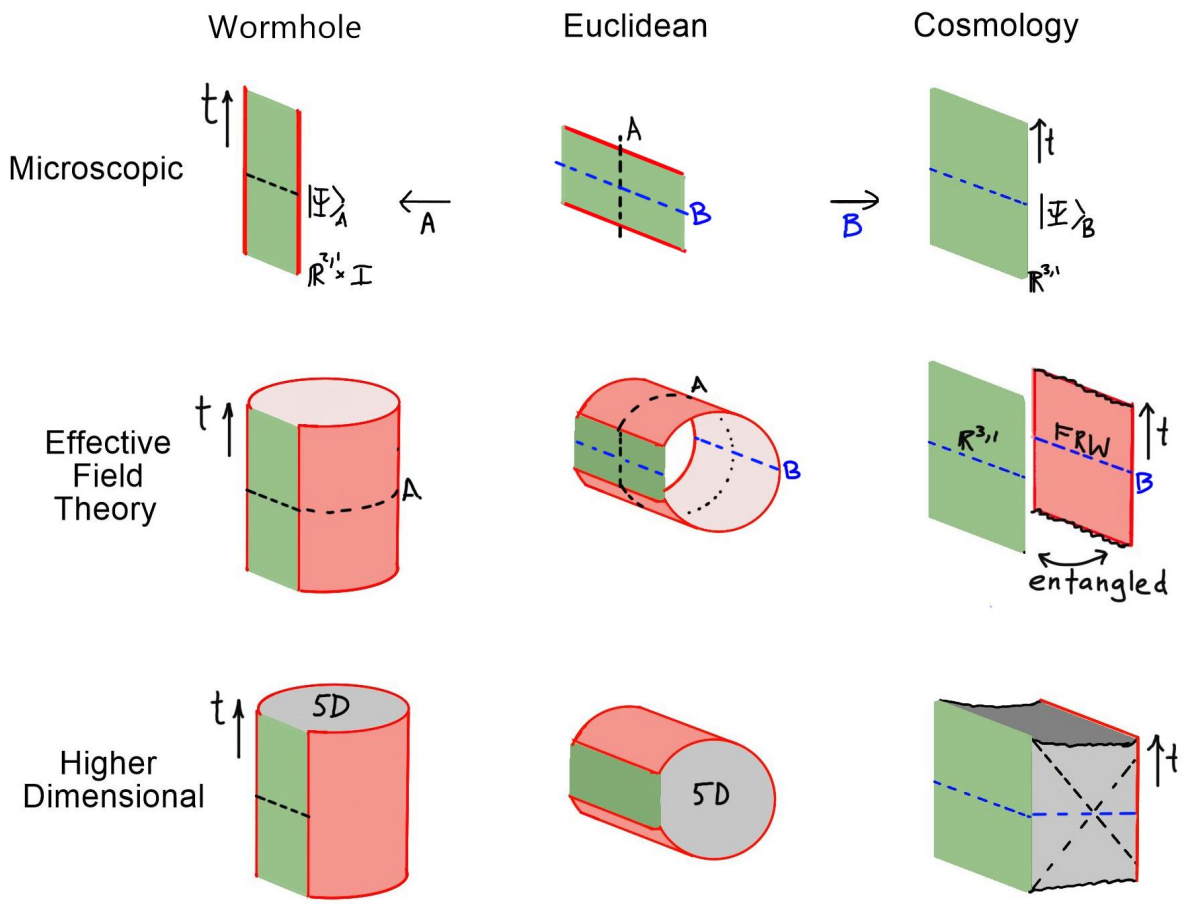

Figure 5.6: Nine different but equivalent perspectives. Top row: the Euclidean path integral for the 3D-4D-3D theory (middle-top) can be sliced in two different ways to the vacuum state of the Lorentzian 3D-4D-3D theory or a complex excited state of the 4D CFT. The middle row shows the holographic dual descriptions of these pictures in the general case where the 4D theory is not holographic. The Euclidean description (center) can be understood as a gravitational path integral that can be sliced to define the static Lorentzian wormhole or the cosmology, entangled with an auxiliary 4D CFT. When the 4D CFT is holographic, we have a higher-dimensional gravity description (bottom row).

This "path integral slicing duality" implies an exact equivalence between certain observables for the two Lorentzian states. The Euclidean path integral with operators inserted on the intersection of the two slices will have an interpretation as the expectation value of some observables in one Lorentzian picture and some closely related observables in the other Lorentzian picture; these are equal since they are computed in exactly the same way.

In our application, the Euclidean path integral in the 3D-4D-3D QFT corresponds to a Euclidean gravitational path integral that includes contributions from a dominant saddle point geometry (the Euclidean wormhole) and fluctuations around this. The geometry and fluctuations here determine the background geometry and quantum states in the two Lorentzian pictures. To the extent that we can describe the Lorentzian physics in terms of quantum field theory on a background saddle-point geometry, we can say that the field theory observables in the cosmology picture will be directly related to field theory observables in the wormhole picture, since again they arise from the same Euclidean path integral.

The simplest case is to consider some observables that live at the intersection of the two slices. For example, we can consider in the Euclidean effective field theory picture some correlation function of local operators restricted to an $\mathbb{R}^2$ in the $\mathbb{R}^3$ that forms the midpoint of the wormhole. This Euclidean correlation function is equal to some correlation function in the cosmology at the time-reflection symmetric surface, and also equal to a vacuum correlation function of operators at the midpoint of the wormhole in the Lorentzian wormhole picture. In this way, any cosmological observable that lives in an $\mathbb{R}^2$ at the time-symmetric point is equal to a vacuum observable in the wormhole picture, as shown in Figure 5.4.

More generally, time-dependent observables in each Lorentzian theory are related by analytic continuation to observables in the Euclidean theory, so time-dependent observables in the two Lorentzian theories will be related by a double analytic continuation. We have already seen that this applies to the scale factor in the background geometry. But it should also apply to other observables, such as the equal time correlation functions of the stress-energy tensor that encode the physics of the CMB. Thus, by understanding the vacuum observables in the Lorentzian wormhole picture, we should be able to answer almost any question about the physics of the cosmology.

In the remainder of this chapter, we focus on the effective field theory description, and the relation between the cosmological observables in the FRW Universe and vacuum observables in the wormhole geometry dual to the vacuum state of the 3D-4D-3D theory.

5.3 Implications for background cosmology

In this section, we focus on the background cosmology, describing how the scale factor evolution and stress-energy tensor evolution are related in the cosmology and wormhole pictures.

Assuming the validity of four-dimensional effective field theory, we expect that it should be a good approximation when discussing the background geometry to use the semiclassical Einstein equation,

$$R_{\mu\nu} - \frac{1}{2} g_{\mu\nu} R - \frac{3}{L^2} g_{\mu\nu} = 8\pi G \langle T_{\mu\nu} \rangle \ , \tag{5.6}$$

where L is the AdS length associated with the underlying 3D CFTs. It will be useful to begin by explicitly describing the background geometries and evolution equations in the two pictures.

Background geometry and stress-energy tensor: cosmology

As we discussed above, in the cosmology picture we have a background geometry

$$ds^2 = -dt^2 + a^2(t)(dw^2 + \delta_{ij} dx^i dx^j) \ , \tag{5.7}$$

where $a(t)$ is time-reversal symmetric.

The homogeneous part of the stress-energy tensor takes the form[42]

$$T^{tt} = \rho(t) \qquad T^{ij} = \frac{1}{a^2(t)}\delta^{ij}p(t) \qquad T^{ww} = \frac{1}{a^2(t)}p(t) \ . \tag{5.8}$$

where ρ and p are the conventionally defined energy density and pressure. These will also be time-reversal symmetric. In terms of the Hubble parameter $H = \dot{a}/a$, the covariant conservation equation $\nabla_\mu T^{\mu\nu} = 0$ gives

$$\dot{\rho} = -3H(\rho + p) \tag{5.9}$$

which can be used to express p in terms of ρ and a. Finally, Einstein's equations relate ρ and a by the Friedmann equation

$$H^2 + \frac{1}{L^2} = \frac{8\pi G}{3}\rho \ . \tag{5.10}$$

Taking the time derivative of (5.10) and using (5.9), we have also that

$$\dot{H} = -4\pi G(p + \rho) \ . \tag{5.11}$$

In this cosmology picture, we expect that the stress-energy tensor has various contributions, including vacuum energy of fields as well as matter and radiation.

Background geometry and stress-energy tensor: wormhole

Let us now see how the scale factor and stress-energy tensor in the cosmology are related directly to those in the Lorentzian wormhole spacetime.

In the wormhole picture, we can describe the metric as

$$ds^2 = d\tau^2 + a_E^2(\tau)(-d\zeta^2 + \delta_{ij}dx^i dx^i) \ . \tag{5.12}$$

Here, $a_E(\tau)$ is obtained from $a(t)$ by analytic continuation $t^2 \leftrightarrow -\tau^2$. It is symmetric under reversal of τ and grows exponentially for $\tau \to \pm\infty$ corresponding to the two asymptotically AdS boundaries.

In this picture, the stress-energy tensor is

$$T^{\tau\tau} = -\rho_E(\tau) \qquad T^{ij} = \frac{1}{a^2(t)}\delta^{ij}p_E(\tau) \qquad T^{\zeta\zeta} = -\frac{1}{a_E^2}p_E(\tau) \ , \tag{5.13}$$

where ρ_E and p_E are related to ρ and p by analytic continuation $t^2 \leftrightarrow -\tau^2$.

The energy conservation equation gives

$$\frac{d\rho_E}{d\tau} = -\frac{3}{a_E}\frac{da_E}{d\tau}(\rho_E + p_E) \tag{5.14}$$

and the analogue of the Friedmann equation gives

$$-\left(\frac{1}{a_E}\frac{da_E}{d\tau}\right)^2 + \frac{1}{L^2} = \frac{8\pi G}{3}\rho_E \ . \tag{5.15}$$

[42]Here and below, quantum expectation values are implied when writing components of the stress-energy tensor.

5.3.1 Energy from vacuum energy

We see that the time evolution $\rho(t)$ of the cosmological energy density, is directly related to a component of the vacuum stress tensor in the wormhole picture as

$$\rho(t) = -T_{\tau\tau}(\tau = it) \tag{5.16}$$

where the right side is real because of the $\tau \to -\tau$ symmetry.

The pressure in the cosmology picture is

$$p(t) = T^{\zeta}{}_{\zeta}(\tau = it) \ , \tag{5.17}$$

where the right side is minus the proper energy density in the wormhole picture. Here, $p(t)$ is also real by the τ-reflection symmetry. While $T_{\tau\tau}$ and $T^{\zeta}{}_{\zeta}$ represent components of the vacuum stress energy tensor in the wormhole picture (i.e. a Casimir stress-energy tensor in the system with two boundaries), the functions $\rho(t)$ and $p(t)$ represent the full stress-energy tensor in the cosmology, including both vacuum and non-vacuum contributions. Thus, in a realistic example, the stress-energy tensor from matter, dark matter, and vacuum in the cosmology picture would all arise from vacuum energy in the wormhole picture. They could be computed from knowledge of the effective field theory in the wormhole and are thus determined without specific knowledge of the big bang or the initial state in the cosmology picture.

5.3.2 Analytic structure of the scale factor

The $\tau \to -\tau$ reflection symmetry and AdS asymptotics in the wormhole picture imply that the wormhole scale factor $a_E(\tau)$ is an even function of τ (defining $\tau = 0$ to be the middle of the wormhole) that grows exponentially for $\tau \to \pm\infty$.[43]

The Lorentzian scale factor $a(t)$ is obtained from $a_E(\tau)$ by analytic continuation $\tau \to it$, so it will also be an even function of t. That $a_E(\tau)$ has the asymptotics of a cosh function suggests an oscillatory piece in the real time scale factor $a(t)$ (since cosh continues to a cosine), but this does not necessarily imply a periodic cosmology. For example, in the simple example $a_E^2(\tau) = \cosh(2\tau/L)$ that arises from a $\Lambda < 0$ + radiation cosmology, we find $a^2(t) = \cos(2t/L)$ which goes to zero for $t = \pm\pi/(2L)$. Thus, we get a big-bang/big-crunch.

For other choices of $\hat{a}_E(z)$ with AdS asymptotics, we can have big-bang/big-crunch scale factors with different functional form or periodic scale factors. However, the physically allowed scale factors will be determined by the dynamics of the theory.

5.3.3 Vacuum energy in the wormhole picture

To understand the possibilities for the scale factor and stress-energy tensor evolution in the cosmology picture, we need to understand the possibilities for the vacuum energy in the wormhole picture.

Here, it is important that the metric is dynamical, so one needs to understand the vacuum configuration of a dynamical metric coupled to quantum fields (including the metric itself).

Assuming the validity of four-dimensional effective field theory, we expect that it should be a good approximation to self-consistently solve the semiclassical Einstein equation (5.6) where $\langle T_{\mu\nu} \rangle$ represents the vacuum energy of the fields (presumably, including metric fluctuations) in our effective theory on the background with metric g. That is, we find the vacuum energy of the effective field

[43] Alternatively, the scale factor $\hat{a}_E(z)$ in conformal coordinates (see appendix D) has simple poles at $\pm z_0$, with no other poles in $[-z_0, z_0]$.

theory on a fixed geometry of the form (5.12), giving some functional of the scale factor $\hat{a}_E(z)$, and then include this functional on the right-hand side of the Einstein equation. In this calculation, it is important to take into account the 4D CFT coupling fields in the two asymptotically AdS regions.

The vacuum energy calculation will generally be divergent in the continuum QFT limit, but it is natural in the gravitational context to assume a cutoff at the Planck scale, $M_{UV} = 1/\sqrt{G}$. In this case, for a renormalizable quantum field theory, the divergent pieces of the stress-energy tensor should take the form of local terms that may involve the curvature.

The cosmological constant problem

The leading potential divergence takes the form $\langle T_{\mu\nu} \rangle = \hat{\Lambda} g_{\mu\nu}$, giving a quantum correction to the cosmological constant. Here, $\hat{\Lambda}$ could have contributions of order $1/G^2$, M^2/G, or $M^4 \log(M^2 G)$ for some mass scale M associated with the effective theory. Any of these would be problematic for realistic cosmology: this is the usual cosmological constant problem.

An acceptably small cosmological constant / curvature scale in the 4D geometry dual to a single 3D CFT can be arranged by making an appropriate choice of CFT. Supersymmetric AdS compactifications of string theory with acceptably small curvature scale and small extra dimensions have been argued to exist recently in [166, 167]. These should correspond to some dual superconformal theory where the smallness of the curvature / cosmological constant relative to the Planck scale is related to the large number of degrees of freedom. Evidently, any $\langle T_{\mu\nu} \rangle \propto g_{\mu\nu}$ contributions to the stress-energy tensor in the effective field theory description of the 4D bulk must cancel. This can likely be understood as a result of supersymmetry in the bulk effective theory.

Coupling in a 4D theory with many fewer local degrees of freedom in a way that preserves supersymmetry and conformal invariance should not affect the dual geometry significantly; this is known to be true in various examples where the dual geometries are known explicitly [175].

In the full setup for the cosmology picture, we break supersymmetry by introducing another boundary theory; this preserves supersymmetry on its own, but the two boundaries together break supersymmetry. There is a well known example where such non-local breaking of supersymmetry in the CFT does not lead to large contributions to the bulk stress-energy tensor. For a supersymmetric holographic conformal field theory compactified on a circle with antiperiodic boundary conditions for fermions, supersymmetry is broken by the boundary conditions on the circle, but the vacuum state is believed to be dual to a geometry with the same scale of curvature as in the dual of the theory with supersymmetric (periodic) boundary conditions for fermions [180]. From an effective field theory point of view, the point may be that the same cancellations that avoided large contributions to the stress-energy tensor in the supersymmetric case persist here.[44]

An alternative argument for the absence of corrections to the cosmological constant is that in the cosmology picture, the dual theory is just the 4D CFT with unbroken supersymmetry. However, the effective theory in the cosmology also then has an underlying supersymmetry but may look non-supersymmetric because of our choice of state (e.g. due to the time-dependent scalar fields). In this case, the leading divergent contributions to the stress-energy tensor should be absent since they are independent of the state and vanish for the vacuum state of a supersymmetric theory.

[44] A useful example may be the calculation of Casimir energy density in a supersymmetric theory where the supersymmetry is broken by boundary conditions. In general Casimir energy calculations, after introducing a regulator, the energy density for infinite volume is subtracted from the energy density with boundaries, and then the regulator is removed to yield a finite result. For a supersymmetric theory, energy density in infinite volume would vanish, so the full energy density should also be finite, even though the boundary conditions break supersymmetry.

Renormalization of the Newton constant

The next potential divergence comes at order $1/G$ and is proportional to the Einstein tensor, $\langle T_{\mu\nu}\rangle \sim 1/G(R_{\mu\nu} - g_{\mu\nu}R)$. Since this is multiplied by $8\pi G$ in the Einstein equation, it comes in at the same order as the Einstein tensor on the left side. Thus, we can think of it as renormalizing the Newton constant by an order one amount. Such contributions can occur even for supersymmetric theories.

R^2 terms

The final possibility for divergent terms are R^2 corrections with coefficients of order $\log(M^2G)$. Since they come into the Einstein equations multiplied by G, they will only be comparable to the Einstein term in regions of the geometry where the curvature is close to the Planck scale, e.g. near the initial and final time in the cosmology picture. We expect that they can be ignored in the wormhole picture.

Finite terms

The remaining part of the stress-energy tensor, finite in the $G \to 0$ limit, can be understood as a Casimir energy density associated with the fields. This part is essential for ending up with a wormhole geometry that can give rise to a cosmological spacetime, since the other significant terms are the Einstein term and cosmological constant term that together give rise to a single-sided pure AdS spacetime.

If the scale of curvature is of order the AdS scale L throughout the geometry, the Einstein term and the cosmological constant term in the Einstein equations will both be of order $1/L^2$. In this case, the Casimir energy density must be of order $1/(GL^2)$ to have a comparable effect. Naively, the scale of the energy density for a field theory with c_0 fields in a geometry with length scale L would be c_0/L^4. The number of fields in our effective theory is expected to be relatively small, so we require that the Casimir energy density is larger than its "natural" value by a factor of $L^2/(Gc_0) \sim c_{3D}/c_0$. Thus, we have the unusual situation of needing a vacuum energy that is anomalously *large*.

A more specific quantitative connection between the Casimir energy density and the scale of curvature in the geometry is provided by evaluating the $++$ component of the Einstein equation at the middle of the wormhole where $\hat{a}'_E = 0$. For this component, the cosmological constant term does not contribute, so the connection between the curvature scale and the energy density is more direct. We have that

$$T_{++} = \frac{1}{8\pi G}R_{++} = -\frac{1}{4\pi G}\frac{\hat{a}''_E}{\hat{a}_E} \sim -\frac{1}{G}\frac{1}{\ell^2} = -\frac{\ell^2}{G}\frac{1}{\ell^4}\,, \tag{5.18}$$

where we have chosen coordinates such that $a(0) = 1$, and ℓ is the length scale associated with the curvature at the midpoint of the wormhole. Thus, to get $\ell \gg \sqrt{G}$, i.e. a wormhole that is large compared to the Planck scale, we need negative null Casimir energy that exceeds the geometrical scale $1/\ell^4$ by a large factor $\frac{\ell^2}{G}$. In appendix E, we show that the integrated null-energy along a null path from one asymptotically AdS boundary to the other must also be negative. Thus, the averaged null energy condition is also violated, but this is typical for Casimir energies.

Since such a large factor is absent for the Casimir energy density of a field on a space with a periodic spatial direction, the interface in the effective field theory picture between the fields on the wormhole and the non-gravitational 4D CFT fields must play an essential role. To understand whether certain interfaces can give rise to such enhancement, [5, 56] studied holographic models of interface quantum field theories. Remarkably, it was found that the needed enhancement of Casimir

energy appears for special choices of the interface physics. We will discuss these results in detail in the next chapter. The somewhat surprising appearance of this energy enhancement provides some evidence for the viability of the class of models we are studying.

Classical scalar field contributions

Another possible contribution to the stress-energy tensor which is consistent with the symmetries of the wormhole geometry is to have one or more scalar fields with a non-trivial classical profile $\phi(\tau)$. We will see below that having non-trivial scalars is generic when the 3D CFT that we start with has relevant or marginally relevant operators, as the variation of these scalars reflect possible RG flows that we might have with this 3D CFT in the UV [181].

With varying scalars, potential terms and derivative terms will both contribute to the stress-energy tensor and back-react on the geometry. In the cosmology picture, we will in this case have a time-dependent scalar field. We will see in Section 5.3.6, and in much more detail in Chapter 8, that this can give rise to a phase of accelerated expansion before the recollapse.

The presence of a non-trivial scalar field does not remove the need for a large Casimir energy. For example, in the wormhole picture with conformal distance coordinate z, we have that the contribution of the scalar field to the null energy is

$$T_{++} = \partial_z \phi \partial_z \phi > 0 \,. \tag{5.19}$$

This gives a positive contribution to the left side of equation (5.18), so the large negative Casimir energy is still required to agree with the right side of the equation.

5.3.4 Example: CFT matter

We now describe a few simple examples of our scenario at the level of effective field theory.

To begin, we review the case where the matter in the gravitational part of our effective field theory is taken to be a CFT [56]. This is not what is expected from the microscopic models, but it has the advantage of being analytically tractable. In particular, the form of the stress-energy tensor is determined up to an overall constant by conformal invariance.

To find the form of stress-energy tensor, we can make use of conformal coordinates (see Appendix D) and perform a conformal transformation to flat space $\mathbb{R}^{2,1} \times [-z_0, z_0]$. Conformal invariance and 2+1 Poincaré symmetry imply that the vacuum stress tensor in this conformal frame takes the form

$$T_{zz} = -\frac{3}{z_0^4} F(z_0) \qquad T_{\mu\nu} = \eta_{\mu\nu} \frac{1}{z_0^4} F(z_0) \tag{5.20}$$

where F is a dimensionless constant that could depend on the ratio between z_0 and any other parameter with dimensions of length, for example the width of the strip of 4D CFT that couples the two asymptotically AdS regions, or some parameter associated with the interface.

We recall that the field theory in the wormhole geometry is coupled at its boundaries via a 4D CFT on a strip. The constant F can depend on our CFT, the non-gravitational CFT that couples the fields at the boundaries of the wormhole, and the physics of the interface between the two CFTs.

In the original conformal frame, the stress tensor using conformal coordinates becomes

$$T_{zz} = -\frac{1}{\hat{a}_E^2} \frac{3}{z_0^4} F + T_{zz}^{CA} \qquad T_{\mu\nu} = \eta_{\mu\nu} \frac{1}{\hat{a}_E^2} \frac{1}{z_0^4} F + T_{\mu\nu}^{CA} \tag{5.21}$$

where T_{zz}^{CA} and $T_{\mu\nu}^{CA}$ are terms due to the 4D conformal anomaly. In general, these are a specific combination of curvature squared terms whose coefficients depend on our choice of CFT. As in our

discussion above, we expect that these can be ignored when the curvature of the geometry is much larger than Planck scale, i.e. away from the big bang/big crunch. We will drop them for now in our discussion of the wormhole picture.[45]

Ignoring the conformal anomaly, the zz component of Einstein's equation gives

$$\left(\frac{\hat{a}'_E}{\hat{a}_E}\right)^2 - \frac{\hat{a}_E^2}{L^2} = -\frac{8\pi G}{z_0^4} F \frac{1}{\hat{a}_E^2} \,, \tag{5.22}$$

where L is the AdS radius. Integrating this we obtain

$$\int_{a_0}^{\hat{a}_E(z)} \frac{da}{\sqrt{\frac{a^4}{L^2} - \frac{8\pi G F}{z_0^4}}} = z \tag{5.23}$$

where a_0 is the minimum value of $\hat{a}_E$ where $\hat{a}'_E = 0$,

$$a_0 = \frac{1}{z_0}(8\pi G F L^2)^{\frac{1}{4}} \,. \tag{5.24}$$

For $z = z_0$, we have $\hat{a}_E \to \infty$, so we get

$$\int_{a_0}^{\infty} \frac{da}{\sqrt{\frac{a^4}{L^2} - \frac{8\pi G F}{z_0^4}}} = z_0 \tag{5.25}$$

which gives

$$F = \frac{\mathcal{I}^4 L^2}{8\pi G} \,. \tag{5.26}$$

where

$$\mathcal{I} = \int_1^{\infty} \frac{dx}{\sqrt{x^4 - 1}} = \frac{\Gamma\left(\frac{3}{2}\right)\Gamma\left(\frac{1}{4}\right)}{\Gamma\left(\frac{3}{4}\right)} = \frac{\sqrt{2}}{2} K\left(\frac{\sqrt{2}}{2}\right) \approx 1.311 \,. \tag{5.27}$$

We recall that F represents the energy density in units of the geometrical length scale in the conformal frame, where we have a CFT Minkowski space between two boundaries separated by z_0. As we discussed above, this would normally be expected to be of order the central charge c_0 of the CFT we are considering, but here we need it to take a much larger value $L^2/G \sim c_{3D}$, i.e. comparable to the central charge of the underlying holographic 3D CFT. However, such anomalously large values can arise with appropriate boundary physics, at least in certain holographic CFTs. We will discuss this in detail in the next chapter.

Lorentzian solutions with CFT matter

It is straightforward to work out the Lorentzian cosmology that arises from this example. Again ignoring the conformal anomaly term, and using (5.26), the Friedmann equation gives (in proper time coordinates)

$$\left(\frac{\dot{a}}{a}\right)^2 + \frac{1}{L^2} = \frac{\mathcal{I}^4 L^2}{z_0^4} \frac{1}{a^4} \,. \tag{5.28}$$

This is equivalent to standard cosmological evolution with radiation and a negative cosmological constant. The Universe expands from a big bang to a maximum scale factor and then contracts

[45] We will see that this assumption implies $F \sim L^2/G$, so that the conformal anomaly term is indeed smaller than the term we keep by a factor of $1/F \ll 1$.

again. We can choose coordinates so that the maximum scale factor is $a = 1$ when $\dot{a} = 0$. This gives $z_0 = \mathcal{I}L$. Defining $t = Ls$ so that s is the time in units of the curvature scale L, the evolution equation simplifies to

$$\left(\frac{\dot{a}}{a}\right)^2 + 1 = \frac{1}{a^4} \,, \tag{5.29}$$

with solution $a = \sqrt{\cos(2s)}$. In terms of the comoving time variable t, the metric is thus simply

$$ds^2 = -dt^2 + \cos\left(\frac{2t}{L}\right) d\vec{x}^2 \,. \tag{5.30}$$

so we have a big-bang / big-crunch cosmology with total proper age $L\pi/2$ determined by the AdS scale in the wormhole picture.

As discussed in [56], the conformal anomaly terms can alter the behavior near the big bang and big crunch. For example, the special case where the conformal anomaly contributes only first-derivative terms to the Friedmann equation leads to an equation whose solution cannot be extended back past an initial time with energy density $T_{00} \sim 1/(c_0 G^2)$ where c_0 is a measure of the number of degrees of freedom in the effective field theory.

5.3.5 Non-conformal effective field theory

In microscopic examples, we expect that the effective field theory describing quantum fields in our setup will be some non-conformal field theory.

Here, the stress-energy tensor computed on a fixed background will be some more complicated functional of the scale factor; in conformal coordinates we can represent this as

$$T_{zz} = -\frac{1}{a^2}\frac{3}{z_0^4} F_a(z) \,. \tag{5.31}$$

The dependence of F on a may be complicated and non-local. In the cosmology picture, the resulting stress tensor evolution will also be more complicated and reflect the RG behavior of the field theory.

5.3.6 Evolution with a scalar field

It is natural to consider the possibility of one or more scalar fields with classical values that depend on time in the cosmology picture or on the τ coordinate of the wormhole. Such scalar field configurations preserve the spacetime symmetries of the setup and lead to models with time-dependent dark energy. In order to explain the current observations of an accelerating Universe using our framework, having a time-dependent scalar field at some positive value of its potential is required, or at least is the simplest possibility.

The presence of scalar fields is generic in the gravitational effective field theories that correspond to our microscopic models. According to the AdS/CFT correspondence, we have a light bulk scalar field for each low-dimension scalar operator in the CFT, with the scalar field mass related to the operator dimension (for the case of a 3D CFT) by[46]

$$m^2 L^2 = \Delta(\Delta - 3) \,. \tag{5.32}$$

[46]This gives a constraint $m^2 L^2 > -9/4$, which is the Breitenlohner-Freedman bound for 4D gravity theories with stable AdS vacua. It is not completely clear that such stability is required in our setup; it might be interesting to explore whether models based on more general gravitational theories (perhaps dual to unstable or non-unitary 3D CFTs) could be sensible.

If the CFT is chosen so that the 4D cosmological constant $1/L^2$ is small, the scalar masses (which set the scale of the derivatives of the potential near the origin) will also be small. The result is that when these scalar fields vary, it is natural for them to be changing non-trivially throughout the spacetime.

If the CFT has both relevant and irrelevant scalar operators, the asymptotic values of the scalar fields will correspond to a saddle of the potential with both positive and negative directions. Generically, the potential will also have higher order terms, and these tend to make the potential positive for large values of the fields (assuming the AdS solution dual to our 3D CFT is stable). For example, in the 4D gauged supergravity models associated with 3D SCFTs with extended supersymmetry, the scalar potential is a quartic polynomial [182]. In models with less supersymmetry, the potential can be much more complicated (see e.g. [183] and references therein for examples).

For solutions of the dual gravitational theory that are controlled by our 3D CFT in the UV, the most generic situation is to have scalar fields associated with the relevant or marginally relevant operators of the theory vary from the saddle-point values as we move away from the AdS boundary. These solutions correspond to taking the dual quantum field theory to be an RG flow obtained by perturbing the CFT with a relevant operator.[47] The strict CFT is a special case where all such perturbations are set to zero.

In this section, we will describe the physical effects of such varying scalar fields in some generality, showing that they can lead to a phase of accelerated expansion. A more detailed analysis of these setups will be discussed in Chapter 8.

Scalar field evolution in the wormhole picture

It is convenient to start with the radial evolution of the scalar field in the wormhole picture. Here, using proper distance coordinates, the equation of motion for scalar fields ϕ_i with potential $V(\vec{\phi})$[48] is

$$\phi_i'' + 3H_E\phi_i' - \partial_i V(\vec{\phi}) = 0 \tag{5.33}$$

(where $H_E \equiv a_E'/a_E$) and the field makes a contribution

$$\rho_E^\phi = -\frac{1}{2}(\partial_\tau \vec{\phi})^2 + V(\vec{\phi}) \tag{5.34}$$

to the right side of the scale factor evolution equation (5.15). In this picture, the evolution of $\vec{\phi}$ with τ is equivalent to the time evolution of a particle in a potential $-V(\vec{\phi})$ with damping coefficient $3H_E$ that becomes constant in the asymptotically AdS regions. We are interested in time-symmetric solutions, so the derivative of $\vec{\phi}$ should vanish at the midpoint of the wormhole. Moving away from the time-symmetric point, a_E increases,[49] so the evolution of $\vec{\phi}$ going away from this point will correspond to ordinary damped motion in the inverted potential.

For a given potential, the possible time-symmetric solutions will be in one-to-one correspondence with the value $\vec{\phi}_0$ of the scalar field at the midpoint of the wormhole. If $\vec{\phi}_0$ corresponds to an extremum of $V(\vec{\phi})$ the scalar will be constant throughout the geometry, and $V(\vec{\phi}_0)$ will be the cosmological constant. Otherwise, $\vec{\phi}$ will move downward (initially along the steepest path) in the inverted potential as we move toward the AdS boundary, as shown in Figure 5.7 (left).

[47] Even if we start with the strict 3D CFT, such perturbations might be induced by the coupling to other 3D CFT via the 4D CFT.

[48] It will be convenient to absorb the cosmological constant into the definition of the scalar potential; we will assume this throughout this section.

[49] The second time derivative of the scale factor is negative at the time-reversal symmetric point of the cosmology, so the second τ derivative is positive at the midpoint of the wormhole.

Behavior at the AdS boundary

As we have explained above, having a varying scalar field as we go to the asymptotically AdS regions corresponds to the underlying 3D CFT being deformed in the UV by a relevant or marginally relevant scalar operator.[50] In this case, the scalar will descend to a value $\vec{\phi}_B$ corresponding to an extremum of $-V$ (or rise to an extremum of V) at the boundaries where $V(\vec{\phi})$ is still negative.[51] Alternatively, going away from the boundary, the scalar rolls down a direction in the potential $V(\vec{\phi})$ with negative second derivative, corresponding to a massless or negative mass-squared scalar that still satisfies the Breitenlohner-Freedman bound [184].

Scalar field evolution in the cosmology picture

In the cosmology picture, the scalars will take the values $\vec{\phi}_0$ at the time-symmetric point and have vanishing time derivatives here.

The equation of motion in the cosmology picture with comoving (proper time) coordinates is

$$\ddot{\phi}_i + 3H\dot{\phi}_i + \partial_i V(\vec{\phi}) = 0 \tag{5.35}$$

and the field makes a contribution

$$\rho^\phi = \frac{1}{2}(\partial_t \vec{\phi})^2 + V(\vec{\phi}) \tag{5.36}$$

to the energy density appearing on the right side of the Friedmann equation (5.10).

As is familiar from discussions of inflationary cosmology, the dynamics of the scalar field is that of a particle in a potential $V(\vec{\phi})$ with time-dependent damping coefficient $3H$, such that we have usual damping in the expanding phase of the Universe and anti-damping in the contracting phase (or evolving backwards towards the big bang). In order to be stationary at the time-symmetric point, the scalars should be rolling up the potential before this. As we described above, a typical potential in a theory supporting a stable AdS vacuum will have interaction terms that make the potential bounded below and positive for large values of the field. Thus, in the anti-damped motion going back toward the big bang, a typical situation would be for the scalar to descend to some lower value of the potential before rising again to positive values (time-reverse of Figure 5.7, right).

A phase of accelerated expansion

Going backward from the time-symmetric point, we have a phase of decelerated expansion while the scalar potential is negative. But at earlier times when the scalar potential reaches positive values, we can have a phase of accelerated expansion. Whether or not such a phase exists depends on the details of the potential, and in particular whether the scale factor reaches $a = 0$ going backwards in time before the scalar potential reaches large enough values to dominate over the matter and radiation.

If the accelerated expansion in our Universe is explained in this way, the scalar must be rolling sufficiently slowly at the $V > 0$ point corresponding to the present time to be consistent with the observations. In Chapter 8 we investigate in detail whether there exist potentials giving rise to evolution that satisfies observational cosmological constraints.

[50] We ignore the case where the scalar blows up at the asymptotically AdS boundary, since we are assuming that the UV behavior corresponds to some well-defined CFT.

[51] In some cases, it might be that the scalar will oscillate before settling to this extremum. However, the relation (5.32) gives a lower bound $m^2L^2 \geq -9/4$. At least in the asymptotic region where $a'/a = 1/L$, the equation (5.33) for the scalar evolution corresponds to overdamped or critically damped motion, so there won't be oscillations in this region.

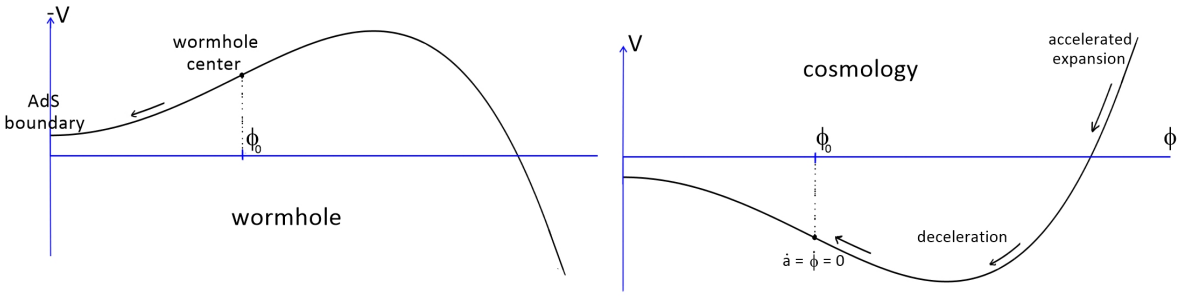

Figure 5.7: Scalar field potential $V(\phi)$. Left: evolution of the scalar from the wormhole centre to the asymptotically AdS region corresponds to damped motion in the inverted potential $-V$ with damping "constant" $3a'_E/a_E$. The evolution of the scalar is dual to the RG flow induced by perturbing the dual CFT by a relevant operator. Right: Evolution of the scalar field in the cosmology from early times to the time-reversal symmetric point corresponds to damped motion in the potential V with damping constant $3\dot{a}/a$. The initial positive values of the potential typically give rise to a phase of accelerated expansion before deceleration and collapse.

Inflation at early times?

In our setup, the potential takes small values in the wormhole solution and for the late time cosmology (near the time-symmetric point) by construction (choosing an appropriate 3D CFT). However, in the surrounding "landscape" of string theory, the more generic values for the potential are expected to be closer to Planck scale. It is possible that the initial conditions for the matter/radiation dominated phase were set up by an early period of inflation where the scalar potential took much larger values, but it is not clear that such a phase is generic in our models or that it would happen at an energy scale where effective field theory is valid.

However, as we have emphasized above, it appears to be unnecessary in our model to understand the details of the early Universe physics in order to compute cosmological perturbations. Cosmological observables in our model are computed most naturally in the wormhole picture where the effective field theory should be valid everywhere and the quantum state is time-independent. Here, the scalar field only explores a small region of the potential near the saddle that corresponds to the dual 3D CFT.

So while there may be inflation in the early Universe of the cosmology picture, and the physics of inflation may provide an explanation for the origin of perturbations, etc... in that picture, understanding the details of this early Universe physics is not necessary to extract the predictions of the model. The wormhole picture provides in some sense a dual picture of the physics, with a different explanation for the origin of correlations relevant to cosmological observables. We will discuss this further in Section 5.4.

Evolution from the initial time

In our scenario, it is most natural to consider the evolution of the scalar field from the asymptotically AdS boundary to the midpoint of the wormhole and then backward in time to the early Universe as we have described. But it is also helpful to envision the evolution in the other direction, since this corresponds to more intuitive ordinary damped motion in the potential.

The evolution is summarized in Figure 5.7. Starting from a positive value of the potential and some large density of matter and radiation (that may have come from an inflationary phase)

the scalar will roll down[52] to some negative value of the potential V before rising again. The potential might oscillate up and down multiple times due to the motion of the scalar in the vicinity of a minimum. At the time-symmetric point, the scalar comes to rest at a point $\vec{\phi}_0$ between two extrema, approaching this point along an upward trajectory of steepest increase.

The scalar field also takes the value $\vec{\phi}_0$ at the midpoint of the wormhole in the dual picture, but going away from this point evolves via damped motion in the inverted potential $-V$, eventually descending to the extremum that corresponds to our dual 3D CFT. The initial conditions required to get a time-symmetric scale factor (i.e. $\dot{\vec{\phi}} = 0$ when $\dot{a} = 0$) and end up in the wormhole picture at a non-minimal extremum of $-V$ would appear to be finely tuned in the cosmology picture, but the microscopic setup guarantees these will arise.

Symmetry breaking

Having a non-zero scalar field expectation value away from the asymptotically AdS regions may be associated with a breaking of gauge symmetry and/or supersymmetry, such that the low-energy effective field theory relevant to the description of physics near the middle of the wormhole or in the cosmology picture is different than the effective field theory describing physics in the asymptotically AdS regions (which would be supersymmetric in microscopic models built from a 3D SCFT). If there is supersymmetry in the effective theory for the asymptotically AdS regions, a challenge is to explain why the scale of SUSY breaking is so much larger than the scale of the vacuum energy in the low energy effective description of the cosmology. This may be explained fairly naturally if it is the value of the scalar field that sets the supersymmetry breaking scale, since the typical potentials in 4D gravity theories dual to CFTs remain of order $8\pi GV \sim 1/L^2$ when the scalar fields themselves have Planck scale variations.[53] As we have described above, if such scalar field expectation values and other features of the state are the only thing that breaks supersymmetry in the cosmology picture, the supersymmetric cancellations that prevent a large quantum correction to the cosmological constant may persist.

It would be useful to understand the possibilities for the low energy physics of theories obtained by starting from a supersymmetric 4D gravity with with an AdS vacuum and breaking symmetries via expectation values for scalars in directions corresponding to relevant operator deformations in the CFT.

5.4 Fluctations about the background

The Euclidean path integral that defines our model corresponds to a gravitational path integral; we have been assuming this will be dominated by a saddle-point configuration that corresponds to the background geometry we have been discussing. However, the path integral also includes fluctuations about the background geometry. In the cosmology picture, these fluctuations correspond to different possible realizations of structure in the Universe. Thus, the microscopic wavefunction describes an ensemble of possible cosmologies, rather than a single instance.

We can ask about the size of the perturbations (e.g. via the variance of various quantities in the ensemble) and also about the correlations between perturbations in typical elements of the ensemble. Information about these cosmological perturbations is contained in the correlation functions of the

[52] A more general possibilitiy is that the scalar will move up the potential before rolling down, or have various oscillations.

[53] For example, a typical Lagrangian density would be $(\partial\phi)^2 - c_0/(GL^2) + c_2/L^2\phi^2 + c_4 G/L^2\phi^4$, with c_i order one, so $8\pi GT$ will stay of order $1/L^2$ as ϕ takes values of order $1/\sqrt{G}$.

stress-energy tensor and other fields, and ultimately in the Euclidean QFT path integral that defines the microscopic state.

For example, we can consider the two-point function of the difference of the energy density from background $\langle(\rho(x)-\bar{\rho})(\rho(0)-\bar{\rho})\rangle$; the $x=0$ case gives the variance at a point. While the overall energy density expectation value $\bar{\rho}$ is spatially constant (since our setup preserves translation invariance), the individual configurations contributing to the wavefunction of the Universe will be inhomogeneous, and the quantitative information about these inhomogeneities can be extracted from the two-point function.

As we have emphasized above, since the same microscopic Euclidean path integral that defines the state of the cosmology is associated with the vacuum state of the confining gauge theory, the fluctuations that give rise to cosmological structure have an alternative interpretation as vacuum fluctuations in the wormhole picture. Correlations in the cosmology picture are related directly to the vacuum correlations in the wormhole picture.

For example, in a realistic cosmology with a Maxwell field, correlation functions of the energy density of this field (which would tell us about CMB observables) are related by analytic continuation to correlations of the stress tensor component $T_{\tau\tau}$ for the same field in the wormhole picture. In particular, any energy density correlators at the time-symmetric point of the cosmology are simply equal to the vacuum correlators $T_{\tau\tau}$ at the midpoint of the wormhole, provided all the operators sit in the same two dimensional plane, i.e. the plane formed by the two coordinates in $\mathbb{R}^3$ that are spatial in both pictures.

In the wormhole picture, correlation functions of bulk fields should be related in a relatively simple way to the correlation functions of operators in the microscopic field theory, using an HKLL-type prescription appropriate to our background geometry. That is, the bulk operator should correspond to a linear combination of local operators in the underlying field theory (mostly localized to the pair of 3D CFTs). So one could in principle use the microscopic field theory to calculate cosmological observables, though in practice, employing the effective field theory description in the wormhole picture should be adequate for most questions.

An important next step will be to investigate the behavior of the correlators in our model and understand the predictions for cosmology. However, there is already one promising qualitative feature.

An alternative to inflation or a dual description?

A distinctive feature in the density perturbations observed via the CMB is that there are correlations between regions of the Universe that would have never been in causal contact if we assume simple cosmological evolution since the big bang. The theory of inflation naturally explains these correlations by introducing an early period of accelerated expansion. However, in our model, these correlations can be explained in a different way. They arise naturally since the cosmological correlators are directly related to vacuum correlators in the wormhole picture, and in a vacuum state on a static geometry, it is natural to have correlations at all scales (e.g. any two points have been in causal contact).

We note also that the standard horizon and flatness problems addressed by inflation are naturally explained by the $\mathbb{R}^3$ symmetry of the model and the fact that the natural "initial" state lives at the time-symmetric surface. On the other hand, we don't know whether perturbations in our model agree with cosmological observations at the quantitative level.

While one possibility is that our model provides an alternative to inflation, it is also possible that the wormhole picture provides a dual description of the same physics. It may be that in the cosmology picture there is inflation and that this generates the density perturbations in the usual

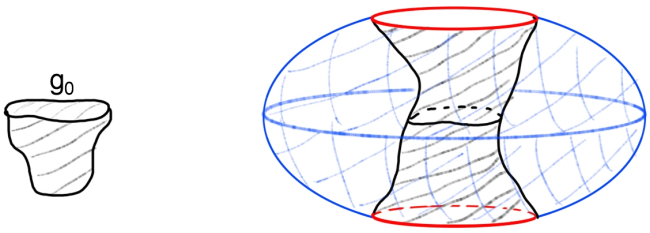

Figure 5.8: Left: Geometry contributing to the Hartle-Hawking wavefunction of the Universe $\Psi[g_0]$, defined as a gravitational path integral over topologies with the only boundary corresponding to the metric g_0. Right: A contribution to the gravitational path integral in our setup. In this case, the Euclidean gravity configurations have asymptotically AdS boundaries in the Euclidean past and future, and the fields at these boundaries are coupled together. The pictures correspond to the case of a closed Universe (spatial slices S^1 in the picture); the flat Universe we are focusing on can be obtained by taking the sphere volume to infinity.

way. In this case, the results must agree with the calculations in the wormhole picture where no knowledge of the early-Universe physics or the inflationary potential is required. In this scenario, the inflationary physics would be dual to the vacuum physics of the wormhole in a similar way to how field theory and gravity can provide different explanations for the same phenomenon in AdS/CFT.

5.4.1 The wavefunction of the Universe in the effective field theory description

While the microscopic quantum state describing the cosmology is constructed using a CFT path integral, we can also think about the state of the Universe from the effective field theory point of view as arising from a certain Euclidean gravity path integral in the effective field theory picture.

It is interesting to contrast this path integral with the one that Hartle and Hawking considered [139]. Hartle and Hawking suggested that the wavefunction of the Universe most naturally arises from a wavefunction $\Psi[g_0]$ where the probability amplitude for a field configuration g_0 is given by a Euclidean gravitational path integral over all four-dimensional Euclidean geometries / field configurations having g_0 as the data at a boundary, with no other boundaries allowed.

In our approach, the state of the Universe may also be naturally understood as arising from a Euclidean path integral. In the effective field theory description, the gravitational configurations contributing to the path integral used for computing observables have asymptotically AdS boundaries in the Euclidean past and future, and the fields in these asymptotic regions are coupled together via a non-gravitational CFT, as shown in Figure 5.8. This non-gravitating field theory serves as an anchor for the fluctuating geometries contributing to the gravitational path integral. The holographic picture suggests that these geometries should be homologous to the fixed geometry of the non-gravitational field theory.

A qualitative difference between our case and the Hartle/Hawking picture is that the fields in our cosmological spacetime are in a mixed state, entangled with the fields in the non-gravitational quantum field theory. Tracing out these auxiliary fields may play a role in understanding how an ensemble of classical cosmologies arises from the wavefunction of the Universe in our model.

5.4.2 The arrow of time

The special state in our cosmology is time-symmetric, so one must understand how the arrow of time emerges for observers in the model. The same issue arises for the Hartle-Hawking proposal, and there have been a number of previous discussions (see e.g. [185]). In [148], following Page [185], it was suggested that the model might describe an ensemble of different cosmologies, some of which have arrows of time in one direction and some of which have arrows of time in the other direction. Here, we point out an interesting alternative, motivated by the idea that i) the arrow of time relates to the classical physics experienced by observers, ii) the emergence of classicality involves decoherence, and iii) that the physics of decoherence should occur either with forward quantum evolution or backward quantum evolution. The idea is that there might be two complementary bases of states, for which the basis elements are not time-reversal invariant, but the two bases are related by time-reversal. The in and out bases of states in discussions of scattering in quantum field theory provide an example. The full state can either be expressed in terms of the forward basis or the backward basis. Using the forward basis and tracing over some unobserved environmental degrees of freedom, we get an ensemble of states that might represent possible cosmologies with a forward arrow of time. Doing the same starting with the backward basis, we would then get an ensemble of possible cosmologies with a backward arrow of time. This picture has the intriguing property that each possible forward cosmology could be mathematically represented as a complicated superposition of backward cosmologies. However, further work is required to understand whether this possibility is sensible.

5.5 Discussion

In this chapter, we have described a possible framework for cosmology motivated by two guiding principles (where the second was suggested by the first):

- There should be a fully non-perturbative microscopic description of the theory.
- There should be a preferred state.

In other words, we are exploring the most optimistic possible scenario for understanding the large-scale physics of our Universe. Unlike our "bubble of cosmology" model from Chapter 4, the cosmologies described in this chapter are globally (rather than just locally) homogeneous and isotropic.

The first principle, together with our current understanding of string theory, led us to focus on the possibility that the fundamental cosmological constant in the effective theory describing our Universe is negative. The existence of an asymptotically AdS analytic continuation suggested both a fundamental description involving 3D CFTs and a preferred state constructed using a Euclidean path integral. An unexpected consequence is the existence of a dual physical system whose vacuum state encodes most of the cosmological physics.

The resulting Universe has a number of attractive features. Homogeneity, isotropy, and flatness are consequences of the symmetry of the model (and the fact that the present state of the Universe is most naturally understood via backward evolution from the time-symmetric point). The equivalence between cosmological observables and vacuum observables in the dual wormhole system provides a natural explanation for the existence of correlations at all scales. This relation also means that any cosmological observables can be computed in principle without knowledge of the physics near the big bang, and without detailed knowledge of the UV completion. In particular, even if there is inflation at early times in the cosmology description, we can compute cosmological perturbations in the dual picture without knowledge of the inflationary potential.

The simplest toy example of our setup (with CFT matter) gives the simplest nontrivial $\Lambda < 0$ cosmology with radiation and cosmological constant leading to a big-bang / big crunch Universe. This Universe does not have an accelerating phase, but more generic examples of our setup have time-dependent scalar fields leading to time-dependent dark energy. These may exhibit a phase of accelerated expansion before the collapse and a phase of matter/radiation domination before that. We will explore this possibility in Chapter 8.

The small cosmological constant is related to the large number of degrees of freedom in the underlying 3D CFTs and (likely) the presence of supersymmetry in the fundamental description. The gauge group for the effective theory is controlled by the global symmetry group of the underlying 3D CFT; microscopic supersymmetric examples with almost any global symmetry group are known. Finally, both the model and the state are completely specified by our choice of 3D and 4D CFTs.

5.5.1 Challenges

We emphasize that it is still an open question to demonstrate definitively that there are fully microscopic examples of this cosmological scenario, and a further challenge to understand whether examples of such models make predictions that are consistent with observations at a quantitative level. An important question is to verify that 3D-4D-3D quantum field theory systems of the type we have described can be dual to a Lorentzian wormhole. To demonstrate the viability of these models more directly, there are various options. For the fully microscopic examples suggested in [56], a classical type IIB supergravity calculation (or alternatively, a strongly coupled field theory calculation) is required to verify that the dual geometries have the right properties. Alternatively, one could try to understand precisely the four-dimensional effective gravitational theory for a microscopic example and understand how this can support a wormhole. Better understanding when and how quantum field theories can exhibit the appropriate vacuum energies to support a static Lorentzian planar wormhole is clearly an important step.

To understand whether the model presented in this chapter can give rise to realistic examples of cosmology, there are many things to check. First, it is necessary to verify that the model presented here is consistent with observations constraining the background cosmology, i.e. the scale factor. We will begin to explore this question in Chapter 8, where we will show that acceleration is a generic feature of the types of scalar potentials described here, and that potentials exist which result in a $\Lambda < 0$ cosmology which has a scale factor that perfectly matches that of a standard ΛCDM model with $\Lambda > 0$. Moreover, following our work it was verified that the potential energy from a time-dependent scalar field (which can have a negative extremum) can quite generically provide cosmological evolution in agreement with redshift vs brightness type Ia supernovae data [186]. These results suggest that, at least at the level of the background cosmology, practitioners used to to working with $\Lambda > 0$ cosmologies have nothing to fear in making the transition to $\Lambda < 0$.

Of course there are other tests which our cosmological model must pass before it can be taken seriously as a model of our Universe. It will be important to check whether the cosmological perturbations in our models can have the right magnitude and correlations, and whether we can satisfy numerous other phenomenological constraints, e.g. obtaining the Standard Model as an effective theory and getting the right amount of dark matter and baryon asymmetry.[54] Since accelerated expansion in our models relies on having one or more time-dependent scalar fields with a very flat potential, it must be understood why other effects of such light scalar fields (e.g. long range forces or time-dependent couplings) have not been observed.[55]

[54] The time-dependent scalar fields that are generic in this class of models may be helpful in explaining the baryon asymmetry [187].

[55] A simple possibility is that these scalar fields are in the dark sector; fermions coupling to the scalar via $\phi\bar{\psi}\psi$

Regardless of whether the scenario presented here turns out to be fully realistic, it may still allow us to make progress on fundamental questions about quantum cosmology, just as we have learned about the quantum description of black holes through AdS/CFT.

5.5.2 Cosmological Islands

The fact that the effective field theory description of our cosmology includes an auxiliary system with which the fields in the cosmological spacetime are entangled is related in an intriguing way to observations in [179]. There, the authors asked when regions of cosmological spacetimes could be "entanglement islands", regions whose degrees of freedom are entangled with some other disconnected system in the effective field theory such that the two parts together form a proper quantum subsystem with a generalized entropy (and thus potentially dual to a quantum subsystem of a microscopic theory). They found that for certain $\Lambda < 0$ flat cosmologies, large enough spatial systems at times close enough to the recollapse point satisfy the criteria to be an island. In that analysis it was not clear what the complementary disconnected system or the microscopic description could be. Our analysis suggests that exactly in the case where [179] found islands, we can give a microscopic description, and the microscopic description indeed involves an auxiliary system with which the fields in the cosmology picture are entangled.

We can also argue directly that large enough subsystems of our cosmology are islands. Consider a ball-shaped region of radius R in the microscopic 4D CFT. For large enough R, this will encode not only the physics of the same region in the 4D CFT in the effective description, but also part of the cosmology. To see this, consider a ball of radius R in the auxiliary system on the time-symmetric slice. This will have thermal entropy scaling like R^3. When R is much larger than the thermal scale, the fields in this region will be mostly purified by fields in the cosmology picture. It should thus be possible choose a similar ball-shaped region of the cosmology (also on the time-symmetric slice) with size proportional to R such that the entropy of the combined system now scales as R^2, coming from degrees of freedom near the boundaries of the two balls. Thus, for large enough R, this combined system with a cosmological island has smaller generalized entropy and provides the correct dual description of the microscopic CFT region.

This is even clearer when the 4D CFT is holographic. In this case, an RT surface for a ball-shaped region in the microscopic theory that remains outside the horizon will have area scaling like R^3 for large R, while an RT surface that enters the horizon and ends on a spherical region of the ETW brane will have area that scales like R^2 for large R. So for large enough R, the latter surface is preferred, and the entanglement wedge includes part of the cosmology. This transition in entangling surfaces and the appearance of islands on the cosmological brane was originally observed and studied in [102].

We can also take the limit where the 4D CFT region size goes to infinity, in which case the entire time-symmetric slice in the cosmology is an island. Hence, the 4D CFT state at the time-symmetric point already has enough data to encode the entire cosmological evolution without any CFT time evolution. This is consistent with the cosmological time evolution being emergent and unrelated to the 4D CFT time evolution.[56] Moreover, in the special case where the 4D CFT is holographic, the Wheeler-DeWitt patch of the time-symmetric point includes the entire end-of-the-world brane trajectory, in agreement with the general analysis.

couplings in the underlying theory will have large masses when ϕ has large expectation values. For a more detailed discussion, see e.g. [188, 189].

[56] The disconnection between cosmological time evolution and CFT time evolution is even more evident if we consider that islands at the time-symmetric point $t = 0$ of the cosmology can be part of the entanglement wedge of regions R of the 4D auxiliary CFT even at late CFT times $t_{\mathrm{CFT}} > 0$ [179].

It is interesting to ask which other cosmological spacetimes can support islands - this may give us a hint whether any other types of cosmologies might have a holographic description similar to the one we are considering. This question was considered in some generality in [179] and [190, 191]. For $\Lambda < 0$ ball-shaped islands continue to be possible for closed or open Universes (i.e. where the spatial curvature is positive or negative), provided that the radius of curvature is sufficiently large [191]. This is consistent with the fact that the microscopic approach suggested in this chapter can be generalized to positive or negative spatial curvature by replacing the $\mathbb{R}^3$ in the construction with S^3 or H^3. The curvature scale for these must be sufficiently large compared to the size of the interval separating the 3D CFTs to end up with the desired confining phase [102].

For $\Lambda \geq 0$, it was found that no islands are possible in flat [179] or open [191] cosmologies. For closed cosmologies (i.e. with positive spatial curvature), a new island candidate is given by the whole cosmological Universe, regardless of the sign of Λ. Thus, it is interesting to ask whether some special state of a 4D CFT on S^3 might also encode the physics of cosmological spacetimes with S^3 spatial geometry and $\Lambda \geq 0$. It is not clear how such a state could arise from a Euclidean path integral, though.

5.5.3 Summary of features

Whether or not the models we are describing turn out to be viable for realistic cosmology, they have a number of interesting features that might be useful in future approaches. To conclude the chapter, we highlight some of the particular features that appear and that might inform future research.

First, we have various motivations to consider $\Lambda < 0$ cosmology:

- We take the existence of a complete, non-perturbative microscopic description as a guiding principle for describing cosmology. Given the present state of our understanding of string theory, this suggest that we focus more on the $\Lambda < 0$ possibility.
- Specifically, with $\Lambda < 0$, we avoid the vacuum instabilities and complicated bubbling multiverse picture that appears in $\Lambda > 0$ discussions. While this picture may dynamically give rise to anthropically allowed positive values of Λ if enough $\Lambda > 0$ string vacua exist [104], it seems difficult to establish that the required landscape of vacua exists (see e.g. [42]), and difficult to imagine what a microscopic description of such a scenario could look like.
- Considering models with time-dependent scalar fields (which can lead to an accelerated expansion phase even if $\Lambda < 0$) is natural in that this is the most general situation consistent with the symmetries of cosmological spacetimes. It is also natural from the string theory point of view, since the best understood regions of the string landscape with small positive potential energy are regions near AdS minima where we have excited some scalar fields.

An interesting feature of $\Lambda < 0$ is that it suggests there may be a natural state for the cosmology constructed from a Euclidean theory:

- Many natural $\Lambda < 0$ cosmological backgrounds have time-reversal symmetry about the $\dot{a} = 0$ point, and these time-symmetric geometries have an analytic continuation to a reflection-symmetric Euclidean geometry. The corresponding Euclidean gravity theory can be used to define a natural state for the cosmology. For this choice:
- The time-reversal symmetry of the background spacetime extends to the quantum state.
- The cosmological observables (for the full quantum state describing the ensemble of possible cosmologies) are analytic functions of coordinates.

- The late time cosmological observables can be calculated precisely without a detailed knowledge of the big bang or initial conditions in the cosmology picture.
- The cosmological observables are related to the vacuum observables in a dual picture. This naturally implies correlations between regions of the Universe that were never in causal contact.

There are interesting features related to the holographic description:

- Three-dimensional holographic quantum field theories play an essential role in the description of the physics. Since these provide descriptions of vacuum AdS solutions, it is natural that they would continue to play an important role if we add a non-zero density of matter/radiation/scalar potential, etc. In our construction, the three-dimensional theory no longer appears in the physical degrees of freedom of the holographic description, but still appears in the path integral that constructs the state.
- The fundamental microscopic degrees of freedom housing the quantum state of the Universe are not conventionally holographic. In our example, they are a small N CFT. These holographic degrees of freedom are not "at the boundary" of the cosmological spacetime. Using the language of recent discussions of black hole evaporation, the cosmological spacetime is an "island." Related to this, we have that:
- The particles/fields in the effective description of cosmology are entangled with an auxiliary system that does not interact directly with the cosmology. Tracing out these auxiliary degrees of freedom, we have a mixed state of the cosmological effective field theory, describing an ensemble of different cosmologies.
- The full history of the Universe is encoded in the state of the underlying 4D CFT at a single time, and should not be affected by changes to the CFT Hamiltonian at earlier or later times. Thus, time evolution in the cosmology seems unrelated to time evolution in the underlying CFT. We can say that time in the cosmology is emergent.
- Finally, the scalar field potential in the effective theory is directly related to properties of the underlying 3D CFT. Taking the number of CFT degrees of freedom to be very large (as would seem appropriate for describing the entire Universe) naturally leads to both a small cosmological constant and small derivatives for the scalar potential.

In special cases where the 4D field theory may also be holographic, we have that:

- The cosmological spacetime lives behind the horizon of a black hole, and the cosmological singularities are related to the black hole initial and final singularities.
- In our specific setup, the cosmological physics lives on a brane in a higher-dimensional spacetime.
- Gravity is localized to the brane because the 3D CFTs associated with the four-dimensional physics have many more local degrees of freedom than the 4D CFT associated with the five-dimensional physics.

Finally, the models have some interesting consequences for phenomenological issues:

- The only input to the model is the choice of the underlying coupled 3D/4D field theory. The gauge group of the effective theory for the cosmology is determined by the global symmetry of the 3D CFT.

- The quantum state in the cosmology, and thus the cosmological perturbations are fixed given the choice of Euclidean effective field theory.
- Correlations between regions of the Universe that were never in causal contact arise naturally because they are related to vacuum correlators in a dual picture.
- If the microscopic 4D CFT (and the dual gravity theory) is supersymmetric, this supersymmetry is only broken by the state in the cosmology picture. This may allow supersymmetric cancellations in the leading contribution to the cosmological constant to persist and explain why the cosmological constant can remain small. In the wormhole picture, supersymmetry is broken explicitly, but only by nonlocal effects (the incompatibility of the two boundary conditions). Again, this seems to avoid large corrections to the cosmological constant.
- The Friedmann equation implies that the total energy density at the time-symmetric point vanishes, so the magnitude of the (negative) dark energy is equal to the magnitude of the remaining energy. The time scale for the variation of these quantities is the age of the Universe, so the dark energy and other sources of energy are expected to have a similar order of magnitude for most of the age of the Universe. This may help explain the cosmological coincidence problem.

Chapter 6

Negative energy enhancement

In this chapter we address a specific issue which arose in the construction of the previous chapter. Recall that the outcome of this construction was an *indirect* holographic description of time symmetric, homogeneous and isotropic, $\Lambda < 0$ cosmologies. The holographic description is indirect because these cosmological spacetimes don't contain any asymptotically AdS regions. Instead, analytic continuations of these spacetimes *do* contain asymptotically AdS regions; in fact they are Euclidean or Lorentzian asymptotically AdS wormhole geometries. The wormhole geometries can be described microscopically using AdS/CFT, and therefore (through the analytic continuations) so can the cosmology.

An apparent issue that this raises is related to the static Lorentzian wormhole geometry which is the double analytic continuation of the cosmological spacetime. In equation (5.18) we showed that the Einstein equation imposes a strong requirement for a symmetric, static wormhole with curvature length scale ℓ at it is midpoint, namely that the null energy density T_{++} at the middle of the wormhole must be of order

$$T_{++} \sim -\frac{\ell^2}{\ell_{\rm Pl}^2}\frac{1}{\ell^4}, \tag{6.1}$$

where $\ell_{\rm Pl}$ is the Planck length. There are two potential concerns regarding this expression.

First, T_{++} must be negative at the centre of the wormhole. This is actually not a concern because T_{++} can contain contributions from quantum fields, and it is well known that vacuum fluctuations of a quantum field in a finite volume can produce negative energy densities. This is the Casimir effect [192], of which the simplest example is the negative vacuum energy in the electromagnetic field between two parallel conducting plates and which induces an observable attraction between the plates [193]. Indeed, the traversable wormhole geometry is qualitatively not much different from this simple setup: it consists of a vacuum state of a quantum field on a geometry filling in the space between two boundaries. Thus we expect vacuum fluctuations to contribute negatively to T_{++}.

A second feature of equation (6.1) is the required *magnitude* of the negative vacuum fluctuations. The factor $1/\ell^4$ represents the magnitude of fluctuations which we expect from a Casimir energy, i.e. a value which is set by the geometric scale ℓ of the setup. For example, the vacuum energy density of the electromagnetic field between two parallel conducting plates is equal to $-\pi^2/(180\ell^4)$ where ℓ is the distance between the plates [192]. However equation (6.1) has an additional factor $\ell^2/\ell_{\rm Pl}^2$. Since the curvature length scale in the wormhole is the same as the curvature length scale in the cosmology, ℓ is also a cosmological length scale. Therefore the additional factor $\ell^2/\ell_{\rm Pl}^2$ is huge for realistic cosmologies, and the required negative energy to support a cosmological scale wormhole is larger in magnitude from the expected value $-1/\ell^4$ by this huge factor.

The purpose of this chapter is to explain why such anomalously large negative energies are not only possible but also *expected* in the wormhole geometries in our construction. The key feature which induces this anomalous effect is the specific coupling which exists between the two ends of the wormhole. Recall that the wormhole effective field theory is dual to a pair of 3D microscopic CFTs coupled by an auxiliary 4D CFT. As we discussed in the last chapter the 4D CFT is required to have many fewer degrees of freedom than the 3D CFTs. Thus in the effective description the effective

4D non-gravitational theory (the dual of the microscopic 4D CFT) will have many fewer degrees of freedom than the wormhole (the dual of the 3D CFTs). In summary, we have an effective picture of a two-part system consisting of a wormhole plus non-gravitational theory living on a circle S^1 times $\mathbb{R}^3$, with the wormhole and non-gravitational theory each occupying part of the circle, and with one system (the wormhole) having many more local degrees of freedom than the other system (non-gravitational theory).

In this chapter we will consider a toy model of this setup in which we maintain the topology of the two-part system but in which we make the simplifying assumption that both systems are holographic field theories. Under this simplifying assumption we will be able to show that if one of the systems has many more degrees of freedom than the other, then it is also possible for it to have an anomalously large negative energy density, exactly as we would hope. This result therefore provides a non-trivial consistency check on our holographic cosmology/wormhole construction.

6.1 Introduction

It is well known that quantum field theories can exhibit various forms of negative energy [192]. For example, in a d-dimensional CFT with one periodic spatial direction (labeled by z) of width w, the energy density takes the form

$$T_{\mu\nu} = \frac{F}{w^d}\eta_{\mu\nu} \qquad T_{zz} = -(d-1)\frac{F}{w^d} \tag{6.2}$$

where F is a dimensionless constant that can be positive for some CFTs. In this case, if k is a null vector whose spatial component is in the z direction, both T_{00} and T_{kk} are negative. The value of F is typically of the order of the central charge of the CFT.[57]

More generally, we can consider such a CFT on $\mathbb{R}^{d-2,1}$ times a strip of width w in the z direction with various choices of boundary physics or couplings between the two sides of the strip. In all cases, assuming that the $(d-2)+1$ dimensional Poincaré symmetry is unbroken, the vacuum stress-energy tensor is constrained to take the form (6.2). It is interesting to ask whether there is some upper bound on F for a given CFT.[58]

In this note, we consider the situation where the CFT (which we call CFT_1) is coupled to another CFT (called CFT_2) at the two edges of the strip. The second CFT may also be on a strip, so that the full compact direction is periodic, as shown in Figure 6.1, or it may be extended infinitely in the $\pm z$ directions.

We take both CFTs to be holographic with an Einstein gravity dual, and as we did in Chapter 3 we model the interface between the CFTs via a constant tension domain wall; see also [76, 87, 89]. The parameters in the gravitational description are the AdS lengths in each region and the tension of the domain wall. The gravity solutions dual to the vacuum state of the interface theory are obtained by solving the vacuum Einstein equations together with the Israel junction conditions [88] at the interface, with the requirement that the asymptotic behavior of the solution matches with the geometry of the CFT setup. From the solutions, we can read off the stress-energy tensor for each CFT via the usual holographic dictionary.

We report the value of the energy density (specifically the parameter F) for each CFT as a function of the two AdS lengths, the interface tension, and the relative amount of the compact

[57] Throughout this chapter, we will use the term "central charge" in general dimensions to denote a parameter that measures the number of degrees of freedom. A specific such quantity is the entropy density for the CFT on $\mathbb{R}^{d-1,1}$ in units of the temperature.

[58] Alternatively, we can consider the CFT on an open interval of width w and ask if there is a maximum/supremum for F among allowed density matrices with stress-energy tensor of the form 6.2.

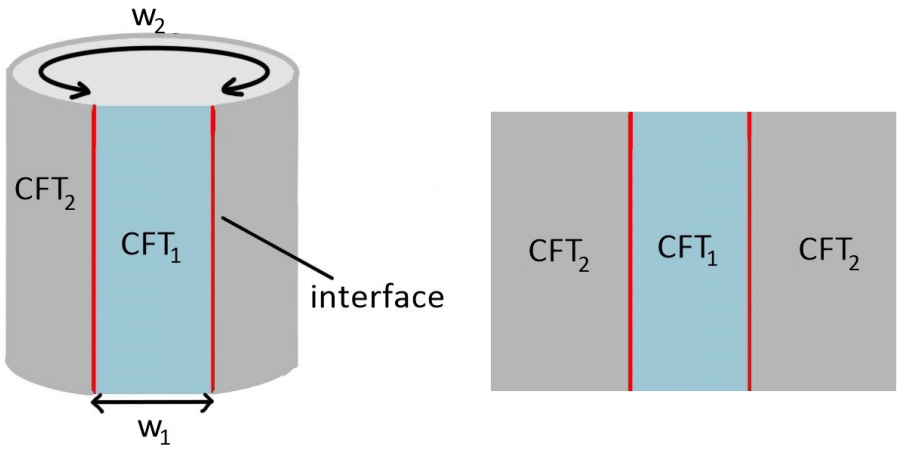

Figure 6.1: CFT configurations for which we study the energy density of the vacuum state (vertical direction is time). Left (basic setup): two CFTs, each on $\mathbb{R}^{d-2,1}$ times an interval are glued together on a periodic direction. Right: in the $w_2 \to \infty$ limit, we have a layer of CFT_1 inside CFT_2.

direction covered by the two CFTs. In CFT language, the AdS lengths and the interface tension in the holographic model correspond to generalized "central charges" associated with the two CFTs and the interface. These provide a measure of the number of degrees of freedom for the CFTs and for the interface. The CFT and interface central charges are expected to decrease monotonically under bulk and interface RG flows, respectively [77, 85, 86, 194–203].

Enhanced negative energies

As we discussed in Chapter 3, the bulk interface tension is constrained to lie within a certain range of positive values in order that the interface can reach the AdS boundary. A striking result of our analysis is that for CFTs of dimension 2+1 or larger, the energy density in the CFT with larger central charge diverges in the limit where the interface tension approaches the lower critical value. Thus, within the context of the holographic model, there is no upper bound for the parameter F.

For 1+1 dimensional CFTs, we do not see this effect. Here, F in our model is bounded from above by $c\pi/6$, the value for the CFT on a periodic direction with antiperiodic boundary conditions for fermions.

The bulk solutions that give rise to large negative energies have an interesting structure, shown in Figure 6.3b. We recall that the solution dual to the vacuum state of a CFT with one periodic direction (assuming anti-periodic boundary conditions for fermions) is the "AdS-soliton" [180, 204] geometry in which the periodic direction smoothly contracts in the bulk. For our solutions with a large negative energy in CFT_1, the region of the bulk associated with CFT_1 is a portion of a multiple cover of the AdS soliton geometry that winds multiple times around the central point but does not include the central point where we would have a conical singularity. It is this winding that allows a negative energy with magnitude larger than a CFT on a periodically identified compact direction with the same width.

The enhancement of negative energies persists when the relative size of the CFT_2 interval goes to zero or infinity. In the former case, we end up with CFT_1 on a periodic direction with a particular kind of defect at one location on this periodic direction. In the latter case, we end up with a layer of CFT_1 surrounded by CFT_2 of infinite extent as in the right side of Figure 6.1. This latter case is particularly interesting since it could be relevant to real three-dimensional materials.

For specific microscopic CFTs, the allowed interfaces are constrained, and it seems likely that there would be some finite upper bound on F for each specific choice of CFT_1 and CFT_2. It would be interesting to verify this and to understand how large F can be relative to the value corresponding to CFT_1 with a periodic direction.

Related work

A detailed investigation of such holographic interface CFTs was recently carried out in [205] for both zero and finite temperature in the case of 1+1 dimensional CFTs. Our work complements this paper, in that we mainly focus on the higher-dimensional cases. In particular, the enhancement of negative energy that we find does not appear for 1+1 dimensional CFTs considered in [205]. It would be interesting, following [205] to extend our results to finite temperature in order to work out the phase diagrams more completely in the higher dimensional cases. This is significantly more challenging with two or more spatial directions, since the dual geometries will generally not be portions of the AdS soliton and/or Schwarzschild solutions.

Anomalously high transition temperatures?

While we have not carried out the explicit analysis of the finite temperature case, we argue in the discussion that the properties of the bulk interfaces in the cases with anomalously large vacuum energies would also give rise to anomalously high transition temperatures to the high-temperature phase. It would be interesting to verify this and understand whether it could be relevant to the physics of real-world layered materials.

Outline

The remainder of the chapter is structured as follows. In Section 6.2, we describe in more detail the field theory configurations we will consider. In Section 6.3, we review the holographic model for these interface CFTs and the calculation of vacuum energy for one of the holographic CFTs with a single periodic direction. In Section 6.4, we use the holographic model to compute the vacuum energies in the theory with two CFTs arranged as shown in Figure 6.1. In Section 6.5, we suggest a field theory mechanism for the enhancement of negative energies, pointing out that negative Casimir energies in simple free-field calculations are enhanced when infrared modes are removed. We conclude with a brief discussion in Section 6.6.

6.2 Field theory setup

In this section, we consider quantum field theories built from one or more CFTs, where CFT_i lives on $R^{d-2,1}$ times an interval of width w_i. At the boundaries of these intervals, the CFTs may be joined to another CFT via a conformal interface, or we may have a conformal boundary theory. We refer to the direction along the various intervals as z and use Greek indices to refer to the $R^{d-2,1}$ directions.

Assuming that the vacuum state preserves the geometrical $(d-2)+1$ dimensional Poincaré symmetry, the stress-energy tensor in each CFT must take the form[59]

$$T_{\mu\nu} = \eta_{\mu\nu} f(z) \qquad T_{zz} = g(z) \qquad T_{\mu z} = 0 \,. \tag{6.3}$$

[59] Here, quantum vacuum expectation values are implied.

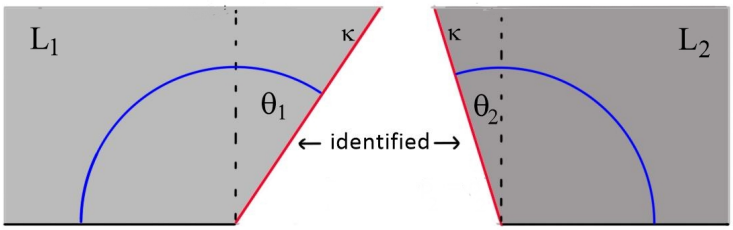

Figure 6.2: Asymptotic behavior of the bulk solutions. The bottom edge of the two diagrams is the AdS boundary. The red lines are identified and represent the interface brane of tension κ separating the two bulk regions with AdS lengths L_1 and L_2. The blue surface is an extremal surface, which can be related by the RT formula to the entanglement entropy of the homologous boundary region, containing the interface.

The conservation relation $\partial^a T_{ab} = 0$ with $b = z$ implies that $g(z)$ is constant. For conformal field theories, the stress-energy tensor must also be traceless, so we have that $(d-1)f = -g$. Finally, by dimensional analysis, we can write

$$T^{(i)}_{\mu\nu} = \eta_{\mu\nu}\frac{F_i}{w_i^d} \qquad T^{(i)}_{zz} = -\frac{(d-1)F_i}{w_i^d} \qquad T^{(i)}_{\mu z} = 0\ . \tag{6.4}$$

The constant F_i can depend only on the dimensionless ratios between w_is, together with our choice of CFTs and interfaces.

Our goal in this chapter is to understand the behavior of F_i as a function of the w_is in various cases and in particular to understand how large F_i can be.

6.3 Holographic interface CFTs

We will mostly consider a simple holographic model for the interface CFTs as discussed in Chapter 3 and [89]. As a brief review, in this setup the gravity dual of each CFT is Einstein gravity, and the interfaces correspond to domain walls in the bulk between regions of different AdS lengths L_i. The gravitational equations are the Einstein equations together with the second Israel junction condition

$$K_{1ab} - K_{2ab} = \kappa h_{ab} \tag{6.5}$$

where $\kappa \equiv 8\pi G_D T/(d-1)$ is defined in terms of the domain wall tension T and K_{1ab} and K_{2ab} represent the extrinsic curvatures for the interface, computed with the bulk metrics on either side, with the normal vector pointing from region 1 to region 2 in each case.

We also assume the first junction condition, which enforces that there is a well-defined metric on the interface equal to the metric induced from the bulk metric on either side,

$$h_{1ab} - h_{2ab} = 0\ . \tag{6.6}$$

6.3.1 Asymptotic behavior of the interface

For an interface between CFTs dual to gravitational theories on AdS with AdS lengths L_1 and L_2, the asymptotic geometry near the interface may be described as a patch of Poincaré AdS_{d+1} with AdS length L_1 glued onto a patch of Poincaré AdS_{d+1} with AdS length L_2. The domain wall

approaches the boundary at a constant Poincaré angle in each region, given by Eqs. (3.16) and (3.17),

$$\sin(\theta_1) = \frac{1}{2}\left(\kappa L_1 + \frac{1}{\kappa L_1} - \frac{L_1}{\kappa L_2^2}\right), \tag{6.7}$$

$$\sin(\theta_2) = \frac{1}{2}\left(\kappa L_2 + \frac{1}{\kappa L_2} - \frac{L_2}{\kappa L_1^2}\right) . \tag{6.8}$$

Recall that here θ_i is the angle by which the domain wall deviates from the normal to the AdS boundary in Poincaré coordinates. Positive θ corresponds to an obtuse angle with the AdS boundary, as shown in Figure 6.2.

From these equations, we found that κ must lie within the range

$$\kappa \in (\kappa_-, \kappa_+) \equiv \left(\left|\frac{1}{L_1} - \frac{1}{L_2}\right|, \frac{1}{L_1} + \frac{1}{L_2}\right). \tag{6.9}$$

Domain walls with tensions outside this range cannot reach the asymptotic boundary.

6.3.2 Bulk geometries

The symmetries of our system imply that the bulk geometry in the region associated with CFT_i is a portion of the double analytically continued planar Schwarzschild geometry

$$ds^2 = L_i^2 f_i(r) dz^2 + \frac{dr^2}{f_i(r)} + r^2 d\vec{x}^2 \tag{6.10}$$

where

$$f_i(r) = \frac{r^2}{L_i^2} - \frac{\mu_i}{r^{d-2}} . \tag{6.11}$$

This geometry is also known as the "AdS soliton" [180, 204]. Here, the radial coordinate r increases from a minimum value

$$r_H = (\mu_i L_i^2)^{\frac{1}{d}} , \tag{6.12}$$

the location of the horizon in the analytically continued geometries, to $r = \infty$, the location of the AdS boundary. The coordinates z and x^μ are defined to be dimensionless; these are related by a constant scaling to the coordinates in the field theory.

When the included region contains the point $r = r_H$, the z coordinate must be periodic with period

$$\beta = \frac{4\pi}{d} \mu_i^{-\frac{1}{d}} L_i^{1-\frac{2}{d}} \tag{6.13}$$

to avoid a conical singularity. However, more generally, we can have some region of a multiply wound version of this geometry with a conical excess at $r = r_H$ provided that the region we keep does not include this conical singularity.

6.3.3 CFT stress tensor

For a CFT state described holographically by a portion of the geometry (6.10), the expectation value of the stress tensor can be read off via the standard holographic dictionary [206]. If the field theory coordinates are related to the dimensionless gravity coordinates via

$$x^\mu_{\text{ft}} = \ell x^\mu_{\text{grav}} , \qquad z_{\text{ft}} = \ell z_{\text{grav}} , \tag{6.14}$$

then the expectation value of the CFT stress tensor is

$$T_{\mu\nu} = \frac{1}{\ell^d} \eta_{\mu\nu} \frac{\mu}{L^{d-2}} \frac{L^{d-1}}{16\pi G} , \qquad T_{zz} = -\frac{d-1}{\ell^d} \frac{\mu}{L^{d-2}} \frac{L^{d-1}}{16\pi G} . \tag{6.15}$$

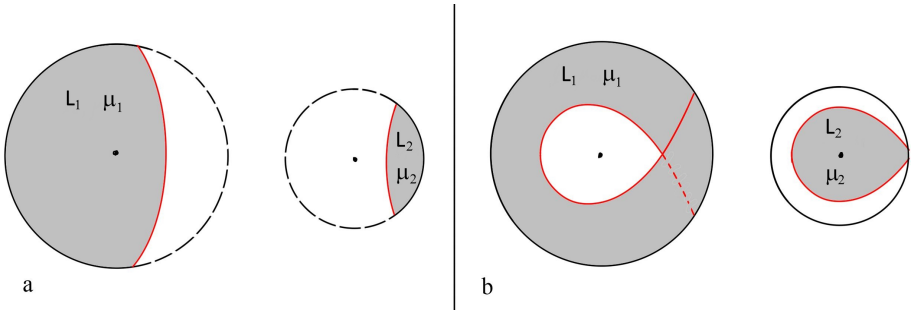

Figure 6.3: Gravitational solutions for interface CFTs (shaded regions are kept). (a) Regions of AdS soliton solutions dual to the separate CFTs on periodic directions are glued together along an interface. (b) For an interface tension approaching a lower critical value, the outer region is multiply wound relative to the original AdS soliton geometry, leading to an enhanced negative energy for the CFT with more degrees of freedom.

6.3.4 Single CFT with a periodic direction

We begin by reviewing the holographic results for the vacuum stress tensor of a single CFT on $R^{d-2,1} \times S^1$ where the S^1 has length w [180, 204]. In this case, one possible dual geometry is just a periodic identification of Poincaré AdS^{d+1}. For this geometry, the stress tensor vanishes.

However, in cases where the S^1 is allowed to contract in the bulk geometry (where we have antiperiodic boundary conditions for fermions) we can also have the solution (6.10). Since the period of the z coordinate in gravity is (6.13) and the field theory period is defined to be w, the parameter ℓ in (6.14) is

$$\ell = w \frac{d}{4\pi} \mu^{\frac{1}{d}} L^{\frac{2}{d}-1} , \tag{6.16}$$

so from (6.15), the stress tensor takes the form (6.4) with

$$F = F_\beta \equiv \left(\frac{4\pi}{d}\right)^d \frac{L^{d-1}}{16\pi G} . \tag{6.17}$$

Up to a numerical factor of order one, this is the central charge of the CFT, providing a measure of the number of degrees of freedom. Thus, in units of the circle size, we have a negative Casimir energy of order the CFT central charge.

It is interesting to ask whether there could be any other solution that gives a lower energy. It was conjectured in [204] that no such solutions exist. In the context of interface theories, we might wonder whether it is possible to lower the energy by having a static bubble of AdS with a different value of the cosmological constant in the interior of the geometry, as shown in Figure F.1. In Appendix F, we show that while such solutions exist in some cases (requiring κ less than the lower critical value for the domain wall to reach the AdS boundary), they are perturbatively unstable and give solutions with higher energy than the AdS soliton.

6.4 Vacuum energies for interface CFTs

Now we consider the case where the S^1 is divided into two parts, with CFT$_1$ on an interval of width w_1 and CFT$_2$ on an interval of width w_2, as in Figure 6.1. The dual geometries are built from patches of geometries (6.10) with parameters (L_1, μ_1) and (L_2, μ_2) joined along an interface, as shown in Figure 6.3, or Figure 6.5 in the case where $\mu_1 = \mu_2 = 0$.

6.4.1 Interface equations from the junction conditions

Following the same techniques employed in Chapter 3 (see also [1, 92, 205]) we can make use of the junction conditions to derive the equations governing the trajectory of the bulk interface.

Without loss of generality, we can identify the coordinates x^μ in the two patches. The first junction condition then implies that the r coordinates must also match along the interface.

The interface is described by a trajectory $z_1(r)$ in the geometry (6.10) dual to CFT_1 and $z_2(r)$ in the region dual to CFT_2; we will consider a region of the interface where the z coordinate in the CFT_1 region increases toward the interface and the z coordinate in the CFT_2 region increases away from the interface.

As described in Chapter 3 the junction conditions lead to the relation

$$L_1 f_1 \frac{dz_1}{ds} + L_2 f_2 \frac{dz_2}{ds} = \kappa r, \tag{6.18}$$

where s is the proper length along the interface. The definition of the proper length parameter s (and the first junction condition that induced geometries on either side of the interface match) gives

$$L_i^2 f_i \left(\frac{dz_i}{ds}\right)^2 + \frac{1}{f_i}\left(\frac{dr}{ds}\right)^2 = 1\,. \tag{6.19}$$

Together, these yield

$$\left(\frac{dr}{ds}\right)^2 - V_{\text{eff}}(r) = 0 \qquad\qquad V_{\text{eff}}(r) \equiv f_1 - \left(\frac{f_2 - f_1 - \kappa^2 r^2}{2\kappa r}\right)^2\,, \tag{6.20}$$

and

$$\begin{aligned} L_1 \frac{dz_1}{dr} &= -\frac{1}{f_1\sqrt{V_{\text{eff}}}}\left(\frac{1}{2\kappa r}(f_1 - f_2) + \frac{1}{2}\kappa r\right) \\ L_2 \frac{dz_2}{dr} &= \frac{1}{f_2\sqrt{V_{\text{eff}}}}\left(\frac{1}{2\kappa r}(f_2 - f_1) + \frac{1}{2}\kappa r\right)\,, \end{aligned} \tag{6.21}$$

where the signs correspond to the conventions described above. The first equation tells us that $r(s)$ will be the trajectory of a particle with zero energy in a potential $-V_{\text{eff}}(r)$.

6.4.2 Holographic results for the energy density

We now make use of the interface solutions to provide results for the energy densities in the two-CFT setup of Figure 6.1.

In this case, it will be convenient to study the ratio

$$E_i \equiv \frac{F_i^{\frac{1}{d}}}{F_\beta^{\frac{1}{d}}} \tag{6.22}$$

of the scale of energy density for each CFT on the strip of width w with the scale of energy density for that CFT on a periodic direction of length w. This will be a function of the dimensionless ratio

$$x \equiv \frac{w_2}{w_1}\,. \tag{6.23}$$

In our holographic setup, $E_1(x)$ will also depend on the ratio $u = L_2/L_1$ of AdS lengths (related to the ratio of central charges of the two CFTs), and the dimensionless ratio $e = (\kappa - \kappa_-)/(\kappa_+ - \kappa_-) \in$

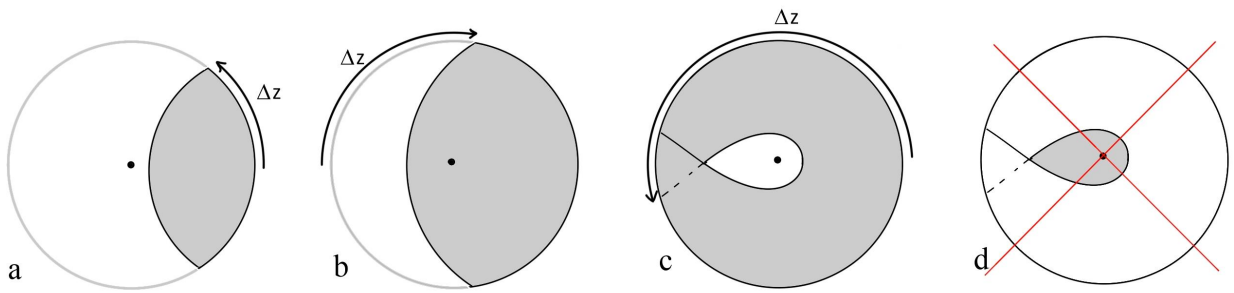

Figure 6.4: Types of bulk regions associated with CFTs on a strip. The central dot corresponds the Euclidean horizon of the geometry. (a) The region does not include the Euclidean horizon. (b) The region includes the Euclidean horizon. (c) The region does not include the Euclidean horizon and is multiply wound. (d) Windings less than zero are not allowed.

$[0,1]$, related to the interface central charge. All together, we have a function $E_1(x;u,e)$. The function $E_2(x;u,e)$ for CFT_2 is related to this by

$$E_2(x;u,e) = E_1(1/x;1/u,e)\ , \tag{6.24}$$

so we will focus on E_1.

In practice, we can study $E_1(x;u,e)$ by first choosing L_1, L_2 and κ corresponding to u and e. The parameter x and the energy E_1 will then both be determined by the choice of $\mu \equiv \mu_2/\mu_1$ in a way that we now explain.

To find x and E_1, it is convenient to define R_i to be the fraction of the asymptotic z coordinate in the solution (6.10) covered by the patch associated with CFT_i. This can be larger than one in the case of multiply wound patches as in Figure 6.4c. From the symmetry of the setup, we have that

$$R_2(x;u,e) = R_1\left(\frac{1}{x};\frac{1}{u},e\right) \tag{6.25}$$

so it suffices to focus on R_1.

The parameter R_1 is related in a simple way to the change Δz_1 in z as we move from the point $r = r_0$ where the interface is closest to the center, determined by

$$V(r_0) = 0\ , \tag{6.26}$$

to the asymptotic boundary. From (6.21), this change is given by

$$\Delta z_1 \;=\; -\frac{1}{L_1}\int_{r_0}^{\infty}\frac{dr}{f_1\sqrt{V_{eff}}}\left(\frac{1}{2\kappa r}(f_1-f_2)+\frac{1}{2}\kappa r\right). \tag{6.27}$$

The relation between R_1 and Δz_1 depends on whether or not the region that we are keeping includes the centre point $r = r_H$, as we can see from Figure 6.4. When the retained region does not include the center, the range of z_1 for the included region is $2\Delta z_1$ and we have $R_1 = 2\Delta z_1/\beta_1$. Otherwise, Δz_1 is negative, the range of z_1 for the included region is $\beta_1 + 2\Delta z_1$, and we have $R_1 = 1 + 2\Delta z_1/\beta_1$.

The retained region includes the centre if and only if dz_1/dr is negative as r increases from r_0. Since f_1 and V_{eff} are always positive, the sign of dz_1/dr is determined by the sign of $f_2 - f_1 - \kappa^2 r^2$ at $r = r_0$. At the phase boundary in parameter space where this quantity changes sign, the interface

crosses the centre point, so we have $r_0 = r_H = (\mu_1 L_1^2)^{1/d}$. In this case, the phase boundary simplifies as

$$f_2(r_0) - f_1(r_0) - \kappa^2 r_0^2 = 0 \qquad \leftrightarrow \qquad \frac{\mu_2}{\mu_1} = \frac{L_1^2}{L_2^2} - \kappa^2 L_1^2 \,. \tag{6.28}$$

We see that $f_2(r_0) - f_1(r_0) - \kappa^2 r^2$ is negative for sufficiently large μ_2, so the condition for our region to include the centre is

$$\frac{\mu_2}{\mu_1} > \frac{L_1^2}{L_2^2} - \kappa^2 L_1^2 \,. \tag{6.29}$$

Thus, we finally have

$$R_1 = \begin{cases} \frac{2\Delta z_1}{\beta_1} & \frac{\mu_2}{\mu_1} < \frac{L_1^2}{L_2^2} - \kappa^2 L_1^2 \\ 1 + \frac{2\Delta z_1}{\beta_1} & \frac{\mu_2}{\mu_1} > \frac{L_1^2}{L_2^2} - \kappa^2 L_1^2 \end{cases} \tag{6.30}$$

In terms of R_1 and R_2, the ratio x is given by

$$x = \frac{R_2 \beta_2}{R_1 \beta_1} \,, \tag{6.31}$$

where β is defined in (6.13).

The function E_1 defined in (6.22) that determines the energy of CFT_1 is exactly the same as R_1:

$$E_1 = R_1 \,. \tag{6.32}$$

We can understand this as follows. For an interface solution with some R_1 that corresponds to CFT_1 on a strip of width w_1, the energy density for this CFT is the same as that of CFT_1 on a periodic direction of length w_1/R_1, since this would have the same local bulk solution and the same identification between bulk coordinates and field theory coordinates. Thus,

$$T_{ab}[w_1] = T_{ab}^{periodic}[w_1/R_1] = T_{ab}^{periodic}[w_1] R_1^d \tag{6.33}$$

where in the last step we have used dimensional analysis. Then

$$E_1 = \left(\frac{T_{ab}[w_1]}{T_{ab}^{periodic}[w_1]} \right)^{\frac{1}{d}} = R_1. \tag{6.34}$$

6.4.3 Zero energy solutions

In addition to the solutions described above, we sometimes have solutions that give zero vacuum energy in each CFT. These are depicted in Figure 6.5. For these solutions, the local geometry is just Poincaré-AdS, with interfaces at fixed angles given by the expressions (6.7) and (6.8). To avoid self-intersection, these solutions are only allowed when the domain walls in each region tilt away from each other, which requires that θ_1 and θ_2 in (6.7) and (6.8) are positive. We find that this will be true when

$$\kappa > \sqrt{\left| \frac{1}{L_1^2} - \frac{1}{L_2^2} \right|} \,. \tag{6.35}$$

This gives

$$e > \frac{1}{1 + \sqrt{\frac{u+1}{|u-1|}}}. \tag{6.36}$$

Since these solutions have zero energy while the other solutions have negative energy, the zero energy solutions will only correspond to the ground state when solutions of the other type do not exist.

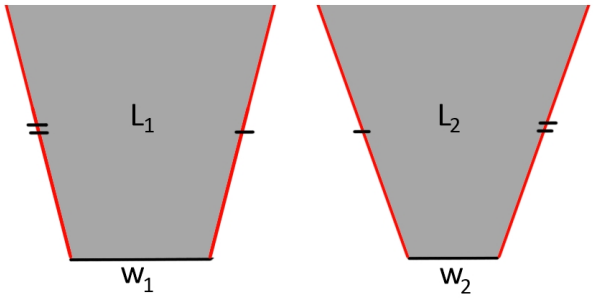

Figure 6.5: Alternate bulk solutions corresponding to our CFT setup. These solutions have zero vacuum energy. The two regions are joined along the domain walls as shown.

6.4.4 Analytic results

In this section, we provide analytic expressions for E_1 and x in terms of the parameters

$$\mu = \frac{\mu_2}{\mu_1} \ , \qquad u = \frac{L_2}{L_1} \ , \qquad e = \frac{\kappa - \kappa_-}{\kappa_+ - \kappa_-} \ . \tag{6.37}$$

From (6.31) and (6.25), the general expression for x is

$$x = \mu^{-\frac{1}{d}} u^{1-\frac{2}{d}} \frac{R_1\left(\frac{1}{u}, \frac{1}{\mu}, e\right)}{R_1\left(u, \mu, e\right)}. \tag{6.38}$$

We now give the result for $E_1 = R_1$ in the cases $u > 1$ and $u < 1$.

Case $u > 1$

For $u > 1$, the relation between κ and e is

$$\kappa = \frac{1}{L_1} - \frac{1}{L_2} + \frac{2e}{L_2} \ . \tag{6.39}$$

Defining

$$\begin{aligned}
\alpha_0 &= \frac{1}{2} \frac{u^2(1-\mu)^2}{(u-1+2e)\sqrt{(1-\mu u)^2 + 4e\mu(u-1+e)} + 2(1+\mu)(1-e)(u+e) - (1+u)(1+u\mu)} \\
\alpha_1 &= \frac{1}{2} \frac{u^2(1-\mu)}{(u-1)(u+2e)+2e^2} \\
\alpha_2 &= \frac{(u-1)(u+2e)+2e^2}{\sqrt{e(1-e)(u+e)(u-1+e)}}
\end{aligned}$$

and

$$\mathcal{I}_d(a,b,c) = \int_1^\infty y^{-\frac{1}{d}} dy \frac{y-a}{(y-b)\sqrt{(y-1)(y+c)}} \tag{6.40}$$

we have that

$$r_0^d = \mu_1 L_1^2 \alpha_0(u,e,\mu) \tag{6.41}$$

and

$$\frac{2\Delta z_1}{\beta_1} = -\frac{1}{4\pi} \frac{\alpha_2}{\alpha_0^{\frac{1}{d}}} \mathcal{I}_d\left(\frac{\alpha_1}{\alpha_0}, \frac{1}{\alpha_0}, \frac{\alpha_2^2 \alpha_1^2}{4\alpha_0^2}\right). \tag{6.42}$$

In this case, we have from (6.30)

$$E_1 = R_1 = -\frac{1}{4\pi}\frac{\alpha_2}{\alpha_0^{\frac{1}{d}}}\mathcal{I}_d\left(\frac{\alpha_1}{\alpha_0}, \frac{1}{\alpha_0}, \frac{\alpha_2^2\alpha_1^2}{4\alpha_0^2}\right) + \Theta\left[\mu - \left(1+\frac{2e}{u}\right)\left(\frac{2}{u} - 1 - \frac{2e}{u}\right)\right] \tag{6.43}$$

where Θ is the step function.

Case $u < 1$

For $u < 1$, the relationship between κ and e is

$$\kappa = \frac{1}{L_2} - \frac{1}{L_1} + \frac{2e}{L_1}\,. \tag{6.44}$$

In this case, $\frac{2\Delta z_1}{\beta_1}$ is given by the same expression as above but with

$$\begin{aligned}
\alpha_0 &= \frac{1}{2}\frac{u^2(1-\mu)^2}{(1-u+2eu)\sqrt{(1-\mu u)^2 + 4ue\mu(1-u+ue)} + 2u(1+\mu)(1-e)(1+eu) - (1+u)(1+u\mu)} \\
\alpha_1 &= \frac{1}{2}\frac{u(\mu-1)}{(1-u)(1-2e) - 2e^2u} \\
\alpha_2 &= -\frac{(1-u)(1-2e) - 2e^2u}{\sqrt{e(1-e)(1+eu)(1-u+eu)}}
\end{aligned}$$

In this case, we have from (6.30)

$$E_1 = R_1 = -\frac{1}{4\pi}\frac{\alpha_2}{\alpha_0^{\frac{1}{d}}}\mathcal{I}_d\left(\frac{\alpha_1}{\alpha_0}, \frac{1}{\alpha_0}, \frac{\alpha_2^2\alpha_1^2}{4\alpha_0^2}\right) + \Theta\left[\mu - (1-2e)\left(\frac{2}{u} - 1 + 2e\right)\right] \tag{6.45}$$

where Θ is the step function.

6.4.5 Results

We now describe the results for $E_1(x; u, e)$ in various cases.

For a given u we find that solutions with a connected interface exist up to some critical value $e^*(u) = e^*(1/u)$. Above this value, there is no choice of μ for which both R_1 and R_2 are greater than 0 (i.e. the interface solution always self-intersects in one of the regions). In this case, the dual solution is of the type described in Section (6.4.3), and the energy density in each CFT is zero. The phase diagram showing the values of e for which we have a connected solution with negative energy densities is shown in Figure 6.6.

Plots of $E_1(x, u, e)$ vs x are given for various u and e below the critical value in Figure 6.7 for $d = 4$ and $d = 2$. The plots for $d = 3$ are qualitatively similar to those for $d = 4$.

For $u > 1$, we find that the value of E_1 is always less than 1, approaching $E_1 = 1$ when $x \to 0$. Physically, this indicates that when CFT_2 has greater central charge than CFT_1, and as the width of the CFT_2 strip goes to zero, the energy density reduces to that of CFT_1 on a periodic direction. In other words, when the interfaces come together, we get a trivial interface. On the other hand, when $u < 1$ (i.e. when CFT_2 has smaller central charge than CFT_1), we do not get a trivial interface when $x \to 0$. This was noted for $d = 2$ in [205].

We have a particularly dramatic effect for $d > 2$ in the case where e becomes small (i.e. the interface tension approaches the lower critical value). Here we get values $E_1 > 1$, with E_1 diverging

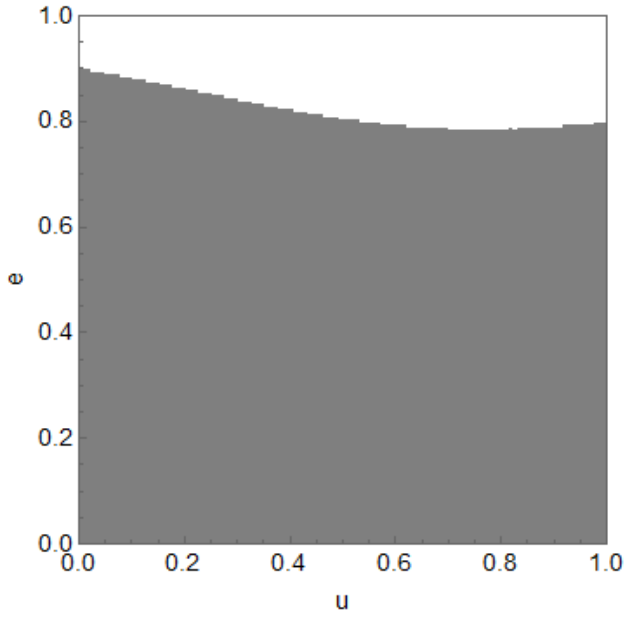

Figure 6.6: Phase diagram in $d = 4$: shaded regions indicate values of $e = (\kappa - \kappa_-)/(\kappa_+ - \kappa_1)$ and $u = L_2/L_1$ for which a connected solution exists and the vacuum energy is negative, while unshaded regions indicate values for which a connected solution does not exist and the vacuum energy is zero.

in the limit $e \to 0$. This means that the magnitude of the negative energy density for CFT_1 in this setting exceeds that of CFT_1 on a periodic direction of the same size, by an amount that becomes arbitrarily large for $e \to 0$. The maximum value of E_1 (obtained for $x \to 0$) is plotted as a function of e for $d = 4$ and $u = 1/2$ in Figure 6.8.

In the next section, we analyze this interesting case of $u < 1$ and small e analytically.

6.4.6 Analytic results in the limit $\kappa \to \kappa_-$ for $L_2 < L_1$

Our numerical results suggest that for $d > 2$, E_1 diverges in the limit $\kappa \to \kappa_-$ ($e \to 1$) in the case where we have $L_2 < L_1$ ($u < 1$). Let us now consider this limit analytically.

For cases where $\mu < 1/u$ (we will see that this is the relevant regime below), we find that in the limit $e \to 0$,

$$\begin{aligned} \alpha_0 &\to \frac{1-\mu u}{4e} \\ \alpha_1 &\to \frac{1}{2}\frac{u(\mu-1)}{1-u} \\ \alpha_2 &\to -\frac{\sqrt{1-u}}{\sqrt{e}}\,. \end{aligned}$$

Then, defining

$$\mathcal{I}_0 \equiv \frac{4^{\frac{1}{d}}}{4\pi}\int_1^\infty \frac{dy}{y^{\frac{1}{2}+\frac{1}{d}}\sqrt{y-1}} = \frac{4^{\frac{1}{d}}}{4\pi}B\left(\frac{1}{2},\frac{1}{d}\right) = \frac{4^{\frac{1}{d}}}{4\pi}\frac{\Gamma\left(\frac{1}{2}\right)\Gamma\left(\frac{1}{d}\right)}{\Gamma\left(\frac{1}{2}+\frac{1}{d}\right)} \tag{6.46}$$

we get from (6.45)

$$R_1 = \frac{2\Delta z_1}{\beta_1} \approx \frac{\mathcal{I}_0}{e^{\frac{1}{2}-\frac{1}{d}}}\frac{\sqrt{1-u}}{(1-\mu u)^{\frac{1}{d}}} \tag{6.47}$$

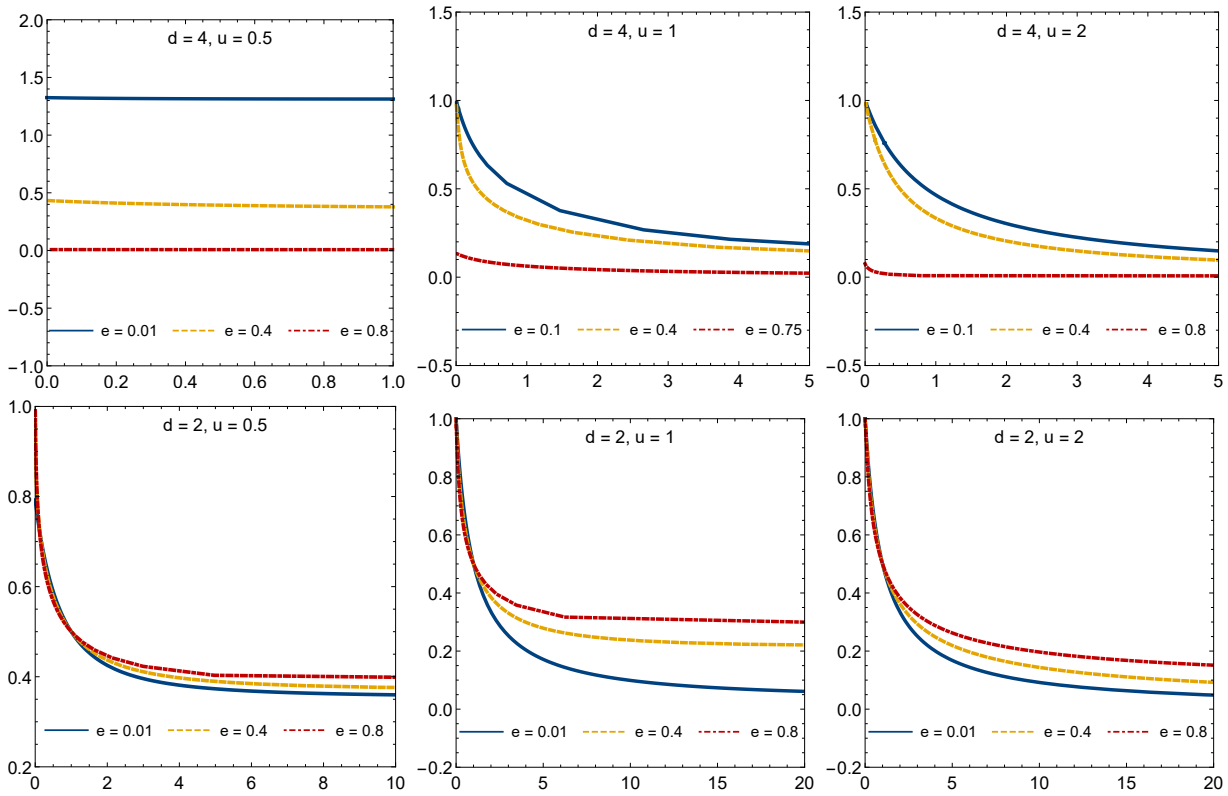

Figure 6.7: Plots of $E_1 \equiv F_1^{1/d}/F_\beta^{1/d}$ versus $x \equiv w_2/w_1$.

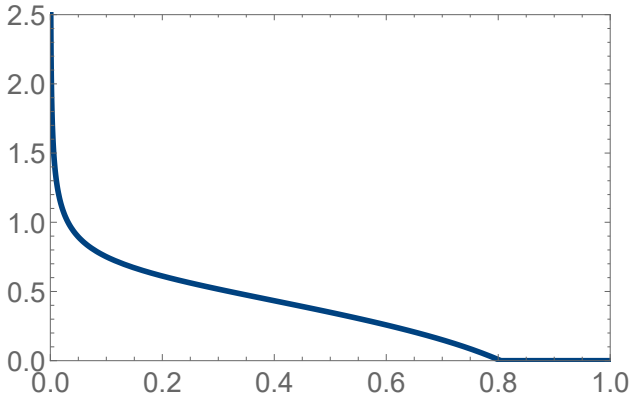

Figure 6.8: Plot of $E_1^{\max}$ as a function of e for $d = 4$ and $u = 0.5$. Note that $E_1^{\max} \to \infty$ as $e \to 0$, showing that we can have arbitrarily large negative energy enhancement in this critical limit. On the other hand $E_1^{\max} = 0$ for e larger than some critical value (0.8 in this example).

and using (6.43)

$$R_2 = R_1\left(\frac{1}{u}, \frac{1}{\mu}, e\right) \approx 1 - \mu^{\frac{1}{d}} u^{\frac{2}{d}-1} \frac{\mathcal{I}_0}{e^{\frac{1}{2}-\frac{1}{d}}} \frac{\sqrt{1-u}}{(1-\mu u)^{\frac{1}{d}}} \,. \tag{6.48}$$

Using (6.38), we find that the relationship between x and μ to leading order in e is

$$\mu(x) = \frac{e^{\frac{d}{2}-1}}{u^2}\left(\frac{u}{(1+x)\sqrt{1-u}\mathcal{I}_0}\right)^d \tag{6.49}$$

From this, we find that the expressions for $E_1 = R_1$ and $E_2 = R_2$ at leading order in e are

$$\begin{aligned} E_1 &\approx \frac{1}{e^{\frac{1}{2}-\frac{1}{d}}}\mathcal{I}_0\sqrt{1-u} \\ E_2 &\approx \frac{x}{1+x} \end{aligned}$$

We note that E_1 is independent of x at leading order in e; the leading x dependence for E_1 may be obtained by multiplying the leading order expression by $(1 + \frac{1}{d}u\mu(x))$.

Thus, we see that for $d > 2$, $E_1 = R_1$ can be made arbitrarily large by taking e small. In this case, E_1 varies very little as a function of x, while R_2 varies from 0 to 1 as x varies from 0 to ∞.

6.4.7 Extension to defect CFTs and layered CFTs

We note that the enhancement of negative vacuum energies that we have observed persists in the limits $x \to 0$ and $x \to \infty$.

In the $x \to 0$ case, the width of the CFT_2 strip goes to zero, so the layer of CFT_2 becomes a defect in CFT_1. As pointed out in [205], there are cases when this defect is non-trivial, such that in the holographic dual we still have a wedge of the gravity dual of CFT_2 emerging from the asymptotic boundary (similar to [207]) which closes off in the interior to form a bubble. This corresponds to the two boundaries of the bulk interface on the right in Figure 6.3b coming together.

In the $x \to \infty$ case, we end up with a layer of CFT_1 inside an infinite bulk of CFT_2 on $\mathbb{R}^{d-1,1}$. In this limit, $\mu_2 \to 0$ and the bulk region dual to CFT_2 is locally pure AdS. Thus, periodicity is not required for the negative energy enhancement that we observe.

6.5 Field theory toy model

Let us try to understand the field theory mechanism that allows enhanced negative vacuum energies. We have found that for CFT_1 on a strip of width w, coupling the two sides via another CFT with lower central charge can lead to negative vacuum energies much larger in magnitude than for CFT_1 on a periodic direction of width w.

A significant feature of the dual geometries in this case is that the region associated with CFT_1 is a thin strip that wraps the AdS soliton geometry multiple times, with $r_0 \gg r_H$. Since the middle part of the geometry is removed, it would appear that the infrared modes of the field theory are suppressed somehow by the interaction with CFT_2. We note that the (artificial) suppression of infrared modes also leads to large negative energies in simple free-field theory toy models.

Consider first a free scalar field in 1+1 dimensions on a periodic direction of length L. The Casimir energy density may be calculated by introducing a UV regulator, calculating the regularized energy density with the periodic direction of length L, subtracting the regularized energy density for $L \to \infty$, and then removing the UV regulator (for details, see for example [208]). The result is

$$T_{00} = -\frac{\pi}{6L^2} \,. \tag{6.50}$$

This includes contributions from the individual modes with wave number $2\pi n/L$. Now, suppose we artificially remove the modes with $|n| \leq k$. These provided a finite contribution to the vacuum energy density,

$$\begin{aligned} T_{00}^{|n|\leq k} &= \frac{1}{L}\sum_{n=-k}^{k}\frac{1}{2}\omega_n \\ &= \frac{1}{L}\sum_{n=-k}^{k}\frac{1}{2}\frac{2\pi|n|}{L} \\ &= \frac{\pi k(k+1)}{L^2}\,. \end{aligned}$$

Thus, the total Casimir energy with these modes removed would be

$$T_{00} = -\frac{\pi}{L^2}(k(k+1)+\frac{1}{6})\,. \tag{6.51}$$

In terms of the scale $\Lambda_{IR} = k/L$ associated with the minimum wavelength, this gives

$$T_{00} = -\pi\left(\Lambda_{IR}^2 + \frac{\Lambda_{IR}}{L} + \frac{1}{6L^2}\right)\,. \tag{6.52}$$

Similar results are obtained for the Casimir energy of a higher-dimensional free scalar on $S^1 \times R^{d-2,1}$ if we remove modes with small ω. Here, it is convenient to temporarily take the infinite spatial directions to be compact, each with length A. Letting n and $\vec{n}$ be the mode numbers in the original periodic direction and the other spatial directions, we consider eliminating modes whose wave numbers satisfy

$$\sqrt{\left(\frac{n}{L}\right)^2 + \left(\frac{\vec{n}}{A}\right)^2} < \Lambda_{IR}\,. \tag{6.53}$$

The contribution of these modes to the Casimir energy is

$$T_{00}^{IR} = \frac{1}{LA^{d-2}}\frac{1}{2}\sum_{IR}\sqrt{\left(\frac{2\pi n}{L}\right)^2 + \left(\frac{2\pi\vec{n}}{A}\right)^2}\,. \tag{6.54}$$

Assuming that $\Lambda_{IR} \gg 1/L$, we can approximate the sum by an integral to obtain

$$T_{00}^{IR} \approx \frac{1}{2(2\pi)^{d-1}}\int_{|\vec{k}|<2\pi\Lambda_{IR}} d^{d-1}k|\vec{k}| = \frac{\pi\Omega_{d-2}}{2d}\Lambda_{IR}^d\,, \tag{6.55}$$

so the Casimir energy with the IR modes removed behaves as

$$T_{00} \approx -\frac{\pi\Omega_{d-2}}{2d}\Lambda_{IR}^d \tag{6.56}$$

with corrections controlled by powers of $1/(L\Lambda_{IR})$.

Recalling that the usual Casimir energy density in this case is of order[60] $-1/L^d$ we see that removing the IR modes leads to a large enhancement by a factor of order $(L\Lambda_{IR})^d$.

In these free field toy models, we have simply removed the IR modes by hand. In these cases, it seems unlikely that there is some way to couple the two sides of a CFT on a strip that has the effect

[60] Specifically, we have $-\zeta(3)/(2\pi L^3)$ for $d = 3$ and $-\pi^2/(90L^4)$ for $d = 4$.

of removing these modes. In the holographic models, this suppression of the IR modes happens dynamically, since the dual geometries show that the interior region of the geometry dual to CFT_1 is absent.

In the end, it is not clear whether the field theory effect pointed out here is relevant to the enhanced negative energies in the strongly coupled holographic models. In particular, the free field theory calculations behave similarly in $d = 2$ and $d > 2$, while in the holographic model, the large negative energies appear only for $d > 2$.

6.6 Discussion

In this chapter, we have made use of a holographic model for interface CFTs to demonstrate a surprising enhancement of negative vacuum energy for a CFT on a strip. This effect occurs when both sides of the strip are coupled to a CFT with fewer degrees of freedom, and the interfaces are of the right type, corresponding to a bulk interface tension close to a critical value.

In the context of the holographic model, we can make the magnitude of the negative energy density arbitrarily large for a strip of fixed width by tuning the bulk interface tension arbitrarily close to a lower critical value. For specific microscopic CFTs[61], we may not have a continuously variable parameter associated with the interface, so it is interesting to understand whether there exist interfaces that have these qualitative properties. We note that the bulk interface tension is positively related to a central charge associated with the interface, which is expected to decrease under renormalization group flows (see e.g. [77]). Thus, the interfaces that give rise to the more negative energies may be expected to be the ones with minimal values of this central charge that have no relevant perturbations. An interesting class of microscopic models to study would be those where the bulk CFTs are $\mathcal{N} = 4$ supersymmetric Yang-Mills theory with different gauge group rank and/or gauge coupling, and the defects correspond three-dimensional SCFTs [83] which individually preserve half the original supersymmetry but together break the supersymmetry. As discussed in [56], despite the absence of supersymmetry, these models may still have a weakly curved dual description in terms of type IIB supergravity.

It would be very interesting if the negative energy enhancement we observe here is relevant to some real-world systems with a layer of one material inside another material, either for two or three dimensional materials. While our modes are holographic, with a large number of local degrees of freedom, it is not clear that this large number of local degrees of freedom is essential for the effect.

Anomalously high transition temperatures in layered materials?

We have focused on the vacuum properties, but it would be interesting to understand more completely the physics at finite temperature, generalizing the results of [205] to higher dimensions. In particular, it would be interesting to see how stable the solutions with enhanced negative energies are to finite temperature perturbations.

For a holographic CFT with one periodic direction (with antiperiodic boundary conditions for fermions), we have a phase transition when the inverse temperature equals the length of the periodic direction [180]. Above this temperature, the thermal circle is contractible in the bulk. The CFT with a compact direction can be understood as a confining gauge theory from the lower-dimensional point of view, and the phase transition is a deconfinement transition. In the layered situation, we similarly expect a phase transition to a high temperature phase where the thermal circle becomes contractible. The naive scale for this transition would be the width of the CFT_1 layer. However,

[61] See [78–83] for top-down examples of holographic interface CFTs.

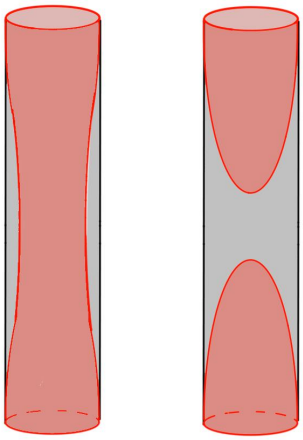

Figure 6.9: Bulk region associated with CFT_1 (shown in grey) at low (left) and high (right) temperature. As the interface tension approaches the lower critical value, we expect that the transition temperature must be increasingly large in order to admit the high-temperature phase disconnected solution (right) which avoids intersection of the domain walls.

we found that the bulk solution corresponding to a CFT_1 layer can be that corresponding to the CFT with a periodic direction whose length is much smaller than the width of the interval. In this case, we expect that this higher temperature scale sets the transition temperature.

To see this, we note that during the transition in the interface case, the bulk interfaces associated with the two CFT interfaces become disconnected and the thermal circle is contractible in the bulk, as shown in Figure 6.9. In the limit where the interface tension approaches the lower critical value (where the local state of CFT_1 is similar to that of a CFT on a circle much smaller than the width of the strip), the angle of intersection between the interface and the AdS boundary becomes small. In this case, we expect that the upper interface in the right side of Figure 6.9 extends further and further down from the interface. Having a solution as in the right of Figure 6.9 which avoids intersection of the two interfaces would require an increasingly large temperature (small periodic direction) relative to the width of the interval (vertical direction) as the tension is lowered to the critical value. Thus, we expect that the transition temperature will become large in this limit. If this is correct, it means that the large negative energy density in the CFT_1 region will persist to relatively high temperatures.

It would be interesting to explore whether a similar mechanism could lead to anomalously high transition temperatures for holographic layered materials exhibiting other low-temperature phases, e.g. those exhibiting superconductivity. There is a wealth of fascinating phenomena associated with layered materials in real-world condensed matter systems (e.g. high-T_c cuprate superconductors). It would be nice to understand whether the underlying field theory mechanism responsible for the anomalously large vacuum energies and anomalously high transition temperatures (assuming our qualitative arguments for the latter are correct) in our holographic model is relevant to observable phenomena in experimentally realizable layered materials.

Implications for our cosmological model

The motivation for studying the field theory setups in this chapter was our holographic cosmological model formulated in Chapter 5. Recall that in this model $\Lambda < 0$ big-bang / big-crunch cosmologies are dual to eternally traversable Lorentzian wormholes, which can only be supported by a large amount of negative null energy density. The results of the present chapter show that

such anomalously large null energy densities are indeed possible if i) the matter in the wormhole is a holographic CFT, ii) the interface between the wormhole and the coupled 4D non-gravitational EFT is appropriately tuned, and iii) if the wormhole has many more degrees of freedom than the non-gravitational EFT. Given that the latter condition is a key feature of our construction, which is required for gravity localization on the wormhole/cosmology, the results of this chapter provide a non-trivial consistency check for our holographic cosmology model.

Chapter 7

Building the holographic dictionary

We saw in Chapter 5 that a large class of spatially flat big-bang / big-crunch cosmologies with negative cosmological constant are related by analytic continuation to asymptotically AdS traversable wormholes with planar cross section. Furthermore we discussed how such wormhole geometries may be dual to a pair of 3D holographic CFTs coupled via auxiliary degrees of freedom to give a theory that confines in the infrared. In this chapter, we begin to populate the *holographic dictionary* defining this duality by investigating how observables in the wormhole geometry are related to observables in the confining non-gravitational theory, and vice versa.

We explain how the wormhole geometry is reflected in i) the spectrum, ii) the two-point functions, and iii) the entanglement entropies of the confining theory. To that end we provide an explicit algorithm to reconstruct the wormhole scale factor (which uniquely determines its geometry) from entanglement entropies, heavy operator two-point functions, or light operator two-point functions (which contain the spectrum information). In the latter case the physics of the bulk scalar field dual to the light operator is closely related to the quantum mechanics of a one-dimensional particle in a potential derived from the scale factor, and the problem of reconstructing the scale factor from the two-point function is directly related to the problem of reconstructing this Schrödinger potential from its spectrum.

7.1 Introduction

In this chapter, we study the possible holographic description of Lorentzian geometries with two asymptotically AdS planar boundaries, with metric of the form

$$ds^2 = a^2(z)(dz^2 - dt^2 + dx^2 + dy^2), \tag{7.1}$$

where $z \in (-z_0, z_0)$ and $a(z)$ has simple poles at the locations $z = \pm z_0$ of the two asymptotic AdS boundaries. We have seen that such geometries make an intriguing appearance as the double analytic continuation of time-reversal symmetric $\Lambda < 0$ big-bang / big-crunch cosmologies. Following [140] we argued that understanding the holographic description of such wormholes may lead to microscopic models of cosmological physics, perhaps even relevant to our Universe.

In this chapter, we will assume that gravitational solutions of this type exist and can be described holographically, and we will attempt to understand the required properties of this holographic description. The pair of asymptotically AdS boundaries in the wormhole suggests a holographic description involving a pair of CFTs. These must be highly entangled with each other in the state corresponding to the wormhole since the two asymptotic regions are connected in the interior. Since it is possible to travel from one boundary to the other causally through the spacetime, these CFTs must also be interacting.

Various recent works [141, 170, 171, 209, 210] have suggested specific ways to obtain traversable wormholes by coupling a pair of holographic CFTs. In Chapter 5 we proposed that four-dimensional examples with geometry (7.1) might arise by coupling a pair of 3D CFTs via an auxiliary four-dimensional field theory. The 4D theory has many fewer local degrees of freedom than the 3D

theories, but (via a renormalization group flow) strongly modifies the IR physics so that the IR theory is confining, with a ground state in which the two 3D CFTs are strongly entangled.

In this chapter, we will be somewhat agnostic about how the CFTs associated with the two asymptotically AdS regions are coupled and ask instead how the wormhole physics is reflected in the state of the CFT degrees of freedom. We ask two general questions about the relationship between planar traversable wormhole geometries and observable properties in the dual field theory.

Question 1: *What observables in the microscopic field theory signal the presence of a dual eternal traversable wormhole?*

This first question is the subject of Section 7.2. We identify multiple signatures of the presence of a wormhole in the observables of the dual microscopic theory.

First, the theory has a discrete mass spectrum of particles characteristic of a confining gauge theory. In the wormhole geometry, the two asymptotic boundaries correspond to the UV of the field theory, while the middle of the wormhole corresponds to an IR "end" of the geometry that is a finite distance from any interior point. Having an IR end characterizes a geometry whose dual field theory is confining.[62] With this feature, the various bulk fields exhibit a discrete set of modes that correspond to towers of particles (glueballs, etc) with a discrete set of masses in the dual field theory.

In Section 7.2.1 we study in detail the spectra that arise from scalar fields in the wormhole and how these depend on the scale factor $a(z)$. Scalar fields in the wormhole geometry with normalizable boundary conditions can be decomposed into components associated with a discrete set of radial wavefunctions $u_i(z)$. These solve an auxiliary Schrodinger problem with potential

$$V(z) = \frac{a''(z)}{a(z)} + m^2 a^2(z) \, . \tag{7.2}$$

The associated eigenvalues λ_i give the values of the mass squared for the associated scalar particles in the 3D theory.

In Section 7.2.2 we describe how the wormhole geometry implies a specific behavior for the two-point functions of scalar operators in the confining field theory, providing expressions for the one-sided and two-sided two-point functions in terms of the wormhole scale factor.

The wormhole geometry also has implications for the behavior of entanglement entropies of subregions of the microscopic theory, as we describe in Section 7.2.3. For example, considering the entanglement entropy for a region that includes a ball of radius R in each CFT, we expect a phase transition as the radius is increased past some critical radius where the RT surface changes from being disconnected to being connected.

The second question that we ask is the following:

Question 2: *How can the wormhole geometry be reconstructed from microscopic observables?*

We address this question in Section 7.3, where we identify three different observables from which to retrieve the behavior of the scale factor $a(z)$ appearing in equation (7.1).

In Sections 7.3.1-7.3.5 we show how to reconstruct the scale factor using the mass spectra of scalar particles in the confining gauge theory arising from scalar fields in the bulk geometry. The spectrum

[62] See e.g. [180, 211] for previous models of holographic confining gauge theories. In Witten's original model, we have an internal S^1 contracting smoothly to zero at the IR end; in the wormhole geometry, we have an S^0 that contracts smoothly to zero.

associated with a given scalar field can be extracted from the two-point function of the corresponding scalar operator, as explained in Section 7.3.1. Using the spectral information associated with a single massless scalar, or any two scalar fields of arbitrary different masses, we can reconstruct the scale factor. The problem of reconstructing the wormhole geometry from mass spectra reduces to the question of whether, given the discrete spectrum of a Schrödinger equation, we can reconstruct the potential $V(z)$ which generates it. This is a particular case of an inverse Sturm-Liouville problem [212, 213], a well-known mathematical question which, in its two-dimensional version, is frequently formulated as "can one hear the shape of a drum?" [214]. Although the answer to this question is negative for generic potentials, the symmetry of our configuration and the AdS asymptotics turn out to be enough to render the inverse problem solvable. We provide an explicit algorithm in Section 7.3.4, first to reconstruct the Schrödinger potential appearing in (7.2) and then using the potentials for a pair of different mass scalars (or a single potential for $m^2 \leq 0$) to reconstruct the scale factor. We give an explicit example in Section 7.3.5.

The second microscopic observable we can use to reconstruct the wormhole geometry is the two-point function of 3D CFT operators with large scaling dimension, corresponding to heavy bulk scalar fields (see Section 7.3.6). Such correlators can be evaluated in the geodesic approximation [215] leading to a functional dependence on the scale factor $a(z)$. Inverting this relationship by solving an integral equation allows us to reconstruct the wormhole metric in terms of microscopic correlators.

The third observable we consider, in Section 7.3.7, is the entanglement entropy of a strip-shaped subsystem in one of the two 3D CFTs. Similarly to the analysis for heavy correlators, the area of the Ryu-Takayangi (RT) surface [216] associated with such subregions has a functional dependence on the scale factor. Once inverted, this relationship yields the wormhole scale factor in terms of the entanglement entropy of the dual microscopic theory.

Applications to cosmology

The holographic description of planar asymptotically AdS wormhole geometries studied in this chapter is an essential part of the framework introduced in Chapter 5 for describing certain time-symmetric $\Lambda < 0$ big-bang / big crunch cosmologies holographically. Recall that in that setup, the quantum state encoding the cosmological spacetime and the quantum state encoding the wormhole spacetime arise from two different slicings of the same Euclidean field theory path integral, and the observables in the two pictures are related by an analytic continuation of two spacetime coordinates. In particular, the cosmological scale factor in conformal time is the analytic continuation of the wormhole scale factor $a(z)$, and so a complete knowledge of the wormhole geometry implies a complete knowledge of the cosmological evolution. Therefore, the wormhole reconstruction procedures developed in Section 7.3 imply that the cosmological scale factor can be reconstructed from simple confining field theory observables as well.[63] We will comment further on these aspects in Section 7.3.4 and in Section 7.4, where we give our concluding remarks.

7.2 From the wormhole to the microscopic theory

Let us consider a planar traversable wormhole geometry

$$ds^2 = a^2(z)(-dt^2 + dx^2 + dy^2 + dz^2), \tag{7.3}$$

[63] Probing the cosmological evolution without relying on the connection to the wormhole is a highly complex task [56, 102, 152, 217] (see also [153, 218] for lower-dimensional examples, and [219, 220] for related discussions), so this approach gives an explicit example of the power of the "slicing duality" introduced in Chapter 5.

with $t, x, y \in R$, and $z \in (-z_0, z_0)$ a coordinate with finite range. We assume that the wormhole connects two asymptotically AdS regions at $z = \pm z_0$, near which the scale factor $a(z)$ has the asymptotic form

$$a(z) \sim \frac{L}{z_0 \pm z} = \frac{\sqrt{-3/\Lambda}}{z_0 \pm z} \tag{7.4}$$

where $\Lambda < 0$ is the cosmological constant and L is the corresponding AdS length. We will also assume that the wormhole is symmetric, $a(z) = a(-z)$. As discussed in Chapter 5, such a geometry arises via a double analytic continuation from a large class of spatially flat, time-reversal symmetric Friedmann-Roberston-Walker (FRW) cosmologies with $\Lambda < 0$.

Recall that while the state of the cosmological effective field theory in these models is highly excited and thus generally difficult to study, the corresponding state in the wormhole picture is simply the canonical vacuum state. This in principle allows one to study a wide class of cosmological observables (e.g. density perturbations, the CMB spectrum, etc.) by studying the vacuum physics in the traversable wormhole background. Moreover, since the wormhole connects two asymptotically AdS regions, we expect the physics in the wormhole to be dual to a pair of non-gravitational, microscopic 3D CFTs living on the two AdS boundaries $\mathbb{R}^{1,2}$. Our goal in this chapter will be to better understand how the effective low energy physics in the wormhole is related to the underlying microscopic physics of the two coupled 3D CFTs. As such, this question does not refer to the cosmology picture, and thus could be of interest outside the cosmological context.

7.2.1 Scalar particle spectrum from bulk scalar field

Let us begin by considering the simple situation in which the effective field theory in the wormhole consists of a single free scalar field ϕ of mass m.[64] The vacuum of the scalar field corresponds to the vacuum state of the dual microscopic theory. We will compute the excitation spectrum of the scalar in the wormhole, and thus obtain the mass spectrum of particles in the microscopic theory.

The excitation spectrum of the field ϕ on the wormhole background can be found by canonically quantizing ϕ. We begin by finding a complete set of mode solutions to the wave equation $(\Box - m^2)\phi = 0$. Translation invariance in the x, y, and t directions ensures a basis of solutions of the form

$$f_{k_x,k_y,i}(t, x, y, z) = \frac{1}{2\pi\sqrt{2\omega}a(z)} e^{-i\omega t} e^{ik_x x} e^{ik_y y} u_i(z), \tag{7.5}$$

which, after substituting into the wave equation, gives a Schrödinger equation for the modes u_i, namely

$$-u_i''(z) + V(z)u_i(z) = \lambda_i u_i(z). \tag{7.6}$$

The frequencies ω are related to the transverse momenta k_x, k_y and the eigenvalues λ_i via

$$\omega = \sqrt{k_x^2 + k_y^2 + \lambda_i}, \tag{7.7}$$

and the Schrödinger potential $V(z)$ is defined in terms of the wormhole scale factor $a(z)$ by

$$V(z) \equiv \frac{a''(z)}{a(z)} + m^2 a^2(z). \tag{7.8}$$

[64] This would be expected to hold precisely in a strict large N limit of the dual field theory and approximately for large but finite N.

Since the scale factor, by assumption, has the symmetry $a(z) = a(-z)$, the same is true for the potential, $V(z) = V(-z)$. Furthermore the scale factor has the asymptotic AdS form (7.4) near the boundaries, and so the potential is of the asymptotic form

$$V(z) \sim \frac{\alpha}{(z_0 \pm z)^2}, \tag{7.9}$$

$$\alpha \equiv 2 - 3m^2/\Lambda. \tag{7.10}$$

From the Schrödinger equation we see that the two possibilities for the asymptotic behavior of $u(z)$ are either $u(z) \sim (z_0 \mp z)^{\Delta_+}$ or $u(z) \sim (z_0 \mp z)^{\Delta_-}$, where

$$\Delta_\pm \equiv \frac{1 \pm \sqrt{1+4\alpha}}{2}. \tag{7.11}$$

We call the former solutions *normalizable*, and the latter *non-normalizable*[65].

The canonical quantization of the scalar field is obtained by writing it as a mode sum

$$\hat{\phi}(t,x,y,z) = \sum_i \int dk_x \int dk_y \Big[f_{k_x,k_y,i}(t,x,y,z)\hat{a}_{k_x,k_y,i} + f^*_{k_x,k_y,i}(t,x,y,z)\hat{a}^\dagger_{k_x,k_y,i} \Big], \tag{7.12}$$

where $\hat{a}_{k_x,k_y,i}$ and $\hat{a}^\dagger_{k_x,k_y,i}$ are canonically commuting creation and annihilation operators for the modes $f_{k_x,k_y,i}$, and the vacuum state of the theory is defined as the state $|0\rangle$ which is annihilated by all the annihilation operators. We will assume that the modes appearing in the sum are normalizable, so that the excitations created by the creation operators are normalizable excitations.[66] Since we have chosen the modes f to be positive frequency with respect to the timelike Killing vector field ∂_t, this canonical vacuum state is the lowest energy state with respect to the Hamiltonian generating time translations in t.

In order for the field ϕ to canonically commute with its conjugate momentum field, it is necessary and sufficient that the mode functions $f_{k_x,k_y,i}$ are orthonormal in the Klein-Gordon inner product. This implies the normalization condition

$$\int_{-z_0}^{z_0} dz\, u_i(z) u_j(z) = \delta_{ij}. \tag{7.13}$$

Since the z coordinate has a finite range, the set of normalizable solutions u_i to the Schrödinger equation is discrete, justifying the use of the discrete label $i = 0, 1, 2, \ldots$.

Having canonically quantized the scalar field, we can read off its energy spectrum. The Hamiltonian for a free scalar field is

$$\hat{H} = \sum_i \int dk_x \int dk_y\, \omega_{k_x,k_y,i} \left(\hat{a}^\dagger_{k_x,k_y,i}\hat{a}_{k_x,k_y,i} + \frac{1}{2} \right), \tag{7.14}$$

and thus, from Eq. (7.7), the energy spectrum of single particle excitations of the field ϕ is given by $\omega = \sqrt{k_x^2 + k_y^2 + \lambda_i}$. Since this is a free theory, the multi-particle spectrum is simply obtained by adding together single particle excitations.

[65] The terms "normalizable" and "non-normalizable" are meaningful only for $\alpha \geq 3/4$. For $-1/4 < \alpha < 3/4$, both solutions are normalizable in L^2 norm, and there are two non-equivalent quantizations of the scalar field, depending on whether we quantize the "normalizable" (standard quantization) or "non-normalizable" (alternative quantization) part of the scalar field. When this ambiguity is present, we will focus here on the standard quantization scheme.

[66] This implies that the states created by acting on the vacuum with the creation operators have position space wavefunctions which are L^2 normalizable.

We expect that the spectrum of excitations in the wormhole is equal to the spectrum of excitations in the dual microscopic theory. The dispersion relation $\omega = \sqrt{k_x^2 + k_y^2 + \lambda_i}$ suggests that in the (2+1)-dimensional microscopic theory[67] the particle excitations have momenta $\vec{k} = (k_x, k_y)$ and a discrete spectrum of squared masses $m_i^2 = \lambda_i$. Indeed, in the particular construction considered in Chapter 5, the dual microscopic theory flows in the infrared towards a confining gauge theory on $\mathbb{R}^{2,1}$, which we expect to exhibit a discrete particle spectrum.

Therefore we find that the wormhole scale factor, and hence the corresponding FRW scale factor, determines the mass spectrum of scalar particles in the underlying microscopic theory. It would be interesting to understand which microscopic theories correspond to FRW cosmologies with realistic scale factors. We will not pursue this question here, but it could be an interesting area for future work. Instead we will now discuss correlators of scalar operators in the microscopic theory and understand how they are related to the geometry of the bulk wormhole.

7.2.2 Scalar two-point functions

Given the geometry of the wormhole, we would like to understand what are the correlation functions of the CFT operator dual to a bulk scalar field.[68] Then in Section 7.3 we will study the inverse problem: how to reconstruct the wormhole geometry from a knowledge of the microscopic correlators.

Computing CFT correlators from a knowledge of the bulk geometry is straightforwardly done using the extrapolate dictionary of AdS/CFT: we compute the bulk correlators, and extrapolate them to the boundary to obtain correlators of 3D CFT operators in the dual confining theory. Let us work this out for the two-point function.

From (7.12), the bulk vacuum Wightman function evaluates to[69]

$$G^+(x,x') \equiv \langle 0|\, \phi(x)\phi(x')\, |0\rangle = \sum_n \int dk_x \int dk_y f_{k_x,k_y,n}(x) f^*_{k_x,k_y,n}(x'). \tag{7.15}$$

Using the expression (7.5) for the mode functions, this can be simplified to

$$G^+(x,x') = \frac{1}{4\pi a(z)a(z')} \sum_n u_n(z)u_n(z') \int_{k_n}^\infty d\omega e^{-i\omega\Delta t} J_0\left(\Delta x_\perp \sqrt{\omega^2 - k_i^2}\right), \tag{7.16}$$

where $\Delta t \equiv t - t'$, $\Delta x_\perp \equiv \sqrt{(x-x')^2 + (y-y')^2}$, and we recall that $u_n(z)$ are eigenfunctions of the Schrödinger equation (7.6), with corresponding eigenvalues $k_n^2 \equiv \lambda_n$. Finally, the ω integral can be evaluated to give [221]

$$G^+(x,x') = \frac{1}{4\pi a(z)a(z')\sqrt{-\Delta t^2 + \Delta x_\perp^2}} \sum_{n=0}^\infty u_n(z)u_n(z') \exp\left(-k_n\sqrt{-\Delta t^2 + \Delta x_\perp^2}\right), \tag{7.17}$$

with the square roots taking values on their principal branch.

[67] Note that the dual microscopic theory is (3+1)-dimensional (two 3D CFTs coupled by 4D auxiliary degrees of freedom), as we have pointed out. However, it flows in the IR to a gapped effective (2+1)-dimensional theory [217]. When we refer to the full dual theory as being (2+1)-dimensional, we have in mind such an effective gapped theory. This should not be confused with the two 3D CFTs living at the two asymptotic boundaries, and coupled by the auxiliary 4D degrees of freedom.

[68] In our paper [3] we also discuss bulk gauge fields, but I have chosen to omit this discussion in this thesis.

[69] In the rest of the chapter we will omit the $\hat{}$ on quantum operators.

Consider now the CFT two-point function of the operator $\mathcal{O}$ which is dual to the field ϕ. This can be obtained by taking the points z and z' to the boundary, and removing powers of $z_0 \pm z$ and $z_0 \pm z'$ so that the expression is independent of z and z'. Concretely, $a(z) \sim 1/(z_0 - |z|)$ as $z \to \pm z_0$. Meanwhile the mode functions are of the form $u_n(z) \sim u_n^+(z_0 + z)^{\Delta_+}$ near $z = -z_0$, where u_n^+ is the normalizable coefficient, chosen such that the modes are normalized as in (7.13). Since $u_n(z)$ is even if n is even and odd if n is odd, near $z = +z_0$ the mode functions are of the form $u_n(z) \sim (-1)^n u_n^+(z_0 - z)^{\Delta_+}$.

Since the wormhole has two boundaries, at $z = \pm z_0$, we have two types of insertions of the operator $\mathcal{O}$ into correlation functions. We denote an insertion of $\mathcal{O}$ at position (t, x, y) at the boundary $z = -z_0$ by $\mathcal{O}_-(t, x, y)$, and similarly for an insertion at the boundary $z = +z_0$. Thus there are two types of two-point functions: $\langle \mathcal{O}_\pm \mathcal{O}_\pm \rangle$ and $\langle \mathcal{O}_\pm \mathcal{O}_\mp \rangle$. The extrapolation procedure gives

$$\langle \mathcal{O}_\pm(t, x, y)\mathcal{O}_\pm(t', x', y') \rangle = \frac{1}{4\pi\sqrt{-\Delta t^2 + \Delta x_\perp^2}} \sum_{n=0}^{\infty} (u_n^+)^2 \exp\left(-k_n \sqrt{-\Delta t^2 + \Delta x_\perp^2}\right), \tag{7.18}$$

for the one sided correlators, and

$$\langle \mathcal{O}_\pm(t, x, y)\mathcal{O}_\mp(t', x', y') \rangle = \frac{1}{4\pi\sqrt{-\Delta t^2 + \Delta x_\perp^2}} \sum_{n=0}^{\infty} (-1)^n (u_n^+)^2 \exp\left(-k_n \sqrt{-\Delta t^2 + \Delta x_\perp^2}\right), \tag{7.19}$$

for the two sided correlators. Given the wormhole scale factor, the mode functions $u_n(z)$ and normalizations u_n^+ can be computed, and the $\mathcal{O}\mathcal{O}$ two-point functions can be evaluated. Therefore, the behavior of scalar operator correlators in the dual confining theory is uniquely fixed by the wormhole geometry.

7.2.3 Entanglement entropy

Another boundary observable in which we expect to see a clear signature of the presence of the wormhole is the entanglement entropy of subregions of the dual microscopic theory. For example, consider the behavior of the entanglement entropy for a region $A = A_L \cup A_R$ — where A_L and A_R are identical-sized subregions of the left and right 3D CFTs respectively — as we vary the size of A. In the presence of a wormhole, we expect to observe a phase transition in the entanglement entropy related to a bulk transition from a disconnected RT surface (dominant for small A) to a connected RT surface going through the wormhole (dominant for large A). The transition occurs because the disconnected surfaces have a regulated area that eventually grows like the volume of the boundary region, while the connected surface has an area that eventually grows like the area of the boundary region. In the absence of a wormhole geometry connecting the two 3D theories living on the two boundaries, there is no such phase transition. We leave further investigation of the properties of holographic entanglement entropies in our setup to future work.

7.3 Reconstructing the wormhole

So far we have discussed how properties of the microscopic theory, such as its particle spectrum and correlators, are related to the geometry of the wormhole. Now let us ask the inverse question: can we reconstruct the wormhole geometry from properties of the underlying confined microscopic theory? We will find that such a reconstruction is indeed possible if we have access to certain observables of the microscopic theory.

The first example of such an observable is given by the two-point functions $\langle \mathcal{O}_1 \mathcal{O}_1 \rangle$ and $\langle \mathcal{O}_2 \mathcal{O}_2 \rangle$ in the confining theory of two 3D CFT scalar operators $\mathcal{O}_1$ and $\mathcal{O}_2$ of different scaling dimensions[70]. Our wormhole reconstruction algorithm from these two-point functions can be summarized as follows.

First, in Section 7.3.1, we show how a knowledge of the scalar two-point function $\langle \mathcal{O}\mathcal{O} \rangle$ in the microscopic confining theory allows one to obtain the mass spectrum of the associated scalar particle excitations, which is equal to the spectrum of modes of a bulk scalar field with some mass m. Then, in Section 7.3.2, we show how the mass spectrum associated with an operator $\mathcal{O}_i$ can be used to reconstruct the Schrödinger potential which gives rise to this spectrum. From (7.8) we know that this potential is given directly in terms of the wormhole scale factor and the mass of the scalar field ϕ_i dual to the operator $\mathcal{O}_i$. In Section 7.3.3 we show how a knowledge of two such potentials, associated with two scalar operators $\mathcal{O}_1$ and $\mathcal{O}_2$ of different dimensions, allows one to invert this relationship and obtain the scale factor.[71] We summarize the entire algorithm in Section 7.3.4 and provide an example of reconstruction in Section 7.3.5. The reconstruction algorithm for the wormhole geometry from boundary scalar two-point functions should be regarded as one of the main results of this chapter. Finally, in Section 7.3.6 and 7.3.7 we explain how the wormhole scale factor can be reconstructed from correlators of 3D CFT operators with large scaling dimension, and from the entanglement entropy of strip-shaped subregions of one of the two 3D CFTs.

7.3.1 Mass spectrum from two-point function

In equation (7.18) and (7.19) we wrote down the CFT two-point functions $\langle \mathcal{O}_\pm \mathcal{O}_\pm \rangle$, in which both insertions of the operator $\mathcal{O}$ are inserted into the same same wormhole boundary, and $\langle \mathcal{O}_\pm \mathcal{O}_\mp \rangle$, where one insertion is into the CFT at $z = +z_0$ and the other insertion into the CFT at $z = -z_0$. Namely

$$G_{++}(s) \equiv \langle \mathcal{O}_\pm(x) \mathcal{O}_\pm(x') \rangle = \frac{1}{4\pi s} \sum_{n=0}^{\infty} (u_n^+)^2 \exp\left(-k_n s\right), \tag{7.20}$$

$$G_{+-}(s) \equiv \langle \mathcal{O}_\pm(x) \mathcal{O}_\mp(x') \rangle = \frac{1}{4\pi s} \sum_{n=0}^{\infty} (-1)^n (u_n^+)^2 \exp\left(-k_n s\right), \tag{7.21}$$

where $s \equiv \sqrt{-(t-t')^2 + (\boldsymbol{x} - \boldsymbol{x}')^2}$.

Let us consider these correlators in the regime where s is imaginary, $s = i\xi$, namely

$$G_{++}(\xi) = \frac{1}{4\pi i \xi} \sum_{n=0}^{\infty} (u_n^+)^2 \exp\left(-i k_n \xi\right), \tag{7.22}$$

$$G_{--}(\xi) = \frac{1}{4\pi i \xi} \sum_{n=0}^{\infty} (-1)^n (u_n^+)^2 \exp\left(-i k_n \xi\right). \tag{7.23}$$

[70] The operators $\mathcal{O}_1, \mathcal{O}_2$ are operators associated with the two 3D CFTs living at the two asymptotic boundaries, but their expectation value is computed in the full confining theory obtained by coupling the two 3D CFTs by auxiliary 4D degrees of freedom.

[71] Note that a single potential associated with a massless bulk scalar field is sufficient to reconstruct the scale factor. For $m^2 < 0$ (but above the BF bound) a single potential may also be enough to reconstruct the geometry, though we only have numerical evidence for this. For $m^2 > 0$, a single potential is not sufficient.

Multiplying by $i\xi$ and taking the Fourier transform gives

$$G_{++}(k) \equiv \int_{-\infty}^{\infty} d\xi\, i\xi G_{++}(\xi) e^{ik\xi} = \frac{1}{2}\sum_{n=0}^{\infty}(u_n^+)^2\delta(k-k_n), \tag{7.24}$$

$$G_{+-}(k) \equiv \int_{-\infty}^{\infty} d\xi\, i\xi G_{+-}(\xi) e^{ik\xi} = \frac{1}{2}\sum_{n=0}^{\infty}(-1)^n(u_n^+)^2\delta(k-k_n), \tag{7.25}$$

and so we see that the spectrum of scalar excitations, $k_n^2 = \lambda_i$, is simply obtained from the peaks in the Fourier transforms of the two-point correlators, while the normalizations u_n^+ are obtained from the amplitudes of the peaks. Interestingly, it is possible to obtain this information either from the one-sided or two-sided correlators. Notice that to obtain the spectrum above a given scale k_0, we need to probe the two-point function on distance scales $\xi < 1/k_0$. From the analysis of Section 7.2.1, we can identify this spectrum of scalar excitations with the discrete spectrum of modes associated with a bulk scalar field.

7.3.2 The inverse Sturm-Liouville problem

Suppose now that, perhaps starting from CFT correlators as in the previous section, we obtain the spectrum λ_i of scalar excitations associated with a given operator $\mathcal{O}$ in the microscopic theory, which we can identify with the discrete spectrum of modes for a bulk scalar field. We know from the analysis in Section 7.2.1 that the λ_i are eigenvalues to the Schrödinger equation (7.6),

$$-u_i''(z) + V(z)u_i(z) = \lambda_i u_i(z), \tag{7.26}$$

where the potential $V(z)$ is related to the scale factor of the wormhole. Given the potential, the problem of finding the eigenvalues λ_i (i.e. diagonalizing the Hamiltonian) is called a Sturm-Liouville problem. Here, we are interested in the inverse Sturm-Liouville problem problem: finding the potential $V(z)$ from a given spectrum λ_i.[72]

Under the assumption of a generic potential the solution to the inverse Sturm-Liouville problem is not unique [212, 213]. However the potentials that are of interest to us are not completely generic; we are assuming that the wormhole geometry is even $a(z) = a(-z)$, and so the potential is also even, $V(z) = V(-z)$. In the context of wormholes that arise from cosmological models [217], this symmetry of the geometry arises from the $\mathbb{Z}_2$ symmetry present in both the Euclidean CFT path integral used to define the theory, as well as the choice of slicing of this path integral which defines the state of the theory. It has been shown in [213] that if the potential is even and integrable, $\int_{-z_0}^{z_0} V(z) < \infty$, then the inverse Sturm-Liouville problem can be solved. Namely, there exists an efficient algorithm which allows one to reconstruct the potential $V(z)$ given its spectrum.

Unfortunately we cannot directly apply these results to solve our inverse Sturm-Liouville problem, because our potential diverges as $1/z^2$ near the AdS boundaries (see Eq. (7.9)) and hence is not integrable. In this section we will upgrade the reconstruction algorithm in [213] to allow for potentials with AdS asymptotics. We will make the following assumptions:

Assumptions

1. The domain of z is $(-z_0, z_0)$ for some $z_0 > 0$;

[72] The question "can one hear the shape of a drum?" [214] — i.e. "Can one determine the geometry of a two-dimensional manifold from a knowledge of the spectrum of the Laplace operator?" — is a higher dimensional analog to the inverse Sturm-Liouville problem.

2. The potential is symmetric, $V(z) = V(-z)$;

3. The potential diverges as $\frac{\alpha}{(z_0-|z|)^2} + \frac{\beta}{(z_0-|z|)}$ at $z = \pm z_0$, with $\alpha > -1/4$ and $\beta \in \mathbb{R}$;

4. The normalizable spectrum $\{\lambda_j\}$ to the Schrödinger equation (7.26) is known.

Let us make some comments about these assumptions. From equation (7.9) we see that the parameter α characterizing the leading divergence of the potential is given by $\alpha = 2 + m^2L^2$, where L is the AdS length in the asymptotically AdS regions, and m is the mass of the scalar field. The assumption $\alpha > -1/4$ is therefore equivalent to the Breitenlohner-Freedman (BF) bound $m^2L^2 > -d^2/4$, with $d = 3$ the spatial dimension of the wormhole [184, 222]. We are also allowing for a subleading divergent term in $V(z)$ proportional to some other constant β.[73] We see from (7.8) that such a term in the potential is expected to arise from general scale factors with boundary asymptotics of the AdS form.

As we have already seen, for a potential with leading divergence of the form in assumption 3, the series expansion near $z = -z_0$ of a solution to the Schrödinger equation (7.26) is

$$u(z) = u^{(-)}(-z_0)(z + z_0)^{\Delta_-}(1 + \dots) + u^{(+)}(-z_0)(z + z_0)^{\Delta_+}(1 + \dots), \tag{7.27}$$

where

$$\Delta_\pm \equiv \frac{1}{2} \pm \bar{\Delta}, \tag{7.28}$$

$$\bar{\Delta} \equiv \frac{1}{2}\sqrt{1 + 4\alpha}, \tag{7.29}$$

and $u^\pm(-z_0)$ are numerical coefficients. The omitted terms in the above expansion are of subleading order in the distance $z + z_0$ from the boundary. We say that the term proportional to $u^{(+)}(-z_0)$ is normalizable at $z = -z_0$, and the term proportional to $u^{(-)}(-z_0)$ is non-normalizable at $z = -z_0$. We have a similar expansion at $z = +z_0$, with normalizable and non-normalizable coefficients $u^{(+)}(z_0)$ and $u^{(-)}(z_0)$. We define the *normalizable eigenfunctions* of the Schrödinger equation (7.26) to be those eigenfunctions for which the non-normalizable component vanishes at both endpoints, $u^{(-)}(-z_0) = u^{(-)}(z_0) = 0$. The *normalizable spectrum* is the set of eigenvalues associated with the normalizable eigenfunctions.

Note that the normalizable eigenfunctions are indeed normalizable in L^2 norm. Perhaps somewhat confusingly, if $\alpha < 3/4$, eigenfunctions which are non-normalizable at one or both endpoints are also normalizable in L^2 norm. This is related to the ambiguity — which arises when a scalar field in AdS has a mass in the range $-d^2/4 < m^2L^2 < -d^2/4 + 1$ — in deciding which part of the field to identify with the expectation value of the dual CFT operator, and which part to identify with the source of the dual CFT operator. For simplicity we will always associate the normalizable eigenfunctions with the expectation values of the dual operators, which in the bulk is the statement that, as we have done in Section 7.2.1, we will expand the scalar field in terms of a complete set of normalizable eigenfunctions of the wave equation.

We will now show how to reconstruct the potential $V(z)$ from its spectrum, subject to these assumptions. The main idea is to reconstruct the unknown potential $V(z)$ from some known "test" potential $\tilde{V}(z)$ which has the same asymptotic spectrum as $V(z)$. Our first task is to determine the test potential $\tilde{V}(z)$.

[73] In principle, we could also have some subleading divergent term with a different non-integer power, but we will restrict our analysis to this case.

Finding the test potential

We want to find a test potential $\tilde{V}(z)$ such that the eigenvalues $\tilde{\lambda}_j$, $j = 0, 1, 2, \ldots$, of the eigenvalue problem

$$-u''(z) + \tilde{V}(z)u(z) = \tilde{\lambda}u(z), \tag{7.30}$$

$$u^{(-)}(\pm z_0) = 0, \tag{7.31}$$

are asymptotically equal to λ_j for $j \to \infty$. To find such a $\tilde{V}(z)$, let us consider solving the equation $-u''(z)+V(z)u(z) = \lambda u(z)$ on the interval $z \leq 0$, in the limit $\lambda \to \infty$. If $V(z)$ contains terms which are bounded on $z \leq 0$, then the term proportional to λ dominates over these terms and we can simply replace these bounded terms by their average value over $z \leq 0$. Besides this constant, the only terms which remain are the divergent pieces of $V(z)$ on $z \leq 0$, which we know by assumption to be $\frac{\alpha}{(z_0+z)^2} + \frac{\beta}{z_0+z}$, although we do not know the values of α and β a priori. By making the same argument for $z > 0$, we conclude that in the limit $\lambda \to \infty$, the potential $V(z)$ can effectively be replaced by

$$\tilde{V}(z) \equiv \frac{\alpha}{(z_0 - |z|)^2} + \frac{\beta}{z_0 - |z|} + c, \tag{7.32}$$

where α, β, c are unknown constants. Our goal is to determine these constants. We will do this by equating the asymptotic spectrum $\tilde{\lambda}_j$ associated with this $\tilde{V}(z)$ with the asymptotic part of the given spectrum λ_j.

The potential $\tilde{V}(z)$ is simple enough that we can explicitly compute its asymptotic spectrum. As we show in Appendix G, up to terms that go to zero as $j \to \infty$, the spectrum at large j is

$$\tilde{\lambda}_j \sim Zj^2 + Aj + B\log(j) + C, \tag{7.33}$$

where Z, A, B, C are given by

$$Z = \left(\frac{\pi}{2z_0}\right)^2, \tag{7.34}$$

$$A = \left(\frac{\pi}{2z_0}\right)^2 2\Delta_+, \tag{7.35}$$

$$B = \frac{\beta}{z_0}, \tag{7.36}$$

$$C = \left(\frac{\pi}{2z_0}\right)^2 \left(\Delta_+^2 - \frac{4\alpha}{\pi^2}\right) + \frac{\beta}{z_0}\left[\log(\pi) - \psi(\Delta_+)\right] + c, \tag{7.37}$$

with $\psi(x)$ being the digamma function and Δ_+ was defined in (7.28). Notice that $Z > 0$. As we saw, the Breitenlohner-Freedman bound requires $\alpha > -1/4$, and so $A > 0$ as well. Meanwhile, B and C can take on any real values. These restrictions on Z, A, B, C, together with equation (7.33), constitute the necessary asymptotic conditions on the sequence λ_j in order for it to correspond to the spectrum of a scalar field in a symmetric wormhole geometry which connects two asymptotically AdS regions. We will assume that the spectrum from which we are trying to reconstruct the wormhole geometry is of this form. In this case we know that there exists a solution to the inverse Sturm-Liouville problem; we will try to find this solution.

Recall that our current goal is to obtain the test potential $\tilde{V}(z)$ defined in (7.32). Given the spectrum λ_j we can deduce the values Z, A, B, C, and then we can invert equations (7.34)-(7.37) to

give z_0, α, β and c in terms of Z, A, B, C:

$$z_0 = \frac{\pi}{2\sqrt{Z}}, \tag{7.38}$$

$$\alpha = \frac{A}{4Z}\left(\frac{A}{Z} - 2\right), \tag{7.39}$$

$$\beta = \frac{\pi B}{2\sqrt{Z}}, \tag{7.40}$$

$$c = -\frac{A}{4\pi^2}\left[\frac{(\pi^2-4)A}{Z} + 8\right] - B\left[\log(\pi) - \psi\left(\frac{A}{2Z}\right)\right] + C. \tag{7.41}$$

Therefore, given a spectrum λ_j with the correct asymptotic form, we can obtain the test potential $\tilde{V}(z)$. The spectrum $\tilde{\lambda}_j$ associated with the test potential will be asymptotically equal to λ_j, as desired.

Notice that, solely from this asymptotic analysis, we can already make several conclusions about some large scale features of the wormhole geometry, and the associated Schrödinger potential $V(z)$. For instance, from (7.34) we see that the leading (quadratic in j) term in the asymptotic expansion of the spectrum λ_j determines z_0, the coordinate width of the wormhole geometry. Meanwhile the term linear in j determines the leading (α/z^2) divergence of the potential near the AdS boundaries, and hence the cosmological constant. The subleading $\log(j)$ term gives the β/z divergence of the potential, and the term constant in j gives the average value c of the non-singular terms in the potential.

It is in accordance with our intuition from AdS/CFT that the values α and β, which are related to the AdS asymptotics of the wormhole geometry, are associated with the UV asymptotics of the spectrum λ_j. Interestingly we also see that what might be considered the two most extremely IR features of the wormhole — the size of the wormhole z_0 and the average value c — are also determined by the asymptotic form of the spectrum. Heuristically we can say that the asymptotic spectrum encodes the large scale features of the wormhole.

In order to determine the finer details of the wormhole, and in particular the potential $V(z)$, we will need to make use of our knowledge of the spectrum λ_k at finite k. In fact we will find that the eigenvalue λ_k encodes the features of the potential on coordinate distance scales of the order z_0/k, and so if we are only interested in reconstructing the features of the potential (and thus of the scale factor) on scales larger than z_0/N, then to a good approximation it is enough to only know the finite subset $\{\lambda_1, \lambda_2, \ldots, \lambda_N\}$ of the full spectrum.[74] Let us now work out the details of this reconstruction.

Reconstructing the true potential from the test potential

Having obtained the test potential $\tilde{V}(z)$ from the asymptotic spectrum, let us now discuss how to reconstruct the true potential $V(z)$. The main idea of the reconstruction algorithm is based on the study of inverse Sturm-Liouville problems by Ref. [213], but adapted to allow for singular potentials such as ours.

We begin by defining $u(z,\lambda), \tilde{u}(z,\lambda), v(z,\lambda)$ and $\tilde{v}(z,\lambda)$ as the solutions to the following initial

[74] Of course we also need the asymptotic form of λ_j in order to obtain the large scale structure of the potential.

value problems on $z \in (-z_0, z_0)$:

$$u: \begin{cases} u''(z,\lambda) = \big[V(z) - \lambda\big] u(z,\lambda) \\ u^{(+)}(-z_0,\lambda) = \frac{1}{2\bar{\Delta}} \\ u^{(-)}(-z_0,\lambda) = 0 \end{cases} \qquad v: \begin{cases} v''(z,\lambda) = \big[V(z) - \lambda\big] v(z,\lambda) \\ v^{(+)}(+z_0,\lambda) = \frac{1}{2\bar{\Delta}} \\ v^{(-)}(+z_0,\lambda) = 0 \end{cases} \tag{7.42}$$

$$\tilde{u}: \begin{cases} \tilde{u}''(z,\lambda) = \big[\tilde{V}(z) - \lambda\big] \tilde{u}(z,\lambda) \\ \tilde{u}^{+}(-z_0,\lambda) = \frac{1}{2\bar{\Delta}} \\ \tilde{u}^{-}(-z_0,\lambda) = 0 \end{cases} \qquad \tilde{v}: \begin{cases} \tilde{v}''(z,\lambda) = \big[\tilde{V}(z) - \lambda\big] \tilde{v}(z,\lambda) \\ \tilde{v}^{(+)}(+z_0,\lambda) = \frac{1}{2\bar{\Delta}} \\ \tilde{v}^{(-)}(+z_0,\lambda) = 0 \end{cases} \tag{7.43}$$

Here primes denote z derivatives and recall that $\bar{\Delta} = \sqrt{\alpha + 1/4}$. As before we are using the notation $u^{(\pm)}(z_0,\lambda)$ for the normalizable $(+)$ and non-normalizable $(-)$ parts of $u(z,\lambda)$ at $z = z_0$, and similarly at $z = -z_0$. The reason for the choice of normalization $1/(2\bar{\Delta})$ is explained in Appendix H. Notice that while u and $\tilde{u}$ are by definition always normalizable (and hence non-diverging) at the left boundary $z = -z_0$, in general they are non-normalizable (and thus in general diverging) at the right boundary $z = +z_0$. Similarly the v and $\tilde{v}$ are normalizable at the right boundary, but non-normalizable at the left one. However the discrete set of functions $u_j(z) \equiv u(z,\lambda_j)$ and $v_j(z) \equiv v(z,\lambda_j)$ are eigenfunctions of the Schrödinger equation with potential V and normalizable boundary conditions at the left *and* right boundaries, and so these functions are completely regular on the entire wormhole. Analogously, $\tilde{u}_j(z) \equiv \tilde{u}(z,\tilde{\lambda}_j)$, $\tilde{v}_j(z) \equiv \tilde{v}(z,\tilde{\lambda}_j)$ are also regular in $[-z_0, z_0]$.

With this in mind, we define the *Wronskian* $\omega(\lambda)$ as the non-normalizable part of $u(z,\lambda)$ at the right boundary, namely

$$\omega(\lambda) \equiv -\lim_{z\to z_0} \frac{u(z,\lambda)}{(z_0 - z)^{\Delta_-}}, \tag{7.44}$$

so that $\omega(\lambda) = 0$ if and only if λ is a normalizable eigenvalue of the Schrödinger equation (7.26) with potential $V(z)$. The following lemma, which we prove in Appendix H, will play a crucial role in our reconstruction of $V(z)$ from $\tilde{V}(z)$:

Lemma 1. *For any L^2 integrable function $f(z)$ on $z \in (-z_0, z_0)$ the following identity holds:*

$$f(z) = \sum_{j=0}^{\infty} \frac{\tilde{v}_j(z) \int_{-z_0}^{z} dy\, u_j(y) f(y) + \tilde{u}_j(z) \int_{z}^{z_0} dy\, v_j(y) f(y)}{\omega'(\lambda_j)}. \tag{7.45}$$

Let us set $f(z)$ equal to $u_0(z)$, the eigenfunction of the Schrödinger equation corresponding to the lowest eigenvalue λ_0. A basic fact from Sturm-Liouville theory states that $u_j(z)$ has j roots, and so $u_0(z) > 0$. Using the orthonormality of the $u_j(z)$ in the L^2-norm, the lemma gives

$$u_0(z) = \tilde{u}_0(z) + \frac{1}{2} \sum_j \tilde{y}_j \int_{-z_0}^{z_0} dx\, u_j(x) u_0(x), \tag{7.46}$$

where

$$\tilde{y}_j(z) \equiv 2 \frac{\tilde{v}_j(z) - (-1)^j \tilde{u}_j(z)}{\omega'(\lambda_j)}, \tag{7.47}$$

Differentiating (7.46) twice and using the differential equations satisfied by $u_0(z)$ and $\tilde{u}_0(z)$, we obtain

$$V(z) u_0(z) = \tilde{V}(z) u_0(z) + \sum_j \big[\tilde{y}_j(z) u_j(z)\big]' u_0(z). \tag{7.48}$$

Finally, since $u_0(z) > 0$ this implies

$$V(z) = \tilde{V}(z) + \sum_j \big[\tilde{y}_j(z) u_j(z)\big]'. \tag{7.49}$$

Equation (7.49) relates the unknown, true potential $V(z)$ to the test potential $\tilde{V}(z)$, the latter having already been determined in the previous section. However this formula is not sufficient for determining $V(z)$, because the eigenfunctions $u_j(z)$ appearing inside this formula implicitly depend on $V(z)$ through the Schrödinger equations

$$u_j''(z) = \big[V(z) - \lambda_j\big] u_j(z). \tag{7.50}$$

Instead, we should think of (7.49) together with the Schrödinger equations (7.50) as a coupled system of non-linear ODEs for the unknown functions $V, u_0, u_1, u_2, \ldots$.

If we restrict j to the interval $0, 1, \ldots, j_{\max}$, then

$$\begin{cases} V(z) = \tilde{V}(z) + \sum_{j=0}^{j_{\max}} \big[\tilde{y}_j(z) u_j(z)\big]', \\ u_j''(z) = \big[V(z) - \lambda_j\big] u_j(z), \quad j = 0, 1, \ldots, j_{\max} \end{cases} \tag{7.51}$$

forms a closed system of $j_{\max} + 2$ equations for $j_{\max} + 2$ unknown functions $V, u_0, u_1, \ldots, u_{j_{\max}}$. For a given value of $j_{\max}$, denote $V_{j_{\max}}(z)$ as the solution for $V(z)$ obtained by solving this finite system of equations. Since $\tilde{y}_j \to 0$ as $j \to \infty$[75], we expect that the corrections to $V_{j_{\max}}$ become smaller and smaller as we increase $j_{\max}$ to larger and larger values, and that in the limit $j_{\max} \to \infty$ we obtain the true potential $V(z)$.

In practice, we will restrict to a finite $j_{\max}$ and thus obtain an approximation to the true potential $V(z)$. Since the functions u_j and $\tilde{y}_j$ oscillate on scales of order z_0/j, we can think of this as being a good approximation to the true potential on coordinate distance scales larger than $z_0/j_{\max} \sim 1/(\sqrt{Z} j_{\max})$.[76] We will explicitly see this feature in the example reconstruction presented in Section 7.3.5.

Let us briefly comment on a subtlety which arises when we attempt to solve the truncated system of ODEs (7.51). The issue is that in order to obtain $\tilde{y}_j$ via equation (7.47), we need to compute the derivatives of the Wronskian, $\omega'(\lambda_j)$. However the Wronskian is defined in (7.44) in terms of the mode function $u(z, \lambda)$, which depends on the potential $V(z)$, and so it appears that $\omega'(\lambda_j)$ must be solved for simultaneously with the system of equations for $V(z)$ and u_j. Although this is possible, there is an elegant approach due to [213] which allows us to independently and efficiently compute $\omega(\lambda_j)$ prior to computing $V(z)$ and u_j.

The main idea is to observe that, from its definition, the function $\omega(\lambda)$ is equal to zero if and only if $\lambda = \lambda_j$. It can then be shown [213] that $\omega(\lambda)$ is an entire function of order $1/2$ and thus by the Hadamard factorization theorem can be written as $\omega(\lambda) = A \prod_i (1 - \lambda/\lambda_i)$, where A is some normalization constant which can be determined by considering the large λ limit, in which $\lambda_j \to \tilde{\lambda}_j$ and $u_j \to \tilde{u}_j$. Differentiating and setting $\lambda = \lambda_j$ gives

$$\omega'(\lambda_j) = -\frac{\tilde{u}_j^{(-)}(z_0)}{\lambda_j - \tilde{\lambda}_j} \prod_{i \neq j}^{\infty} \frac{(\lambda_j - \lambda_i)}{(\lambda_j - \tilde{\lambda}_i)} \approx -\frac{\tilde{u}_j^{(-)}(z_0)}{\lambda_j - \tilde{\lambda}_j} \prod_{i \neq j}^{j_{\max}} \frac{(\lambda_j - \lambda_i)}{(\lambda_j - \tilde{\lambda}_i)}, \tag{7.52}$$

[75] To see this note that as $j \to \infty$ we have that $\lambda_j \to \tilde{\lambda}_j$ and hence in this limit $\tilde{u}_j$ and $\tilde{v}_j$ both approach the jth eigenfunction of the Schrödinger equation with potential $\tilde{V}$. Since the jth eigenfunction of a symmetric Sturm-Liouville problem has parity $(-1)^j$ we see that $\tilde{v}_j = (-1)^j \tilde{u}_j$ and hence $\tilde{y}_j \to 0$.

[76] The *scale independent* features of the potential $V(z)$, namely the amplitudes of the $1/z^2$ and $1/z$ AdS divergences at the AdS boundaries and the average value of the non-diverging piece of $V(z)$, were determined from the asymptotic (large j) part of the spectrum.

where we have approximated $\lambda_j \approx \tilde{\lambda}_j$ for $j > j_{\max}$. This formula allows us to approximate $\omega'(\lambda_j)$ from quantities that we are given (λ_j) and quantities which we can easily compute ($\tilde{\lambda}_j$ and $\tilde{u}_j$).

7.3.3 Solving for the scale factor from $V(z)$

Having reconstructed the potential V, we now want to obtain the wormhole scale factor by solving the non linear ODE (7.8) for $a(z)$. It is convenient to define the scale factor in AdS units $\tilde{a}(z) = a(z)/L$, in terms of which the ODE takes the form

$$\tilde{a}''(z) + (\alpha - 2)\tilde{a}^3(z) - V(z)\tilde{a}(z) = 0 \tag{7.53}$$

where we used $m^2L^2 = \alpha - 2$, and α is the parameter entering the definition of the test potential. In order to find a unique solution for $\tilde{a}(z)$, we need to impose initial conditions for $\tilde{a}(z)$ and its derivative at some point $z \in (-z_0, z_0)$. However, we only know that the scale factor is symmetric (and therefore $\tilde{a}'(0) = 0$), and that its asymptotic behavior is given by equation (7.4), which in AdS units becomes

$$\lim_{z \to \mp z_0} \tilde{a}(z) = \frac{1}{z_0 \pm z}. \tag{7.54}$$

In general settings and without further assumptions, this information is not enough to uniquely determine the scale factor from a single reconstructed potential. Let us understand this in some more detail.

If the bulk scalar field is massless, which implies $\alpha = 2$, there is a unique symmetric solution to the ODE (7.53) with the correct asymptotics (7.54). In fact, in this case the ODE reduces to a linear ODE. Therefore, given a symmetric solution of the ODE with some initial condition $\tilde{a}(0)$, all other solutions differ by a multiplicative constant. Only one solution in such family has the correct coefficient (i.e. 1) for the divergent term. We conclude that a single potential associated to a bulk massless scalar field is enough to reconstruct the wormhole geometry. On the other hand, for $\alpha \neq 2$ (corresponding to $m^2 \neq 0$) it is non-trivial to understand whether there is a unique symmetric solution to (7.53) with the correct asymptotics.

In order to shed light on this problem, it is useful to consider the generic ansatz[77]

$$\tilde{a}(z) = \frac{1}{z_0 + z} + \frac{1}{z_0 - z} + R(z) \tag{7.55}$$

where $R(z)$ is a symmetric function, regular in $z \in [-z_0, z_0]$. Suppose we have a solution $\tilde{a}_1(z)$ to the ODE (7.53) of the form (7.55). Let us consider a second solution of the form $\tilde{a}_2(z) = \tilde{a}_1(z) + f(z)$ where $f(z)$ is a symmetric function, regular in $z \in [-z_0, z_0]$. $\tilde{a}_2(z)$ is by construction symmetric and of the form (7.55), i.e. it has the correct asymptotic behavior. Substituting $\tilde{a}_2(z)$ in the ODE (7.53) and using the fact that $\tilde{a}_1(z)$ is also a solution, we find that $f(z)$ must satisfy

$$\begin{cases} \frac{f''(z)}{f(z)} - \frac{\tilde{a}_1''(z)}{\tilde{a}_1(z)} + (\alpha - 2)[f(z) + 2\tilde{a}_1(z)][f(z) + \tilde{a}_1(z)] = 0 \\ f'(0) = 0 \\ f(\pm z_0) < \infty \end{cases} \tag{7.56}$$

For $\alpha = 2$ (massless bulk scalar field), the problem (7.56) has no non-trivial solutions, because all the candidate solutions of (7.56) are proportional to $\tilde{a}_1(z)$, which is divergent at $z = \pm z_0$, and

[77] Note that this is the most generic ansatz giving rise to a potential of the form we are considering (specified in Assumption 3 in Section 7.3.2). In particular, it implements the symmetry of the scale factor and the AdS asymptotic behavior at the two boundaries, while introducing no further divergences in the potential besides the quadratic and linear ones appearing in our assumptions.

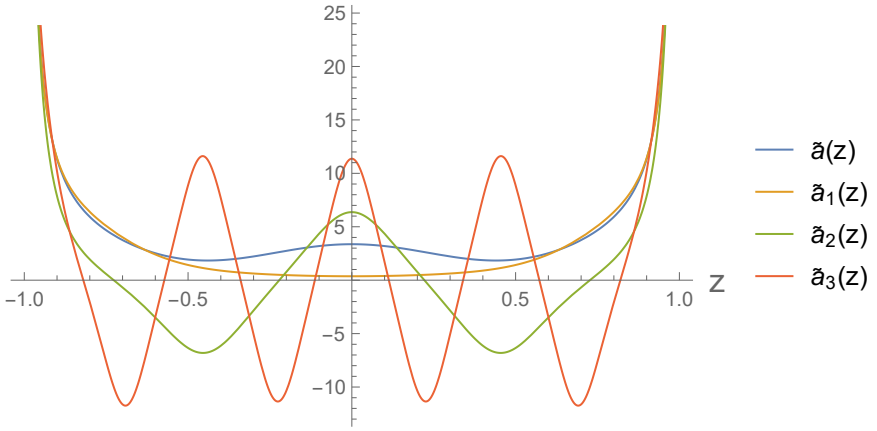

Figure 7.1: Multiple solutions of the ODE (7.53) with potential $V(z)$ defined by the scale factor (7.57), with $z_0 = 1$ and $mL = 3/2$. The solutions displayed are the original scale factor (7.57) $\tilde{a}(z)$, and additional solutions of the form $\tilde{a}_i(z) = \tilde{a}(z) + f_i(z)$, where $f_i(z)$ is a solution of (7.56). In particular, they are solutions of (7.56) with initial conditions $f_1(0) = -3$, $f_2(0) = 3$, $f_3(0) = 8$. The solutions $\tilde{a}_i(z)$ are symmetric and display the asymptotic behavior (7.54). In general, there are infinite solutions of this form.

therefore violate $f(\pm z_0) < \infty$. This result is supported by our numerical analysis, and confirms our expectation that there is a unique symmetric solution of the ODE (7.53) with asymptotic behavior (7.54) when $\alpha = 2$: the spectrum of a massless scalar field is sufficient to reconstruct the wormhole geometry.

For $\alpha > 2$ (massive, non-tachyonic bulk scalar field, $m^2 > 0$), our numerical analysis suggests that, in general, there are infinitely many solutions to the system (7.56). For example, consider the scale factor[78]

$$\tilde{a}(z) = \frac{1}{z_0 + z} + \frac{1}{z_0 - z} + \cos\left(\frac{2\pi z}{z_0}\right) + \exp\left[-\frac{1}{(z_0^2 - z^2)}\right], \tag{7.57}$$

from which we can easily compute the corresponding potential $V(z)$. However, the system (7.56) then has multiple solutions, only one of which corresponds to the scale factor $\tilde{a}(z)$ which we started with (see Figure 7.1). Without additional information it is not possible to pick out the correct scale factor over the other valid solutions, $\tilde{a}_1, \tilde{a}_2$, etc. Therefore, the solution of the ODE (7.53) is not uniquely determined by symmetry and by the asymptotic behavior (7.54). We can conclude that, for $m^2 > 0$ and without further assumptions on the properties of the scale factor, we cannot reconstruct the wormhole geometry from a single potential $V(z)$, i.e. from a single scalar field spectrum.

Finally, for $\alpha < 2$ (tachyonic bulk scalar field, $m^2 < 0$), our numerical analysis suggests that there is no solution of (7.56). Although we have no mathematical proof for the non-existence of a solution of the problem (7.56), the numerical evidence and the fact that multiple solutions of the ODE (7.53) exist for any $\alpha > 2$ but a unique solution exists for $\alpha = 2$ points towards the existence of a unique symmetric solution of the ODE (7.53) with the correct asymptotics (7.54) when $\alpha < 2$. Therefore, we expect that the spectrum of a single tachyonic scalar field is sufficient to reconstruct the wormhole geometry.

From the discussion above we can conclude that, without making additional assumptions about

[78] Note that this form of the scale factor has no particular physical meaning. We included the last term to emphasize that the presence of non-perturbative contributions (at $z = \pm z_0$) does not prevent the existence of multiple solutions. The same result was obtained for several different forms of the scale factor.

the sign of m^2 or the analyticity of the scale factor, it is not possible to reconstruct the wormhole geometry from a single scalar spectrum. In particular, although for $m^2 \leq 0$ one spectrum is sufficient to reconstruct the scale factor, for $m^2 > 0$ additional data is required to perform the task.

Taking a different route, we will now show that if we have access to two scalar field spectra for two non-interacting bulk scalar fields of different mass (for any sign of m^2), the wormhole geometry can be uniquely reconstructed. Note that two spectra are always sufficient to reconstruct the scale factor, but the discussion in the previous paragraphs suggests that they might not be necessary.

Reconstructing the wormhole from two scalar spectra

Let us now assume that we have access to two distinct mass spectra of scalar particles in the dual confining gauge theory, corresponding to two non-interacting scalar fields with different masses in the same wormhole geometry. Suppose that, given the knowledge of the two spectra, we reconstructed the two associated potentials $V_1(z)$ and $V_2(z)$ using the procedure described in the previous subsections. We can then evaluate the ODE (7.53) for the two potentials at $z = 0$, and take their difference. Since $\tilde{a}(z)$ is the same in both equations, and we can obtain the values of α_1, α_2 from the asymptotic spectra, this yields an initial condition for the scale factor at the centre of the wormhole:

$$\tilde{a}(0) = \tilde{a}_0 \equiv \sqrt{\left| \frac{V_1(0) - V_2(0)}{\alpha_1 - \alpha_2} \right|}. \tag{7.58}$$

We can now solve the ODE (7.53) for any of the two potentials imposing initial conditions at the centre of the wormhole: $\tilde{a}(0) = \tilde{a}_0$, $\tilde{a}'(0) = 0$. This uniquely determines the wormhole scale factor.

It is worth noting that this procedure holds for any form of the scale factor (even in the non-physical case where it is not positive everywhere) and for both signs of m^2. Moreover, since in generic settings we expect to have multiple scalar fields in the wormhole geometry [217, 223], it is reasonable, and in fact to be expected, that we can have access to multiple spectra of scalar particles in the dual confining gauge theory.

7.3.4 Wormhole reconstruction algorithm

Let us summarize the algorithm that allows us to reconstruct the wormhole geometry from two scalar mass spectra in the underlying microscopic theory.[79] These spectra may be given as input data, or they may be obtained from a knowledge of the microscopic correlators, as explained in Section 7.3.1. We will assume that the spectra are of the asymptotic form $\lambda_j \sim Zj^2 + Aj + B\log j + C$, with $Z, A > 0$ and B, C arbitrary. As we have seen, this is a necessary condition for a microscopic spectrum to have a dual description in terms of a free scalar field in a wormhole background. The reconstruction algorithm is as follows:

1. Start with the first spectrum; call it λ_j. Fit the asymptotic values of λ_j to the curve $Zj^2 + Aj + B\log j + C$ and determine the constants Z, A, B, C.
2. Using (7.38)-(7.41) determine z_0, α, β, c, and from (7.32) construct $\tilde{V}(z)$.
3. Choose an integer $j_{\max} > 0$. The wormhole scale factor will be accurately reconstructed on scales larger than $z_0/j_{\max}$.

[79] As discussed above, if we have access to a spectrum associated with a bulk scalar field with $m^2 \leq 0$, there is no need for a second spectrum. We can therefore skip step 10, and solve the ODE (7.53) imposing that the scale factor is symmetric and has the correct asymptotics (7.54).

4. Compute the lowest $j_{\max}+1$ eigenvalues $\tilde{\lambda}_0, \tilde{\lambda}_1, \ldots, \tilde{\lambda}_{j_{\max}}$ by solving the Schrödinger equation

$$-u''(z) + \tilde{V}(z)u(z) = \tilde{\lambda}_j u(z), \tag{7.59}$$

subject to normalizable boundary conditions, $u^{(-)}(\pm z_0) = 0$. We are using $u^{(+)}$ and $u^{(-)}$ to denote the normalizable and non-normalizable components to mode functions; see (7.27).

5. Define $\bar{\Delta} \equiv \sqrt{\alpha + 1/4}$. For $0 \leq j \leq j_{\max}$ compute $\tilde{u}_j(z)$ by solving

$$\tilde{u}_j''(z) = \left[\tilde{V}(z) - \lambda_j\right]\tilde{u}_j(z), \tag{7.60}$$

subject to the initial conditions

$$\tilde{u}_j^{(+)}(-z_0) = \frac{1}{2\bar{\Delta}}, \tag{7.61}$$

$$\tilde{u}_j^{(-)}(-z_0) = 0. \tag{7.62}$$

6. For $0 \leq j \leq j_{\max}$, obtain $\omega'(\lambda_j)$ from (7.52).

7. For $0 \leq j \leq j_{\max}$, define $\tilde{y}_j(z) \equiv 2\frac{\tilde{u}_j(-z) - (-1)^j \tilde{u}_j(z)}{\omega'(\lambda_j)}$.

8. Determine $u_0, u_1, \ldots, u_{j_{\max}}$ by solving the system of equations

$$u_j''(z) = \left(\tilde{V}(z) + \sum_{i=0}^{j_{\max}} \left[\tilde{y}_i(z)u_i(z)\right]' - \lambda_j\right) u_j(z) \tag{7.63}$$

subject to the boundary conditions

$$u_j^{+}(-z_0) = \frac{1}{2\bar{\Delta}}, \tag{7.64}$$

$$u_j^{-}(-z_0) = 0. \tag{7.65}$$

9. Obtain the potential by setting

$$V(z) = \tilde{V}(z) + \frac{1}{2}\sum_{j=0}^{j_{\max}} \Big(\left[\tilde{y}_j(z)u_j(z)\right]' + \left[\tilde{y}_j(-z)u_j(-z)\right]'\Big). \tag{7.66}$$

Here we have ensured by hand that the reconstructed $V(z)$ is symmetric, since this is not automatically true for finite $j_{\max}$.[80]

10. Repeat steps 1-9 to reconstruct the potential associated with the second spectrum. Now we have reconstructed two potentials, $V_1(z)$ and $V_2(z)$, from the respective asymptotic spectra. The value of the scale factor at the centre of the wormhole is then given by

$$\tilde{a}(0) = \tilde{a}_0 \equiv \sqrt{\left|\frac{V_1(0) - V_2(0)}{\alpha_1 - \alpha_2}\right|} \tag{7.67}$$

where $\tilde{a}(z) = a(z)/L$.

[80] We would like the approximate potential to be symmetric so that the resulting scale factor in the wormhole picture is symmetric and thus the analytically continued scale factor in the cosmology picture is real.

11. Compute the wormhole scale factor by solving

$$\begin{cases} \tilde{a}''(z) + (\alpha - 2)\tilde{a}^3(z) - V(z)\tilde{a}(z) = 0 \\ \tilde{a}(0) = \tilde{a}_0 \\ \tilde{a}'(0) = 0 \end{cases} \tag{7.68}$$

12. Finally, if one is interested in the corresponding FRW scale factor, it can be obtained by analytic continuation. Numerically this can be approximated by flipping the sign of every other non-zero term in the Taylor expansion of $\tilde{a}(z)$ around $z = 0$. Namely,

$$\tilde{a}_{\mathrm{FRW}}(t) \approx \sum_n \frac{(-1)^{n/2}}{n!} \frac{d^{2n}\tilde{a}(z)}{dz^{2n}}\Big|_{z=0} t^{2n}. \tag{7.69}$$

7.3.5 Numerical example of wormhole reconstruction

In this subsection we provide an explicit example of implementation of the reconstruction algorithm summarized in Section 7.3.4. The scale factor we wish to reconstruct has the analytic form

$$\tilde{a}(z) = \frac{1}{z_0 + z} + \frac{1}{z_0 - z} + 2\cos\left(\frac{2\pi z}{z_0}\right) \tag{7.70}$$

where we set $z_0 = 1$. This scale factor does not have any specific physical meaning, and in particular it does not analytically continue to a Big Bang-Big Crunch cosmological scale factor. However, it is simple enough for the reconstruction to not be computationally too expensive, while its behavior is non-trivial enough to make the reconstruction example significant.

As a first step, we need to compute the asymptotic spectra of two potentials $V_1(z)$ and $V_2(z)$ of the form

$$V(z) = \frac{a''(z)}{a(z)} + m^2 L^2 a^2(z) \tag{7.71}$$

for two different choices of mL, and the first few eigenvalues of the same potentials, i.e. $\lambda_j^{(1)}$, $\lambda_j^{(2)}$ for $j < j_{max}$. This data will serve as input for the reconstruction procedure. Our choices of masses is $m_1 L = 1/2$, $m_2 L = 3/2$, and we choose $j_{\max} = 50$, i.e. we reconstruct the potentials from their first 51 eigenvalues. The first step in our algorithm is to fit the asymptotic spectra as in equation (7.33) (see Figure 7.2). Using equations (7.38), (7.39), (7.40) and (7.41), this yields $z_0 = 1$ for both spectra and the parameters of the test potentials (7.32):

$$\begin{aligned} &\alpha_1 = 2.250097, \qquad \beta_1 = -3.737523, \qquad c_1 = 33.996971; \\ &\alpha_2 = 4.249159, \qquad \beta_2 = 6.267183, \qquad c_2 = 21.274552. \end{aligned} \tag{7.72}$$

We can then compute the first 51 eigenvalues of the two test potentials defined as in (7.32), and apply the rest of the algorithm described in Section 7.3.4 to reconstruct the two potentials $V_1(z)$ and $V_2(z)$ from their spectra. Plots of the reconstructed potentials, together with the respective test potentials (7.32) and the exact potentials computed directly from the scale factor (7.70) are reported in Figure 7.3. The reconstructed potentials match the exact potentials up to corrections of order $1/j_{max} \sim 10^{-2}$, as expected.

We have now completed steps 1-9 of the reconstruction algorithm of Section 7.3.4 for two spectra, and reconstructed the two potentials $V_1(z)$ and $V_2(z)$ to good accuracy. The last two steps allow us to obtain the wormhole scale factor from such potentials. First, we must obtain the initial condition

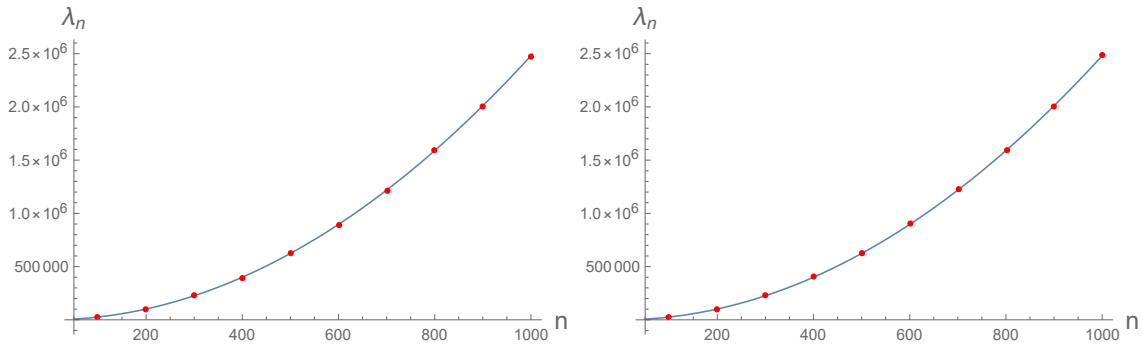

(a) (b)

Figure 7.2: Asymptotic spectra generated by the potentials (7.71) for $\tilde{a}(z)$ given by (7.70). The fitted data also include all eigenvalues with $j \in [80, 99]$ and $j \in [901, 999]$, omitted in the plots. (a) $mL = 1/2$. The result of the fit is $Z_1 = 2.467401$, $A_1 = 10.270160$, $B_1 = -3.737523$, $C_1 = 39.926397$. (b) $mL = 3/2$. The result of the fit is $Z_2 = 2.467401$, $A_2 = 12.934720$, $B_2 = 6.267183$, $C_2 = 36.382785$.

$\tilde{a}(0) = \tilde{a}_0$ as in equation (7.58). We could do this by directly subtracting $V_1^{\rm rec}(0)$ from $V_2^{\rm rec}(0)$, which would already allow us to obtain the initial condition to good accuracy, and obtain a good reconstruction of the wormhole scale factor. However, note that the reconstructed potentials have an oscillating behavior around $z = 0$, because we only used a finite amount of eigenvalues to perform the reconstruction (see Figure 7.3). Therefore, we can further improve the accuracy of the initial condition by averaging $V_1^{\rm rec}(z)$ and $V_2^{\rm rec}(z)$ over one oscillation period around $z = 0$, and then using such average values in place of $V_1^{\rm rec}(0)$, $V_2^{\rm rec}(0)$ in (7.58). Using this procedure and the values (7.72) of α_1 and α_2, we obtain $\tilde{a}_0 = 3.989952$, where the exact value is $\tilde{a}_0^{\rm true} = 4$ (note that the error is again of order $1/j_{\rm max}$, as expected). Finally, we can solve the ODE (7.53) for either $V_1(z)$ or $V_2(z)$ with initial conditions $\tilde{a}(0) = \tilde{a}_0$, $\tilde{a}'(0) = 0$, and obtain the wormhole scale factor. The numerically reconstructed $\tilde{a}_{\rm rec}(z)$ is reported in Figure 7.4 along with the exact scale factor (7.70). The two agree with very good accuracy, up to corrections of order $1/j_{\rm max}$.

7.3.6 Scale factor from heavy correlators

In the previous sections we have shown how to reconstruct the wormhole geometry given certain information about the dual confining gauge theory. In particular we found that the reconstruction is possible if we are given two sets of microscopic correlators, associated with 3D CFT scalar operators $\mathcal{O}_1$ and $\mathcal{O}_2$ of different scaling dimensions. The duals of these operators are scalar fields of different masses living in the wormhole geometry. So far we have not assumed anything about the masses of these scalar fields, i.e. we have made no restrictions on the dimensions of the microscopic operators.

However, we will now see that the situation is much simpler if we have access to the two-point correlator of a heavy operator $\mathcal{O}$, i.e. an operator with a large scaling dimension. Namely we will find that a knowledge of this correlator is sufficient to reconstruct the wormhole geometry; there is no need for additional information from a different operator.

The key observation which allows for such a simplification is to note that for a scalar field of large mass m the spatial two-point function in the wormhole is given approximately by

$$\langle \phi(x)\phi(y)\rangle \sim e^{-mL(x,y)}, \tag{7.73}$$

where L is the geodesic distance between x and y. Via the extrapolate dictionary, this leads to a

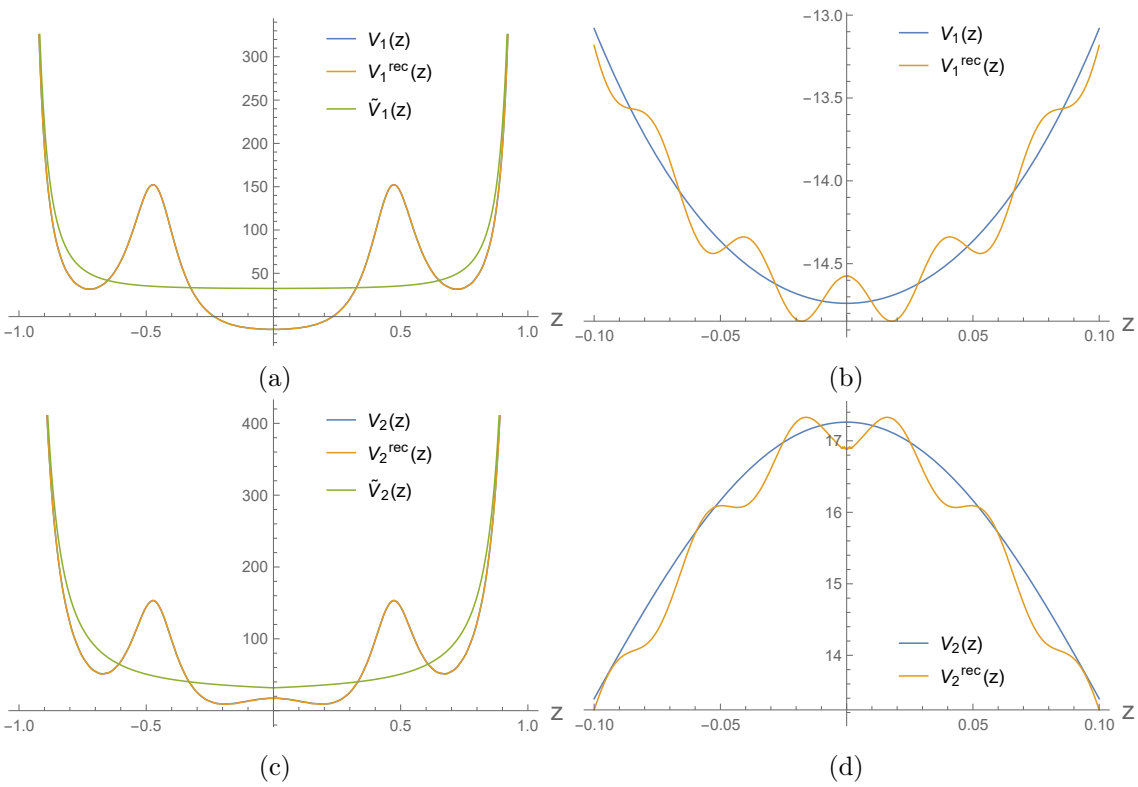

Figure 7.3: True potentials $V_i(z)$ (computed by equation (7.71) with $\tilde{a}(z)$ given by (7.70)), reconstructed potentials $V_i^{\text{rec}}(z)$, and test potentials $\tilde{V}_i(z)$ (given by equation (7.32) with parameters (7.72)) as a function of z. (a) $V_1(z)$, $V_2^{\text{rec}}(z)$, and $\tilde{V}_1(z)$ for $mL = 1/2$. (b) Detail of $V_1(z)$ and $V_1^{rec}(z)$ around $z = 0$ for $mL = 1/2$. As expected, the reconstructed potential is a good approximation to the true potential up to corrections of order $1/j_{\max} \sim 10^{-2}$. (c) $V_2(z)$, $V_2^{\text{rec}}(z)$, and $\tilde{V}_2(z)$ for $mL = 3/2$. (d) Detail of $V_2(z)$ and $V_2^{rec}(z)$ around $z = 0$ for $mL = 3/2$. As expected, the reconstructed potential is a good approximation to the true potential up to corrections of order $1/j_{\max} \sim 10^{-2}$.

spatial two-point function

$$\langle \mathcal{O}(w)\mathcal{O}(0)\rangle \sim e^{-mL(w)} \tag{7.74}$$

for the heavy operator $\mathcal{O}$ dual to the field ϕ, where L is the regulated length of the geodesic. See [215] for a review. Since geodesics are manifestly associated with the geometry of the spacetime, it seems plausible that a knowledge of various geodesic lengths via the correlators of $\mathcal{O}$ is enough information to explicitly reconstruct the wormhole. We will now show that this is indeed the case. The discussion is similar to [224] though our final approach is somewhat different and we get a more explicit result.

Let us begin by expressing the wormhole metric in the form

$$ds^2 = A^2(z)dz^2 + B^2(z)dx_\mu dx^\mu. \tag{7.75}$$

This can be mapped to the familiar conformally flat gauge by changing to a coordinate $\tilde{z}$ defined by $Adz = Bd\tilde{z}$. Letting x be one of the spatial coordinates of the field theory, we have that spatial

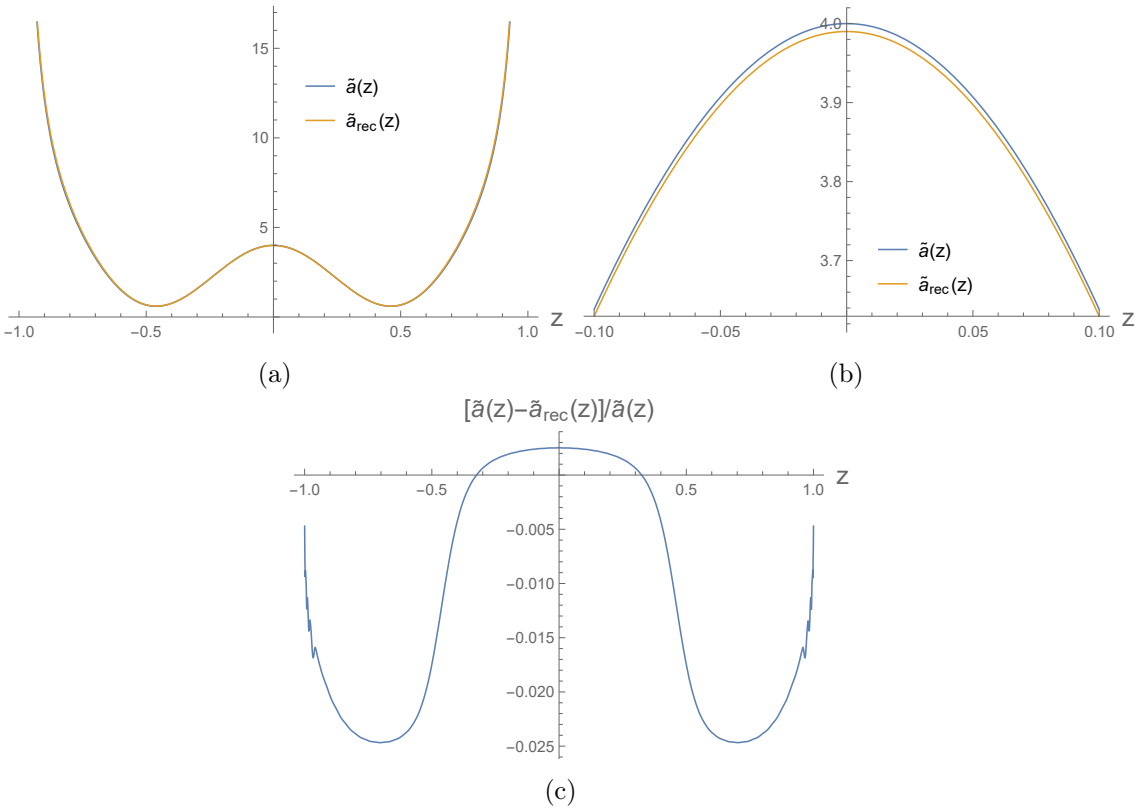

Figure 7.4: True scale factor $\tilde{a}(z)$ (given by equation (7.70)) and reconstructed scale factor $\tilde{a}_{rec}(z)$ as a function of z. (a) The scale factors are almost indistinguishable at large scales. (b) Detail around the centre of the wormhole at $z = 0$. (c) Discrepancy between the true scale factor and the reconstructed scale factor, quantified by $[\tilde{a}(z) - \tilde{a}_{rec}(z)]/\tilde{a}(z)$. As expected, the reconstruction is accurate up to corrections of order $1/j_{max} \sim 10^{-2}$.

geodesics $z(x)$ lying in the $z - x$ plane are determined by extremizing the action

$$S = \int dz \sqrt{A^2(z) + B^2(z) \left(\frac{dx}{dz}\right)^2} \,. \tag{7.76}$$

The conserved quantity associated with translation invariance in the x direction is

$$p_x = \frac{\partial \mathcal{L}}{\partial x'} = \frac{B^2(z)}{\sqrt{A^2(z) \left(\frac{dz}{dx}\right)^2 + B^2(z)}}. \tag{7.77}$$

While the action itself (giving the length of a geodesic) diverges, the variation of the action with respect to one of the endpoints is finite. We recall that the variation of the action about an on shell configuration with respect to an endpoint variation δx_i in the direction x_i can be expressed as

$$\delta S = p_i \delta x_i \,. \tag{7.78}$$

Taking x_i to be the direction x we find

$$\frac{\delta S}{\delta x} = p_x. \tag{7.79}$$

For geodesics with two endpoints at the same asymptotic boundary separated by w, there will be some deepest point $z_*(w)$ to which the geodesic penetrates. At this point, $dz/dx = 0$, so from (7.77) we have that $p_x = B(z_*)$. Thus, we have the relation

$$B(z_*) = \frac{\delta S}{\delta x} \equiv S_1(w). \tag{7.80}$$

The right side here can be computed from CFT data. Namely, the regulated version of the geodesic length S is given by $L(w)$ and so using the heavy correlator (7.74) we obtain

$$S_1(w) = -\frac{1}{m}\frac{d}{dw}\ln\langle \mathcal{O}(w)\mathcal{O}(0)\rangle. \tag{7.81}$$

Now, using $p_x = B(z_*)$ and (7.77) gives us an equation for dx/dz which can be integrated along half the geodesic curve to obtain another relation between w and z_*. Namely

$$w/2 = \int_{z_\infty}^{z_*} dz \frac{A(z)}{B^2(z)} \frac{1}{\sqrt{\frac{1}{B^2(z_*)} - \frac{1}{B^2(z)}}}, \tag{7.82}$$

where z_∞ is the asymptotic value of the coordinate z.[81] By a choice of gauge, we can take $B(z)$ to be any convenient function. In this case, the CFT data $S_1(w)$ and the known function $B(z)$ can be used in equation (7.80) to write w on the left side of (7.82) as some function of z_*. The equation (7.82) can then be understood as an integral equation (specifically, a weakly singular Volterra equation of the first kind) for the remaining undetermined metric function $A(z)$.

The integral equation

$$f(s) = \int_a^s \frac{y(t)dt}{\sqrt{g(s) - g(t)}} \tag{7.83}$$

for $y(t)$ has solution

$$y(s) = \frac{1}{\pi}\frac{d}{ds}\left[\int_a^s dt \frac{f(t)g'(t)}{\sqrt{g(s) - g(t)}}\right]. \tag{7.84}$$

Applying this to our case, we have that

$$A(z) = -\frac{1}{\pi}B^2(z)\frac{d}{dz}\left[\int_{z_\infty}^{z} d\hat{z} \frac{w(\hat{z})B(z)B'(\hat{z})}{B^2(\hat{z})\sqrt{B^2(\hat{z}) - B^2(z)}}\right] \tag{7.85}$$

Via this equation and (7.80), we are able to fully determine the metric in terms of the heavy microscopic two-point function.

We can make things more explicit by choosing the function $B(z)$ to be equal to $S_1(z)$. In this case, from (7.80) we have

$$S_1(z_*) = S_1(w), \tag{7.86}$$

so we have $z_* = w$. Thus, our choice of B corresponds to taking the z coordinate of a point in the wormhole to be the width of a CFT interval whose geodesic penetrates to that point. Then, from (7.85) we have

$$A(w) = -\frac{1}{\pi}S_1^2(w)\frac{d}{dw}\left[\int_0^w d\hat{w} \frac{\hat{w}S_1(w)S_1'(\hat{w})}{S_1^2(\hat{w})\sqrt{S_1^2(\hat{w}) - S_1^2(w)}}\right], \tag{7.87}$$

[81] This assumes that z increases toward the interior. Otherwise the limits of integration would be reversed.

and the metric is given by

$$ds^2 = A^2(w)dw^2 + S_1^2(w)dx_\mu dx^\mu. \tag{7.88}$$

In this way, we have explicitly expressed the metric in terms of the microscopic data encoded in the function $S_1(w)$ via equation (7.81).

The form (7.88) of the reconstructed metric suggests the change of variables

$$\mu(w) = -\frac{1}{\pi}\left[\int_0^w d\hat{w}\frac{\hat{w}S_1(w)S_1'(\hat{w})}{S_1^2(\hat{w})\sqrt{S_1^2(\hat{w}) - S_1^2(w)}}\right] . \tag{7.89}$$

In terms of this radial coordinate, we have simply

$$ds^2 = S_1^4(w(\mu))d\mu^2 + S_1^2(w(\mu))dx_\mu dx^\mu. \tag{7.90}$$

7.3.7 Metric from entanglement entropy

Via a very similar analysis, we could also extract the metric from the entanglement entropy for a strip-shaped subsystem of one of the 3D CFTs.[82]

We consider the entanglement entropy of a strip of width w in one of the 3D CFTs. We assume that the result is well approximated by the area of a RT surface in the dual 4D traversable wormhole.[83]

The entanglement entropy has the usual UV divergence but also an IR divergence due to the infinite volume of the strip. We consider the quantity

$$s_1(w) = \frac{d}{dw}s(w) \tag{7.91}$$

where $s(w)$ is the entanglement entropy per unit of length of the strip. In this case, it will be convenient to take the metric as

$$ds^2 = \frac{A^2(z)}{B(z)}dz^2 + B(z)dx_\mu dx^\mu \ , \tag{7.92}$$

where A and B are in general different than the similarly named functions in Section 7.3.6. With this choice, the expression for the action determining the extremal surface trajectory is precisely the same as the expression (7.76) that we used in the previous section. Precisely the same analysis then tells us that if we choose $B(z) = s_1(z)$, such that z is identified with w (i.e. the width of a strip whose RT surface barely reaches our point z^*), then the remaining metric function is

$$A(w) = -\frac{1}{\pi}s_1^2(w)\frac{d}{dw}\left[\int_0^w d\hat{w}\frac{\hat{w}s_1(w)s_1'(\hat{w})}{s_1^2(\hat{w})\sqrt{s_1^2(\hat{w}) - s_1^2(w)}}\right] . \tag{7.93}$$

However, differently from Section 7.3.6, the final metric is

$$ds^2 = \frac{A^2(w)}{s_1(w)}dw^2 + s_1(w)dx_\mu dx^\mu. \tag{7.94}$$

In this case, a change of variables analogous to (7.89) with $S_1 \to s_1$ gives

$$ds^2 = s_1^3(w(\mu))d\mu^2 + s_1(w(\mu))dx_\mu dx^\mu. \tag{7.95}$$

[82] To be precise, we should also include some part of the 4D CFT here, but since this has many fewer local degrees of freedom, we expect that the precise choice if this region shouldn't matter too much.

[83] This expectation could be modified significantly if the volume of the internal space present in the UV-complete realization of our setup changes with radial position.

7.4 Discussion

In this chapter we have investigated the relationship between observables in a bulk theory with an AdS planar eternal traversable wormhole background geometry and observables in the corresponding dual confining microscopic theory. We have studied what properties of the microscopic theory can be deduced from the existence of a bulk dual wormhole, and, conversely, how the wormhole geometry can be reconstructed from observables in the microscopic theory.

The presence of the wormhole determines specific properties of the dual microscopic theory: spectrum of massive particles, existence of a massless sector (see [3] for details), properties of two-point functions, and entanglement structure. In particular, the behavior of bulk quantum scalar fields implies the existence of a discrete spectrum of massive scalar particles.

On the other hand, certain observables in the microscopic confining theory (two-point functions of two 3D CFT scalar operators with different scaling dimensions, correlators of 3D CFT operators with large scaling dimensions, and entanglement entropies of subregions of the microscopic theory) allow one to reconstruct the dual wormhole geometry. A central result of the chapter is the explicit algorithm we derived to reconstruct the wormhole metric from two-point functions of 3D CFT scalar operators.

Recall that our motivation for studying the wormhole geometries discussed in this chapter was their relationship, via a double analytic continuation, to big-bang / big-crunch cosmologies. Therefore an important consequence of our findings in this chapter is that the FRW metric can be obtained from microscopic confining gauge theory observables by reconstructing the wormhole geometry, and then analytically continuing the resulting scale factor.

On the other hand if we do not make use of the duality presented by the analytic continuation (which we call the "slicing duality" in Chapter 5), the FRW Universe is encoded in a very complex way into the physics of a specific highly excited state of only the microscopic 4D auxiliary degrees of freedom coupling the two 3D CFTs. In fact, in a doubly holographic setup, where the auxiliary degrees of freedom are also holographic, the cosmology can be understood as living on an end-of-the-world (ETW) brane behind the horizon of a 5D black hole [102, 152]. As we discussed in Chapter 5, in this viewpoint the cosmology can be seen as an "entanglement island" associated with large subregions of the 4D auxiliary system. In both interpretations, reconstructing the cosmological evolution using observables in the excited state of the 4D auxiliary system requires computing expectation values of extremely complicated field theory operators[84]. Nonetheless, by means of the slicing duality the cosmological evolution can be probed by reconstructing the corresponding wormhole geometry using confining field theory observables as simple as the spectrum of massive particles or two-point functions of operators with large scaling dimension, and then analytically continuing the scale factor. This fact shows explicitly how the slicing duality allows one to relatively easily reconstruct holographic cosmologies which would naively be extremely complex to probe.

[84] It has been shown in [102] that the entanglement entropy at early times of sufficiently large subregions of the boundary field theory can probe the cosmological scale factor. In fact, the RT surface associated with such subregions penetrates the black hole horizon and ends on the ETW brane, in analogy with the analysis of Hartman and Maldacena [225].

Chapter 8

Towards realistic cosmologies

We have analyzed the analytic connection between a large class of $\Lambda < 0$ big-bang / big crunch cosmologies and asymptotically AdS wormholes. This connection enables a possible holographic realization of cosmology. One of the features of this construction, discussed qualitatively in Chapter 5, is that these models generically have time-dependent scalar fields that could, despite the negative cosmological constant, give rise to cosmologies with a period of accelerated expansion. In this chapter we explore this possibility more quantitatively. We first demonstrate via explicit effective field theory examples that models with an asymptotically AdS Euclidean continuation can also exhibit a period of accelerated expansion without fine tuning. We then show that certain more tuned examples can give predictions arbitrarily close to a $(\Lambda > 0)$CDM model. Thus by construction we will prove that, at least at the level of the background (i.e. without consideration of fluctuations), our model is capable of describing realistic cosmologies.[85] Finally, we demonstrate via an explicit construction that the potentials of interest can arise from a superpotential, thus suggesting that these solutions may be compatible with an underlying supersymmetric theory.

8.1 Introduction

In this chapter, we consider the viability of models of cosmology based on gravitational effective theories associated to a dual CFT via the AdS/CFT correspondence. These EFTs have a negative extremum in their scalar potential (the negative cosmological constant, $\Lambda < 0$) with an associated stable AdS solution. But they also have cosmological solutions of FRW form, including flat big bang matter/radiation cosmologies. Naively, these would not be realistic because of the negative cosmological constant. However, we will argue via examples that in the solutions that are most likely to have a holographic description, there will generically be time-dependent scalar fields whose potential energy can give rise to an accelerating phase in the cosmology without significant fine-tuning. We will show further that the resulting scale factor evolution can match observations.

The initial motivation to study cosmological models based on EFTs with holographic duals is the goal of finding a complete quantum gravity description for *some* four-dimensional big bang cosmology, realistic or not. Since some solutions of these $\Lambda < 0$ effective theories have a known microscopic description via holography, it is plausible that holographic tools may play a role in coming up with a microscopic description of the cosmological solutions as well.

We have explored in earlier chapters the precise role that holography might play: cosmological solutions with $\Lambda < 0$ and some combination of matter and radiation are time-symmetric big-bang / big-crunch spacetimes whose analytic continuations are wormhole geometries with asymptotically AdS regions for Euclidean time $\tau \to \pm\infty$ (see [226] for an early study of accelerating cosmologies in similar setups). This suggests a picture where the Euclidean theory is defined holographically via a pair of 3D CFTs and observables in the cosmology are related by analytic continuation to observables in this Euclidean theory.

As we have discussed, the existence of dual CFTs associated to the asymptotically AdS regions

[85] Here by "realistic" we mean "in agreement with observations".

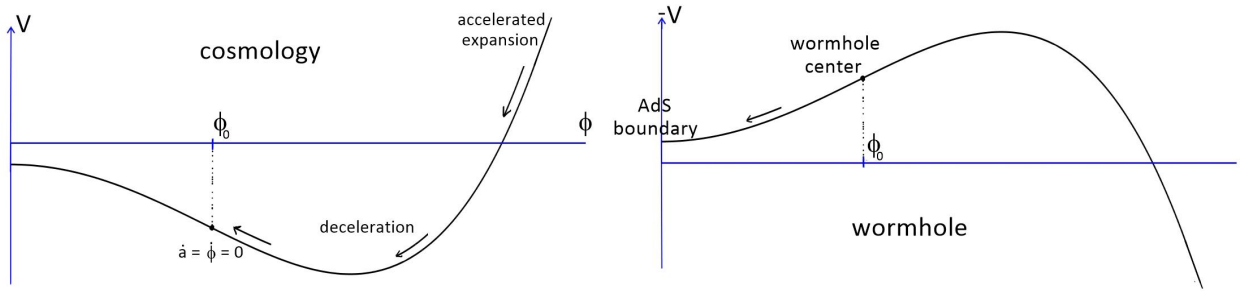

Figure 8.1: Evolution of the scalar field ϕ in a typical potential $V(\phi)$ in the cosmology and its Euclidean continuation.

in the Euclidean solution suggests that the solutions will often also have non-trivial scalar fields. Scalars with $m^2 < 0$ will be present in the effective field theory in the fairly generic situation that the CFTs have relevant scalar operators.[86] These scalar fields vanish at the asymptotically AdS boundary, but in the most generic asymptotically AdS solutions, the $m^2 < 0$ scalars turn on as we move away from the boundary. This is associated with RG flow in the dual CFT. The radial dependence of the scalar field in the wormhole translates to a time-dependence of the scalar field in the cosmology.

The main goal of the present chapter is to show that these scalar fields can naturally give rise to an accelerating period in the cosmology, and that in some cases, the acceleration can be realistic, with the cosmological scale factor matching arbitrarily well with the scale factor of conventional models that provide a good fit to observational data.[87]

A typical potential for a scalar field associated with a relevant CFT operator is shown in Figure 8.1 (left). The negative m^2 gives the quadratic decrease in V for small ϕ, while the eventual increase is due to the interaction terms that would typically be present; for example, a higher-order polynomial potential should eventually be positive and growing if the EFT is stable.

In the Euclidean solution, the evolution of the scalar field from the middle of the wormhole to the AdS boundary corresponds to the damped motion of a particle in the potential $-V$ with damping constant $3a'/a \equiv 3(da/d\tau)/a$. In order for this extremum to be associated with a stable AdS solution, we must satisfy the Breitenlohner-Freedmann bound $V'' > -9/(4L^2_{\rm AdS})$, which turns out to correspond to the fact that the motion of the scalar field towards the extremum is overdamped. Thus, the simplest evolution of the scalar in the wormhole is a simple monotonic evolution from a lower value of the potential (i.e. a higher value of $-V$) at the middle to the higher extremal value at the boundaries, as shown in Figure 8.1 (right).

In the cosmology, the value of the scalar at the time-symmetric point is the same as the value of the scalar at the middle of the Euclidean wormhole. The evolution back towards the big bang or forwards towards the big crunch corresponds to the anti-damped motion of the scalar in the potential V, initially moving in the direction towards the positive part of the potential. In many cases, the scalar will reach the positive region of the potential before the scale factor goes to zero, so part of the cosmological evolution has positive dark energy.

As we have seen this opens up the possibility that some of these $\Lambda < 0$ models might exhibit an accelerating phase. To check this, we study various explicit examples in Section 8.2. We first verify that solutions based on the scalar evolution shown in Figure 8.1 can lead to periods of accelerated expansion in the cosmology without excessive fine-tuning. We find examples of simple potentials

[86] Recall that the scalar masses are related to operator dimensions by $m^2 L^2_{\rm AdS} = \Delta(\Delta - 3)$.

[87] See [227] for an early study of accelerating negative Λ cosmologies compatible with data.

that give rise to acceleration for generic values of their parameters, meaning in a codimension zero region of the parameter space.

Next, we check that by taking an appropriately chosen potential, we can find models with acceleration where the scale factor is arbitrarily close to ΛCDM or wCDM models for the past evolution. These models are finely tuned, but we include them as a demonstration that the framework can in principle give results consistent with observations. For realistic cosmology, we want to match observations, not ΛCDM, and this requirement allows a much broader class of potentials. We return to this point in the discussion.

If the effective field theory describing cosmology is related to some underlying CFT, an interesting possibility is that this CFT and the corresponding effective theory is supersymmetric,[88] and that this supersymmetry is broken in the cosmology by the time-dependent scalar field expectation value. The physics of such a model is surely very complicated. If the underlying effective theory is some gauged supergravity, the scalar expectation value would break gauge symmetry and supersymmetry, and the low energy effective field theory relevant to the cosmology would arise via RG flow in which various fields would become strongly coupled (as in QCD). We will not attempt to understand any of these things here, but ask instead a fairly naive question: can the scalar potentials giving rise to realistic time-symmetric cosmologies with asymptotically AdS Euclidean continuations arise from a superpotential in a supersymmetric effective field theory? In Section 8.3, we show that it is always possible to find a superpotential giving rise to a given scalar potential, and provide an explicit algorithm to construct such a superpotential.[89] We further show that an approximation of the superpotential is sufficient to accurately obtain the regions of the scalar potential relevant for the cosmological evolution.

The results of this chapter are explorations to see what is possible at the level of effective field theory; we have not attempted to investigate whether the detailed potentials giving rise to realistic cosmological backgrounds can arise from microscopic constructions in string theory. But the fact that $\Lambda < 0$ effective theories are not immediately ruled out suggests that cosmological models with asymptotically AdS continuations (and thus potential holographic descriptions) have a chance of being realistic. We discuss various directions for further investigation in Section 8.4.

8.2 Accelerating cosmologies from asymptotically AdS Euclidean geometries

Throughout this chapter, we will consider spatially flat cosmological solutions

$$ds^2 = -dt^2 + a(t)^2 d\vec{x}^2 \tag{8.1}$$

of $\Lambda < 0$ effective field theories. For simplicity, we will consider models with a single scalar field with potential $V(\phi)$. Allowing matter and radiation, the equations of motion are

$$\ddot{\phi} + 3H\dot{\phi} + \frac{dV}{d\phi} = 0\,, \qquad H^2 = \frac{8\pi G}{3}\left[\frac{1}{2}\dot{\phi}^2 + V(\phi) + \frac{\rho_R}{a^4} + \frac{\rho_M}{a^3}\right]\,, \tag{8.2}$$

where $H = \dot{a}/a$.

The solutions we are interested in are time-symmetric and arise via analytic continuation from real Euclidean solutions

$$ds^2 = d\tau^2 + a_E(\tau)^2 d\vec{x}^2 \tag{8.3}$$

[88] It has been conjectured that holographic CFTs with standard dual gravitational effective field theories must be supersymmetric [228], though this is not proven or widely accepted.

[89] To the best of our knowledge, no such algorithm appeared in the literature before.

For the Euclidean solution, the equations of motion are

$$\phi_E'' + 3H_E\phi_E' - \frac{dV}{d\phi_E} = 0\,, \qquad H_E^2 = \frac{8\pi G}{3}\left[\frac{1}{2}(\phi_E')^2 - V(\phi_E) - \frac{\rho_R}{a_E^4} - \frac{\rho_M}{a_E^3}\right]\,, \tag{8.4}$$

where $a_E(\tau) = a(i\tau)$, $\phi_E(\tau) = \phi(i\tau)$, and $H_E(\tau) = H(i\tau)$.

We would like to find potentials $V(\phi)$ and solutions $a(t), \phi(t)$ with the following properties.

- The scale factor evolution matches observational constraints, including a recent phase of accelerated expansion.
- The solution is time-reversal symmetric about a recollapse point.
- The analytic continuation of the solution (taking $t \to i\tau$ where $t = 0$ is the recollapse point) is asymptotically AdS for $\tau = \pm\infty$.
- The scalar field satisfies the Breitenlohner-Freedman (BF) bound $V'' > -9/(4L_{\rm AdS}^2)$ at the two asymptotic AdS boundaries in the Euclidean solution.

8.2.1 Constraints on the potential

There are a variety of constraints on the scalar potential V coming from these requirements.

First consider the solution in Lorentzian time, i.e. the "cosmology picture". In order to have a time-symmetric solution, $a(t)$ and $\phi(t)$ must be even functions (taking $t = 0$ to be the recollapse time, so that our present era corresponds to negative times) with $\dot{a}(0) = 0$ and $\dot{\phi}(0) = 0$. The Friedmann equation shows that the potential must be negative at this time-symmetric point, since $H = 0$ here and V must cancel the remaining (positive) sources of energy density.

The scalar evolution equation is that of a particle in a potential with damping $3H$ which is positive during the expanding phase. In order for the scalar field to have zero time derivative at the time-symmetric point, this particle must stop at $t = 0$, and this is only possible if it is ascending the potential just prior to $t = 0$. Thus, going forward from the present time, the scalar field must descend from positive to negative values of the potential and then rise and stop at some ϕ_0, passing through some minimum along the way.

In the Euclidean continuation, i.e. the "wormhole picture", the evolution equations are given in (8.4). Since $\ddot{a}(t = 0) < 0$, we have $a_E''(\tau = 0) > 0$. For a solution that is asymptotically AdS as $\tau \to \pm\infty$, a must behave as $e^{H_{\rm AdS}|\tau|}$ for large $|\tau|$, so the simplest possibility is that a is monotonically increasing from $\tau = 0$ towards each boundary. In this case, the evolution of ϕ towards the boundary is the same as the damped motion of a particle in potential $-V$. The scalar ϕ should approach a constant as $\tau \to \pm\infty$, so the inverted potential $-V$ should have a minimum here. Without loss of generality, we will take such a minimum to be located at $\phi = 0$.

Thus, the simplest possibility for the shape of the overall potential is that shown in Figure 8.1 with the evolution in the cosmology picture and the wormhole picture covering different regions of the potential as shown. We have argued in the introduction that this shape is natural for effective field theories associated with holographic CFTs.

A final constraint comes from requiring that the AdS solution that describes the two asymptotic regions is stable to scalar perturbations. This requires that the scalar field mass (the second derivative of the potential) satisfies the BF bound

$$\left.\frac{d^2V}{d\phi^2}\right|_{\phi=0} \geq \frac{9}{4}V(0), \tag{8.5}$$

where we chose units such that $8\pi G/3 = 1$, in which $V(0) = -1/L^2_{\rm AdS}$. The condition (8.5) also ensures that the scaling dimensions of the corresponding operator in the dual microscopic theory is real as required for a unitary quantum field theory.

This bound turns out to have a simple implication for the scalar evolution towards the extremum at $\phi = 0$. First notice that, in order to ensure the existence of the AdS asymptotic regions in the wormhole picture, the scalar potential energy term must be the dominant contribution on the right-hand side of the Euclidean Friedmann equation (8.4) as $\tau \to \pm\infty$. This implies $H(\tau) \to H_{\rm AdS} \equiv \sqrt{-V(0)}$ as $\tau \to \pm\infty$. By inspecting the scalar field evolution equation in (8.4) it is then immediate to conclude that the BF bound (8.5) is equivalent to the condition for the scalar field motion to be overdamped in the vicinity of the extremum of the potential at $\phi = 0$. Therefore, moving from the centre of the wormhole towards the asymptotic boundaries, the scalar field will simply evolve from $\phi = \phi_0$ to $\phi = 0$, settling at the minimum of the inverted potential $-V$ without any oscillation occurring in the asymptotic region.

To summarize, starting from the present value of the scalar potential, we require that it decreases to negative values and then increases to an extremum with a negative value, where the second derivative of the potential at the extremum satisfies equation (8.5).

In the presence of the constraints needed for the setup to admit a dual holographic description—i.e. the fact that the potential needs to be negative at the time-symmetric point, have a negative minimum between the positive region and the inversion point, and a negative maximum with a small second derivative corresponding to the AdS vacuum in the Euclidean picture—it is less clear whether a phase of accelerated expansion can be supported by the positive region of a potential. In fact, for generic potentials and generic initial conditions at the time-symmetric point, the scalar field might not reach the positive region of the potential during the cosmological evolution, or reach it but not in a slow-roll regime. For instance, our numerical analysis indicates that a simple quartic potential satisfying all the requirements imposed by holography cannot support a phase of accelerated expansion. In particular, an accelerating phase can be obtained only by significantly violating the BF bound at the negative maximum.

In the following we will therefore first show that, for a simple one-parameter family of exponential potentials satisfying all our constraints, a phase of accelerated expansion can be obtained for generic choices of initial conditions and of the potential's parameter. We will then show that choosing more complicated potentials and appropriately fine-tuning one of their parameters, it is possible to reproduce to arbitrary accuracy the scale factor evolution predicted by more standard cosmological models such as ΛCDM and wCDM.

8.2.2 Existence and genericity of an accelerating phase

Starting with a potential satisfying these constraints, we can look for solutions with the desired properties.

As initial conditions at the symmetric point $t = \tau = 0$, we can take[90]

$$\phi(0) = \phi_0, \qquad a(0) = 1, \tag{8.6}$$

with vanishing derivatives $\dot{a}(0) = a'(0) = \dot{\phi}(0) = \phi'(0) = 0$. The matter and radiation densities are constrained via the Friedmann equation at $t = 0$ as

$$\rho_R + \rho_M = -V(\phi_0)\ . \tag{8.7}$$

[90] In this convention, a will be less than one at the present time for examples applicable to realistic cosmology, but we can rescale $a(t) \to a(t)/a(t_0)$ to give the scale factor corresponding to the conventions of Sections 8.2.3 and 8.2.4.

In the approximation where radiation can be neglected (valid for most of the cosmological history and everywhere in the wormhole solution), the matter density is fixed by $V(\phi_0)$, so the solution is fully specified by ϕ_0, the scalar field value at $t = 0$.

We would first like to check that it is possible to have an accelerating phase of cosmology before the recollapse without significant fine-tuning of the potential. Evolving backward in time from the recollapse point in the cosmology picture, the scalar field evolution corresponds to antidamped motion in the potential V; it is natural that the scalar reaches positive values of the potential, however this does not immediately imply an accelerating phase. Such a phase further requires the positive scalar potential to dominate over all other sources of energy density. This does not always happen: it may be that the growth of matter density, radiation density, or scalar kinetic energy outpaces the increase in scalar potential as $a \to 0$ or that the scale factor decreases to zero (i.e. we reach the big bang) before the potential energy dominates. Thus, it is not true that we get an accelerating phase for all potentials of the type shown in Figure 8.1 and all initial conditions.

On the other hand, it is not difficult to find examples of potentials and initial conditions that do give rise to acceleration. Here we study a simple example of a potential that satisfies all of our criteria and exhibits acceleration over a significant fraction of the combined parameter space of potential parameters and the initial condition ϕ_0. For just this subsection, we restrict to a simplified model with only radiation and scalar field contributions to the stress tensor; we set the matter contribution to zero for the purposes of this demonstration.

We consider a potential that is even about the AdS extremum $\phi = 0$ with mass $m^2 = -9/4$ at the BF bound,

$$V(\phi) = -1 - \frac{9}{8}\phi^2 + V_{\text{int}}(\phi) \, . \tag{8.8}$$

In order to make the potential bounded from below and take positive values for larger ϕ, we include terms at higher-order in ϕ^2. We have found that simply adding a ϕ^4 term does not give solutions with an accelerating phase. Instead, we consider a one-parameter family of even interaction potentials

$$V_{\text{int}}(\phi) = e^{g\phi^2} - g\phi^2 - 1, \tag{8.9}$$

where the last two terms are subtracted off to give an interaction potential starting at order ϕ^4.

We consider solutions for various model parameters g and initial condition ϕ_0. These solutions are obtained by numerically integrating the coupled scalar and Friedmann equations starting from the turning point where $\phi = \phi_0$ and $H = \dot{\phi} = 0$. We set $\rho_M = 0$ and determine the value of ρ_R from $V(\phi_0)$ using (8.2). The system is numerically integrated back in time towards the big bang, then we numerically check if a given solution has a numerically detectable period of accelerated expansion.

In Figure 8.2, we show the space of parameters (g, ϕ_0) that leads to a period of accelerated expansion in the cosmology picture before the recollapse. We see that a significant region of the space where the parameters are of order 1 yields an accelerating phase. Thus, cosmological acceleration can be obtained without significant fine-tuning of the model or initial conditions.

We can also consider how the mass of the field affects the allowed parameter space. In Figure 8.3 we show the evolution of the parameter space exhibiting accelerated expansion as m^2 becomes less negative. We see that accelerated expansion becomes rapidly less generic as m^2 increases. Conversely, we have also observed that if m^2 is allowed to go below the BF bound, then a period of acceleration becomes more generic. Qualitatively, this is because the slope of the potential near the turning point (which in the present model is controlled mostly by the value of the mass) must be steep enough for the anti-damped scalar field to quickly gain kinetic energy as we evolve back towards the big bang (or forward towards the big crunch). This is necessary for the scalar field to reach the positive region of the potential before the scale factor vanishes.

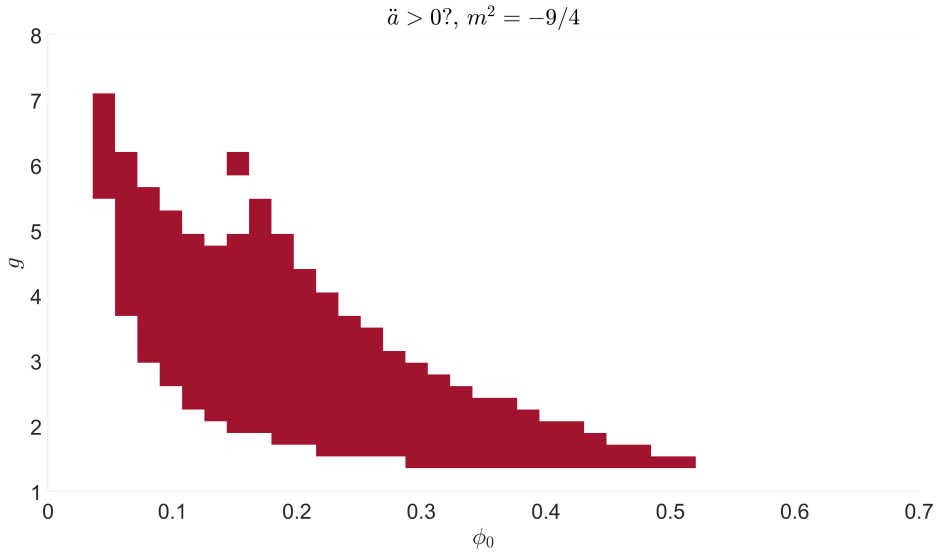

Figure 8.2: Space of model parameter g and initial condition ϕ_0 for the exponential potential of Eqs. (8.8) and (8.9). Solutions of the equations of motion (8.2) and (8.4) with parameter g and initial condition ϕ_0 contained in the red region exhibit an accelerating phase.

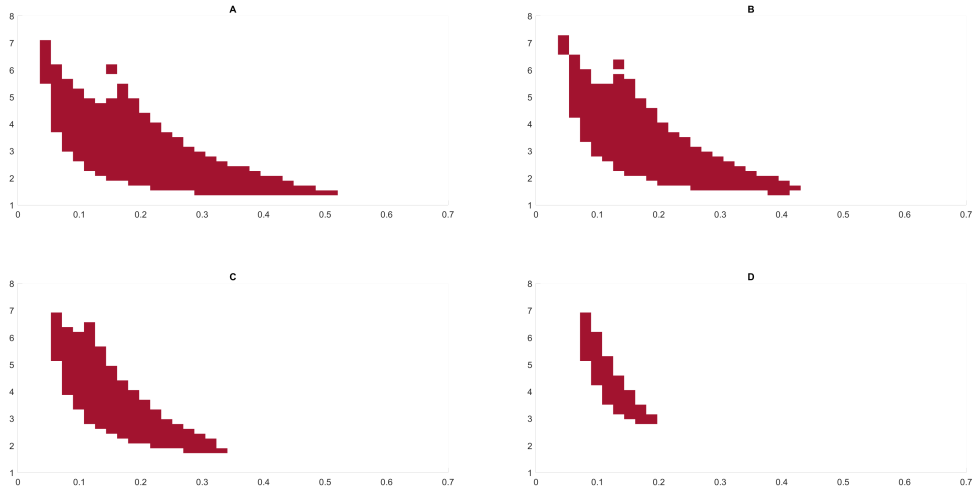

Figure 8.3: Panel (A) is the same as Figure 8.2 with $m^2 = -9/4$. Panels (B), (C), and (D) correspond to masses $m^2 = -8/4$, $m^2 = -7/4$, and $m^2 = -6/4$, respectively. Clearly it becomes much less generic to have a period of accelerated expansion as m^2 increases.

There is no particular physical significance to the form of the potential we have chosen; below, we will see that the exponentially increasing behaviour of the potential for large ϕ is not necessary to obtain acceleration.

8.2.3 An example matching flat ΛCDM

As a first example of a phenomenologically realistic cosmology based on the framework introduced in Chapter 5, we study potentials able to reproduce to good accuracy the standard ΛCDM model (with positive Λ). These are potentials satisfying all the properties outlined above and having a nearly flat positive region.

For our numerical analysis it is useful to work in units such that $8\pi G/3 = 1$ and to introduce rescaled variables

$$\tilde{t} = H_0 t, \qquad \Omega_i = \frac{\rho_i^{\text{now}}}{H_0^2}, \qquad \tilde{H} = \frac{H}{H_0}, \qquad \tilde{V}(\phi) = \frac{V(\phi)}{H_0^2}\ , \tag{8.10}$$

where ρ_i^{now} are the energy densities at the present time. The equations of motion then read

$$\ddot{\phi} + 3\tilde{H}\dot{\phi} + \frac{d\tilde{V}}{d\phi} = 0\,, \qquad \tilde{H}^2 = \frac{1}{2}\dot{\phi}^2 + \tilde{V}(\phi) + \frac{\Omega_R}{a^4} + \frac{\Omega_M}{a^3} \tag{8.11}$$

in the cosmology picture, and

$$\phi_E'' + 3\tilde{H}_E\phi_E' - \frac{d\tilde{V}}{d\phi_E} = 0\,, \qquad \tilde{H}_E^2 = \frac{1}{2}(\phi_E')^2 - \tilde{V}(\phi_E) - \frac{\Omega_R}{a_E^4} - \frac{\Omega_M}{a_E^3} \tag{8.12}$$

in the wormhole picture, where overdots and primes now represent derivatives with respect to rescaled time variables. With this choice, both the Lorentzian time $\tilde{t} = H_0 t$ and the Euclidean time $\tilde{\tau} = H_0\tau$ are measured in units of the Hubble time $1/H_0$. We also adopt the convention $a(\tilde{t}_0) = 1$ where $\tilde{t}_0 < 0$ is the present time. This implies that at the time-symmetric point the initial condition for the scale factor is $a(0) = a_0 > 1$. The $\tilde{t}/\tilde{\tau}$ derivatives of a and ϕ vanish at the symmetric point $\tilde{t} = \tilde{\tau} = 0$. Given a value for the density parameters Ω_R and Ω_M and a choice of a_0, the initial condition for the scalar field is determined by the Friedmann equation at $\tilde{t} = 0$:

$$\frac{\Omega_R}{a_0^4} + \frac{\Omega_M}{a_0^3} = -\tilde{V}(\phi_0)\ . \tag{8.13}$$

Let us now consider a five-parameter family of potentials given by

$$\tilde{V}(\phi) = \tilde{V}_0(\phi) + \tilde{V}_0(-\phi) - B, \tag{8.14}$$

where

$$\tilde{V}_0(\phi) = \frac{A-B}{2}\text{erf}\left(\frac{\phi - X}{\Delta}\right) + C\exp\left[-\left(\frac{\phi - X}{\Delta}\right)^2\right] + \frac{A+B}{2}, \tag{8.15}$$

and erf is the error function. An example of the potential (8.14) is plotted in Figure 8.4. The parameter $A > 0$ fixes the height of the plateau for large values of ϕ and determines the value of the positive vacuum energy driving the accelerated expansion in the cosmology picture, while $B < 0$ gives the value of the negative cosmological constant in the asymptotic AdS regions in the wormhole picture. The parameters $C < 0$, $X > 0$ and $\Delta > 0$ determine the depth, location, and width of the deep valleys present in the potential, respectively. In order to reproduce the ΛCDM model, the value of A must match the value of the positive vacuum energy observed in our Universe.

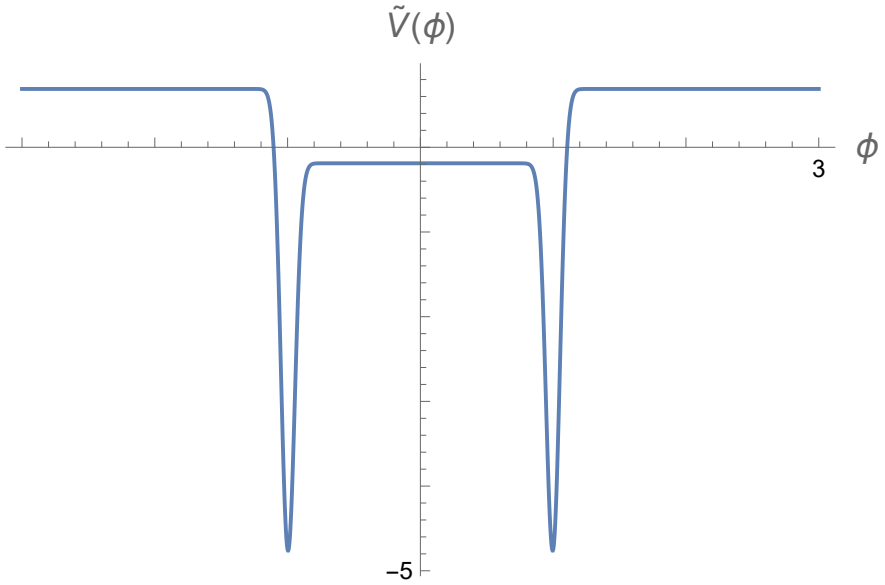

Figure 8.4: An example of the potential (8.14). A fixes the value of $\tilde{V} > 0$ at the positive plateau, B the value of $\tilde{V}(0)$, i.e. the negative cosmological constant in the asymptotically AdS regions of the wormhole solution. C, X, Δ determine the depth, location, and width of the deep valleys present in the potential.

We can then study solutions of the cosmology and wormhole equations of motion (8.11) and (8.12) with potential given by equations (8.14) and (8.15). We choose the values for the cosmological parameters obtained by the *Planck* 2018 collaboration using TT, TE, EE + lowE + lensing + BAO data [6]:

$$\Omega_R = 9.18 \times 10^{-5}, \qquad \Omega_M = 0.311, \qquad \Omega_\Lambda = 0.6889, \tag{8.16}$$

where Ω_Λ is the density parameter associated with the vacuum energy today. We further choose the initial condition $a_0 = 2$ for the scale factor at the time-symmetric point, while the scalar field initial condition ϕ_0 is determined by equation (8.13) once the five parameters of the potential are fixed.[91] In our numerical solutions depicted in Figures 8.5, 8.6, and 8.8, they are taken to be

$$A = 0.6889, \qquad B = -0.03, \qquad C = -5, \qquad X = 1, \qquad \Delta = 0.0726775778709, \tag{8.17}$$

yielding $\phi_0 = 0.817319$.

We point out that the present model is very finely tuned and, moreover, contains a relatively large number of free parameters (namely 7: the potential parameters in equation (8.17) plus the present day matter and radiation densities). However we remind the reader that the purpose of this section is simply to demonstrate that our framework is capable of giving results consistent with observations, in this case by directly matching ΛCDM. Ultimately however we want to match observations, not ΛCDM, and this requirement allows for a much broader class of potentials which are *not* finely tuned and which can contain fewer free parameters. We will comment on this in the discussion section of this chapter (see also [229]).

[91] We remind the reader that the initial conditions for the cosmology and wormhole pictures are the same. Note also that in general there are multiple solutions of equation (8.13). As we have explained above, we are interested in a solution such that ϕ_0 lies between a minimum and a maximum of the potential.

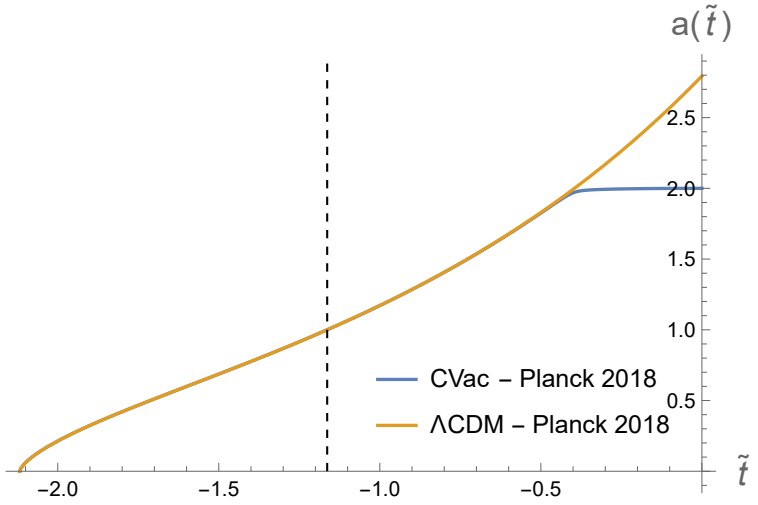

Figure 8.5: Scale factor evolution for the cosmological solution obtained using the *Planck* cosmological parameters (8.16) (denoted by "CVac"). The potential parameters are given in Equation (8.17). The scale factor for the corresponding ΛCDM solution is also depicted. The two scale factors are indistinguishable until the present day $\tilde{t} = \tilde{t}_0 = -1.16342$ (where $a(\tilde{t}_0) = 1$) — indicated by the black dashed line — and beyond. Deviations in our solution from the ΛCDM behaviour become evident at late times as the Universe approaches the turning point at $\tilde{t} = 0$. The contraction phase in our solution, not depicted here, can be obtained by time-reversal.

Cosmological solution

By an appropriate fine-tuning of the potential's parameters (see Appendix I.1) leading to the values (8.17), the cosmological evolution reproduces to very good accuracy the one predicted by the corresponding ΛCDM solution between the early Universe and the present day $\tilde{t} = \tilde{t}_0$, see Figure 8.5. For $\tilde{t} > \tilde{t}_0$, the potential energy eventually decreases and becomes negative as the scalar field rolls down the potential, while the kinetic energy K_ϕ increases. Finally, the scalar kinetic energy decreases and vanishes as we reach the time-symmetric point $\tilde{t} = 0$ (where we impose our initial conditions for both the cosmological and the wormhole solutions). See Figure 8.6.

As a consistency check, we verified that the luminosity distance

$$d_L(z) = \frac{1}{H_0 a(t)} \int_{\tilde{t}}^{\tilde{t}_0} \frac{dt'}{a(t')}\,, \qquad 1 + z = \frac{1}{a(t)}, \tag{8.18}$$

computed from our solution[92] agrees with the Pantheon+SH0ES type Ia supernova (SN Ia) data [8]. In particular, we found that the luminosity distance in our solution is indistinguishable from the one generated by the corresponding ΛCDM solution in the range of redshifts z covered by the SNIa data; see Figure 8.7. Therefore, our model fits the data as well as the ΛCDM model. Due to the well-known Hubble tension issue [230], this also implies that the solution obtained using the *Planck* 2018 parameters (8.16) is in tension with supernovae data. We also studied a solution generated using cosmological parameters obtained from supernovae observations [7], which clearly matches data much better. Whether specific realizations of our models could help solve the Hubble tension is an interesting open question that we plan to investigate in future work.

[92]For the solution obtained using the *Planck* cosmological parameters (8.16) we can use the value of H_0 measured by *Planck*, i.e. $H_0^{planck} = 67.66$ km s^{-1} Mpc^{-1}.

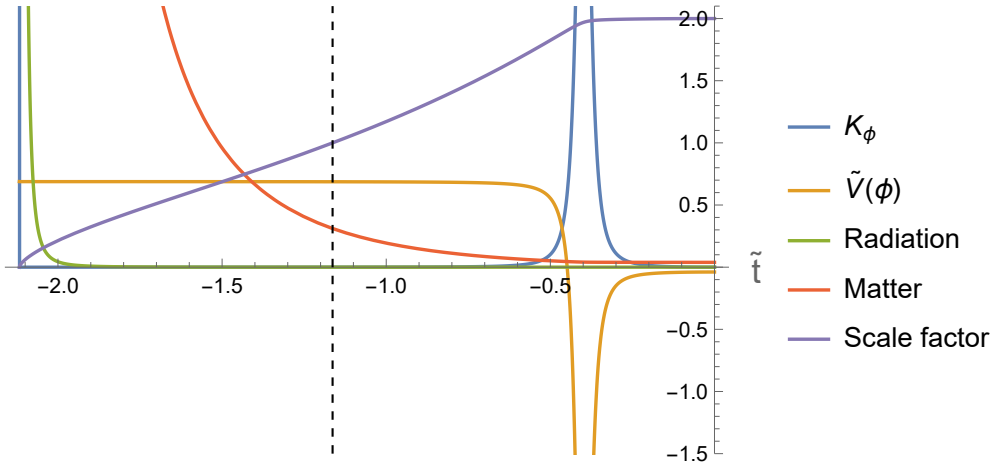

Figure 8.6: Scalar field kinetic (K_ϕ) and potential ($\tilde{V}$) energies, radiation contribution Ω_R/a^4, matter contribution Ω_M/a^3, and scale factor $a(\tilde{t})$ as a function of time $\tilde{t}$ for the expansion phase of our cosmological solution obtained using the *Planck* cosmological parameters (8.16). The potential parameters are given in Equation (8.17). The contraction phase can be obtained by time-reversal. The black dashed line indicates the present day $\tilde{t} = \tilde{t}_0 = -1.16342$ for which $a(\tilde{t}_0) = 1$. K_ϕ is negligible for most of the evolution until the present day. The Universe undergoes a radiation-dominated and a matter-dominated era before the current potential energy-dominated era. In the future, the potential energy will decrease and the kinetic energy increase and become dominant as the scalar field rolls down the potential. Finally, the kinetic energy vanishes as the Universe reaches its turning point at $\tilde{t} = 0$, where initial conditions for our numerical solutions are imposed.

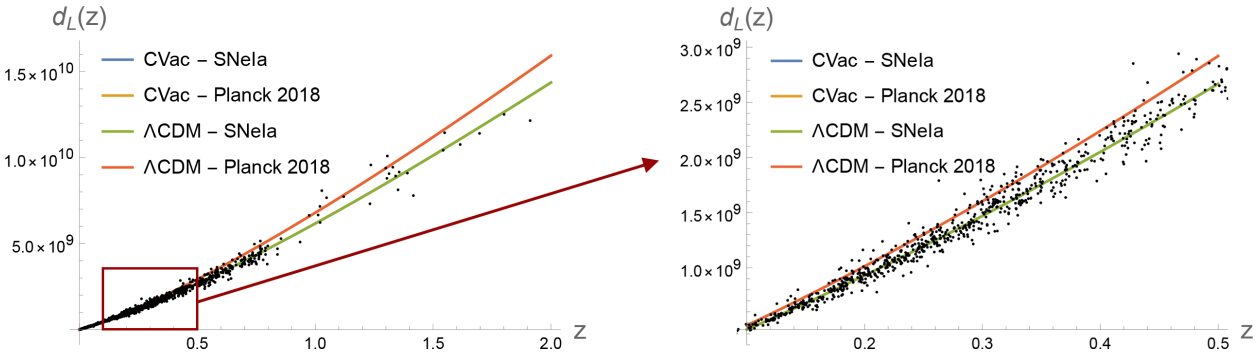

Figure 8.7: Luminosity distance $d_L(z)$ computed for two solutions involving rolling scalars (denoted by "CVac") and their corresponding ΛCDM solutions. For the *Planck* 2018 solution, the cosmological parameters are given in equation (8.16), the potential parameters in equation (8.17), and we used $H_0^{\text{Planck}} = 67.66$ km s^{-1} Mpc^{-1} [6]. For the SNeIa solution, the cosmological parameters are given by[93] $\Omega_R = 9.96 \times 10^{-5}$, $\Omega_M = 0.338$, $\Omega_\Lambda = 0.662$, $H_0^{\text{SN}} = 73.4$ km s^{-1} Mpc^{-1} [7], and the potential parameters are $A = 0.662$, $B = -0.03$, $C = -5$, $X = 1$, $\Delta = 0.0716914850735$; this yields $\phi_0 = 0.824448$. The Pantheon+SH0ES experimental data are also depicted [8]. Our cosmological solutions and their corresponding ΛCDM solutions are indistinguishable, meaning that our model matches supernovae data as well as the ΛCDM model. Notice that the solutions generated using *Planck* 2018 cosmological parameters are in tension with some of the other data, while the ones generated using cosmological parameters derived from supernovae observations agree with data: this is a manifestation of the Hubble tension.

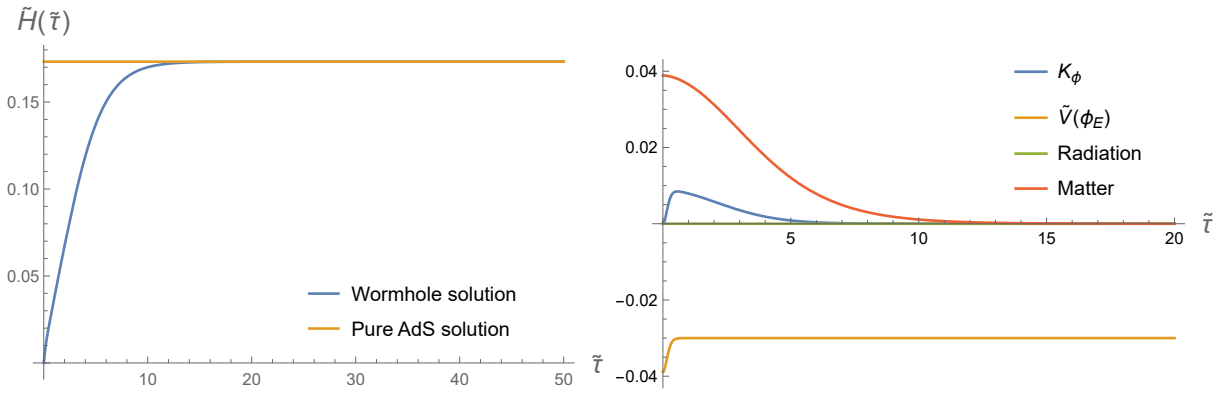

Figure 8.8: Wormhole solution from the centre of the wormhole towards the asymptotic boundary at $\tilde{\tau} = \infty$, obtained using the *Planck* cosmological parameters (8.16). The potential parameters are given in equation (8.17). The evolution from the centre of the wormhole towards the other asymptotic boundary at $\tilde{\tau} = -\infty$ is obtained by reflection symmetry around $\tilde{\tau} = 0$. (Left) Hubble parameter as a function of the coordinate $\tilde{\tau}$. The value of the Hubble parameter for the corresponding pure AdS solution $\tilde{H}_\infty = \sqrt{B}$ is also depicted. In the asymptotic region $\tilde{\tau} \to \infty$ the wormhole solution approaches pure AdS. (Right) Scalar field kinetic and potential energies, radiation contribution Ω_R/a_E^4, and matter contribution Ω_M/a_E^3 as a function of the coordinate $\tilde{\tau}$ along the wormhole direction. As we move towards the AdS asymptotic boundary (i.e. as we increase $\tilde{\tau}$), the overdamped scalar field approaches its value $\phi_E = 0$ at the AdS boundary and its kinetic energy vanishes. The radiation and matter contributions are suppressed as the scale factor increases, and in the asymptotic region the negative scalar potential energy $\tilde{V}(0)$ is dominant: the solution approaches an AdS vacuum solution.

Wormhole solution

First, we remark that the potential under consideration with the parameters (8.17) used in our numerical analysis satisfies the BF bound (8.5). As a result of the scalar field's overdamped motion described above, the scale factor in the wormhole solution $a_E(\tilde{\tau})$ increases away from the wormhole centre, the matter and radiation terms are suppressed as $\tilde{\tau}$ increases or decreases from $\tilde{\tau} = 0$, and the scalar kinetic energy K_ϕ becomes negligible as $\phi_E \to 0$ (see Figure 8.8, right panel). Therefore, for $\tilde{\tau} \to \pm\infty$ the solution approaches pure AdS with vacuum energy density parameter given by $\Omega_\Lambda = 3\tilde{V}(0) = 3B$. As a consequence, the scale factor takes the asymptotic form $a(\tilde{\tau}) \to \exp(\sqrt{-B}\tilde{\tau})$ as $\tau \to \pm\infty$ and the Hubble parameter approaches a constant value $\tilde{H}(\tilde{\tau}) \to \tilde{H}_\infty = \sqrt{-B}$ (see Figure 8.8, left panel). These results confirm the existence, within the class of models introduced in [231, 232], of well-defined wormhole solutions associated with cosmological solutions able to reproduce to arbitrary accuracy the predictions of the ΛCDM model.

We would like to point out that, from a top-down point of view, there is reason to be skeptical about the existence of the type of potentials studied in this subsection on the grounds of Swampland conjectures. In particular, the de Sitter conjecture [41, 233, 234] would appear to rule out potentials with very flat regions such as the ones introduced in equations (8.14) and (8.15). Nonetheless, this class of nearly-flat potentials is a useful starting point for our discussion. Indeed, the present analysis suggests that sufficient fine-tuning allows us to reproduce arbitrarily well the predictions of the ΛCDM model between the early Universe and the present time while preserving the existence of a wormhole solution with the scalar field satisfying the BF bound at the two asymptotic AdS boundaries. A similar conclusion remains valid for more general potentials, as we will now see.

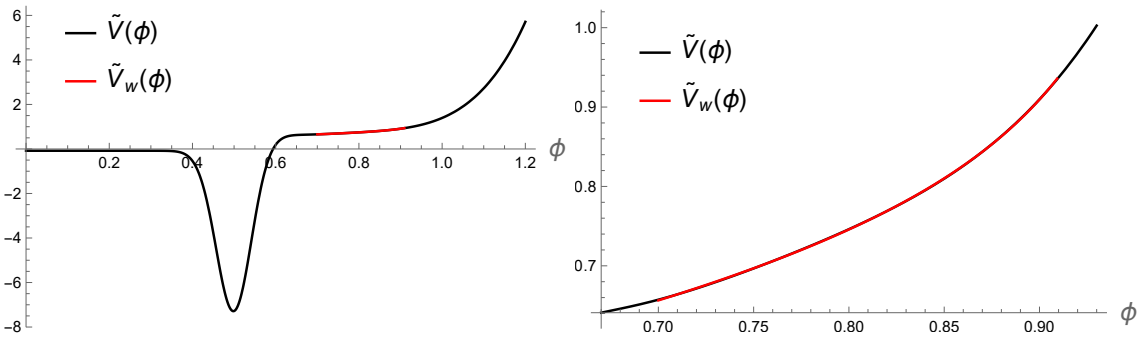

Figure 8.9: Rescaled potentials for the model $V(\phi)$ and reconstruction $V_w(\phi)$, where the region of the latter probed by the scalar field in the range $z \in (z_{\min}, z_{\max})$ is shown. The right-hand plot is a close-up on this region. The precise form of the model $V(\phi)$ can be found in Appendix I.2.

8.2.4 An example matching flat wCDM

Though we have considered a flat potential to make direct contact with the ΛCDM model, such tuning of the scalar potential is not at all necessary, and we can consider a broader class of models consistent with direct observations of Ω_M and the scale factor $a(t)$, which may involve scalar evolution over a range of potential values $\Delta V/V = O(1)$.

For concreteness, we consider the spatially flat wCDM model,[94] since direct constraints on the cosmological parameters for these models from type Ia supernova observations, using the Pantheon+SH0ES data set, are provided in [7]. We recall that this model consists of modifying the dark energy contribution in the ΛCDM model, by replacing the cosmological constant with a perfect fluid governed by the equation of state $\rho = wp$, with w constant. The corresponding Hubble expansion is given by

$$H(z) = H_0\sqrt{\Omega_M(1+z)^3 + \Omega_\Lambda(1+z)^{3(1+w)}}\,, \tag{8.19}$$

where Ω_Λ is the density parameter for the dark energy, so that $\Omega_\Lambda = 1 - \Omega_M$ with the assumption of spatial flatness. The constraints on the parameters of this model from [7] are

$$H_0 = (73.5 \pm 1.1)\ \text{km s}^{-1}\ \text{Mpc}^{-1}\,, \quad \Omega_M = 0.309^{+0.063}_{-0.069}\,, \quad w = -0.90 \pm 0.14\,. \tag{8.20}$$

We can reproduce the evolution of the wCDM cosmology over an arbitrarily large range of redshifts using our scalar field model. With the assumption that only a single scalar field is relevant to the cosmological evolution, we can actually deduce the potential associated with this scalar field given $a(t)$ and Ω_M. To see this, note that from the Friedmann equations the kinetic energy can be expressed as

$$K(t) \equiv \frac{1}{2}\dot{\phi}^2 = -\frac{1}{8\pi G}\dot{H} - \frac{3}{16\pi G}\Omega_M H_0^2 \frac{1}{a^3}\,, \tag{8.21}$$

and we can take the square root and integrate, to obtain

$$\phi(t) = \phi(t_0) + \int_{t_0}^{t} d\hat{t}\sqrt{-\frac{1}{4\pi G}\dot{H}(\hat{t}) - \frac{3}{8\pi G}\Omega_M H_0^2 \frac{1}{a^3(\hat{t})}}. \tag{8.22}$$

Similarly, the potential energy is

$$V(t) = \frac{1}{8\pi G}\dot{H} + \frac{3}{8\pi G}H^2 - \frac{3}{16\pi G}\Omega_M H_0^2 \frac{1}{a^3}\,. \tag{8.23}$$

[94] We neglect radiation in this subsection.

We can alternatively express these in terms of the redshift z and adopt the rescaled quantities introduced in the previous subsection, obtaining

$$\begin{aligned}\phi(z) &= \phi_0 + \int_0^z dz' \, \frac{\sqrt{\frac{1}{4\pi G}(1+z')\tilde{H}(z')\tilde{H}'(z') - \frac{3}{8\pi G}(1+z')^3\Omega_M}}{(1+z')\tilde{H}(z')}, \\ \tilde{V}(z) &= -\frac{1}{8\pi G}(1+z)\tilde{H}(z)\tilde{H}'(z) + \frac{3}{8\pi G}\tilde{H}(z)^2 - \frac{3}{16\pi G}(1+z)^3\Omega_M \, .\end{aligned} \tag{8.24}$$

We may then substitute the rescaled version of the Hubble expansion from equation (8.19) into these expressions.

In the scalar field model, the effective equation of state parameter $w \equiv P/\rho$ is given by

$$w = \frac{\frac{1}{2}\dot{\phi}^2 - V}{\frac{1}{2}\dot{\phi}^2 + V} \, , \tag{8.25}$$

which is straightforwardly obtained from the stress-energy tensor of a spatially homogeneous scalar field. For a general scalar theory, w will be redshift dependent, but with appropriate choice of scalar potential, we may recover solutions for which w is approximately constant over an arbitrarily large range of redshifts. We denote by $V_w(\phi)$ the scalar potential reconstructing the wCDM model for all $z > 0$. For the best-fit parameters of wCDM listed above, we show part of the reconstructed potential $\tilde{V}_w(\phi) = V_w(\phi)/H_0$ in Figure 8.9.

Since the Pantheon+SH0ES data used to deduce the cosmological parameter constraints probe only redshifts in the range $z \in (z_{\min}, z_{\max})$ with $z_{\min} \approx 10^{-3}$ and $z_{\max} \approx 2.26$, we are free to consider any scalar potential $V(\phi)$ that coincides with $V_w(\phi)$ in the region over which the scalar solution evolves in this range of redshifts. In Figure 8.9, we also plot a rescaled scalar potential $\tilde{V}(\phi) = V(\phi)/H_0$ agreeing with $\tilde{V}_w(\phi)$ in the appropriate range, but that satisfies the "UV constraints" necessary for the existence of an analytic continuation of the cosmological solution to an asymptotically AdS wormhole. The precise form of the potential $\tilde{V}(\phi)$, as well as our method for constructing the potential and the appropriate initial conditions for the cosmological solution, are given in Appendix I.2. In the left panel of Figure 8.10, we plot the equation of state evolution $w(z)$ extracted directly from the time-symmetric cosmological solutions in the model with potential $\tilde{V}(\phi)$, confirming that they reproduce that of the wCDM model with the desired precision, while in the right panel of Figure 8.10 we confirm that the analytic continuation of these solutions have AdS asymptotics.

We emphasize that, while we have only aimed here to reproduce the wCDM model over the region $z \in (z_{\min}, z_{\max})$ where it has been constrained by SNe Ia data, we could recover the same model over an arbitrarily large redshift interval through suitable choice of the scalar potential.

8.3 Supersymmetric models

In our discussion so far, we have considered an effective gravitational field theory involving scalar fields with dynamics controlled by an effective potential V. We have shown that such a theory could describe the background dynamics of our Universe while also admitting a Euclidean continuation suggestive of a dual CFT description.

The most well-understood examples of gravitational theories which are dual to CFTs are supersymmetric. It is thus interesting to ask whether there exist supersymmetric theories whose effective low energy descriptions contain scalar fields with potentials V, which give rise to effective cosmological dynamics. In these examples, supersymmetry could be broken by the time-dependent scalar

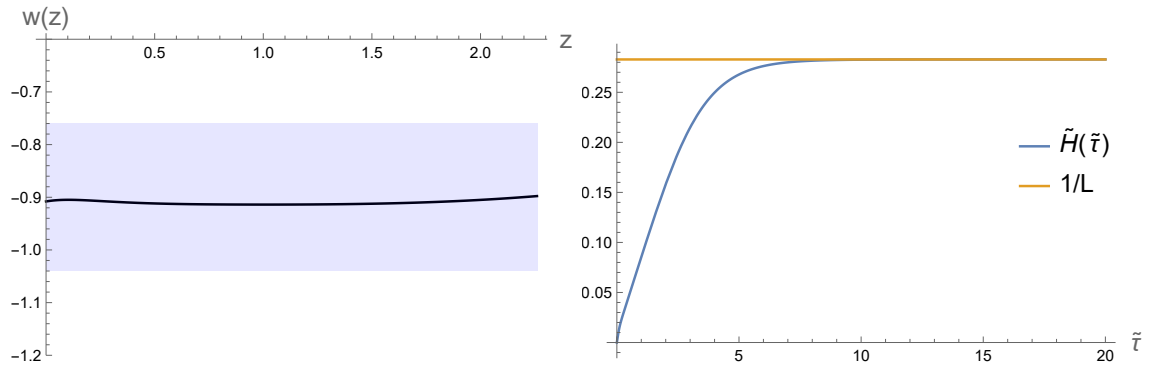

Figure 8.10: (Left) Equation of state parameter w versus redshift z for time-symmetric solutions to the model $\tilde{V}(\phi)$, with shaded region given by the Pantheon+SH0ES constraint. (Right) Euclidean evolution of $\tilde{H}(\tilde{\tau})$, with $\frac{1}{L} \equiv \sqrt{-V(0)}$ plotted for reference. In the asymptotic region $\tilde{\tau} \to \infty$ the wormhole solution approaches pure AdS, as expected. The precise form of the potential $\tilde{V}(\phi)$ can be found in Appendix I.2.

field expectation value. Note that here we will not be concerned with whether the supersymmetric theories under consideration have explicitly known CFT duals. Instead we simply wish to understand whether supersymmetry is consistent with the restricted class of scalar potentials which we have considered so far.

We will consider $\mathcal{N} = 1$ supergravity and restrict to considering only the gravity and scalar sectors; presumably one can consistently set the gravitino and chiral fermions to zero in solutions to the full equations of motion. We follow the notation of [235] and we set $8\pi G_{\rm N} = \kappa^2 = 1$ in this section.

The n_c scalar fields ϕ^i of $\mathcal{N} = 1$ supergravity are bottom components of chiral multiplets, such that the theory has bosonic Lagrangian

$$\mathcal{L} = \frac{1}{2}R - K_{i\bar{j}}\partial_\mu\phi^i\partial^\mu\bar{\phi}^{\bar{j}} - V_W(\phi,\bar{\phi})\,, \tag{8.26}$$

where $K_{i\bar{j}} = \partial_i\bar{\partial}_{\bar{j}}K$ is the Kähler metric arising from a Kähler potential K, and V_W is the scalar potential

$$V_W = e^K\left(K^{i\bar{j}}D_iWD_{\bar{j}}\bar{W} - 3|W|^2\right)\,, \qquad D_iW = \partial_iW + K_iW\,, \tag{8.27}$$

defined in terms of the superpotential W.

For simplicity we will consider the case of a single chiral multiplet, $n_c = 1$, and set the Kähler potential to the canonical form $K(\phi,\bar{\phi}) = \bar{\phi}\phi$. Theories with more general Kähler potentials and more chiral multiplets may also be interesting to consider. In our case the scalar potential is given by

$$V_W(\phi) = e^{\phi\bar{\phi}}\left(|W'(\phi) + \bar{\phi}W(\phi)|^2 - 3|W(\phi)|^2\right). \tag{8.28}$$

A specification of W is part of the specification of the supersymmetric theory, with the only restriction on W being that it is a holomorphic function of ϕ. Thus we would like to know whether it is possible to choose W such that V_W is a scalar potential like the ones considered in previous sections, i.e. which gives rise to effective cosmological dynamics.

The scalar field ϕ arising from the supersymmetric theory is a complex field, which we can decompose into two real fields as $\phi = \phi_R + i\phi_I$. Thus V_W is a (real) potential of two real fields, ϕ_R

and ϕ_I, whose dynamics will in general be coupled — the trajectory of ϕ in the complex plane will generally involve motion in both the ϕ_R and ϕ_I directions.

However, although it is certainly possible that the low energy effective field theory describing our Universe contains multiple real scalar fields, in the previous sections we have shown that a single field with potential V is sufficient for the cosmology to be in quantitative agreement with measurements of the scale factor, while still admitting an asymptotically AdS Euclidean continuation. Thus we might hope that we can find a potential V_W such that the dynamics in the ϕ plane is one-dimensional, for example such that ϕ rolls down the real axis, with $\phi_I = 0$ for all times. Moreover, we would like $V_W(\phi_R) = V(\phi_R)$, so that the remaining scalar degree of freedom ϕ_R provides us with the desired cosmological evolution.

We will now show that, even with this restriction that ϕ_I effectively decouples from the dynamics, given any cosmological potential $V(\phi_R)$ it is possible to find a superpotential $W(\phi)$ such that $V_W(\phi_R)$ is, to an arbitrarily good approximation, equal to $V(\phi_R)$ within a given fixed region. Furthermore, in this construction W will be holomorphic everywhere provided that V is. Since the cosmological potentials which we considered in previous sections are generically holomorphic everywhere, this construction will produce holomorphic superpotentials W which give rise to realistic effective cosmological dynamics with Euclidean AdS asymptotics.

Constructing the superpotential

In our construction $W(\phi_R)$ will be real, in which case Eq. (8.28) for $\phi = \phi_R$ reads

$$V_W(\phi_R) = e^{\phi_R^2}\left\{\left[W'(\phi_R) + \phi_R W(\phi_R)\right]^2 - 3W^2(\phi_R)\right\}. \tag{8.29}$$

This is a nonlinear ODE for W and cannot be solved in closed form. To obtain a linear equation, write

$$V_W(\phi_R) = e^{\phi_R^2}\left(W' + (\phi_R + \sqrt{3})W\right)\left(W' + (\phi_R - \sqrt{3})W\right). \tag{8.30}$$

Now let $f(\phi_R)$ be some function, which we define shortly, and consider the linear ODE

$$W'(\phi_R) + (\phi_R - \sqrt{3})W(\phi_R) = f(\phi_R). \tag{8.31}$$

The general solution is the sum of a homogeneous plus inhomogeneous piece,

$$W(\phi_R) = CG(\phi_R) + G(\phi_R)\int_0^{\phi_R} du \frac{f(u)}{G(u)}, \tag{8.32}$$

where C is an arbitrary integration constant, and the homogeneous piece is given by

$$G(\phi_R) = \exp\left(-\frac{1}{2}\phi_R^2 + \sqrt{3}\phi_R\right). \tag{8.33}$$

Substituting this solution for W into (8.30) we obtain the scalar potential

$$V_W(\phi_R) = \tilde{V}(\phi_R)\left(1 + \frac{\tilde{V}(\phi_R)e^{-2\sqrt{3}\phi_R}}{12C^2} + \frac{1}{2\sqrt{3}C^2}\int_0^{\phi_R} du\, \tilde{V}(u)e^{-2\sqrt{3}u}\right). \tag{8.34}$$

where we have defined

$$\tilde{V}(\phi_R) \equiv 2\sqrt{3}Ce^{\phi_R^2} f(\phi_R)G(\phi_R). \tag{8.35}$$

Because we are free to choose f, we are effectively free to choose $\tilde{V}$. We can thus require $V_W(\phi_R) = V(\phi_R)$ and solve (8.34) for $\tilde{V}$. Although this cannot be done in closed form, we can obtain a series approximation for $\tilde{V}$ in powers of $1/C^2$. Notice that C is an arbitrary constant, and so it can be chosen large enough to be a good expansion parameter; we will discuss this in more detail below. Namely, writing

$$\tilde{V}(\phi_R) = \tilde{V}_0(\phi_R) + \frac{1}{C^2}\tilde{V}_2(\phi_R) + \frac{1}{C^4}\tilde{V}_4(\phi_R) + \dots, \tag{8.36}$$

it is possible to recursively solve the equation $V_W(\phi_R) = V(\phi_R)$ for the $\tilde{V}_n$. The first two terms in the expansion are

$$\tilde{V}_0(\phi_R) = V(\phi_R), \tag{8.37}$$

$$\tilde{V}_2(\phi_R) = -\frac{V(\phi_R)}{2\sqrt{3}}\left(\frac{e^{-2\sqrt{3}\phi_R}V(\phi_R)}{2\sqrt{3}} + \int_0^{\phi_R} du\, V(\phi_R)e^{-2\sqrt{3}u}\right), \tag{8.38}$$

and expressions for higher order terms can be straightforwardly obtained by recursion. Substituting (8.35) into (8.32) we obtain the superpotential in terms of $\tilde{V}$,

$$W(\phi_R) = CG(\phi_R)\left(1 + \frac{1}{2\sqrt{3}C^2}\int_0^{\phi_R} du\, \tilde{V}(u)e^{-2\sqrt{3}u}\right), \tag{8.39}$$

and using the series expansion for $\tilde{V}$ in terms of V, we can, perturbatively in powers of $1/C^2$, write the superpotential W in terms of the cosmological potential V:

$$W(\phi_R) = CG(\phi_R)\left[1 + \frac{1}{2\sqrt{3}C^2}\int_0^{\phi_R} du\, V(u)e^{-2\sqrt{3}u} + \mathcal{O}\left(C^{-4}\right)\right]. \tag{8.40}$$

Truncating the expansion

If we use the full expression for $W(\phi_R)$ derived above, including all corrections in powers of $1/C^2$, then we would expect to find an exact equality $V_W(\phi_R) = V(\phi_R)$ for all values of ϕ_R. Of course, it is not possible to work with the infinite series of terms. Instead we can truncate the series expansion of W at n terms, obtaining the truncated superpotential, which we denote W_n. For example, W_2 is obtained by keeping two terms in the expansion,

$$W_2(\phi_R) = CG(\phi_R)\left(1 + \frac{1}{2\sqrt{3}C^2}\int_0^{\phi_R} du\, V(u)e^{-2\sqrt{3}u}\right), \tag{8.41}$$

which results in the scalar potential

$$V_{W_2}(\phi_R) = V(\phi_R)\left(1 + \frac{V(\phi_R)e^{-2\sqrt{3}\phi_R}}{12C^2} + \frac{1}{2\sqrt{3}C^2}\int_0^{\phi_R} du\, V(u)e^{-2\sqrt{3}u}\right). \tag{8.42}$$

Recall that C appeared simply as an undetermined integration constant, and we are free to set it to any value whatsoever. Therefore we have the somewhat unusual freedom to set our expansion parameter $1/C$, and thus the terms truncated in going from W to W_2, as small as we like. In terms of the potentials, given any value of ϕ_R we can make $V_{W_2}(\phi_R)$ arbitrarily close to the cosmological potential $V(\phi_R)$. In other words, as we take C large V_{W_2} converges pointwise to $V(\phi_R)$. If we restrict to values of ϕ_R in any compact subset of the real line, then the convergence is uniform

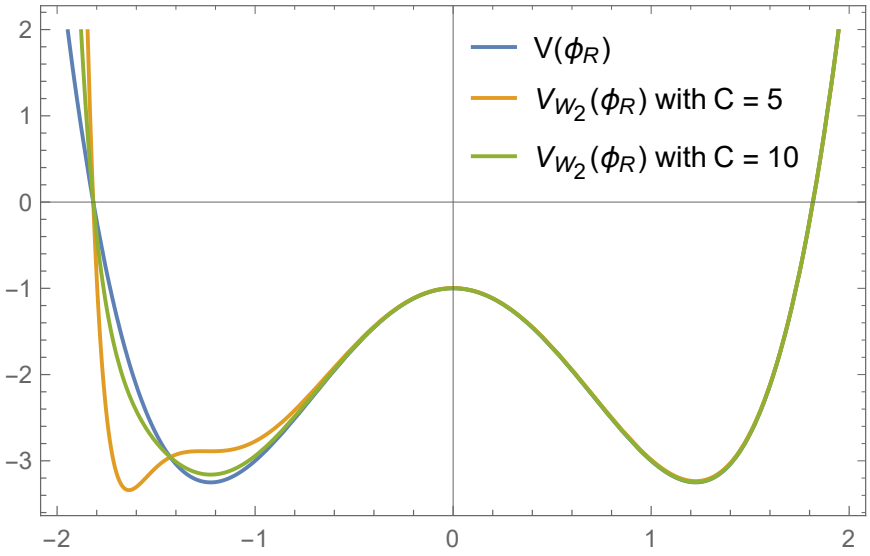

Figure 8.11: Comparison of $V(\phi_R) = -1 - 3\phi_R^2 + \phi_R^4$ and the potential $V_{W_2}(\phi_R)$ given by equation (8.42), obtained from the truncated superpotential W_2 given by Equation (8.41).

within this subset. Thus we have successfully managed to embed any scalar potential V — including cosmological potentials — into a supersymmetric theory, to an arbitrary degree of accuracy.

In Fig. 8.11 we illustrate with a simple example the deviation of V_{W_2} from V for various values of C. Notice that $V_{W_2}(\phi_R)$ is in excellent agreement with $V(\phi_R)$ for $\phi_R > 0$, but for a fixed value of C the agreement breaks down for negative enough values of ϕ_R. This is because the exponential factor in the integrand in (8.41) suppresses the contribution of the subleading term for positive values of ϕ_R, but enhances this same contribution for negative ϕ_R. This effect can be traced back to us choosing to set the second bracketed factor in (8.30) equal to f. Had we chosen to set the first factor equal to f, the same analysis would result in an approximation $V_{W_2}(\phi_R)$ of $V(\phi_R)$ that is accurate for all $\phi_R < 0$, but breaks down for ϕ_R positive enough. Since throughout this chapter we have worked with the convention that the scalar field rolls along the positive real axis, it makes sense to consider, as we have done, the construction which gives an accurate approximation $V_{W_2}(\phi_R) \approx V(\phi_R)$ for positive ϕ_R. Nevertheless, by taking C large enough, we can make $V_{W_2}(\phi_R)$ arbitrarily close to $V(\phi_R)$ for ϕ_R greater than any real ϕ_R^*.

Maximum at $\phi_R = 0$

One potential issue with the truncated potential $V_{W_2}(\phi_R)$ is that it is not symmetric with respect to $\phi_R \to -\phi_R$; see Fig. 8.11. Despite this, from (8.42) we find

$$V'_{W_2}(\phi_R) = V'(\phi_R)\left(1 + \frac{2V(\phi_R)e^{-2\sqrt{3}\phi_R}}{12C^2} + \frac{1}{2\sqrt{3}C^2}\int_0^{\phi_R} du\, V(u)e^{-2\sqrt{3}u}\right), \tag{8.43}$$

and hence $V'_{W_2}(0) = 0$ if $V'(0) = 0$. Thus, although $V_{W_2}(\phi_R)$ is not symmetric, it does have a local maximum at $\phi_R = 0$, allowing for the asymptotically AdS solution $\phi_R = 0$ in the Euclidean continuation. Therefore it is not a problem that $V_{W_2}(\phi_R)$ is not symmetric.

Dynamics of a complex ϕ

So far we have restricted the complex field $\phi = \phi_R + i\phi_I$ to the real line, i.e. we have set $\phi_I = 0$. This has allowed us to explicitly construct the superpotential $W_2(\phi_R)$, which gives a scalar potential $V_{W_2}(\phi_R)$ that is arbitrarily close to the cosmological potential $V(\phi_R)$. Analytically continuing away from the real axis, we obtain the superpotential $W_2(\phi)$ as a function of complex ϕ. Notice from (8.41) that if $V(\phi)$—the analytic continuation of the cosmological potential $V(\phi_R)$—is analytic in some simply connected region of the complex plane containing $\phi = 0$, then $W_2(\phi)$ is analytic in this same region. The cosmological potentials considered in previous sections were analytic everywhere, and so the corresponding superpotential is also analytic everywhere.

The superpotential $W_2(\phi)$ defines a scalar potential $V_{W_2}(\phi)$ for complex values of ϕ via Eq. (8.28),

$$V_{W_2}(\phi) = e^{\phi\bar{\phi}} \left(|W_2'(\phi) + \bar{\phi} W_2(\phi)|^2 - 3|W_2(\phi)|^2 \right). \tag{8.44}$$

Notice that $V_{W_2}(\phi)$ is not holomorphic even if $W_2(\phi)$ is. In fact, $V_{W_2}(\phi)$ is real for all ϕ, and so it cannot be holomorphic. Thus instead of thinking of $V_{W_2}(\phi)$ as a function of a single complex variable ϕ, it makes more sense to think of it as a (real) function of two real variables, ϕ_R and ϕ_I.

By construction we have ensured that $V_{W_2}(\phi)$ restricted to the real axis is approximately equal to the cosmological potential $V(\phi_R)$. An important question is: if at some initial time the values of ϕ and $\dot{\phi}$ are both real (i.e. $\phi_I = 0 = \dot{\phi}_I$), then does ϕ remain real (i.e. does ϕ_I remain zero) throughout its dynamical evolution? In other words we are asking whether the imaginary component of ϕ decouples, leaving only a single real scalar degree of freedom to source the cosmological dynamics.

To answer this, suppose that ϕ is spatially homogeneous and consider the equation of motion for the fields ϕ_R and ϕ_I with potential $V_{W_2}(\phi_I, \phi_R)$,

$$\ddot{\phi}_i + 3H\dot{\phi}_i + \partial_i V_{W_2} = 0. \tag{8.45}$$

Since $W_2(\phi)$ is analytic in the complex plane and real on the real axis, it can be shown that $\overline{W_2(\phi)} = W_2(\bar{\phi})$.[95] Equation (8.44) then implies that $V_{W_2}(\bar{\phi}) = V_{W_2}(\phi)$ which implies that $\partial V_{W_2}/\partial\phi_I$ is identically zero on the real axis. Therefore if ϕ_I and $\dot{\phi}_I$ vanish at some initial time, they vanish for all times; if ϕ starts rolling along the real axis, it stays on the real axis. Hence we are able to construct any effective single field cosmological model, such as those discussed in previous sections, by starting with a supersymmetric Lagrangian.

Stability

Having shown that $\phi_I = 0 = \dot{\phi}_I$ initially implies vanishing ϕ_I for all times, i.e. ϕ_I decouples from ϕ_R, it is important to ask whether the dynamics of ϕ_R is stable against small perturbations which make ϕ_I or $\dot{\phi}_I$ nonzero. Such perturbations will inevitably spontaneously occur due to quantum fluctuations, so it is crucial to consider their effects.

To determine the effects of such small perturbations away from real values of ϕ, we must evaluate $\partial^2 V_W/\partial\phi_I^2$ for $\phi_I = 0$. If this is positive, the potential $V_{W_2}(\phi)$ curves upwards as ϕ moves away from the real axis, and thus the motion along the real axis is stable to small perturbations.

[95] Proof: Since $W_2(\phi)$ is analytic $W_2(\phi) = W_2(\phi_R + i\phi_I) = \sum_{n=0}^{\infty} \frac{1}{n!} W_2^{(n)}(\phi_R)(\phi - \phi_R)^n$. Since $W_2(\phi_R)$ is real $\overline{W_2^{(n)}(\phi_R)} = W_2^{(n)}(\phi_R)$. Hence $\overline{W_2(\phi)} = \sum_{n=0}^{\infty} \frac{1}{n!} W_2^{(n)}(\phi_R)(\bar{\phi} - \phi_R)^n = W_2(\bar{\phi})$.

Equation (8.44) gives $V_{W_2}(\phi)$ for all complex values of ϕ. Setting $\phi = \phi_R + i\phi_I$ and differentiating, we find

$$\left.\frac{\partial^2 V_{W_2}}{\partial \phi_I^2}\right|_{\phi_I=0} = 8e^{2\sqrt{3}\phi_R}C^2 + F_0(\phi_R) + \frac{F_2(\phi_R)}{C^2}, \tag{8.46}$$

where $F_0(\phi)$ and $F_2(\phi)$ are analytic functions (which depend on V) and are thus bounded on any compact set $I \subset \mathbb{R}$. Therefore, since the leading term in this expansion is positive, it is always possible to take C large enough so that $\partial^2 V_{W_2}/\partial\phi_I^2|_{\phi_I=0} > 0$ for any $\phi_R \in I$.[96] In this case the dynamics of ϕ_R along the real axis is guaranteed to be stable under fluctuations in the imaginary directions, and so even at the level of perturbations the field ϕ_I decouples from the dynamics of ϕ_R.[97] Thus we truly have a single field cosmological model, starting from a supersymmetric Lagrangian.

8.4 Outlook

In this chapter, we have argued that accelerated expansion is generic (i.e. arises without fine tuning) in $\Lambda < 0$ cosmologies arising from asymptotically AdS Euclidean wormholes, for simple scalar potentials with a form that is natural in theories with a dual CFT. We found that there exist models of this type which can match ΛCDM to high accuracy at the level of background geometry, so the framework can give realistic cosmologies. We found that the scalar potential in these examples can arise from a superpotential, so the effective field theory can potentially have a supersymmetric point for $\phi = 0$. There are many directions for further study.

Direct reconstruction of the potential

The class of models considered in this chapter make at least two generic predictions: that one should have a dynamical scalar field contributing to the energy density of the Universe and that the Universe should eventually begin to decelerate. With this in mind, it is interesting to consider direct measurements of the scale factor from supernova observations and search for evidence of an evolving scalar field. In principle, the scalar potential in a single field model can be reconstructed directly from knowledge of the scale factor $a(t)$ and Ω_M when radiation can be ignored. The explicit expressions given in equations (8.22) and (8.23) define $V(\phi)$ parametrically. However, Ω_M (the present day matter contribution to the energy density) is not well constrained by direct observation, and the reconstruction of $V(\phi)$ for given Ω_M is quite sensitive to small changes in $a(t)$. As a result, there is actually considerable freedom in the form of the potential that can be consistent with data, and thus considerable room for the types of models considered here.[98]

Indeed, following the work presented here, a more systematic study investigated the constraints imposed by type Ia supernovae data on the possible evolution of a single scalar field over the period of time for which the data was available (roughly half the age of the Universe) [186]. There it was found that the data strongly favour a decreasing potential energy at present, with a significant variation in scalar potential $\Delta V/V \approx 1$ over the period of time corresponding to the available data. We note that it is particularly interesting at present to consider models that go beyond ΛCDM given the Hubble tension [236].

[96] Recall that taking C large is the same limit which ensures $V_{W_2}(\phi_R) \approx V(\phi_R)$ in the first place.

[97] Note that the dynamics is also stable in the double analytically continued (Lorentzian wormhole) picture [231], because $\partial^2 V_{W_2}/\partial\phi_I^2 > 0$ trivially satisfies the BF bound, while $\partial^2 V_{W_2}/\partial\phi_R^2$ satisfies the BF bound by construction.

[98] One example of this flexibility is highlighted in Figure 8.9 which shows in red a potential with significant variation that provides a good fit to the low redshift measurements of the scale factor.

Including fluctuations in a realistic effective field theory model

In this chapter, we have focused entirely on the evolution of the homogeneous background. We found that there are effective theories that are compatible both with the cosmological history obtained from ΛCDM or wCDM and with having a stable asymptotically AdS analytic continuation. It is very interesting to understand whether these effective theories are also capable of reproducing the observed spectrum of fluctuations in the CMB. One question we would particularly like to understand is whether primordial inflation is required or if the existence of the analytic continuation is already enough to give a sensible spectrum of fluctuations.

We also want to understand if the scalar potentials we are considering could have other phenomenological effects. For example, considering fluctuations around a very flat potential raises the prospect of a new long-ranged scalar-mediated force. One can also ask if scalar particles would be produced in any appreciable quantity and, if so, could such particles form a component of dark matter? These are issues that must be addressed to claim a fully realistic model, quite apart from objections to flat potentials arising from Swampland conjectures.

Towards a microscopic construction

Here we have focused exclusively on effective theories, but it remains an important open question to find concrete microscopic realizations of these big-bang / big-crunch cosmologies with a holographic dual. In the search for such constructions, it makes sense to again back off of demanding a fully realistic model. Instead, we can ask if relatively simple models can be found, perhaps corresponding to a pure radiation scenario or a scenario with a relatively simple scalar potential exhibiting some period of acceleration.

It is also interesting to further explore the issue of supersymmetric effective theories. Here we showed that a superpotential can be constructed to match any potential we devise, but presumably not all such superpotentials arise from a UV-complete and supersymmetric microscopic theory.

Chapter 9

Conclusions

A major goal of physics is to better understand the very early Universe. Our present understanding suggests that this was a time when the energy density exceeded the Planck scale, indicating that if we are to make progress towards this goal we will need a theory of cosmology that is valid at trans-Planckian scales. Because the Planck scale is the scale at which quantum gravitational effects are expected to become important, such a cosmological theory should presumably be based on a quantum theory of gravity. In this thesis we have presented a novel formulation for a theory of quantum cosmology which is based on AdS/CFT holography. Here we give a brief summary of our main results.

Summary of results

We started in Chapter 3 by asking a general question in holography: Under which conditions can a holographic conformal field theory CFT_2 describe the gravitational physics dual to a different holographic conformal field theory, CFT_1? We argued that the answer is "when the two CFTs can be non-trivially coupled at an interface". In this case there exists a state of CFT_2 that describes an arbitrarily large bubble of the gravitational system dual to a state of CFT_1. In our setup both the gravitating bubble as well as the exterior region possess a negative cosmological constant, although not necessarily of the same value. Most of our focus was on proving this claim in the simplest case where the state of CFT_1 is the vacuum state, but we also argued on general grounds that this should be true for arbitrary excited states as well, in which case the gravitational "bubble" would contain excitations on top of the $\Lambda < 0$ vacuum.

In Chapter 4 we investigated the possibility that the gravitating bubble is a portion of an FRW cosmology. Unlike in Chapter 3, where the focus was on understand the gravitational solutions associated with a specific CFT setup, here we first constructed the gravitational solution by patching together a bubble of $\Lambda < 0$ + radiation + matter time-symmetric cosmology with an external empty AdS spacetime, and then we investigated whether such a gravitational system can have a good CFT description. By studying the thermodynamics and the Euclidean analytic continuations of these spacetimes, we found strong evidence that a CFT description of these types of spacetimes should in general be possible. Moreover, by studying the extremal surfaces of the geometries we found that in many cases entanglement entropies of CFT subregions provide a direct probe of cosmological physics directly from the microscopic CFT states.

Although the cosmological bubbles in our construction could be made arbitrarily large, we found it desirable from a Copernican perspective to have a holographic description of cosmology that was homogeneous and isotropic on the full spatial slices. Naively this is not possible, since any non-trivial homogeneous and isotropic cosmology would contain matter and/or radiation everywhere, whereas holographic spacetimes are required to be asymptotically empty. Nevertheless, in Chapter 5 we exploited a simple mathematical observation which allowed us to make progress: a large class of $\Lambda < 0$ cosmologies are time-symmetric, meaning that the geometry obtained by analytically continuing the time coordinate to imaginary values is sensible (it has a real metric). Unlike the cosmology, which contracts to a big-bang or a big-crunch in the distant past and future, the Euclidean geometry

generally expands as one moves away from the reflection symmetric surface, and in both directions ends at an asymptotically AdS boundary. Hence the analytic continuation of the cosmology is a Euclidean wormhole with two AdS boundaries. Similarly if we assume that the original cosmology is spatially flat, a second analytic continuation, this time of a spatial coordinate, produces a traversable Lorentzian AdS wormhole. The AdS wormhole spacetimes are microscopically describable using AdS/CFT, and thus by analytic continuation the same is true of the cosmology. More concretely we argued that the microscopic setup describing the gravitational physics should consist of a pair of three-dimensional CFTs coupled via a four-dimensional field theory with many fewer degrees of freedom. We explored in detail the implications of this construction on the background FRW cosmology, and in less quantitative detail the implications for fluctuations about the background.

One of the principal concerns with this construction is the viability of the traversable Lorentzian wormhole, which can only be supported by a negative energy that is larger than the usual Casimir vacuum energy by a factor of order $\ell^2/\ell^2_{\text{Planck}}$. If the wormhole is dual to a cosmology then ℓ is a cosmological length scale, and therefore this required anomalous factor is huge. The goal of Chapter 6 was to show that such an anomalously large negative energy density is natural for the types of systems under consideration. To make this argument we considered a simplified model of the wormhole. While the wormhole is a gravitational system with many degrees of freedom whose two ends are connected by an auxiliary non-gravitational system with many fewer degrees of freedom, we considered a simple setup in which both systems are non-gravitational holographic CFTs. Because both theories in this toy model are holographic we were able to compute their energy densities using AdS/CFT techniques. We thus found that, with an appropriate tuning of the interface coupling between the two CFTs, it is indeed possible for one of the CFTs to have an anomalously large negative energy density, but only if it has many more degrees of freedom than the other CFT. This suggests that the parametrically large negative energy density is linked to the parametrically large relative number of degrees of freedom of the theory, which further suggests that perhaps the same should be true in the wormhole theory, since, as we mentioned, this theory necessarily contains many more degrees of freedom than the non-gravitational theory to which it is coupled.

Having provided strong evidence that the Lorentzian wormhole can be supported with the appropriate amount of negative energy, in Chapter 7 we looked to extend our understanding of the precise relationship between the gravitational physics in the wormhole, and the non-gravitational / quantum mechanical / microscopic dual description. The reason we chose to study the wormhole rather than the cosmology directly is because the wormhole is a simple vacuum spacetime, whereas the fields in the cosmology are in a highly non-trivial excited state. Of course at the end of the calculation we can simply translate (via analytic continuation) any conclusions regarding the wormhole into conclusions regarding the cosmology; thus it makes sense to study whichever system is easier, which in this case is the wormhole. To that end, we investigated the relationship between observable quantities in the wormhole to observable quantities in the microscopic field theory dual to the wormhole. This microscopic theory is *not* a conformal field theory, but rather a pair of 3D CFTs coupled by a 4D field theory. At low energies this field theory setup will generally be defined by a confining gauge theory, that is a theory with a finite energy gap between the vacuum and the lowest excited state. Our purpose in this chapter was to derive explicit two-way mappings between observables in the confining gauge theory (the operator excitation spectrum and entanglement entropies of subregions) to the observables of the wormhole (the metric). These results strengthen our understanding of the quantum mechanical description of AdS wormhole spacetimes, and consequently of time-symmetric $\Lambda < 0$ cosmologies.

Finally in Chapter 8 we explored whether the cosmological constructions that we presented can be made realistic from the perspective of cosmological observations. We started at the ground floor

by exclusively considering the background geometry, i.e. the FRW scale factor. The most obvious potential phenomenological issue with our cosmologies is that they contain a negative cosmological constant, which by itself is unable to produce the accelerated expansion of spacetime necessary to match observations. The reason why this is not a problem is that our cosmologies also naturally contain scalar fields with a non-trivial potential V. The negative cosmological constant indicates a negative extremum for V, but it is plausible, and in fact likely, that other regions in field space give a positive value for V. If the fields are able to access these $V > 0$ regions then it may be possible for the scalar potential energy to drive an accelerated expansion of spacetime. Indeed by considering an example with a single scalar field we confirmed this expectation. First we showed that acceleration is generic, in the sense that a large subspace of potentials and initial conditions results in periods of accelerated expansion before the time-symmetric point in the cosmology. Then we showed that there exist potentials that allow our $\Lambda < 0$ cosmologies to match to arbitrary precision the background dynamics of standard $\Lambda > 0$ cosmology. These results imply that, at least at the level of the background dynamics, there is no reason to fear $\Lambda < 0$ cosmology.

Final remarks

This thesis represents the starting point of an endeavour to understand $\Lambda < 0$ cosmologies quantum mechanically. There are many important directions that are yet to be explored, which we elaborated on in the discussion sections of the previous chapters. Here we note three of the most important.

First, the technical results in this thesis have been obtained from a bottom-up perspective, meaning that we have worked within a simplified model of AdS/CFT in which the gravitational theory is greatly simplified, for example often consisting of just gravity and a scalar field, and the dual CFT is not precisely defined. However, a truly microscopic description of cosmology will require a top-down construction. A guide for future research in this direction should be our discussion in Section 5.2 (first formulated in [56]) of the expected field theory setup, consisting of a pair of supersymmetric 3D conformal field theories coupled via an auxiliary 4D field theory.

Second, while in Chapter 8 we showed that the $\Lambda < 0$ cosmologies are consistent with observational constraints at the level of the background (see also [186]), the make or break for all cosmological models is their ability or inability to accurately predict fluctuations about the background. For example, one of the main successes of standard inflationary cosmology is that it is able to predict CMB fluctuations that match observations. It will be very interesting to see whether our models are capable of making similarly accurate predictions. The likely path forward in this direction will be to compute fluctuations of the relevant quantum fields in the wormhole geometry, since this is a simple vacuum spacetime, and then analytically continue these results to the cosmological domain. As we discussed in Section 5.4, because the wormhole theory is weakly curved, this could provide an explanation for cosmological fluctuations that does not require the presence of a rapidly expanding inflationary regime.

Lastly, if our model of cosmology succeeds in these two directions, i.e. if it admits a top-down microscopic description and is able to predict realistic fluctuations about the background, then we would finally be in a position to try and answer the question that motivated us all along, namely to understand physics at the beginning of the Universe (whatever that may be). We will leave these explorations for future work.

Bibliography

[1] P. Simidzija and M. Van Raamsdonk, *Holo-ween*, *Journal of High Energy Physics* **2020** (Dec., 2020) 28.

[2] A. Sahu, P. Simidzija and M. Van Raamsdonk, *Bubbles of cosmology in ads/cft*, *Journal of High Energy Physics* **2023** (2023) 1–29.

[3] S. Antonini, P. Simidzija, B. Swingle and M. Van Raamsdonk, *Can one hear the shape of a wormhole?*, *JHEP* **09** (2022) 241, [2207.02225].

[4] S. Antonini, P. Simidzija, B. Swingle, M. Van Raamsdonk and C. Waddell, *Accelerating cosmology from $\Lambda < 0$ gravitational effective field theory*, *JHEP* **05** (2023) 203, [2212.00050].

[5] A. May, P. Simidzija and M. Van Raamsdonk, *Negative energy enhancement in layered holographic conformal field theories*, *Journal of High Energy Physics* **2021** (2021) 1–24.

[6] Planck collaboration, N. Aghanim et al., *Planck 2018 results. VI. Cosmological parameters*, *Astron. Astrophys.* **641** (2020) A6, [1807.06209].

[7] D. Brout et al., *The Pantheon+ Analysis: Cosmological Constraints*, 2202.04077.

[8] "Pantheon+SH0ES 2021/2022 data release." https://pantheonplusshOes.github.io.

[9] E. Hubble, *A relation between distance and radial velocity among extra-galactic nebulae*, *Proceedings of the national academy of sciences* **15** (1929) 168–173.

[10] T. Abbott, M. Acevedo, M. Aguena, A. Alarcon, S. Allam, O. Alves et al., *The dark energy survey: Cosmology results with˜ 1500 new high-redshift type ia supernovae using the full 5-year dataset*, *arXiv preprint arXiv:2401.02929* (2024) .

[11] S. Weinberg, *Cosmology*. OUP Oxford, 2008.

[12] S. W. Hawking and G. F. Ellis, *The large scale structure of space-time*. Cambridge university press, 2023.

[13] R. M. Wald, *General relativity*. University of Chicago press, 2010.

[14] A. M. Ghez, S. Salim, N. Weinberg, J. Lu, T. Do, J. Dunn et al., *Measuring distance and properties of the milky way's central supermassive black hole with stellar orbits*, *The Astrophysical Journal* **689** (2008) 1044.

[15] R. Abuter, A. Amorim, N. Anugu, M. Bauböck, M. Benisty, J.-P. Berger et al., *Detection of the gravitational redshift in the orbit of the star s2 near the galactic centre massive black hole*, *Astronomy & Astrophysics* **615** (2018) L15.

[16] R. Abuter, A. Amorim, M. Bauböck, J. Berger, H. Bonnet, W. Brandner et al., *Detection of the schwarzschild precession in the orbit of the star s2 near the galactic centre massive black hole*, *Astronomy & Astrophysics* **636** (2020) L5.

[17] S. W. Hawking and R. Penrose, *The singularities of gravitational collapse and cosmology*, *Proceedings of the Royal Society of London. A. Mathematical and Physical Sciences* **314** (1970) 529–548.

[18] R. Penrose, *Gravitational collapse: The role of general relativity*, .

[19] S. Weinberg, *The quantum theory of fields*, vol. 2. Cambridge university press, 1995.

[20] K. Eppley and E. Hannah, *The necessity of quantizing the gravitational field*, *Foundations of Physics* **7** (1977) 51–68.

[21] D. N. Page and C. Geilker, *Indirect evidence for quantum gravity*, *Physical Review Letters* **47** (1981) 979.

[22] J. Mattingly, *Why eppley and hannah's thought experiment fails*, *Physical Review D* **73** (2006) 064025.

[23] R. Penrose, *On the gravitization of quantum mechanics 1: Quantum state reduction*, *Foundations of Physics* **44** (2014) 557–575.

[24] A. Belenchia, R. M. Wald, F. Giacomini, E. Castro-Ruiz, Č. Brukner and M. Aspelmeyer, *Quantum superposition of massive objects and the quantization of gravity*, *Physical Review D* **98** (2018) 126009.

[25] S. Hossenfelder, *Experimental search for quantum gravity*, in *Workshop on Experimental Search for Quantum Gravity NORDITA, Stockholm, Sweden*, vol. 1010, Springer, 2010.

[26] S. Carlip, *Is quantum gravity necessary?*, *Classical and Quantum Gravity* **25** (2008) 154010.

[27] P. D. Group, R. Workman, V. Burkert, V. Crede, E. Klempt, U. Thoma et al., *Review of particle physics*, *Progress of theoretical and experimental physics* **2022** (2022) 083C01.

[28] C. Rovelli, *Loop quantum gravity*, *Living reviews in relativity* **11** (2008) 1–69.

[29] R. Loll, *Quantum gravity from causal dynamical triangulations: a review*, *Classical and Quantum Gravity* **37** (2019) 013002.

[30] L. Bombelli, J. Lee, D. Meyer and R. D. Sorkin, *Space-time as a causal set*, *Physical review letters* **59** (1987) 521.

[31] M. Planck, *über eine verbesserung der wienschen spektralgleichung*, *Verhandl. Dtsc. Phys. Ges.* **2** (1900) 202.

[32] J. F. Donoghue, *General relativity as an effective field theory: The leading quantum corrections*, *Physical Review D* **50** (1994) 3874.

[33] C. P. Burgess, *An introduction to effective field theory*, *Annu. Rev. Nucl. Part. Sci.* **57** (2007) 329–362.

[34] J. Polchinski, *String Theory*. Cambridge University Press, Oct., 1998, 10.1017/cbo9780511816079.

[35] M. B. Green, J. H. Schwarz and E. Witten, *Superstring Theory: 25th Anniversary Edition*. Cambridge University Press, July, 2012, 10.1017/cbo9781139248563.

[36] P. Fayet and S. Ferrara, *Supersymmetry*, *Physics Reports* **32** (Sept., 1977) 249–334.

[37] E. Witten, *Search for a realistic kaluza-klein theory*, *Nuclear Physics B* **186** (Aug., 1981) 412–428.

[38] E. Witten, *Dynamical breaking of supersymmetry*, *Nuclear Physics B* **188** (Oct., 1981) 513–554.

[39] M. R. Douglas, *The statistics of string/m theory vacua*, *Journal of High Energy Physics* **2003** (May, 2003) 046–046.

[40] S. K. Ashok and M. R. Douglas, *Counting flux vacua*, *Journal of High Energy Physics* **2004** (Jan., 2004) 060–060.

[41] G. Obied, H. Ooguri, L. Spodyneiko and C. Vafa, *De Sitter Space and the Swampland*, 1806.08362.

[42] U. H. Danielsson and T. Van Riet, *What if string theory has no de Sitter vacua?*, *Int. J. Mod. Phys. D* **27** (2018) 1830007, [1804.01120].

[43] J. M. Maldacena, *The Large N limit of superconformal field theories and supergravity*, *Int. J. Theor. Phys.* **38** (1999) 1113–1133, [hep-th/9711200].

[44] P. Di Francesco, P. Mathieu and D. Sénéchal, *Conformal Field Theory*. Springer New York, 1997, 10.1007/978-1-4612-2256-9.

[45] E. Witten, *Anti-de Sitter space and holography*, *Adv. Theor. Math. Phys.* **2** (1998) 253–291, [hep-th/9802150].

[46] S. S. Gubser, I. R. Klebanov and A. M. Polyakov, *Gauge theory correlators from noncritical string theory*, *Phys. Lett.* **B428** (1998) 105–114, [hep-th/9802109].

[47] O. Aharony, S. S. Gubser, J. M. Maldacena, H. Ooguri and Y. Oz, *Large N field theories, string theory and gravity*, *Phys. Rept.* **323** (2000) 183–386, [hep-th/9905111].

[48] M. Ammon and J. Erdmenger, *Gauge/gravity duality: Foundations and applications*. Cambridge University Press, 2015.

[49] I. Heemskerk, J. Penedones, J. Polchinski and J. Sully, *Holography from conformal field theory*, *Journal of High Energy Physics* **2009** (2009) 079.

[50] G. 't Hooft, *Dimensional reduction in quantum gravity*, *Conf. Proc. C* **930308** (1993) 284–296, [gr-qc/9310026].

[51] L. Susskind, *The world as a hologram*, *Journal of Mathematical Physics* **36** (Nov., 1995) 6377–6396.

[52] R. Bousso, *The holographic principle*, *Reviews of Modern Physics* **74** (Aug., 2002) 825–874.

[53] J. D. Bekenstein, *Black holes and the second law*, *Lettere Al Nuovo Cimento Series 2* **4** (Aug., 1972) 737–740.

[54] S. W. Hawking, *Particle creation by black holes*, *Communications In Mathematical Physics* **43** (Aug., 1975) 199–220.

[55] K. S. Thorne, *The Membrane Paradigm for Black-Hole Astrophysics*, p. 209–213. Springer US, 1987.

[56] M. Van Raamsdonk, *Cosmology from confinement?*, *JHEP* **03** (2022) 039, [2102.05057].

[57] R. P. Feynman and A. R. Hibbs, *Quantum mechanics and path integrals*. International series in pure and applied physics. McGraw-Hill, New York, NY, 1965.

[58] O. Aharony, S. S. Gubser, J. Maldacena, H. Ooguri and Y. Oz, *Large n field theories, string theory and gravity*, *Physics Reports* **323** (Jan., 2000) 183–386.

[59] P. van Nieuwenhuizen, *Supergravity*, *Physics Reports* **68** (Feb., 1981) 189–398.

[60] J. M. Maldacena, *Eternal black holes in anti-de Sitter*, *JHEP* **04** (2003) 021, [hep-th/0106112].

[61] S. Ryu and T. Takayanagi, *Holographic derivation of entanglement entropy from AdS/CFT*, *Phys. Rev. Lett.* **96** (2006) 181602, [hep-th/0603001].

[62] B. Swingle, *Entanglement Renormalization and Holography*, *Phys. Rev.* **D86** (2012) 065007, [0905.1317].

[63] M. Van Raamsdonk, *Comments on quantum gravity and entanglement*, 0907.2939.

[64] M. Van Raamsdonk, *Building up spacetime with quantum entanglement*, *Gen. Rel. Grav.* **42** (2010) 2323–2329, [1005.3035].

[65] J. Maldacena and L. Susskind, *Cool horizons for entangled black holes*, *Fortsch. Phys.* **61** (2013) 781–811, [1306.0533].

[66] M. Van Raamsdonk, *Lectures on Gravity and Entanglement*, in *Proceedings, Theoretical Advanced Study Institute in Elementary Particle Physics: New Frontiers in Fields and Strings (TASI 2015): Boulder, CO, USA, June 1-26, 2015*, pp. 297–351, 2017. 1609.00026. DOI.

[67] M. Van Raamsdonk, *Building up spacetime with quantum entanglement II: It from BC-bit*, 1809.01197.

[68] G. Penington, *Entanglement Wedge Reconstruction and the Information Paradox*, 1905.08255.

[69] A. Almheiri, N. Engelhardt, D. Marolf and H. Maxfield, *The entropy of bulk quantum fields and the entanglement wedge of an evaporating black hole*, 1905.08762.

[70] A. Almheiri, R. Mahajan and J. Maldacena, *Islands outside the horizon*, 1910.11077.

[71] H. Ooguri and T. Takayanagi, *Cobordism Conjecture in AdS, to appear*, .

[72] J. McNamara and C. Vafa, *Cobordism Classes and the Swampland*, 1909.10355.

[73] M. Oshikawa and I. Affleck, *Boundary conformal field theory approach to the critical two-dimensional Ising model with a defect line*, *Nucl. Phys. B* **495** (1997) 533–582, [cond-mat/9612187].

[74] P. Liendo, L. Rastelli and B. C. van Rees, *The Bootstrap Program for Boundary CFT_ d*, *JHEP* **07** (2013) 113, [1210.4258].

[75] I. Affleck and A. W. W. Ludwig, *Universal noninteger 'ground state degeneracy' in critical quantum systems*, *Phys. Rev. Lett.* **67** (1991) 161–164.

[76] T. Azeyanagi, A. Karch, T. Takayanagi and E. G. Thompson, *Holographic calculation of boundary entropy*, *JHEP* **03** (2008) 054, [0712.1850].

[77] J. Estes, K. Jensen, A. O'Bannon, E. Tsatis and T. Wrase, *On Holographic Defect Entropy*, *JHEP* **05** (2014) 084, [1403.6475].

[78] M. Chiodaroli, E. D'Hoker and M. Gutperle, *Simple Holographic Duals to Boundary CFTs*, *JHEP* **02** (2012) 005, [1111.6912].

[79] M. Chiodaroli, E. D'Hoker and M. Gutperle, *Holographic duals of Boundary CFTs*, *JHEP* **07** (2012) 177, [1205.5303].

[80] E. D'Hoker, J. Estes and M. Gutperle, *Exact half-BPS Type IIB interface solutions. I. Local solution and supersymmetric Janus*, *JHEP* **06** (2007) 021, [0705.0022].

[81] E. D'Hoker, J. Estes and M. Gutperle, *Exact half-BPS Type IIB interface solutions. II. Flux solutions and multi-Janus*, *JHEP* **06** (2007) 022, [0705.0024].

[82] O. Aharony, L. Berdichevsky, M. Berkooz and I. Shamir, *Near-horizon solutions for D3-branes ending on 5-branes*, *Phys. Rev.* **D84** (2011) 126003, [1106.1870].

[83] B. Assel, C. Bachas, J. Estes and J. Gomis, *Holographic Duals of D=3 N=4 Superconformal Field Theories*, *JHEP* **08** (2011) 087, [1106.4253].

[84] A. Karch and L. Randall, *Open and closed string interpretation of SUSY CFT's on branes with boundaries*, *JHEP* **06** (2001) 063, [hep-th/0105132].

[85] T. Takayanagi, *Holographic Dual of BCFT*, *Phys. Rev. Lett.* **107** (2011) 101602, [1105.5165].

[86] M. Fujita, T. Takayanagi and E. Tonni, *Aspects of AdS/BCFT*, *JHEP* **11** (2011) 043, [1108.5152].

[87] J. Erdmenger, M. Flory and M.-N. Newrzella, *Bending branes for DCFT in two dimensions*, *JHEP* **01** (2015) 058, [1410.7811].

[88] W. Israel, *Singular hypersurfaces and thin shells in general relativity*, *Il Nuovo Cimento B (1965-1970)* **44** (1966) 1–14.

[89] C. Bachas, S. Chapman, D. Ge and G. Policastro, *Energy Reflection and Transmission at 2D Holographic Interfaces*, *Phys. Rev. Lett.* **125** (2020) 231602, [2006.11333].

[90] T. Quella, I. Runkel and G. M. Watts, *Reflection and transmission for conformal defects*, *JHEP* **04** (2007) 095, [hep-th/0611296].

[91] M. Meineri, J. Penedones and A. Rousset, *Colliders and conformal interfaces*, *JHEP* **02** (2020) 138, [1904.10974].

[92] Z. Fu and D. Marolf, *Bag-of-gold spacetimes, euclidean wormholes, and inflation from domain walls in ads/cft*, *Journal of High Energy Physics* **2019** (2019) 40.

[93] P. Kraus, *Dynamics of anti-de Sitter domain walls*, *JHEP* **12** (1999) 011, [hep-th/9910149].

[94] L. Fidkowski, V. Hubeny, M. Kleban and S. Shenker, *The black hole singularity in AdS/CFT*, *JHEP* **02** (2004) 014, [hep-th/0306170].

[95] B. Freivogel, V. E. Hubeny, A. Maloney, R. C. Myers, M. Rangamani and S. Shenker, *Inflation in AdS/CFT*, *JHEP* **03** (2006) 007, [hep-th/0510046].

[96] M. Botta-Cantcheff, P. Martínez and G. A. Silva, *On excited states in real-time AdS/CFT*, *JHEP* **02** (2016) 171, [1512.07850].

[97] A. Christodoulou and K. Skenderis, *Holographic Construction of Excited CFT States*, *JHEP* **04** (2016) 096, [1602.02039].

[98] D. Marolf, O. Parrikar, C. Rabideau, A. Izadi Rad and M. Van Raamsdonk, *From Euclidean Sources to Lorentzian Spacetimes in Holographic Conformal Field Theories*, *JHEP* **06** (2018) 077, [1709.10101].

[99] J. L. Barbon and E. Rabinovici, *Holography of AdS vacuum bubbles*, *JHEP* **04** (2010) 123, [1003.4966].

[100] A. Hamilton, D. N. Kabat, G. Lifschytz and D. A. Lowe, *Local bulk operators in AdS/CFT: A Boundary view of horizons and locality*, *Phys. Rev. D* **73** (2006) 086003, [hep-th/0506118].

[101] A. Hamilton, D. N. Kabat, G. Lifschytz and D. A. Lowe, *Holographic representation of local bulk operators*, *Phys. Rev. D* **74** (2006) 066009, [hep-th/0606141].

[102] S. Cooper, M. Rozali, B. Swingle, M. Van Raamsdonk, C. Waddell and D. Wakeham, *Black hole microstate cosmology*, *Journal of High Energy Physics* **2019** (2019) 1–70.

[103] H.-C. Kim, H.-C. Tarazi and C. Vafa, *Four Dimensional $\mathcal{N} = 4$ SYM and the Swampland*, 1912.06144.

[104] R. Bousso and J. Polchinski, *Quantization of four form fluxes and dynamical neutralization of the cosmological constant*, *JHEP* **06** (2000) 006, [hep-th/0004134].

[105] D. Marolf, *Unitarity and Holography in Gravitational Physics*, *Phys. Rev. D* **79** (2009) 044010, [0808.2842].

[106] A. R. Brown, D. A. Roberts, L. Susskind, B. Swingle and Y. Zhao, *Complexity, action, and black holes*, *Phys. Rev. D* **93** (2016) 086006, [1512.04993].

[107] T. Banks and W. Fischler, *An Holographic cosmology*, hep-th/0111142.

[108] A. Strominger, *The dS / CFT correspondence*, *JHEP* **10** (2001) 034, [hep-th/0106113].

[109] M. Alishahiha, A. Karch, E. Silverstein and D. Tong, *The dS/dS correspondence*, *AIP Conf. Proc.* **743** (2004) 393–409, [hep-th/0407125].

[110] V. Gorbenko, E. Silverstein and G. Torroba, *dS/dS and $T\overline{T}$*, *JHEP* **03** (2019) 085, [1811.07965].

[111] E. Coleman, E. A. Mazenc, V. Shyam, E. Silverstein, R. M. Soni, G. Torroba et al., *de Sitter Microstates from $T\bar{T} + \Lambda_2$ and the Hawking-Page Transition*, 2110.14670.

[112] B. Freivogel, V. E. Hubeny, A. Maloney, R. C. Myers, M. Rangamani and S. Shenker, *Inflation in AdS/CFT*, *JHEP* **03** (2006) 007, [hep-th/0510046].

[113] P. McFadden and K. Skenderis, *Holography for Cosmology*, *Phys. Rev. D* **81** (2010) 021301, [0907.5542].

[114] S. Banerjee, U. Danielsson, G. Dibitetto, S. Giri and M. Schillo, *Emergent de Sitter Cosmology from Decaying Anti–de Sitter Space*, *Phys. Rev. Lett.* **121** (2018) 261301, [1807.01570].

[115] L. Susskind, *Black Holes Hint Towards De Sitter-Matrix Theory*, 2109.01322.

[116] T. Hertog and G. T. Horowitz, *Holographic description of AdS cosmologies*, *JHEP* **04** (2005) 005, [hep-th/0503071].

[117] C. Akers, N. Engelhardt, D. Harlow, G. Penington and S. Vardhan, *The black hole interior from non-isometric codes and complexity*, 2207.06536.

[118] Z. Fu and D. Marolf, *Bag-of-gold spacetimes, Euclidean wormholes, and inflation from domain walls in AdS/CFT*, *JHEP* **11** (2019) 040, [1909.02505].

[119] T. Anous, T. Hartman, A. Rovai and J. Sonner, *Black Hole Collapse in the 1/c Expansion*, *JHEP* **07** (2016) 123, [1603.04856].

[120] V. Balasubramanian, A. Lawrence, J. M. Magan and M. Sasieta, *Microscopic origin of the entropy of black holes in general relativity*, 2212.02447.

[121] A. R. Brown, H. Gharibyan, G. Penington and L. Susskind, *The Python's Lunch: geometric obstructions to decoding Hawking radiation*, *JHEP* **08** (2020) 121, [1912.00228].

[122] S. B. Giddings and A. Nudelman, *Gravitational collapse and its boundary description in ads*, *Journal of High Energy Physics* **2002** (2002) 003.

[123] X. Dong, D. Harlow and A. C. Wall, *Reconstruction of Bulk Operators within the Entanglement Wedge in Gauge-Gravity Duality*, *Phys. Rev. Lett.* **117** (2016) 021601.

[124] G. Penington, *Entanglement Wedge Reconstruction and the Information Paradox*, .

[125] A. Hamilton, D. N. Kabat, G. Lifschytz and D. A. Lowe, *Local bulk operators in AdS/CFT: A Boundary view of horizons and locality*, *Phys. Rev. D* **73** (2006) 086003.

[126] A. Hamilton, D. N. Kabat, G. Lifschytz and D. A. Lowe, *Holographic representation of local bulk operators*, *Phys. Rev. D* **74** (2006) 066009.

[127] N. Engelhardt, G. Penington and A. Shahbazi-Moghaddam, *A world without pythons would be so simple*, *Class. Quant. Grav.* **38** (2021) 234001, [2102.07774].

[128] A. Biasi, O. Evnin and S. Sypsas, *de sitter bubbles from anti–de sitter fluctuations*, *Phys. Rev. Lett.* **129** (Dec, 2022) 251104.

[129] M. Van Raamsdonk, *Spacetime from bits*, *Science* **370** (2020) 198–202.

[130] A. May and M. Van Raamsdonk, *Interpolating between multi-boundary wormholes and single-boundary geometries in holography*, *Journal of High Energy Physics* **2021** (2021) 1–37.

[131] S. Perlmutter, G. Aldering, G. Goldhaber, R. Knop, P. Nugent, P. G. Castro et al., *Measurements of ω and λ from 42 high-redshift supernovae*, *The Astrophysical Journal* **517** (1999) 565.

[132] A. G. Riess, A. V. Filippenko, P. Challis, A. Clocchiatti, A. Diercks, P. M. Garnavich et al., *Observational evidence from supernovae for an accelerating universe and a cosmological constant*, *The Astronomical Journal* **116** (1998) 1009.

[133] P. J. E. Peebles and B. Ratra, *Cosmology with a Time Variable Cosmological Constant*, *Astrophys. J. Lett.* **325** (1988) L17.

[134] B. Ratra and P. J. E. Peebles, *Cosmological Consequences of a Rolling Homogeneous Scalar Field*, *Phys. Rev. D* **37** (1988) 3406.

[135] R. R. Caldwell, R. Dave and P. J. Steinhardt, *Cosmological imprint of an energy component with general equation of state*, *Phys. Rev. Lett.* **80** (1998) 1582–1585, [astro-ph/9708069].

[136] K. Dutta, Ruchika, A. Roy, A. A. Sen and M. M. Sheikh-Jabbari, *Beyond ΛCDM with low and high redshift data: implications for dark energy*, *Gen. Rel. Grav.* **52** (2020) 15, [1808.06623].

[137] L. Visinelli, S. Vagnozzi and U. Danielsson, *Revisiting a negative cosmological constant from low-redshift data*, *Symmetry* **11** (2019) 1035, [1907.07953].

[138] A. A. Sen, S. A. Adil and S. Sen, *Do cosmological observations allow a negative λ?*, 2021.

[139] J. Hartle and S. Hawking, *Wave Function of the Universe*, *Adv. Ser. Astrophys. Cosmol.* **3** (1987) 174–189.

[140] J. M. Maldacena and L. Maoz, *Wormholes in AdS*, *JHEP* **02** (2004) 053, [hep-th/0401024].

[141] B. Freivogel, V. Godet, E. Morvan, J. F. Pedraza and A. Rotundo, *Lessons on Eternal Traversable Wormholes in AdS*, *JHEP* **07** (2019) 122, [1903.05732].

[142] P. Betzios, E. Kiritsis and O. Papadoulaki, *Euclidean Wormholes and Holography*, *JHEP* **06** (2019) 042, [1903.05658].

[143] P. Saad, S. H. Shenker and D. Stanford, *JT gravity as a matrix integral*, 1903.11115.

[144] D. Marolf and H. Maxfield, *Transcending the ensemble: baby universes, spacetime wormholes, and the order and disorder of black hole information*, 2002.08950.

[145] A. Maloney and E. Witten, *Averaging Over Narain Moduli Space*, 2006.04855.

[146] N. Afkhami-Jeddi, H. Cohn, T. Hartman and A. Tajdini, *Free partition functions and an averaged holographic duality*, *JHEP* **01** (2021) 130, [2006.04839].

[147] J. Cotler and K. Jensen, *AdS_3 gravity and random CFT*, 2006.08648.

[148] M. Van Raamsdonk, *Comments on wormholes, ensembles, and cosmology*, *JHEP* **12** (2021) 156, [2008.02259].

[149] M. Van Raamsdonk, *Evaporating Firewalls*, *JHEP* **11** (2014) 038, [1307.1796].

[150] G. Penington, *Entanglement Wedge Reconstruction and the Information Paradox*, 1905.08255.

[151] A. Almheiri, N. Engelhardt, D. Marolf and H. Maxfield, *The entropy of bulk quantum fields and the entanglement wedge of an evaporating black hole*, 1905.08762.

[152] S. Antonini and B. Swingle, *Cosmology at the end of the world*, *Nature Phys.* **16** (2020) 881–886, [1907.06667].

[153] S. Antonini and B. Swingle, *Holographic boundary states and dimensionally reduced braneworld spacetimes*, *Phys. Rev. D* **104** (2021) 046023, [2105.02912].

[154] Z. Wang, Z. Xu, S. Zhou and Y. Zhou, *Partial Reduction and Cosmology at Defect Brane*, 2112.13782.

[155] Z.-Y. Fan, *On holographic braneworld cosmology*, 2106.14376.

[156] A. Karch and L. Randall, *Localized gravity in string theory*, *Phys. Rev. Lett.* **87** (2001) 061601, [hep-th/0105108].

[157] T. Takayanagi, *Holographic dual of a boundary conformal field theory*, *Physical review letters* **107** (2011) 101602.

[158] M. Fujita, T. Takayanagi and E. Tonni, *Aspects of AdS/BCFT*, *JHEP* **11** (2011) 043, [1108.5152].

[159] I. Kourkoulou and J. Maldacena, *Pure states in the SYK model and nearly-AdS_2 gravity*, 1707.02325.

[160] A. Almheiri, *Holographic Quantum Error Correction and the Projected Black Hole Interior*, 1810.02055.

[161] G. Penington, S. H. Shenker, D. Stanford and Z. Yang, *Replica wormholes and the black hole interior*, *Journal of High Energy Physics* **2022** (2022) 1–87.

[162] X. Dong, X.-L. Qi, Z. Shangnan and Z. Yang, *Effective entropy of quantum fields coupled with gravity*, *Journal of High Energy Physics* **2020** (2020) 1–52.

[163] Y. Chen, V. Gorbenko and J. Maldacena, *Bra-ket wormholes in gravitationally prepared states*, *JHEP* **02** (2021) 009, [2007.16091].

[164] J. B. Hartle, S. W. Hawking and T. Hertog, *Accelerated expansion from negative λ*, 2012.

[165] L. Boyle, K. Finn and N. Turok, *C p t-symmetric universe*, *Physical review letters* **121** (2018) 251301.

[166] M. Demirtas, M. Kim, L. McAllister, J. Moritz and A. Rios-Tascon, *Exponentially Small Cosmological Constant in String Theory*, *Phys. Rev. Lett.* **128** (2022) 011602, [2107.09065].

[167] M. Demirtas, M. Kim, L. McAllister, J. Moritz and A. Rios-Tascon, *Small cosmological constants in string theory*, *JHEP* **12** (2021) 136, [2107.09064].

[168] P. Betzios, E. Kiritsis and O. Papadoulaki, *Interacting systems and wormholes*, *JHEP* **02** (2022) 126, [2110.14655].

[169] E. Antonyan, J. Harvey and D. Kutasov, *Chiral symmetry breaking from intersecting D-branes*, *Nucl. Phys. B* **784** (2007) 1–21, [hep-th/0608177].

[170] P. Gao, D. L. Jafferis and A. Wall, *Traversable Wormholes via a Double Trace Deformation*, *JHEP* **12** (2017) 151, [1608.05687].

[171] J. Maldacena and X.-L. Qi, *Eternal traversable wormhole*, 1804.00491.

[172] M. Van Raamsdonk, *Building up spacetime with quantum entanglement II: It from BC-bit*, 1809.01197.

[173] A. Karch and L. Randall, *Locally localized gravity*, *JHEP* **05** (2001) 008, [hep-th/0011156].

[174] D. Gaiotto and E. Witten, *S-Duality of Boundary Conditions In N=4 Super Yang-Mills Theory*, *Adv. Theor. Math. Phys.* **13** (2009) 721–896, [0807.3720].

[175] C. Bachas and I. Lavdas, *Massive Anti-de Sitter Gravity from String Theory*, *JHEP* **11** (2018) 003, [1807.00591].

[176] M. Van Raamsdonk and C. Waddell, *Finding $AdS^5 \times S^5$ in 2+1 dimensional SCFT physics*, *JHEP* **11** (2021) 145, [2109.04479].

[177] C. F. Uhlemann, *Islands and Page curves in 4d from Type IIB*, *JHEP* **08** (2021) 104, [2105.00008].

[178] M. Porrati, *Mass and gauge invariance 4. Holography for the Karch-Randall model*, *Phys. Rev. D* **65** (2002) 044015, [hep-th/0109017].

[179] T. Hartman, Y. Jiang and E. Shaghoulian, *Islands in cosmology*, 2008.01022.

[180] E. Witten, *Anti-de Sitter space, thermal phase transition, and confinement in gauge theories*, *Adv. Theor. Math. Phys.* **2** (1998) 505–532, [hep-th/9803131].

[181] D. Z. Freedman, S. S. Gubser, K. Pilch and N. P. Warner, *Renormalization group flows from holography–supersymmetry and a c-theorem*, hep-th/9904017.

[182] J. Louis and H. Triendl, *Maximally supersymmetric ads 4 vacua in n = 4 supergravity*, *Journal of High Energy Physics* **2014** (Oct, 2014) .

[183] P. Karndumri, *Holographic rg flows and symplectic deformations of n= 4 gauged supergravity*, *Physical Review D* **105** (2022) 086009.

[184] P. Breitenlohner and D. Z. Freedman, *Stability in gauged extended supergravity*, *Annals of physics* **144** (1982) 249–281.

[185] D. N. Page, *Will Entropy Decrease if the Universe Recollapses?*, *Phys. Rev. D* **32** (1985) 2496.

[186] M. Van Raamsdonk and C. Waddell, *Possible hints of decreasing dark energy from supernova data*, *arXiv preprint arXiv:2305.04946* (2023) .

[187] I. Affleck and M. Dine, *A New Mechanism for Baryogenesis*, *Nucl. Phys. B* **249** (1985) 361–380.

[188] S. M. Carroll, *Quintessence and the rest of the world: suppressing long-range interactions*, *Physical Review Letters* **81** (1998) 3067.

[189] L. Amendola, *Coupled quintessence*, *Physical Review D* **62** (2000) 043511.

[190] S. Fallows and S. F. Ross, *Islands and mixed states in closed universes*, *JHEP* **07** (2021) 022, [2103.14364].

[191] R. Bousso and E. Wildenhain, *Islands in closed and open universes*, 2022.

[192] H. B. Casimir, *On the attraction between two perfectly conducting plates*, *Proc. Kon. Ned. Akad. Wet.* **51** (1948) 793.

[193] G. Bressi, G. Carugno, R. Onofrio and G. Ruoso, *Measurement of the casimir force between parallel metallic surfaces*, *Physical Review Letters* **88** (Jan., 2002) .

[194] A. Zamolodchikov, *Irreversibility of the Flux of the Renormalization Group in a 2D Field Theory*, *JETP Lett.* **43** (1986) 730–732.

[195] D. L. Jafferis, I. R. Klebanov, S. S. Pufu and B. R. Safdi, *Towards the F-Theorem: N=2 Field Theories on the Three-Sphere*, *JHEP* **06** (2011) 102, [1103.1181].

[196] I. R. Klebanov, S. S. Pufu and B. R. Safdi, *F-Theorem without Supersymmetry*, *JHEP* **10** (2011) 038, [1105.4598].

[197] H. Casini and M. Huerta, *On the RG running of the entanglement entropy of a circle*, *Phys. Rev. D* **85** (2012) 125016, [1202.5650].

[198] J. L. Cardy, *Is There a c Theorem in Four-Dimensions?*, *Phys. Lett. B* **215** (1988) 749–752.

[199] Z. Komargodski and A. Schwimmer, *On Renormalization Group Flows in Four Dimensions*, *JHEP* **12** (2011) 099, [1107.3987].

[200] M. Nozaki, T. Takayanagi and T. Ugajin, *Central Charges for BCFTs and Holography*, *JHEP* **06** (2012) 066, [1205.1573].

[201] D. Gaiotto, *Boundary F-maximization*, 1403.8052.

[202] N. Kobayashi, T. Nishioka, Y. Sato and K. Watanabe, *Towards a C-theorem in defect CFT*, *JHEP* **01** (2019) 039, [1810.06995].

[203] S. Yamaguchi, *Holographic RG flow on the defect and g theorem*, *JHEP* **10** (2002) 002, [hep-th/0207171].

[204] G. T. Horowitz and R. C. Myers, *The AdS / CFT correspondence and a new positive energy conjecture for general relativity*, *Phys. Rev. D* **59** (1998) 026005, [hep-th/9808079].

[205] C. Bachas and V. Papadopoulos, *Phases of Holographic Interfaces*, 2101.12529.

[206] S. de Haro, S. N. Solodukhin and K. Skenderis, *Holographic reconstruction of space-time and renormalization in the AdS / CFT correspondence*, *Commun. Math. Phys.* **217** (2001) 595–622, [hep-th/0002230].

[207] I. Akal, Y. Kusuki, T. Takayanagi and Z. Wei, *Codimension two holography for wedges*, *Phys. Rev. D* **102** (2020) 126007, [2007.06800].

[208] M. Bordag, U. Mohideen and V. M. Mostepanenko, *New developments in the Casimir effect*, *Phys. Rept.* **353** (2001) 1–205, [quant-ph/0106045].

[209] J. Maldacena, D. Stanford and Z. Yang, *Diving into traversable wormholes*, *Fortsch. Phys.* **65** (2017) 1700034, [1704.05333].

[210] J. Maldacena, A. Milekhin and F. Popov, *Traversable wormholes in four dimensions*, 1807.04726.

[211] T. Sakai and S. Sugimoto, *Low energy hadron physics in holographic QCD*, *Prog. Theor. Phys.* **113** (2005) 843–882, [hep-th/0412141].

[212] B. M. Levitan and M. G. Gasymov, *Determination of a Differential Equation by Two of its Spectra*, *Russian Mathematical Surveys* **19** (Apr., 1964) R01.

[213] O. H. Hald, *The inverse Sturm-Liouville problem with symmetric potentials*, *Acta Mathematica* **141** (1978) 263 – 291.

[214] M. Kac, *Can one hear the shape of a drum?*, *The american mathematical monthly* **73** (1966) 1–23.

[215] T. Faulkner, M. Li and H. Wang, *A modular toolkit for bulk reconstruction*, *JHEP* **04** (2019) 119, [1806.10560].

[216] S. Ryu and T. Takayanagi, *Holographic derivation of entanglement entropy from the anti–de sitter space/conformal field theory correspondence*, *Physical review letters* **96** (2006) 181602.

[217] S. Antonini, P. Simidzija, B. Swingle and M. Van Raamsdonk, *Cosmology from the vacuum*, 2203.11220.

[218] A. Almheiri, A. Mousatov and M. Shyani, *Escaping the Interiors of Pure Boundary-State Black Holes*, 1803.04434.

[219] S. Fallows and S. F. Ross, *Constraints on cosmologies inside black holes*, 2203.02523.

[220] C. Waddell, *Bottom-up holographic models for cosmology*, 2203.03096.

[221] I. S. Gradshteyn and I. M. Ryzhik, *Table of integrals, series, and products*. Academic press, 2014.

[222] P. Breitenlohner and D. Z. Freedman, *Positive energy in anti-de sitter backgrounds and gauged extended supergravity*, *Physics letters B* **115** (1982) 197–201.

[223] S. Antonini, P. Simidzija, B. Swingle and M. Van Raamsdonk, *Cosmology as a holographic wormhole*, 2206.14821.

[224] S. Bilson, *Extracting Spacetimes using the AdS/CFT Conjecture: Part II*, *JHEP* **02** (2011) 050, [1012.1812].

[225] T. Hartman and J. Maldacena, *Time evolution of entanglement entropy from black hole interiors*, *Journal of High Energy Physics* **2013** (2013) , [1303.1080].

[226] B. McInnes, *Answering a basic objection to bang / crunch holography*, *JHEP* **10** (2004) 018, [hep-th/0407189].

[227] R. Cardenas, T. Gonzalez, Y. Leiva, O. Martin and I. Quiros, *A model of the universe including dark energy accounted for by both a quintessence field and a (negative) cosmological constant*, *Phys. Rev. D* **67** (2003) 083501, [astro-ph/0206315].

[228] H. Ooguri and C. Vafa, *Non-supersymmetric AdS and the Swampland*, *Adv. Theor. Math. Phys.* **21** (2017) 1787–1801, [1610.01533].

[229] M. Van Raamsdonk and C. Waddell, *Possible hints of decreasing dark energy from supernova data*, 2305.04946.

[230] E. Di Valentino, O. Mena, S. Pan, L. Visinelli, W. Yang, A. Melchiorri et al., *In the realm of the Hubble tension—a review of solutions*, *Class. Quant. Grav.* **38** (2021) 153001, [2103.01183].

[231] S. Antonini, P. Simidzija, B. Swingle and M. Van Raamsdonk, *Cosmology from the vacuum*, 2203.11220.

[232] S. Antonini, P. Simidzija, B. Swingle and M. Van Raamsdonk, *Cosmology as a holographic wormhole*, 2206.14821.

[233] S. K. Garg and C. Krishnan, *Bounds on Slow Roll and the de Sitter Swampland*, *JHEP* **11** (2019) 075, [1807.05193].

[234] H. Ooguri, E. Palti, G. Shiu and C. Vafa, *Distance and de Sitter Conjectures on the Swampland*, *Phys. Lett. B* **788** (2019) 180–184, [1810.05506].

[235] S. de Alwis, J. Louis, L. McAllister, H. Triendl and A. Westphal, *Moduli spaces in AdS_4 supergravity*, *JHEP* **05** (2014) 102, [1312.5659].

[236] E. Di Valentino, O. Mena, S. Pan, L. Visinelli, W. Yang, A. Melchiorri et al., *In the realm of the hubble tension—a review of solutions*, *Classical and Quantum Gravity* **38** (2021) 153001.

[237] G. J. Galloway, K. Schleich, D. M. Witt and E. Woolgar, *Topological censorship and higher genus black holes*, *Phys. Rev. D* **60** (1999) 104039, [gr-qc/9902061].

[238] D. Colton, *The confluent hypergeometric function. by herbert buchholz. springer-verlag, new york (1969). 238 pp.*, *Canadian Mathematical Bulletin* **13** (1970) 164–164.

Appendix A

Solving the junction conditions

We will derive the expression

$$f_1 \frac{dt_1}{ds} + f_2 \frac{dt_2}{ds} = \kappa r \tag{A.1}$$

starting from the second junction condition

$$K_{1ab} - K_{2ab} = \kappa h_{ab}. \tag{A.2}$$

First, we denote the proper velocity of a particle in the domain wall in the coordinates (t_i, r) as $u^a = (\dot{t}_i, \dot{r}) = (dt_i/ds, dr/ds)$, where we are suppressing the angular components which vanish by spherical symmetry. In Euclidean signature $u^a u_a = 1$ and thus

$$f_i \left(\frac{dt_i}{ds}\right)^2 + \frac{1}{f_i}\left(\frac{dr}{ds}\right)^2 = 1\ . \tag{A.3}$$

The normal to the domain wall, n^a, satisfies $u^a n_a = 0$ and $n^a n_a = 1$. We can easily confirm that $n_a = (-\dot{r}, \dot{t}_i)$ fulfills these requirements. Our choice of sign for n_a is consistent with our convention that this vector points from region 1 into region 2.

Next let us compute the $K_{1\theta\theta} = n_{\theta;\theta}$. Since $n_\theta = 0$ we have

$$K_{1\theta\theta} = -\Gamma^i_{\theta\theta} n_i = -\Gamma^r_{\theta\theta} n_r = r f_1(r) \frac{dt_1}{ds} \tag{A.4}$$

Similarly $K_{2\theta\theta} = -n_{\theta;\theta}$ gives

$$K_{1\theta\theta} = -r f_2(r) \frac{t_2}{ds}, \tag{A.5}$$

where the minus sign arises because the extrinsic curvature is defined using an outward facing normal. Substituting these expressions into the $\theta\theta$ component of (A.2) gives (A.1), as desired. Note that all other angular components of (A.2) lead to the same equation.

Appendix B

Interface trajectories in $D = 3$

For an interface of tension κ between a region with parameters λ_1, μ_1 and parameters λ_2, μ_2, the interface trajectory is determined by

$$\left(\frac{dr}{ds}\right)^2 = V_{eff} \tag{B.1}$$

with

$$V_{eff} = 1 + \lambda_1 r^2 - \mu_1 - \left[\frac{(\lambda_2 - \lambda_1 - \kappa^2)}{2\kappa} r - \frac{\mu_2 - \mu_1}{2\kappa r}\right]^2 . \tag{B.2}$$

The interface reaches a minimum value r_0 where $V_{eff}(r_0) = 0$. We have

$$r_0 = \frac{|\Delta\mu|}{\sqrt{2\kappa^2(1-\mu_1)+(\Delta\lambda-\kappa^2)(\Delta\mu)+2\sqrt{(1-\mu_1)^2\kappa^4+(1-\mu_1)(\Delta\lambda-\kappa^2)\kappa^2\Delta\mu+\kappa^2\lambda_1\Delta\mu^2}}} \tag{B.3}$$

where $\Delta\mu = \mu_2 - \mu_1$ and $\Delta\lambda = \lambda_2 - \lambda_1$.

The trajectories in the λ_1 and λ_2 regions are respectively

$$\begin{aligned} \frac{dt_1}{dr} &= \frac{1}{f_1\sqrt{V_{eff}}}\left(\frac{1}{2\kappa r}(f_1 - f_2) + \frac{1}{2}\kappa r\right) \\ \frac{dt_2}{dr} &= -\frac{1}{f_2\sqrt{V_{eff}}}\left(\frac{1}{2\kappa r}(f_2 - f_1) + \frac{1}{2}\kappa r\right) , \end{aligned} \tag{B.4}$$

where $f_i = 1 + \lambda_i r^2 - \mu_i$. We find that

$$\Delta t_2 \equiv t_2(\infty) - t_2(r_0) = \Delta(\lambda_1, \lambda_2, \mu_1, \mu_2, \kappa) \qquad \Delta t_1 \equiv t_1(\infty) - t_1(r_0) = -\Delta(\lambda_2, \lambda_1, \mu_2, \mu_1, \kappa) \tag{B.5}$$

where

$$\Delta(\lambda_1, \lambda_2, \mu_1, \mu_2, \kappa) = C(K(z) + C_\Pi \Pi(\nu, z)) . \tag{B.6}$$

Here, Π and K are elliptic integral functions defined as

$$\Pi(\nu, z) = \int_0^1 \frac{dt}{(1-\nu t^2)\sqrt{(1-t^2)(1-z^2t^2)}} \qquad K(z) = \Pi(0, z) \tag{B.7}$$

and the the parameters in (B.6) are defined as

$$\begin{aligned} z &= \sqrt{\frac{(\mu_2-\mu_1)^2}{(\mu_2-\mu_1)^2 + 4r_0^4\kappa^2 A}} \qquad \nu = \frac{1-\mu_2}{1-\mu_2+\lambda_2 r_0^2} \\ C &= z r_0 \frac{1}{1-\mu_2}\mathrm{sign}(\mu_2-\mu_1) \qquad C_\Pi = \frac{[(1-\mu_1)\lambda_2 + (1-\mu_2)(\kappa^2-\lambda_1)]r_0^2\nu}{(1-\mu_2)(\mu_1-\mu_2)} \end{aligned} \tag{B.8}$$

The parameter A is defined in (3.29).

For $\mu_1 = 0$ and $\mu_2 = \mu$ these results reduce to those in section 3.4.3.

B.1 Large μ

Continuing to take $\mu_1 = 0$ and $\mu_2 = \mu$, starting from equation (B.5) we find that in the limit of large μ, we have

$$\Delta t_1 = \sqrt{\frac{\kappa}{\mu}} \left(K(z_\infty) - \frac{\pi}{2} z_\infty^2 \, {}_2F_1\left(\frac{1}{2}, \frac{3}{2}; 2|z_\infty^2\right)\right) \tag{B.9}$$

and

$$\Delta t_2 = -\frac{1}{\sqrt{\kappa\mu}} \left(K(z_\infty) + \frac{\kappa+1}{\kappa-1} \Pi\left(1 - \frac{\lambda_2}{(\kappa-1)^2}, z_\infty\right)\right) \tag{B.10}$$

where

$$z_\infty = \sqrt{\frac{\lambda_2 - (\kappa-1)^2}{4\kappa}} \, . \tag{B.11}$$

Here, we have used that for small ν,

$$\Pi(\nu, z) = K(z) + \frac{\pi}{4}\nu \, {}_2F_1\left(\frac{1}{2}, \frac{3}{2}; 2|z^2\right) + \mathcal{O}(\nu^2) \tag{B.12}$$

Appendix C

Comparing on shell actions

For some CFT parameter values there are multiple bulk geometries consistent with the given CFT data. In this case, the geometry that describes the CFT in the semiclassical limit is the one with the lowest value of the Euclidean action.

Recall that the Euclidean action for a domain wall solution is given by:

$$\mathcal{I} = -\frac{1}{16\pi G_D}\Bigg[\int_{\mathcal{M}_1} d^D x\sqrt{g_1}\,(R_1 - 2\Lambda_1) + \int_{\mathcal{M}_2} d^D x\sqrt{g_2}\,(R_2 - 2\Lambda_2) + 2\int_{\mathcal{S}} d^{D-1}y\sqrt{h}(K_1 - K_2) - 2(D-2)\int_{\mathcal{S}} d^{D-1}y\sqrt{h}\kappa\Bigg], \tag{C.1}$$

where we have used $\kappa \equiv 8\pi G_D T/(D-2)$. Taking the trace of the Einstein equation gives

$$R_i = \frac{2D}{D-2}\Lambda_i, \tag{C.2}$$

for $i \in \{1, 2\}$, and taking the trace of the second junction condition, Eq. (3.8) gives

$$K_1 - K_2 = (D-1)\kappa. \tag{C.3}$$

The on shell Euclidean action thus simplifies to

$$\mathcal{I} = -\frac{1}{8\pi G_D}\left[\frac{2\Lambda_1}{D-2}\int_{\mathcal{M}_1} d^D x\sqrt{g_1} + \frac{2\Lambda_2}{D-2}\int_{\mathcal{M}_2} d^D x\sqrt{g_2} + \kappa\int_{\mathcal{S}} d^{D-1}y\sqrt{h}\right]. \tag{C.4}$$

The volume element in region $\mathcal{M}_1$ is

$$d^D x\sqrt{g_i} = r^{D-2}dt_i dr d\Omega_{D-2}, \tag{C.5}$$

where $d\Omega_{D-2}$ is the volume element on S^{D-2}. Parametrizing the domain wall by $t_i = t_i(r)$, we find that the volume element on the domain wall is given by

$$d^{D-1}y\sqrt{h} = r^{D-2}\sqrt{f_i(r)\left(\frac{dt_i}{dr}\right)^2 + \frac{1}{f_i(r)}}\,dr d\Omega_{D-2}. \tag{C.6}$$

Note that the proper time τ for a particle on the domain wall at constant angular coordinates is given by $d\tau^2 = f_i(r)dt_i^2 + dr^2/f_i(r)$. Combining this with the equation of motion (3.27) of the domain wall gives

$$\left(\frac{dt_i}{dr}\right)^2 = \frac{\alpha_i^2(r)}{f_i^2(r)V_{\text{eff}}(r)}, \tag{C.7}$$

and hence the volume element on the domain wall $\mathcal{S}$ is

$$d^{D-1}y\sqrt{h} = \frac{r^{D-2}}{\sqrt{V_{\text{eff}}(r)}}dr d\Omega_{D-2}. \tag{C.8}$$

Using Eqs. (C.5) and (C.8) in the on shell Euclidean action (C.4) and performing the integral over S^{D-2} gives

$$\mathcal{I} = -\frac{\text{Vol}\left(S^{D-2}\right)}{8\pi G_D}\left[\frac{2\Lambda_1}{D-2}\int_{\mathcal{M}_1} r^{D-2}dt_1dr + \frac{2\Lambda_2}{D-2}\int_{\mathcal{M}_2} r^{D-2}dt_2dr + \kappa\int_{\mathcal{S}}\frac{r^{D-2}}{\sqrt{V_{\text{eff}}(r)}}dr\right], \quad \text{(C.9)}$$

where $\text{Vol}\left(S^{D-2}\right)$ is the volume of S^{D-2}. Note that the integrals $\int_{\mathcal{M}_i}$ are now just in the $t_i - r$ plane, while the integral $\int_{\mathcal{S}}$ is just over r. The bounds on these integrals depend on which domain wall geometry we are considering.

C.1 Simplifications in D = 3

Starting from the expression (C.4) for the action and specializing to $D = 3$, we have that

$$\begin{aligned} 4G_3\mathcal{I} &= \int_{\mathcal{M}_1} d\omega_1 + \int_{\mathcal{M}_2} d\omega_2 - \kappa\int_{\mathcal{S}} rd\tau \\ &= \int_{\partial\mathcal{M}_1}\omega_1 + \int_{\partial\mathcal{M}_2}\omega_2 - \kappa\int_{\mathcal{S}} rd\tau \end{aligned} \quad \text{(C.10)}$$

where we are now considering $\mathcal{M}_i$ as regions on the two-dimensional $r - t_i$ plane and we have defined the one-forms

$$\omega_i = \lambda_i r^2 dt_i\ . \quad \text{(C.11)}$$

The non-vanishing contributions to the integral are those corresponding to the cutoff surface, the domain wall, and (in cases $IIA-$ and $IIB-$) the horizon $r = r_{\text{H}}$. In all cases, the contribution from the cutoff surfaces in $\mathcal{M}_1$ and $\mathcal{M}_2$ give

$$4G_3\mathcal{I}_{cutoff} = r_{max}^2 t_{max} \quad \text{(C.12)}$$

up to corrections which vanish in the limit $r_{max} \to \infty$.[99]

To express the contribution from the domain wall $\mathcal{S}$, we can combine the three contributions at the interface into the single integral

$$4G_3\mathcal{I}_{\mathcal{S}} = \int_{\mathcal{S}}(\lambda_1 r^2 dt_1 - \lambda_2 r^2 dt_2 - \kappa r d\tau). \quad \text{(C.13)}$$

Here we are integrating along the direction of increasing r, and so the sign of the second term is changed relative to Eq. (C.10), which required integrating in the opposite direction. To simplify this, we note that $\alpha_i = f_i dt_i/d\tau$, so the second junction condition can be written as

$$f_1 dt_1 - f_2 dt_2 = \kappa r d\tau \quad \text{(C.14)}$$

where τ is taken to increase in the direction of increasing r. Using $f_i = 1 - \mu_i + \lambda_i r^2$, we have that

$$4G_3\mathcal{I}_{\mathcal{S}} = \int_{\mathcal{S}}(-dt_1 + (1-\mu)dt_2) = (1-\mu)\Delta t_2 - \Delta t_1. \quad \text{(C.15)}$$

Here, Δt represents the change in t from the minimum r location on the interface to the asymptotic boundary.[100]

[99] Here, we are taking the asymptotic time coordinate to run from 0 to $S/2$ in the $\lambda = \lambda_1$ region and $S/2$ to t_{max} in the $\lambda = \lambda_2$ region. The result including corrections is $r_{max}^2 t_{max} - t_2(r_{max}) + t_1(r_{max})$.

[100] More precisely, it is the change going to the cutoff surface, but the difference goes to zero when the cutoff surface is taken to infinity.

Finally, in cases where the interior regions includes a Euclidean horizon, we have a contribution

$$4G_3\mathcal{I}_{horizon} = -\lambda_2 r_{\text{H}}^2\beta/2 = (1-\mu)\beta/2. \tag{C.16}$$

Here and above, we are calculating the action only in the region $t \geq 0$. The action in region $t \leq 0$ is equal by symmetry.

In summary, for AdS geometries, the regulated action is

$$4G_3\mathcal{I}^{reg}_{\text{AdS}} = \Delta t_2 - \Delta t_1 \tag{C.17}$$

while for black hole geometries, the regulated action is

$$4G_3\mathcal{I}^{reg}_{BH} = (1-\mu)\frac{S}{2\sqrt{\lambda_2}} - \Delta t_1 \tag{C.18}$$

In this expression, we have used that $S/2 = \sqrt{\lambda_2}\Delta t_2$ in black hole exterior solutions with no horizon, while $S/2 = \sqrt{\lambda_2}(\Delta t_2 + \beta/2)$ in exterior solutions with a horizon.

Appendix D

Cosmological equations in conformal coordinates

For some applications, it is useful to consider the evolution equations that determine the background cosmology and wormhole spacetimes in conformal coordinates in which the metric is a scaled version of Minkowski space.

Background geometry and stress-energy tensor: conformal time

In the cosmology picture, the background metric with conformal time is

$$ds^2 = \hat{a}^2(\eta)(-d\eta^2 + dw^2 + dx_i dx_i) \ . \tag{D.1}$$

Here $\hat{a}(\eta) = a(t)$ and t and η are related by $d\eta/dt = a^{-1}(t)$. In these coordinates, the stress-energy tensor is

$$T^{\eta\eta} = \frac{1}{\hat{a}^2(\eta)}\hat{\rho}(\eta) \qquad T^{ij} = \frac{1}{\hat{a}^2(\eta)}\delta^{ij}\hat{p}(\eta) \qquad T^{ww} = \frac{1}{\hat{a}^2(\eta)}\hat{p}(\eta) \tag{D.2}$$

where $\hat{\rho}(\eta) = \rho(t)$ and $\hat{p}(\eta) = p(t)$.

In these coordinates the Friedmann equation gives

$$\frac{1}{\hat{a}^4}\left(\frac{d\hat{a}}{d\eta}\right)^2 + \frac{1}{L^2} = \frac{8\pi G}{3}\hat{\rho} \tag{D.3}$$

and the conservation equation is

$$\dot{\hat{\rho}} = -\frac{3}{\hat{a}}\frac{d\hat{a}}{d\eta}(\hat{\rho} + \hat{p}) \tag{D.4}$$

Wormhole picture: conformal distance coordinates

It will also be convenient to describe the wormhole in terms of a conformal distance coordinate z, in terms of which the metric is

$$ds^2 = \hat{a}_E^2(z)(dz^2 - d\zeta^2 + dx_i dx_i) \ . \tag{D.5}$$

The scale factor $\hat{a}_E(z)$ is related to $\hat{a}(\eta)$ by analytic continuation $\eta^2 \leftrightarrow -z^2$.

In these coordinates, the range of z is finite, $z \in [-z_0, z_0]$. The coordinate locations $\pm z_0$ correspond to the asymptotically AdS boundaries; the scale factor $\hat{a}_E(z)$ has simple poles at these locations.

The stress-energy tensor in this picture is

$$T^{zz} = -\frac{1}{\hat{a}_E^2(z)}\hat{\rho}_E(z) \qquad T^{\zeta\zeta} = -\frac{1}{\hat{a}_E^2(z)}\hat{p}_E(z) \qquad T^{ij} = \frac{1}{\hat{a}_E^2(z)}\delta^{ij}\hat{p}_E(z) \tag{D.6}$$

where $\hat{\rho}_E$ and $\hat{p}_E$ are related to ρ and p by analytic continuation $\eta^2 \leftrightarrow -z^2$.

The analog of the Friedmann equation in this picture is

$$-\frac{1}{\hat{a}_E^4}\left(\frac{d\hat{a}_E}{dz}\right)^2+\frac{1}{L^2}=\frac{8\pi G}{3}\hat{\rho}_E \tag{D.7}$$

and the conservation equation is

$$\frac{d\hat{\rho}_E}{dz}=-\frac{3}{\hat{a}_E}\frac{d\hat{a}_E}{dz}(\hat{\rho}_E+\hat{p}_E). \tag{D.8}$$

Appendix E

Requirement of negative integrated null energy in the wormhole picture

The requirement of negative null energy at the midpoint of the wormhole can be extended to a requirement for integrated null energy between the two asymptotically AdS boundaries [237].

Considering the expression

$$N \equiv 8\pi G \int d\lambda T_{\mu\nu} \frac{dx^\mu}{d\lambda} \frac{dx^\nu}{d\lambda} \, . \tag{E.1}$$

and taking $x(\lambda)$ to be a null geodesic between the two asymptotically AdS boundaries with λ the affine parameter, we find

$$N = 8\pi G \int \frac{dz}{\hat{a}_E^2(z)} T_{++}(z) = 8\pi G \int dz T^{--}(z) \, . \tag{E.2}$$

Using Einstein's equations, we have that

$$8\pi G T_{++} = R_{++} = 4 \left(\frac{\hat{a}_E'}{\hat{a}_E} \right)^2 - 2 \frac{\hat{a}_E''}{\hat{a}_E} \, . \tag{E.3}$$

Then we can check that

$$\begin{aligned} N &= 2 \int dz \left\{ \frac{d}{dz} \left[\frac{1}{\hat{a}_E} \frac{d}{dz} \frac{1}{a} \right] - \left[\frac{d}{dz} \frac{1}{\hat{a}_E} \right]^2 \right\} \\ &= - \int_{-z_0}^{z_0} dz \left[\frac{d}{dz} \frac{1}{\hat{a}_E} \right]^2 < 0 \, , \end{aligned} \tag{E.4}$$

where $\pm z_0$ are the locations of the two asymptotically AdS boundaries. Near these points, $1/\hat{a}_E(z)$ behaves as $C(z_0 \mp z)$, so the total derivative term in the first line term vanishes.

We conclude that the null energy integrated from one side of the wormhole to the other as in (E.1) must be negative. This is not possible for any ordinary matter satisfying the null energy condition, but it is possible for the vacuum energy of quantum fields, and this is the situation we are considering.

Appendix F

Other possible vacua for the CFT on $\mathbb{R}^{d-2,1} \times S^1$?

Since the non-perturbative gravitational theory dual to a CFT must include domain walls associated with allowed interfaces to other CFTs [1], an interesting possibility is that we could have Poincaré invariant states of a holographic CFT on $R^{d-2,1} \times S^1$ dual to a geometry with a domain wall, as shown in Figure F.1. This would include a region $r < r_0$ of the geometry (6.10) with AdS length L_1 glued into a region $r > r_0$ of the geometry (6.10) with AdS length L_2. For the interior geometry, the periodicity of the z direction must be (3.40) in order to avoid a conical singularity, but for the exterior geometry, we can have any period.

In this case, the extrinsic curvatures measured with respect to region i using a normal vector pointing towards the outer region are

$$K_{zz} = \frac{L_i^2}{2} \frac{\partial f_i}{\partial r} \sqrt{f_i(r)} \qquad K_{\mu\nu} = \eta_{\mu\nu} r \sqrt{f_i(r)} \,, \tag{F.1}$$

so the junction conditions (3.8) give

$$\begin{aligned} r\sqrt{f_1(r)} - r\sqrt{f_2(r)} &= \kappa r^2 \\ \frac{1}{\sqrt{f_1}} \frac{\partial f_1}{\partial r} - \frac{1}{\sqrt{f_2}} \frac{\partial f_2}{\partial r} &= 2\kappa \,. \end{aligned} \tag{F.2}$$

Thus, we can have a solution for some radius r_0 if $v(r_0) = v'(r_0) = 0$, where

$$v(r) \equiv \sqrt{f_1(r)} - \sqrt{f_2(r)} - \kappa r \,. \tag{F.3}$$

From $v(r_0) = 0$, we conclude that the tension must be related to r_0 and the parameters L_1 and L_2 by

$$\kappa = \frac{1}{r_0} \left(\sqrt{f_1} - \sqrt{f_2} \right) \,. \tag{F.4}$$

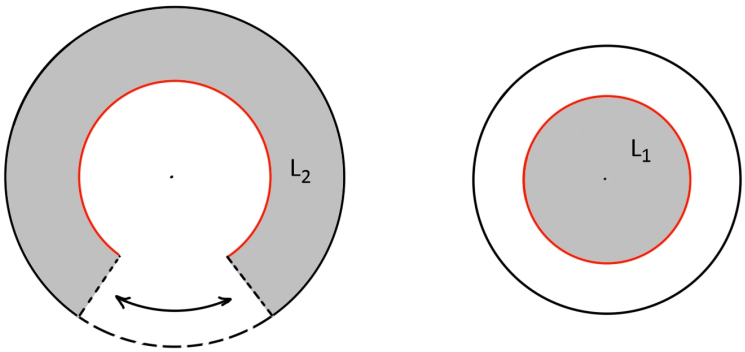

Figure F.1: Possible geometry dual to a CFT on $R^{d-2,1} \times S^1$ with an interior bubble described by a different low-energy effective theory.

The remaining equation gives

$$\frac{d}{dr}\left(\frac{\sqrt{f_1(r)}}{r} - \frac{\sqrt{f_2(r)}}{r}\right)\bigg|_{r=r_0} = 0 \tag{F.5}$$

Solving this, we find

$$r_0^d = \mu_1\mu_2 \frac{\mu_1 - \mu_2}{\left(\frac{\mu_1}{L_2}\right)^2 - \left(\frac{\mu_2}{L_1}\right)^2} \ . \tag{F.6}$$

We must have that r_0 is larger than the minimum value r_H (Equation 6.12) for each region. Defining as before $\mu = \mu_2/\mu_1$ and $u = L_2/L_1$, we must have one of the following options:

$$u > 1 \qquad \frac{1}{u^2} < \mu < \frac{1}{u} \qquad\qquad OR \qquad\qquad u < 1 \qquad \frac{1}{u} < \mu < \frac{1}{u^2} \tag{F.7}$$

From (F.4), we have that

$$\kappa L_1 = \frac{1}{u}\sqrt{\frac{1-\mu u^2}{\mu - 1}}\left(\frac{1}{\sqrt{\mu}} - \sqrt{\mu}\right) \tag{F.8}$$

so we have a positive tension domain wall only for the $u > 1$ case. Thus, the allowed region of parameter space for bubble solutions with positive tension domain walls is

$$u > 1 \qquad\qquad \frac{1}{u^2} < \mu < \frac{1}{u} \ . \tag{F.9}$$

We find that κ increases from 0 to κ_- as μ increases from $1/u^2$ to $1/u$. Thus, the tension is always less than the lower critical value κ_-. Therefore, these domain walls cannot reach the AdS boundary; they are not of the type that corresponds to an interface between two CFTs.

Assuming that such domain walls exist in some cases, we can still consider the energy associated with these solutions. To avoid a conical singularity, the periodicity of z_1 must be given by β_1 in (3.40). The proper distance around the domain wall must match in the inner and outer spacetimes, so the periodicity of z_2 must satisfy

$$L_2\sqrt{f_2}\Delta z_2 = L_1\sqrt{f_1}\beta_1 \ . \tag{F.10}$$

Finally, we have that the ratio of the periodicity of z_2 to the periodicity β_2 in the solution without an interface is

$$R = \frac{\Delta z_2}{\beta_2} = \frac{L_1\sqrt{f_1}\beta_1}{L_2\sqrt{f_2}\beta_2} = (\mu u^2)^{1/d-1} \ . \tag{F.11}$$

We recall that R^d gives the ratio of the energy density to that for the case where the bulk solution is just the usual AdS-soliton. So we would have a lower-energy vacuum if there are any cases with $R > 1$. But the constraints (F.9) imply that $\mu u^2 > 1$, so for positive tension branes, we only get $R < 1$.

We conclude that considering solutions with a bubble does not lead to a lower vacuum energy than we had from the AdS soliton solution.

We have also checked that these solutions are not perturbatively stable. Starting with one of the solutions, we consider keeping the outer geometry fixed while varying the r coordinate of the interface. We continue to impose the first junction condition so that the inner and outer regions join without a discontinuity in the metric. This requires that the parameter μ_1 be adjusted along with the interface radius in a particular way. Evaluating the action for the resulting off-shell configuration, we find that in all cases, our solution represents a local maximum as a function of the interface radius.

Appendix G

Derivation of the asymptotic spectrum

Consider the Schrödinger equation with the "test" potential

$$\tilde{V}(z) \equiv \frac{\alpha}{(z_0 - |z|)^2} + \frac{\beta}{z_0 - |z|} + c \tag{G.1}$$

The potential (G.1) is simple enough that we can explicitly compute the asymptotic form of its normalizable spectrum, $\tilde{\lambda}_j$. Indeed, a simple rescaling of z reduces the corresponding Schrödinger equation to a Whittaker's differential equation, whose solution is well known [238]. First, we note the basic result from Sturm-Liouville theory that since the potential $\tilde{V}(z)$ is even, the normalizable eigenfunctions alternate between even functions $(u_0, u_2, \dots)$ and odd functions $(u_1, u_3, \dots)$. Let us consider the odd eigenfunctions, which are defined, up to normalization, by the condition $u(0) = 0$. The solution to the Schrödinger equation with this "initial" condition at $z = 0$ can be obtained from the solution of the Whittaker's differential equation by an appropriate rescaling of z [238]. The general solution is given by the linear combination

$$u_{\text{odd}}(z, \tilde{\lambda}) = C_1 M_{x,\frac{\mu}{2}}\left(i2(z_0 - |z|)\sqrt{\tilde{\lambda} - c}\right) + C_2 M_{x,-\frac{\mu}{2}}\left(i2(z_0 - |z|)\sqrt{\tilde{\lambda} - c}\right) \tag{G.2}$$

where $M_{x,\frac{\mu}{2}}(y)$ is related to the confluent hypergeometric function of the first kind ${}_1F_1(a; b; y)$ by

$$M_{x,\frac{\mu}{2}}(y) = y^{\frac{1+\mu}{2}} \mathrm{e}^{-\frac{y}{2}} {}_1F_1\left(\frac{1+\mu}{2} - x; 1 + \mu; y\right) \tag{G.3}$$

and we identified

$$x = \frac{i\beta}{2\sqrt{\tilde{\lambda} - c}}; \qquad \mu = 2\bar{\Delta}; \qquad y = i2(z_0 - |z|)\sqrt{\tilde{\lambda} - c} \tag{G.4}$$

where $\bar{\Delta} = \sqrt{1 + 4\alpha}/2$. The first term in the linear combination (G.2) corresponds to the normalizable component of the eigenfunctions, while the second term is the non-normalizable component. Since we are interested in the normalizable spectrum of the potential (G.1), we set $C_2 = 0$.

Then the odd normalizable eigenvalues $\tilde{\lambda}_j$, $j = 1, 3, 5...$, are given by values of $\tilde{\lambda}$ that solve the odd condition $u_{odd}(0, \tilde{\lambda}_j) = 0$.[101] Since we are interested in the asymptotic spectrum, we want to look for solutions $\{\tilde{\lambda}_j\}$ of the odd condition with $\tilde{\lambda}_j \gg 1$. Therefore, we can set $z = 0$ and find the form of the normalizable eigenfunction (first term in equation (G.2)) in the limit of large $\tilde{\lambda}$. Defining $x = i\tau$, $y = i\zeta$ and assuming $\tau \in \mathbb{R}^+$, $\zeta \in \mathbb{R}\backslash\{0\}$, $\mu \in \mathbb{R}$, the function $M_{i\tau,\frac{\mu}{2}}(i\zeta)$ has the

[101] For $-1/4 < a < 0$ the non-normalizable modes also vanish at $z = z_0$. To avoid this difficulty, here we are assuming that $a > 0$. The results for the case $a < 0$ follow by analytic continuation.

following asymptotic expansion for large ζ [238]:

$$M_{i\tau,\frac{\mu}{2}}(i\zeta) \sim \frac{2\Gamma(1+\mu)\exp\left[\frac{\pi}{2}\left(\tau+i\frac{1+\mu}{2}\right)\right]\mathrm{sgn}(\zeta)}{\left|\Gamma\left(\frac{1+\mu}{2}\pm i\tau\right)\right|}\cdot$$

$$\left\{\cos\left[-\tau\log|\zeta|+\frac{\zeta}{2}+\delta-\frac{\pi}{4}(1+\mu)\mathrm{sgn}(\zeta)\right]\sum_{k=0}^{N}\frac{\left(\frac{\tau^2}{\zeta}\right)^k}{k!}\frac{\cos\left[\sum_{r=1}^{k}(\phi_r^{(+)}+\phi_r^{(-)})-\frac{\pi}{2}k\right]}{\prod_{r=1}^{k}\left(\sin\phi_r^{(+)}\sin\phi_r^{(-)}\right)}\right.$$

$$\left.-\sin\left[-\tau\log|\zeta|+\frac{\zeta}{2}+\delta-\frac{\pi}{4}(1+\mu)\mathrm{sgn}(\zeta)\right]\sum_{k=1}^{N}\frac{\left(\frac{\tau^2}{\zeta}\right)^k}{k!}\frac{\sin\left[\sum_{r=1}^{k}(\phi_r^{(+)}+\phi_r^{(-)})-\frac{\pi}{2}k\right]}{\prod_{r=1}^{k}\left(\sin\phi_r^{(+)}\sin\phi_r^{(-)}\right)}\right\} \tag{G.5}$$

where $\Gamma(x)$ is the Euler gamma function, and δ, $\phi_r^{(\pm)}$ are given by

$$\delta=-\frac{i}{2}\log\left[\frac{\Gamma\left(\frac{1+\mu}{2}+i\tau\right)}{\Gamma\left(\frac{1+\mu}{2}-i\tau\right)}\right];\qquad \tan\phi_r^{(\pm)}=\frac{\tau}{r+\frac{-1\pm\mu}{2}}. \tag{G.6}$$

Keeping only terms up to order $1/\sqrt{\tilde{\lambda}-c}$ in equation (G.5), we get (up to an irrelevant multiplicative factor)

$$\begin{aligned}M_{i\tau,\frac{\mu}{2}}(i\zeta)\sim&\cos\left[-\tau\log|\zeta|+\frac{\zeta}{2}+\delta-\frac{\pi}{4}(1+\mu)\mathrm{sgn}(\zeta)\right]\\&+\frac{1-\mu^2}{4\zeta}\sin\left[-\tau\log|\zeta|+\frac{\zeta}{2}+\delta-\frac{\pi}{4}(1+\mu)\mathrm{sgn}(\zeta)\right]+\mathcal{O}\left(\frac{1}{\tilde{\lambda}-c}\right).\end{aligned} \tag{G.7}$$

The discrete set of asymptotic odd eigenvalues $\{\tilde{\lambda}_j\}$ (for odd values of $j\gg 1$) we are looking for is determined by the zeros of equation (G.7). Using equation (G.4), such zeros are given by the $\tilde{\lambda}$'s satisfying

$$\begin{aligned}\sqrt{\tilde{\lambda}-c}=&-\frac{\alpha}{2z_0^2\sqrt{\tilde{\lambda}-c}}+\frac{\beta}{2z_0\sqrt{\tilde{\lambda}-c}}\log\left(2z_0\sqrt{\tilde{\lambda}-c}\right)+\frac{i}{2z_0}\log\left[\frac{\Gamma\left(\Delta_+-\frac{i\beta}{2\sqrt{\tilde{\lambda}-c}}\right)}{\Gamma\left(\Delta_+-\frac{i\beta}{2\sqrt{\tilde{\lambda}-c}}\right)}\right]\\&+\frac{\pi}{2z_0}(\Delta_++2n-1)\end{aligned} \tag{G.8}$$

with $\Delta_+=(1+2\bar{\Delta})/2$ and $n=1,2,3....$ Substituting the expansion ansatz

$$\sqrt{\tilde{\lambda}-c}=a_1n+a_2\log n+a_3+a_4\frac{\log n}{n}+\frac{a_5}{n}+\mathcal{O}\left(\frac{1}{n^2}\right) \tag{G.9}$$

into equation (G.8) and expanding the right hand side up to order $1/n$ yields the values of the $\{a_i\}_{i=1,\dots,5}$. Solving equation (G.9) for $\tilde{\lambda}$ and identifying $n=(j+1)/2$ with j odd, we finally obtain

the expression for the asymptotic spectrum:

$$\tilde{\lambda}_j \sim \left(\frac{\pi}{2z_0}\right)^2 j^2 + \left(\frac{\pi}{2z_0}\right)^2 2\Delta_+ j + \frac{\beta}{z_0}\log(j) + \left(\frac{\pi}{2z_0}\right)^2 \left(\Delta_+^2 - \frac{4\alpha}{\pi^2}\right) + \frac{\beta}{z_0}\left[\log(\pi) - \psi(\Delta_+)\right] + c, \tag{G.10}$$

where $\psi(x)$ is the digamma function. Although we have derived this expansion for j odd, it can immediately be extended also to even values of j, yielding the full asymptotic spectrum (7.33).

Appendix H

Proof of reconstruction lemma

Here we prove the lemma used in the reconstruction algorithm in Section 7.3.2.

Lemma 2. *For any L^2 integrable function $f(z)$ on $z \in (-z_0, z_0)$ the following identity holds:*

$$f(z) = \sum_{j=0}^{\infty} \frac{\tilde{v}_j(z) \int_{-z_0}^{z} dy\, u_j(y) f(y) + \tilde{u}_j(z) \int_{z}^{z_0} dy\, v_j(y) f(y)}{\omega'(\lambda_j)}. \tag{H.1}$$

Proof. Let $f(z)$ be an L^2 integrable function. We define

$$\Phi(z,\lambda) \equiv \frac{\tilde{v}(z,\lambda) \int_{-z_0}^{z} dy\, u(y,\lambda) f(y) + \tilde{u}(z,\lambda) \int_{z}^{z_0} dy\, v(y,\lambda) f(y)}{\omega(\lambda)}. \tag{H.2}$$

Notice that this is well-defined because $u(y,\lambda)$ is integrable at the left boundary, while $v(y,\lambda)$ is integrable at the right boundary. Now consider the contour integral

$$\frac{1}{2\pi i} \int_{\Gamma} d\lambda\, \Phi(z,\lambda), \tag{H.3}$$

where Γ is a large circle in the complex λ plane, whose radius we take to infinity. In this limit, we can evaluate the contour integral in two different ways. First, directly by the residue theorem we find

$$\frac{1}{2\pi i} \int_{\Gamma} d\lambda\, \Phi(z,\lambda) = \sum_{j=0}^{\infty} \frac{\tilde{v}_j(z) \int_{-z_0}^{z} dy\, u_j(y) f(y) + \tilde{u}_j(z) \int_{z}^{z_0} dy\, v_j(y) f(y)}{\omega'(\lambda_j)}, \tag{H.4}$$

where λ_j are eigenvalues of (7.26) with normalizable boundary conditions, and where we define $u_j(z) \equiv u(z,\lambda_j)$, $\tilde{u}_j(z) \equiv \tilde{u}(z,\lambda_j)$, and similarly for the vs.

Alternatively, we can evaluate the above contour integral by first going to the limit of large $|\lambda|$ (since we are taking the radius of the contour Γ to infinity) before using the residue theorem. As we discussed, in the limit $|\lambda| \to \infty$ we can effectively replace $V(z)$ with $\tilde{V}(z)$, and hence $u \to \tilde{u}$, $v \to \tilde{v}$ and $\omega(\lambda) \to \tilde{\omega}(\lambda) \equiv -\tilde{u}^{-}(z_0,\lambda)$. Using the residue theorem we thus obtain

$$\frac{1}{2\pi i} \int_{\Gamma} d\lambda\, \Phi(z,\lambda) = \sum_{j=0}^{\infty} \frac{\tilde{V}_j(z) \int_{-z_0}^{z} dy\, \tilde{U}_j(y) f(y) + \tilde{U}_j(z) \int_{z}^{z_0} dy\, \tilde{V}_j(y) f(y)}{\tilde{\omega}'(\tilde{\lambda}_j)}, \tag{H.5}$$

where $\tilde{U}_j$ and $\tilde{V}_j$ are solutions of the following initial value problems on $z \in (-z_0, z_0)$

$$\tilde{U}_j : \begin{cases} \tilde{U}_j''(z) = \left[\tilde{V}(z) - \tilde{\lambda}_j\right] \tilde{U}_j(z) \\ \tilde{U}_j^{(+)}(-z_0) = \frac{1}{2\tilde{\Delta}} \\ \tilde{U}_j^{(-)}(-z_0) = 0 \end{cases} \qquad \tilde{V}_j : \begin{cases} \tilde{V}_j''(z) = \left[\tilde{V}(z) - \tilde{\lambda}_j\right] v_j(z) \\ \tilde{V}_j^{(+)}(+z_0) = \frac{1}{2\tilde{\Delta}} \\ \tilde{V}_j^{(-)}(+z_0) = 0 \end{cases} . \tag{H.6}$$

Hence $\tilde{U}_j$ and $\tilde{V}_j$ must both be proportional to the j-th normalizable eigenfunction of $u''(z) = \big[\tilde{V}(z) - \lambda\big]u(z)$. Since $\tilde{V}(z)$ is $\mathbb{Z}_2$ symmetric, these eigenfunctions have a parity $(-1)^j$, and thus $\tilde{U}_j(z) = (-1)^j\tilde{V}_j(z)$. Additionally, by using the explicit form G.2 for the normalizable eigenfunctions, it can be verified by direct calculation that $\tilde{\omega}'(\tilde{\lambda}_j) = (-1)^j||U_j||^2$, where $||\cdot||^2$ denotes the L^2-norm, i.e. the norm associated with the Sturm-Liouville inner product. It was in order to obtain this identity that we chose the normalization factor $1/2\bar{\Delta}$ for the normalizable modes in Eqs. (7.42) and (7.43). Therefore (H.5) gives

$$\frac{1}{2\pi i}\int_\Gamma d\lambda\,\Phi(z,\lambda) = \sum_{j=0}^{\infty}\frac{\tilde{U}_j(z)\int_{-z_0}^{z_0} dy\,\tilde{U}_j(y)f(y)}{||U_j||^2}, \tag{H.7}$$

which is precisely the Sturm-Liouville expansion of $f(z)$. Comparing with (H.4) we obtain the identity

$$f(z) = \sum_{j=0}^{\infty}\frac{\tilde{v}_j(z)\int_{-z_0}^{z} dy\,u_j(y)f(y) + \tilde{u}_j(z)\int_{z}^{z_0} dy\,v_j(y)f(y)}{\omega'(\lambda_j)}, \tag{H.8}$$

which completes the proof. □

Appendix I

Details of the potential examples

I.1 Fine-tuning potentials with a flat region

In this appendix we explain how the parameters of potentials with a flat region of the form (8.14)-(8.15) must be chosen and fine-tuned to reproduce the ΛCDM cosmological evolution between the early Universe and the present day.

In order to have a phase of accelerated expansion in the cosmological evolution, the positive potential energy at the plateau (which is fixed by observational data to be $A = \Omega_\Lambda$) must be dominant over every other term on the right-hand side of the Friedmann equation. This implies that the scalar field's kinetic energy K_ϕ must be very small when the field reaches the plateau. Evolving backwards in time from the time-symmetric point $\tilde{t} = 0$ in the cosmology picture, the scalar field behaves like an anti-damped particle. Therefore, intuitively, an accelerated expansion can take place only if $|B| \ll |A|$ — where B sets the value of $V(0)$. In this way, for an appropriately fine-tuned potential, the scalar field just barely makes it up to the plateau and the kinetic energy does not become dominant until very close to the Big Bang (or Big Crunch, if we evolve forward in time from the time-symmetric point).

Next, we must require that the BF bound (8.5) is satisfied. This can be achieved by choosing the value of X to be large enough that the deep valleys are not too close to the maximum at $\phi = 0$, so that $(d^2\tilde{V}/d\phi^2)|_{\phi=0}$ is suppressed. However, X must not be too large, otherwise the cosmological evolution will reach the Big Bang singularity before the scalar field can reach the valleys (and then the plateau): in this case, no accelerated expansion phase occurs.

Moreover, the (negative) parameter C — which controls the depth of the valleys — must be large enough that the scalar field acquires sufficient kinetic energy in its anti-damped motion to reach the positive plateau. But it cannot be too large, or the kinetic energy will be large when the scalar reaches the plateau and no accelerated phase can take place. We remark that no particular fine-tuning has been carried out so far on the parameters: we just identified the general criteria to choose the parameters B, C and X in order for an accelerated expansion to be possible and for the BF bound to be satisfied (we remind that A is fixed by data). The specific choice of their values is arbitrary and irrelevant for the sake of reproducing the ΛCDM evolution.

Finally, we fine-tune the value of Δ[102] to allow the scalar field to reach the plateau with a very small kinetic energy. This yields a phase of accelerated expansion, and will allow us to reproduce the ΛCDM cosmological evolution between the early Universe and the present day.

Note that, as we evolve backwards in time towards the Big Bang, the scalar field's kinetic energy will eventually become dominant. Our goal is to reproduce as best as possible the results of the ΛCDM model, in which there is no such term in the Friedmann equation, between the early Universe and the present day. More precisely, an important criterion for the feasibility of these models is that we should not have a significant departure from ΛCDM between the present time and the time of Big Bang Nucleosynthesis (BBN) (which roughly occurs in the range of temperatures $T \sim 10^9 - 10^{10}$ K), otherwise the abundances of various elements could vary appreciably from those experimentally

[102] Note that we could have instead fixed a value of Δ and fine-tuned the parameter C.

observed. These temperatures correspond to scale factors which are between 10^{-9} and 10^{-10} times smaller than the current value of the scale factor $a(\tilde{t}_0) = 1$. We can therefore ask whether it is possible to tune our model with a rolling scalar such that the scalar field's kinetic energy is a subdominant contribution in the cosmological Friedmann equation for $10^{-10} \lesssim a(\tilde{t}) \leq 1$. In other words, we would like to determine whether the kinetic energy dominance can be pushed sufficiently early in time that it would not impact the predictions of BBN.

By appropriately fine-tuning the parameter Δ we were able to push the crossover between the early kinetic-energy-dominated era and the radiation-dominated era to $\tilde{t} = \tilde{t}^*$ with $\tilde{t}^* - \tilde{t}_{BB} = \mathcal{O}(10^{-13})$ (where $\tilde{t}_{BB}$ corresponds to the Big Bang) in our numerical solutions, corresponding to $a(\tilde{t}^*) = \mathcal{O}(10^{-7})$. We were not able to reach the desired value $a(\tilde{t}^*) = \mathcal{O}(10^{-10})$ because of numerical precision issues related to the excessively small time steps needed, but there is no a priori obstacle in pushing the kinetic-energy-dominated era arbitrarily close to the cosmological singularity.

By implementing this fine-tuning procedure after choosing the *Planck* 2018 cosmological parameters (8.16) and the initial condition $a_0 = 2$, we obtained the set of parameters (8.17) used in our numerical analysis. The same procedure was also used to fine-tune the potential for the solution employing SNIa-derived cosmological parameters depicted in Figure 8.7.

I.2 Scalar potential for wCDM model

For completeness, we provide some details related to the analysis in Section 8.2.4.

To construct a scalar potential $V(\phi)$ agreeing with $V_w(\phi)$ in a suitable region, permitting cosmological solutions which satisfy observational constraints from SNe Ia and have asymptotically AdS Euclidean continuations, we proceed as follows:

1. Determine the redshift dependence of the scalar field $\phi_w(z)$ and potential $V_w(z)$ for the given wCDM model,[103] in the region $z \in (z_{\min}, z_{\max})$ where type Ia supernova data have been used to constrain cosmological parameters. We have the freedom to choose the value $\phi_w(0) \equiv \phi_0$ and the sign of $\phi_w'(0)$; we will take both to be positive. Note however that the present scalar kinetic energy is fixed to
$$\frac{1}{2}\dot{\phi}_w(z=0)^2 = \frac{1}{8\pi G} H_0 H'(0) - \frac{3}{16\pi G} H_0^2 \Omega_M \equiv K_0 \,. \tag{I.1}$$

2. Evaluate $\phi_w(z)$ and $V_w(z)$ for a large sample $\{z_i\}$ of redshifts in the interval $(z_{\min}, z_{\max})$, to obtain an array of pairs $\{(\phi_w^{(i)}, V_w^{(i)})\}$.

3. Choose a model $V(\phi; \{p\}, q)$, with parameters $\{p\}$ and q, satisfying:

   - $V(0; \{p\}, q) < 0$
   - $-\frac{9}{4} < \frac{V''(0;\{p\},q)}{|V(0;\{p\},q)|} < 0$
   - $V(\phi; \{p\}, q)$ behaves as a polynomial for $\phi \gtrsim \phi(z=0)$.

   In our case, the model has a Gaussian trough between $\phi = 0$ and $\phi = \phi_0$, with a height controlled by the parameter q.

[103] The Hubble expansion $H(z)$ for the wCDM model is given in equation (8.19), using the parameters recorded in Section 8.2.4. The redshift dependence of the scalar $\phi(z)$ and potential $V(z)$ may then be computed from $H(z)$ using equation (I.2).

4. Apply the "shooting method" to determine parameters $\{p\}$ and q for which the model has a time-symmetric solution with the correct scalar kinetic energy K_0 at $z = 0$:
   - For various choices of q, use the array $\{(\phi_w^{(i)}, V_w^{(i)})\}$ to determine the best-fit parameters $\{p_{\text{fit}}(q)\}$.
   - Solve the equations of motion for $a(t), \phi(t)$ for the best-fit models $V(\phi; \{p_{\text{fit}}(q)\}, q)$ with each choice of q to determine for which value q_* there exists a future time t for which $\dot{a}(t) = \dot{\phi}(t) = 0$; this determines the model for which the solution has a moment of time symmetry. We use initial conditions $\phi(t_0) = \phi_0$, $\dot{\phi}(t_0) = -\sqrt{2K_0}$, and $a(t_0) = 1$.
5. As a check, evaluate the solution to the model $V(\phi; \{p_{\text{fit}}(q_*)\}, q_*)$ with time-symmetric initial conditions, and verify that the equation of state $w(z)$ behaves appropriately for $z \in (z_{\min}, z_{\max})$, and that the Euclidean continuation has AdS asymptotics.

It will frequently be useful to work with quantities rescaled by the Hubble parameter H_0, as defined in Section 8.2.3.

We observe that the procedure outlined above has significant freedom in the choice of model $V(\phi)$; since our goal is merely to demonstrate the existence of a scalar potential satisfying the list of criteria outlined in the main text, it suffices to construct a specific example.

Constructing an example

We first deduce the redshift dependence of the scalar field $\phi_w(z)$ and the rescaled potential $\tilde{V}_w(z)$ from the rescaled Hubble expansion $\tilde{H}(z)$ for the wCDM model, using

$$\begin{aligned}\phi_w(z) &= \phi_0 + \int_0^z dz' \, \frac{\sqrt{\frac{1}{4\pi G}(1+z')\tilde{H}(z')\tilde{H}'(z') - \frac{3}{8\pi G}(1+z')^3\Omega_M}}{(1+z')\tilde{H}(z')} \\ \tilde{V}_w(z) &= -\frac{1}{8\pi G}(1+z)\tilde{H}(z)\tilde{H}'(z) + \frac{3}{8\pi G}\tilde{H}(z)^2 - \frac{3}{16\pi G}(1+z)^3\Omega_M \, .\end{aligned} \tag{I.2}$$

We also deduce the present time-derivative $\dot{\phi}(\tilde{t}_0)$, where the overdot denotes a derivative with respect to the rescaled time coordinate; in units $\frac{8\pi G}{3} = 1$, we find for the wCDM model

$$\dot{\phi}_w(\tilde{t}_0) = -0.2628687886 \, . \tag{I.3}$$

Next, we choose as our model function

$$\begin{aligned}\tilde{V}(\phi; A, B, C, \Delta, X, \mathbf{V}) &= \tilde{V}_0(\phi; \ldots) + \tilde{V}_0(-\phi; \ldots) \\ \tilde{V}_0(\phi; \ldots) &= \frac{A-B}{2}\text{erf}\left(\frac{\phi - X}{\Delta}\right) + C\exp\left(-\frac{(\phi-X)^2}{\Delta^2}\right) \\ &\quad + \left(\sum_{k=1}^{4}\frac{V_k}{k!}(\phi - X)^k\right)\left(1 + \text{erf}\left(\frac{\phi - X}{\Delta}\right)\right) + \frac{A}{2} \, .\end{aligned} \tag{I.4}$$

This is similar to the asymptotically flat potential introduced in Section 8.2.3 to reproduce the ΛCDM model, though we have effectively replaced the flat region with a polynomial.

We will choose to situate the present time at $\phi_0 = 0.7$, the trough in the potential at roughly $X = 0.5$, the width $\Delta = 0.06$, and to take $B = -0.08$, which fixes the potential at $\phi = 0$ to this value; we choose these values for concreteness, though one could proceed analogously for many suitable

choices of these quantities. Our choices are motivated by the facts that (1) having the trough join suitably to the polynomial piece of the potential requires $(\phi_0 - X)$ to be a few multiples of Δ, and (2) B should be sufficiently large in absolute value that we avoid recollapse in the wormhole picture. The parameter C, controlling the depth of the trough, is the parameter that we will vary for the shooting method.

With these choices, we proceed to apply the shooting method, solving the equation (8.11) with initial conditions $a(t_0) = 0, \phi(t_0) = \phi_0, \dot{\phi}(t_0) = -0.2628687886$, for various choices of C and best-fit (A, V_1, V_2, V_3, V_4). Our procedure yields, to our working precision, the parameters $C = -7.80623080636$ and

$$\begin{gathered} A = 1.13258420902349\,, \quad V_1 = -4.21938633468535\,, \quad V_2 = 50.3190576443637\,, \\ V_3 = -370.514499837809\,, \quad V_4 = 1408.97547041725\,. \end{gathered} \tag{I.5}$$

We plot the corresponding potential $V(\phi)$, as well as $V_w(\phi)$, in Figure 8.9 of the main text. We find that the moment of time symmetry occurs at rescaled time $\tilde{t}$ with

$$\tilde{t} - \tilde{t}_0 = 0.5712956836\,, \tag{I.6}$$

at which time the scale factor and scalar field are given by

$$a(\tilde{t}) = 1.41641139203233\,, \quad \phi(\tilde{t}) = 0.358665688585761\,. \tag{I.7}$$

To check our results, we can solve both the Lorentzian and Euclidean equations of motion (8.11) and (8.12) for the model with scalar potential $V(\phi)$, assuming time-symmetric initial conditions at

$$\phi = 0.358665688585761\,, \tag{I.8}$$

the location suggested by equation (I.7). Assuming that the present time $\tilde{t}_0$ satisfies $a(\tilde{t}_0) = 1$, we can extract the redshift dependence of the equation of state parameter $w(z)$ over the range $z \in (z_{\min}, z_{\max})$ using equation (8.25), and verify that it is approximately constant and equal to the Pantheon+SH0ES value $w = -0.90 \pm 0.14$; we show this in Figure 8.10 in the main text. We can also verify that the Euclidean solution is asymptotically AdS by plotting the rescaled "Euclidean Hubble expansion" $H(\tau)$ and observing that it approaches a constant value, as also shown in Figure 8.10 in the main text.